# OXIDATION OF ZINC SULPHIDE

A Thesis presented for the Research Degree of

DOCTOR OF PHILOSOPHY

of the

COUNCIL FOR NATIONAL ACADEMIC AWARDS

LONDON

by

BODHISATTWA BASAK

John Graymore Chemistry Laboratories,
Department of Mathematical and
Physical Sciences,
Plymouth Polytechnic,
PLYMOUTH,
PL 48 AA,
Devon.

February, 1973.

## ABSTRACT

A physicochemical study has been made of roasting and sintering processes for zinc sulphide ores. The sulphides are oxidised to metal oxides or sulphates according to conditions, e.g. temperature and time of heating, composition of surrounding gases, whether under static or dynamic conditions. The mechanisms and kinetics of oxidation depend also on surface area, crystallite and aggregate sizes of the materials and the presence of any impurities. Thus, for basic oxidation studies, finely-divided zinc sulphide samples have been precipitated from solution at various pH levels and in the presence of different concentrations of eletrolytes. These experimental conditions have been correlated with changes in phase composition, surface area and crystallite and aggregate sizes during the formation of the precipitates and their subsequent ageing in solution at various temperatures.

The oxidation of the two pure zinc sulphides and five ore concentrates were investigated using the techniques of thermal analysis, gas sorption, X-ray diffraction, optical and electron microscopy.

By use of D.T.A., the effects of temperature, time, grain size, flow rate and oxygen content of the air on the roasting of the above materials were determined.

Changes in specific surface and average crystallite size (deduced from gas sorption) illustrate the influence of the zinc sulphate on the sintering of the zinc oxide. Further experiments show the effect of small amounts of lead and iron sulphides on the zinc oxide sintering. Results have been correlated with oxidation rates.

Attempts have been made to apply the basic researches to problems arising with the industrial roasting and sintering of natural ores such as spontaneous ignition (during shipment, storage and processing) and their poor sintering behaviour and incomplete sulphur removal at higher temperature. Improvements obtained by the use of lime and silica additives in the production of sinters have been investigated.

ACKNOWLEDGEMENTS

The author wishes to express his sincere thanks to Dr. D.R. Glasson for his supervision and guidance throughout the course of this work. He also wishes to acknowledge the valuable assistance he has had from Dr. S.A.A. Jayaweera and helpful discussions he has had with Dr. A.B. Meggy.

He is grateful to Dr. A.W. Richards, Research Manager, Imperial Smelting Corporation Ltd., Avonmouth, Bristol for industrial supervision and Mr. C.F. Harris and other members of staff for useful discussions.

He is grateful to Dr. A.B. Meggy and Dr. C.M. Gillett for allowing the use of research facilities, Mr. B. Lakey and other members of the staff for their co-operation and useful discussions.

He would like to thank the Governors of the Polytechnic for granting him the research assistantship.

His thanks are also due to the Polytechnic Library staff for their assistance and Mrs.W. Pawley who typed the manuscript.

CONTENTS

# Chapter 1

## INTRODUCTION AND REVIEW

### 1.1 Introduction

The element of zinc has been known and used for a long time in history. (Mellor, 1946)(1) The metal, which accounts for 0.02% of the earth's crust occurs almost entirely as zinc sulphide, ZnS; this exists in two forms, the much commoner cubic zinc blende or sphalerite and the rarer hexagonal wurtzite. Iron and cadmium are present nearly always as substitutional impurities. Other metals also, e.g. lead, have been removed from the ore during its concentration. The sulphide is converted easily to the oxide by roasting in air. The metal distils when it is heated in a retort with carbon. The following is an outline of the industrial use of zinc sulphide

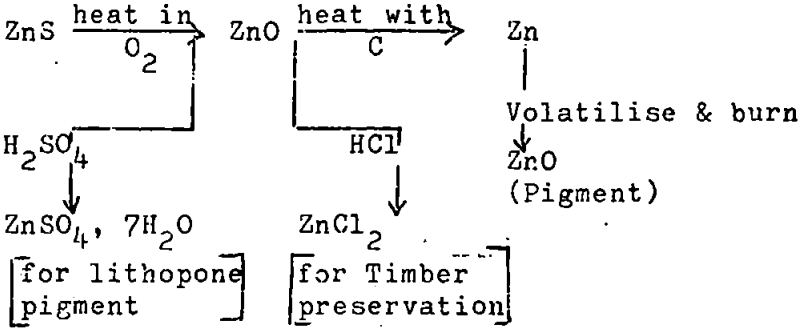


In the presence of impurities, zinc sulphide is phosphorescent and it is used in the manufacture of luminous paint. It is used also to make screens sensitive to X-rays, and when mixed with barium sulphate, it forms the white pigment, lithopone.

The metal is used for 'Galvanising' steel. An alloy with ~4% Al and 0.15 - 1.25% Cu is being employed increasingly for die-casting.

According to M.Hill et al(1970)(2) several ship-loads of concentrates from the Persian Gulf have been recorded to have caught fire. In 1969 the cargo of the "S.S. Aryaman" was reported glowing and large amounts of sulphur dioxide were evolved. At Khorramshahs (a port) fires have occurred in bagged, unbagged and humified material and at Konchke (a mine) a dump of concentrates in woven polypropylene bags ignited in 11 days.

To prevent the self-heating of Bafq concentrates or to minimise the self-heating, so that the material can be stockpiled and shipped in a safe manner, and to determine the 'cause' or 'trigger' of the self-heating, preliminary investigations by M. Hill et al. (1970)(2) have been extended in the present work. Thus, zinc sulphide has been prepared by both wet or dry methods giving both crystalline forms. The oxidation to zinc oxide and zinc sulphate has been studied by thermogravimetric methods. Attempts have been made to correlate the temperature conditions with changes in surface area, crystallite or aggregate sizes and crystal morphology. Effects of variations in the surrounding gas composition, e.g. reduced oxygen content, also have been studied. Likewise, the role of impurities such as iron, lead and copper in the oxidation of zinc sulphide concentrates has been assessed.

## 1.2 Formation of zinc sulphide

Mellor (1946)(1) has summarised the methods of preparation of zinc sulphide by earlier workers. These involve mainly the action of hydrogen sulphide on various zinc salts. The properties and form of the product depends on the conditions of preparation. The summary contains the methods of precipitation of zinc sulphide from solution of gaseous $H_2S$ under different conditions of

hydrogen ion concentration and temperature. He discusses also the phosphorescence of the material.

Zinc sulphide is dimorphic changing from the $\beta$ or cubic modification (sphalerite) at about $1020^{\circ}$ to the $\alpha$ or hexagonal modification (wurtzite). ZnS sublimes at $1185^{\circ}$ and melts at $1850^{\circ}$ with a vapour pressure at 150 atmospheres.

So according to R.A. Laudise et al (1959)(3), the conventional crystal growth techniques are not suitable for its preparation, especially if the cubic modification is desired. Small crystals (<1 mm) of zinc sulphide have been prepared by sublimation and vapour phase reaction. But their size, purity, stoichiometry and luminescence varies. Allen et al (1912)(4) and Kremheller et al (1957)(5) have crystallized ZnS isothermally under hydrothermal conditions, but the increase in particle size was rather small (5 $\mu$.m.). However, R.A. Laudise et al (1959)(3) have grown large crystals in a hydrothermal system where the required supersaturation was produced by a temperature gradient.

R. Dimitrov (1969)(6) has prepared small needle-like ZnS single crystals. His method of preparation is as follows. Zinc sulphide, obtained by precipitation with $H_2S$ from a zinc sulphate solution was used as initial material. The powdered sulphide was briquetted beforehand into small tablets, which (in a quartz vessel) were heated up to 3 hours in a pipe furnace at 1280 K in a current of super-pure nitrogen.

A horizontal Celite furnace was used for the resublimation of ZnS. It was establised that at 1723 K ($1450^{\circ}$C), with a nitrogen current of $6 \times 10^{-3} m^3/3600$ sec (1 hr) ZnS crystals ($6 \times 1 \times 0.2$) $10^{-3}$m in size accumulate in 4 hours on the wall of the quartz tube. The crystallization temperature of the crystals was 1523 K($1250^{\circ}$C).

A hexagonal or cubic ZnS modification was obtained, depending on experimental conditions, particularly the temperature of sublimation and crystallization. A cubic sulphide modification was obtained at a crystallization temperature of 1223 K (950°C).

## 1.3 Crystal Structure and bonding of Zinc sulphide

Zinc blende or sphalerite has a face-centered cubic structure with sulphur atoms occupying the corners and face centres of the unit cell and Zn atoms occupying half the tetrahedral sites. Fig. 1

The structure of Wurtzite can be considered to consist of sulphur atoms occupying the lattice points of a hexagonal close-packed system with the zinc atoms at half the tetrahedral sites Fig. 1

In the structures of diamond, sphalerite and wurtzite each atom is surrounded tetrahedrally by four other atoms. If the atoms are those of Group IV elements or of two elements symmetrically arranged relative to Group IV in the Periodic Table, the number of valence electrons is correct to permit the formation of a tetrahedral covalent bond between each atom and its four neighbours. Compounds exhibiting sphalerite or wurtzite structure are listed in Table 1.

In all of these compounds it is probable that the bonds are covalent with some ionic character (Pauling, 1960)(7).
For the zinc sulphide, ZnS, the extreme covalent structure

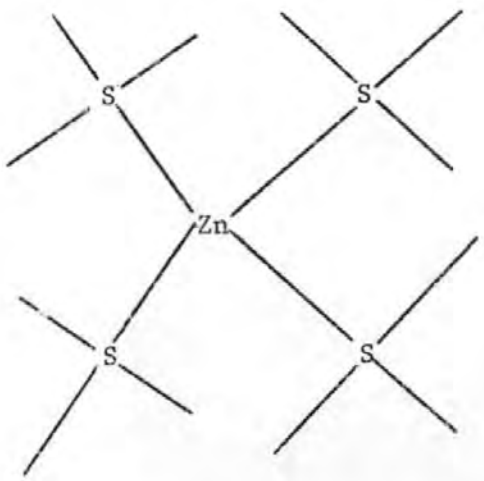

TABLE 1

Comparison of observed interatomic distances in B3 and B4 crystals* with sums of tetrahedral radii.

| | | | | | | | |
|---|---|---|---|---|---|---|---|
| AlN | 1.96 | AlP | 2.36 | AlAs | 2.44 | AlSb | 2.62 |
| B4 | 1.90 | B3 | 2.36 | B3 | 2.44 | B3 | 2.64 |
| GaN | 1.96 | GaP | 2.36 | GaAs | 2.44 | Gasb | 2.62 |
| B4 | 1.95 | B3 | 2.36 | B3 | 2.44 | B3 | 2.63 |
| InN | 2.14 | InP | 2.54 | InAs | 2.62 | Insb | 2.80 |
| B4 | 2.15 | B3 | 2.54 | B3 | 2.62 | B3 | 2.80 |
| BeO | 1.72 | BeS | 2.10 | BeSe | 2.20 | BeTe | 2.38 |
| B4 | 1.65 | B3 | 2.10 | B3 | 2.20 | B3 | 2.41 |
| ZnO | 1.97 | ZnS | 2.35 | ZnSe | 2.45 | ZnTe | 2.63 |
| B4 | 1.97 | B3B4 | 2.35 | B3 | 2.45 | B3 | 2.63 |
| | | Cds | 2.52 | CdSe | 2.62 | CdTe | 2.80 |
| | | B3B4 | 2.53 | B3B4 | 2.63 | B3 | 2.80 |
| | | HgS | 2.52 | HgSe | 2.62 | HgTe | 2.80 |
| | | B3 | 2.52 | B3 | 2.63 | B3 | 2.79 |
| CuF | 1.99 | CuCl | 2.34 | CuBr | 2.46 | CuI | 2.63 |
| B3 | 1.85 | B3 | 2.34 | B3 | 2.46 | B3 | 2.62 |
| BN | 1.58 | SiC | 1.94 | MgTe | 2.72 | AgI | 2.80 |
| B3 | 1.57 | B3B4 | 1.89 | B4 | 2.76 | B3B4 | 2.80 |

* B3 is the sphalerite structure (cubic) and B4 the wurtzite structure (hexagonal).

Figure 1

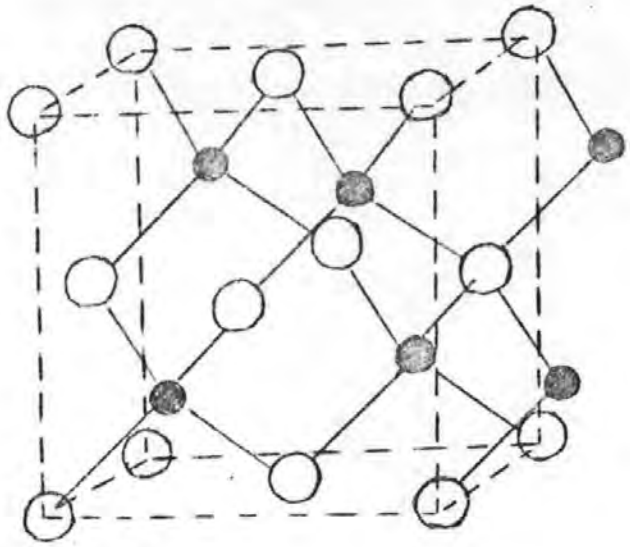

The arrangement of Zinc atoms (small circles) and sulphur atoms (large circles) in sphalerite, the cubic form of Zinc sulphide.

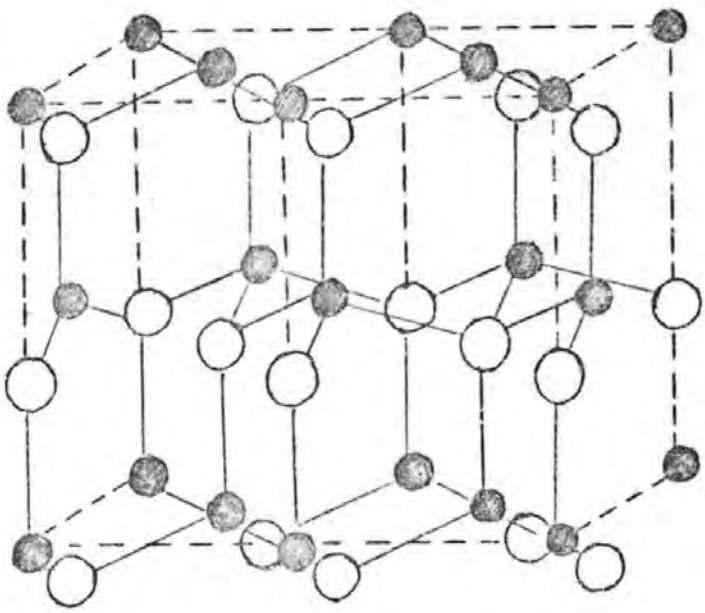

The arrangement of Zinc atoms (small circles) and sulphur atoms (large circles) in wurtzite, the hexagonal form of zinc sulphide. The unit of structure outlined by dashes is the orthahexagonal unit, with edges at right angles to one another. The lengths of the edges of the unit in the basal phase have the ratio $\sqrt{3}/1$, corresponding to the $120^{\circ}$ angles of the hexagonal unit.

places formal charges 2+ on zinc and 2- on sulphur. It is probable that the bonds have enough ionic character in this crystal and in others of similar structure to make the actual charges of the atoms nearly zero; for ZnS, this would require about 50 percent ionic character.

A set of values of tetrahedral covalent radii for the use in compounds of these types is given in Table 2 and represented graphically in Figure 2.

Table 2

TETRAHEDRAL COVALENT RADII/Å

| | | | | | | |
|---|---|---|---|---|---|---|
| | Be | B | C | N | O | F |
| | 1.06 | 0.88 | 0.77 | 0.70 | 0.66 | 0.64 |
| | Mg | Al | Si | P | S | Cl |
| | 1.40 | 1.26 | 1.17 | 1.10 | 1.04 | 0.99 |
| Cu | Zn | Ga | Ge | As | Se | Br |
| 1.35 | 1.31 | 1.26 | 1.22 | 1.18 | 1.14 | 1.11 |
| Ag | Cd | In | Sn | Sb | Te | I |
| 1.52 | 1.48 | 1.44 | 1.40 | 1.36 | 1.32 | 1.28 |
| | Hg | | | | | |
| | 1.48 | | | | | |

Figure 2

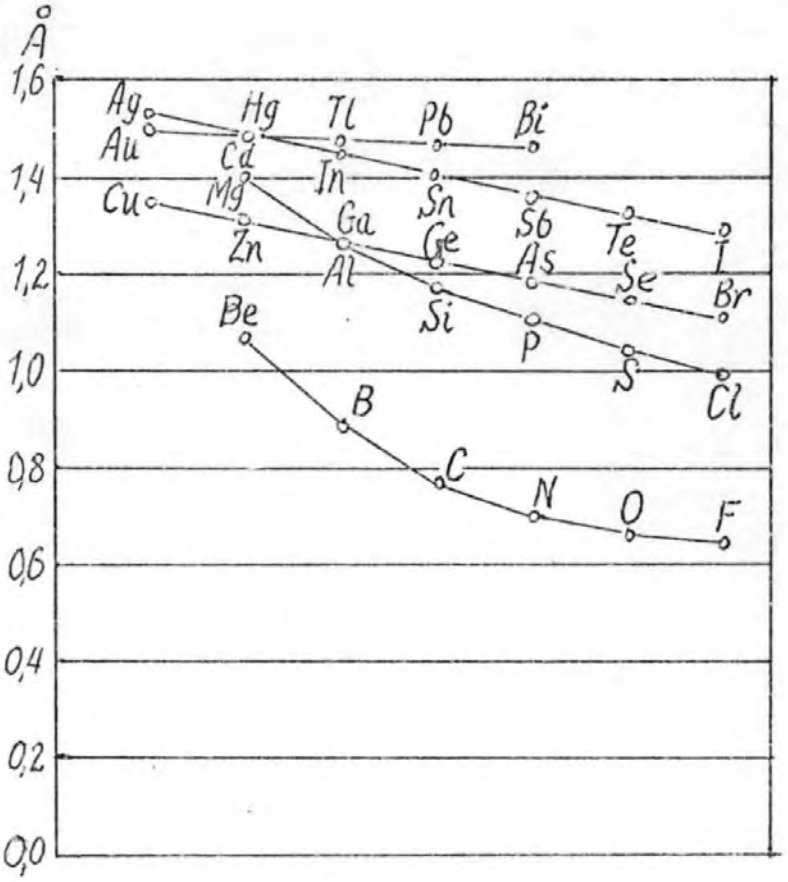


Values of tetrahedral covalent radii for sequences of atoms

## 1.4 Oxidation of Zinc sulphide

The oxidation of zinc sulphide has been a subject of both experimental and theoretical investigations (G.S.G. Beveridge, 1962)(8). The reaction is exothermic and may be considered to be irreversible. Such a reaction has been found to proceed in a topochemical manner. In other words, as the reaction proceeds a progressively thicker outer shell of zinc oxide is formed while the inner core of unreacted sulphide decreases. The reaction may be represented by

$$ZnS(s) + \tfrac{3}{2}O_2(g) = ZnO(s) + SO_2(g)$$

Several possible side reactions may occur, with sulphate formed below 700°C and an interaction between the sulphide and the oxide becoming important at 1400°C.

Studies on the kinetics of roasting of pure zinc sulphide in air carried out by earlier workers have shown that two main processes are involved in the oxidation of zinc sulphide, a kinetic range with activation energies 30 - 70 k.cal/mole at low temperatures and a diffusion-controlled range with low activation energies at high temperatures. Various temperatures have been reported in the literature for the changeover from the kinetic region to the diffusion region. Ong et al (1956)(9), working with single crystals of sphalerite, found that the oxidation rate of sphalerite crystals is linear over the range 700°- 870°C, with an activation energy of 60 k.cal/mole, indicating chemcial control up to 870°C. Cannon and Denbigh (1957)(10), working with small single crystals of zinc sulphide, found that the reaction is controlled by chemical kinetics up to 830°C with an activation energy of about 50 K.Cal/mole.

At low temperatures, between 680°- 830° it has been shown (Cannon et al, 1957)(10) that the rate of movement of the ZnO - ZnS interface depends on the processes taking place at this interface and not on the diffusion through the overlying layer of zinc oxide.

Similar results have been published by Ong et al (1956)(9) for a single crystal of ZnS and by Diev et al, (1955)(12) and Wada et al (1957)(11) for the powdered form. In the lattice, the reaction is chemically controlled up to about 600°C. Beyond this temperature, the rate is controlled by the diffusion of oxygen through the oxide layer; this occurs at a lower temperature than for single crystals because of the much greater surface area available.

The temperature at which the chemical reaction rate first becomes significant increases with decreasing surface area; values of 470 to 540°C are reported for precipitated powdered zinc sulphide by Balikhina et al (1937)(13) and 555 to 750°C for sphalerite crystals by Ongawa et al (1929)(14), Orlev et al (1942)(15) and Cannon et al (1957)(10) depending on the particle size.

Wada and Niva (1957)(11) followed the roasting of zinc sulphide by a weight loss technique using a spring balance. Beveridge (1962)(8) used spherical compacts of zinc sulphide and followed the overall reaction rate by absorbing the gaseous reaction products in hydrogen peroxide solution and estimating their concentration by a conductivity method.

The spherical pellets of zinc sulphide made from Santander concentrates were studied by K.Nateson et al (1969)(16) at a temperature range of 740° to 1020°C. The analysis of their data indicated that the process of oxidation was predominantly controlled by transport through the zinc oxide product layer.

## 1.5 Kinetics of oxidation of Zinc sulphide

The linear oxidation of sphalerite as described by John N. Ong et al (1956)(9) may be considered a heterogeneous gas-solid reaction involving an absorption process on the surface followed by desorption of the products.

According to him, the steps by which the reaction of sphalerite proceeds may be represented as follows :

$$ZnS + O_2 \rightleftarrows ZnS \ldots O_2 \text{ (chemisorption)} \ldots\ldots\ldots\ldots (1)$$

followed by decomposition of the surface site:

$$ZnS \ldots\ldots O_2 \rightarrow \text{(activated state)} \neq ZnO + SO \ldots\ldots\ldots\ldots (2)$$

and

$$2SO + O_2 \rightarrow 2SO_2 \ldots\ldots\ldots\ldots (3)$$

Ultimately resulting in the formation of ZnO and $SO_2$. The postulate that SO exists as an intermediate product has been suggested by M.E. Wadsworth et al (1953)(17). Its presence would be only transitory and it would be immediately removed at the surface by reaction (3).

According to the absolute reaction rate theory of K.J. Laidler (1950)(18) the rate of a reaction may be represented by

$$\text{Rate} = k \cdot \frac{KT}{h} \pi_i C_i e^{-\Delta F^{\neq}/RT}$$

$$= \pi_i C_i K' \ldots\ldots\ldots\ldots\ldots\ldots (4)$$

where $\pi_i C_i$ = the product of the concentration of the reactants

$\Delta F^{\neq}$ = the free energy of activation

$k$ = the transmission coefficient usually taken as unity

$K$ = Boltzman Constant

$h$ = Planck constant

$K'$ = the specific reaction rate constant

If the rate-determining reaction is the thermal decomposition of a surface site, then

$$\text{Rate} = f(\theta)K^{1} \quad \ldots\ldots\ldots\ldots\ldots\ldots(5)$$

Where $f(\theta)$ = some function of the fraction of the surface covered.

The rate then may be written as

$$\text{Rate} = \frac{KT}{h} f(\theta) K_{SR} e^{-\Delta F^{\neq}/RT}$$

$$= \frac{KT}{h} f(\theta) K_{SR} e^{-\Delta H^{\neq}/RT} e^{\Delta s^{\neq}/R} \quad \ldots\ldots\ldots\ldots\ldots\ldots(6)$$

where $K_{SR}$ = constant, which includes a surface roughness factor.

$\Delta H^{\neq}$ = the enthalpy of activation.

$\Delta S^{\neq}$ = entropy of activation.

For the mechanism involving single site adsorption of an oxygen molecule on the surface the reaction appears to be extremely rapid. This may be represented by

$$ZnS \text{ (surface)} + O_2 \rightleftharpoons ZnS \ldots O_2 \text{(surface)}$$

from which $K_1 = \frac{\theta}{1-\theta} \cdot \frac{1}{(O_2)} = e^{-\Delta F_1/RT}$

$\ldots\ldots\ldots\ldots\ldots\ldots(7)$

where $\theta$ = the fraction of the surface covered with adsorbed oxygen

$K_1$ = the equilibrium constant of the adsorption process

$(O_2)$ = the concentration of oxygen in the gas phase

$\Delta F_1$ = the free energy of adsorption

The equilibrium value of $\Delta F_1$ from thermodynamic considerations may be expressed as :

$$\frac{-\Delta F_1}{RT} = \ln K_1 - \ln K_1^{o} = \ln \frac{\prod_{ii} C_p}{\prod_{ii} C_R} - \ln \frac{\prod_{ii} C_p^{o}}{\prod_{ii} C_R^{o}}$$

$\ldots\ldots\ldots\ldots\ldots\ldots(8)$

where $C_p$ = the concentration of the products

$C_R$ = the concentration of the reactants

Superscript o refers to the standard state. The quantity $\ln \prod_{ii} C_p^{o} / \prod_{ii} C_R^{o}$ is arbitrarily chosen such that it equals zero in

the standard state. Since the oxygen concentration is expressed in moles per litre, the standard state is defined as $\theta^{\circ} = 0.5$ and $(O^{\circ}_2) = 1$ mole per litre. Solving equation (7) and (8) the following is obtained :

$$\theta = \frac{K_1(O_2)}{1+K_1(O_2)} \quad \ldots\ldots\ldots\ldots\ldots (9)$$

Assuming that at constant temperature the quantity $K_{SR} \frac{KT}{h} e^{-\Delta F^{\neq}/RT}$ remains constant, then equation (6) may be written in the form :

$$\text{Rate} = K_o \frac{K_1(O_2)}{1+K_1(O_2)}$$

from which a value of $K_1$ may be obtained by simultaneous evaluation of two points on each isotherm.

A plot of log $K_1$ against the reciprocal temperature gives the value of enthalpy of adsorption, $\Delta H_1$ of $O_2$ on sphalerite; it was found to be -59.6K. cal per mole of oxygen with an entropy of adsorption of -39.2 k.cal/K.

The rate of oxidation of the (110) faces of sphalerite studied by K.J. Cannon et al (1957)(10) show that the rate of penetration of oxygen diminished somewhat during the early stages of reaction, but subsequently approached an almost constant rate, the thickness of the oxide layer increasing linearly with the time. The linearity which follows the initial period is consistent with the assumption that the observed rate is 'chemically controlled'. The steady reaction rate as measured in centimeters penetration per second, has been calculated from the linear portion of the curves. A plot of the logarithm of the steady reaction rate against the reciprocal of the absolute temperature over the range 680°C to 830°C, is a linear one and the rate can thus be

represented by the relation :

$$\text{Rate} = \text{const.} \times e^{-E/RT} \quad \ldots\ldots\ldots\ldots (1)$$

with $E = 50$ Kcal/mole

The combined effect of temperature and partial pressure may be represented by

$$\text{Rate} = Ae^{-E/RT} \, p^{\frac{1}{2}} \quad \ldots\ldots\ldots\ldots\ldots (11)$$

where $P$ = the partial pressure in atmosphere

$E$ = 50 Kcal/mole

and A has the value $8.0 \times 10^4$ when the rate is expressed as cm penetration $sec^{-1}$ or the value $3.2 \times 10^3$ when the rate is expressed as moles ZnS $cm^{-2}$ $sec^{-1}$. At temperatures below 830°C the penetration was very uniform over the faces, the ZnO-ZnS interface was sharply defined and the corners of the sulphide core remained sharp. On the other hand, at temperatures above 830°C, the corners began to show a rounding, as in Fig

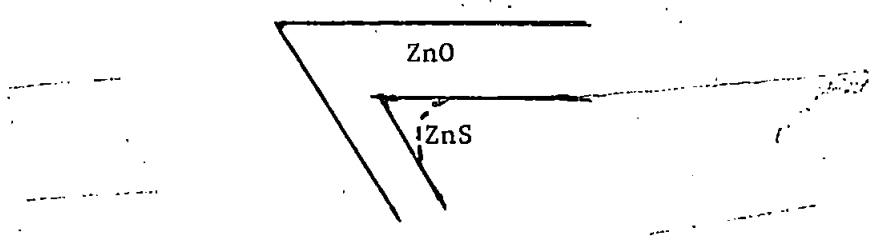


This is clearly due to the diffusion of oxygen or sulphur dioxide through the oxide layer, becoming significant as a rate-controlling factor.

At temperatures over 900°C the penetration becomes very uneven over different parts of the crystal. The uneven penetration was at first thought to be due to cracks or other faults in the crystal, but this does not explain why the effects become marked only above 900°C. It is probably due to thermal instability: the thickness of the oxide layer impedes the escape of the heat of reaction which thereby causes a local rise in temperature and therefore a still further increase in reaction rate.

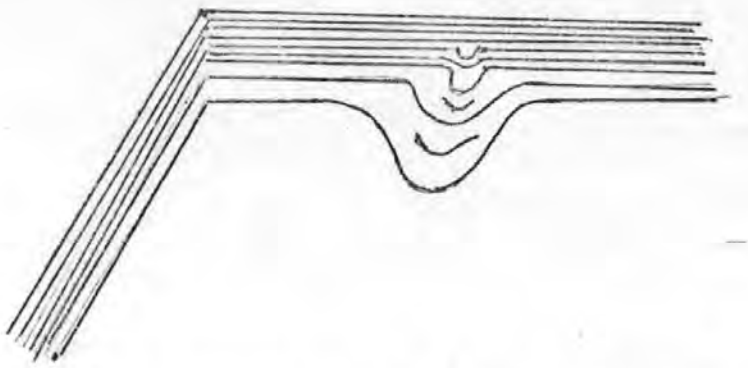

Non-uniform growth pattern of oxide films on ZnS above 900°C.

When crystals were roasted at temperatures above 950°C there was a considerable deposition of woolly zinc oxide on the platinum and silica supports of the roasting tray. At these temperatures it is known that zinc sulphide has an appreciable dissociation pressure, whilst zinc oxide itself is still almost involatile. It seemed, therefore, that evaporation of zinc sulphide was taking place, followed by a vapour-phase oxidation and a deposition of zinc oxide on available surfaces.

An approximate theory of simultaneous reaction at the ZnO-ZnS interface and of diffusion of oxygen through the overlying layer of zinc sulphide has been put forward by K.J.Cannon et al(1957)(10). They consider the ease of reaction at plane surfaces and neglect the effects of edges.

They again apply Fick's law (17) to the inward diffusion of oxygen through the porous zinc oxide, despite the existence of a flow of sulphur dioxide in the reverse direction. The concentration gradient is assumed to be linear, the number of moles of oxygen diffusing in unit time up to unit area of the interface is therefore

$$D(C_o - C)x \quad \ldots\ldots\ldots\ldots\ldots\ldots (111)$$

where D = the diffusion coefficient

x = the oxide layer thickness at time, t

$C$ = the oxygen concentration at the ZnO-ZnS interface.

$C_o$ = the oxygen concentration at the outer surface of the crystal = the concentration in the bulk gas phase in the absence of any appreciable mass transfer resistance in this phase.

The reaction rate at the interface is approximately proportional to the square root of C, the number of moles of oxygen reacting in unit time at unit area of the interface is

$$KC^{\frac{1}{2}} \quad \ldots\ldots\ldots\ldots\ldots (IV)$$

where $K$ = a velocity constant; equating (111) and (IV) at the steady state :

$$KC^{\frac{1}{2}} = D(C_o - C)/x$$

and hence $C = C_o \left(1 + \gamma - \gamma\sqrt{1 + 2/\gamma}\right) \ldots\ldots\ldots (V)$

where $\gamma$ = the dimensionless quantity

$$\gamma = x^2K^2/2D^2C_o \ldots\ldots\ldots\ldots\ldots\ldots\ldots (VI)$$

The penetration rate $\frac{dx}{dt}$ is obtained by multiplying (IV) by (V), the molar volume of zinc sulphide and by a factor 2/3, from the stoichiometry of the reaction. Thus from (IV) and (V) together with these factors :

$$\frac{dx}{dt} = 2/3\ KVC_o^{\frac{1}{2}} \left(1 + \gamma - \gamma\sqrt{1+2/\gamma}\right)^{\frac{1}{2}} \ldots\ldots\ldots (VII)$$

This expression reduces to simpler forms under two limiting conditions :

(1) If $\gamma \ll 1$, which occurs at temperatures at which K is small,

$$\frac{dx}{dt} = \frac{2}{3} KVC_o^{\frac{1}{2}}$$

This corresponds to 'chemical control' since the rate is independent of the thickness or of the value of the diffusion coefficient.

(2) If $\gamma \gg 1$, which occurs at higher temperatures where K is relatively large, $\frac{dx}{dt} = \frac{2}{3} DVC_o/x$

which corresponds to 'diffusion control'. Integrating $x^2 = \frac{4}{3} DVC_o t$ and the thickness is thus proportional to the square root of the time.

1.5a The sintering of Zinc oxide formed on zinc sulphide surfaces

Since solids are involved, reactions which are thermodynamically feasible may be kinetically unfavourable, because of (1) loss of reactive surface through sintering of the solid reactants and products and (2) impedance of the participant gases (oxygen and sulphur dioxide) by the sintered materials. Thus, the degree of sintering affects both chemical and diffusion kinetics as in (1) and (2) respectively.

1.5.1. General principles of the mechanism of sintering

Systems undergoing sintering are of two types, namely:

(1) homogeneous systems consisting of a single component or components which give continuous series of solid solutions.

(2) heterogeneous systems consisting of multiple component systems.

In the homogeneous sintering of a powder, distinction can be made between two overlapping stages of sintering. The first stage is characterized by the formation and growth of bonds, i.e. the contact areas between adjacent powder particles. The growth of these contact areas takes place during the early stages of sintering, and is manifested by improved cohesion of the compact. If the material is electrically conducting, there is rapid increase of conductivity. In the second stage of sintering, the material is densified and the pore volume decreased. Under favourable conditions the pores are practically eliminated.

The surface free energy is considered to be the driving force in both stages of sintering. The energy required for sintering is supplied by the decrease of surface areas or by the replacement of high-energy interfacings by those of lower energy, e.g. grain boundaries. The surface free energy is sufficient to

account for sintering, provided a suitable mechanism is available for the transport of atoms involved in the consolidation of powder compacts. The following five mechanisms are possible in the case of homogeneous materials:

(1) Evaporation followed by condensation

(2) Surface diffusion

(3) Volume diffusion

(4) Viscous flow (Newtonian flow characterized by a linear relationship between strain rate and stress).

(5) Plastic flow (Bingham flow characterized by the existence of a yield stress).

Frenkel (1945)(18) assumed that with both amorphous and crystalline powders, viscous flow would occur under the variation of influence of the capillary forces associated with the curved surfaces of the pores with time. The viscosity may be represented by the equation :

$$\eta = KT/D\,\Omega_o \quad \ldots\ldots\ldots\ldots\ldots\ldots (1)$$

where $\eta$ = viscosity

D = coefficient of self-diffusion

T = thermodynamic temperature

K = constant

$\Omega_o$ = atomic volume

According to Shaler and Wulff (1948)(19), Nabarro (1948)(20) and Herring (1950)(21), at high temperatures, crystalline solids can deform at stresses below the yield point. The mechanism of deformation is considered to be the migration of individual vacancies or atoms, i.e. volume diffusion. The driving force for this migration is the gradient in chemical potential resulting from the differences in stress.

The first demonstration that mass flow by volume diffusion occurs during sintering was provided by Kuczynski (1950)(22). He was the first to provide quantitative proof of this by comparing the observed time-dependence of neck growth with the time-dependences predicted for viscous flow, evaporation condensation, volume diffusion and surface diffusion. He showed that in all four cases, the sintering time, t, to produce a neck of radius, x, should be given by the form:

$$\left(\frac{x}{a}\right)^n = \frac{A(T)t}{a^m} \quad \text{.....(11)}$$

where $a$ = radius of particle

$A(T)$ = a function of temperature only

and $n=2$, $m=1$ for viscous flow

$n=3$, $m=2$ for evaporation-condensation

$n=5$, $m=3$ for volume diffusion

$n=7$, $m=4$ for surface diffusion

$n=6$, $m=6$ for grain boundary growth

Kuczynski's model for neck-growth by volume diffusion is shown in Fig. 3, which shows two spheres in contact, sectioned through their centres. The capillary suction in the neck is then:

$$1/r = 1/x = \frac{\gamma}{r} \quad \text{.....(111)}$$

$\gamma$ = surface tension

$r$ = radius of curvature of the neck surface in the plane of the section.

When a vacancy is formed under the surface of the neck, a quantity of work, $\gamma\delta^3/r$, is done; therefore by capillary suction, where $\delta^3$ is the volume of the vacancy, the thermal energy required to form the vacancy is decreased by this amount. Hence

$$\frac{\Delta C}{C} = \frac{C^1 - C}{C} = \frac{\gamma\delta^3}{rKT} \ll 1 \quad \text{.....(1V)}$$

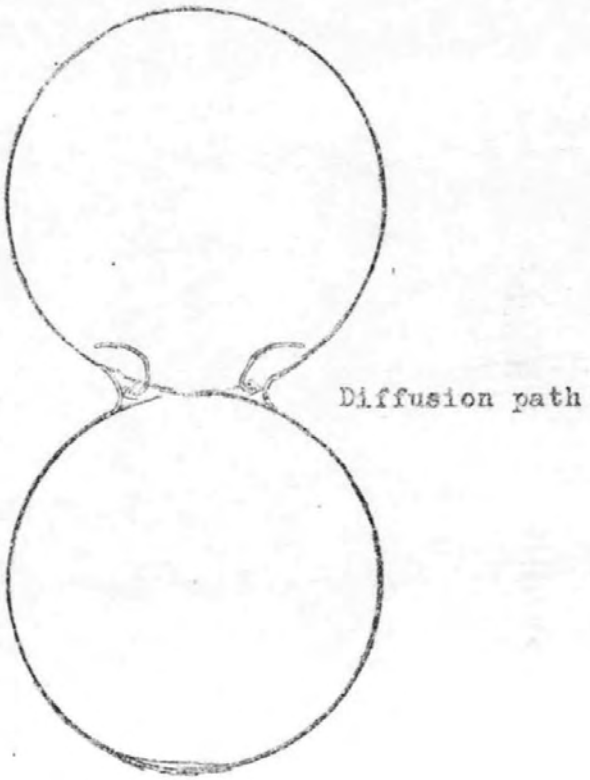


Figure 3 Kuczynski model for initial sintering by vacancies being eliminated at the surface of spheres.

where $C$ = concentration of vacancies in the unstressed crystal

and $C^1$ = concentration of vacancies in the neck.

This expression is identical with that for the increase in the vacancy concentration around a cylindrical pore of radius, r. In case of the vacancy flux away from the neck, Kuczynski assumed in effect that the surface of the latter could be considered as forming one half of the surface of a cylindrical pore, from which there was radial diffusion to sinks on the surfaces of the sphere.

For this case, the vacancy concentration gradient adjacent to the surface is $\frac{\Delta C}{r \ln d/r}$

where d is the distance at which $C^1 = C$; $\ln d/r$ was assumed to be unity. An equation could thus be set up for the rate of increase in the volume of the neck:

$$\frac{(X)^5}{(a)} = \frac{40\gamma\delta^3 Dt}{a^3 KT} \quad \ldots\ldots\ldots\ldots \text{(V)}$$

where $a$ = particle radius

$D$ = coefficient of volume diffusion

Kuczynski's original model assumed that vacancy sinks are confined to the particle surfaces and could only account for densification so long as the pores remain open and inter-connected. Kingery and Berg (1955)(23) showed that the observed rates were too rapid to be accounted for by neck growth due to volume diffusion and proposed a model (Fig. 4) in which a grain boundary existing between two spherical particles is considered to act as the vacancy sink.

Atoms would then flow from the vacancy sinks to the neck surface, as indicated by the arrows, and thus, by spreading out of material at the neck, cause the particles to coalesce. Subsequently Coble and Ellis (1958, 1963)(24,25) concluded that the deformation produced by plastic flow is limited to a fixed value determined by the hot hardness of the material, limited as

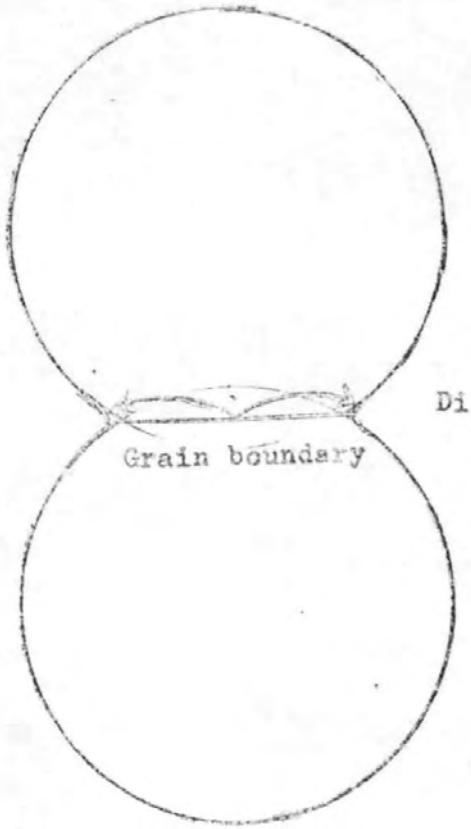


Figure 4 Kingery and Berg model for vacancies eliminated at grain boundary at neck

a mechanism to < 84% theoretical density.

1.5.2 The effect of sintering on the kinetics of zinc sulphide oxidation

G.S.G. Beveridge (1962)(8) found that the physical properties of the originally similar pellets of zinc sulphide used in rate-determining experiments were altered by sintering or partial softening action above about 900°C to an extent dependent upon the temperature level of operation. As the heating temperature rises from 900 to 1200°C, not only does the pellet shrink in size, (its diameter being reduced by 20%, although there is negligible loss in weight), but also its bulk density almost doubles, its internal voidage or porosity decreases to negligible values, and its internal surface (as measured by the BET method) drops to about 5% of its original value. These observations show that the properties begin to alter at about 900°C from their original or low temperature values with the onset of sintering, with most changes occurring in the narrow temperature range 950 - 1050°C.

This sintering action, occurring not only in nitrogen but also in air, will tend to decrease the available surface for reaction, as well as decreasing the size of the entry pores due to fusing of the particulate material in the pellet. It may also cause a blanketing of area, not measurable by the BET method, but it is possible that this might be detected by the bulk density measurements. These measurements of the changes in the physical properties of the zinc sulphide specimens are necessary for any prediction of the over-all reaction rate.

Masakazu Sakaguchi (1970)(26) has studied the oxidation of zinc sulphide powder in oxygen or in an oxygen-hydrogen chloride atmosphere, at 500 - 1150°C. The specific surface area of samples was measured by the gas adsorption method. At 500°C the addition of HCl increased the formation of ZnO on ZnS. The specific

surface area decreased with increase in partial pressure of oxygen. Oxidation rates of zinc sulphide in an atmosphere of oxygen increased with increasing temperature up to 850°C. The addition of HCl, however, retarded the oxidation at that temperature. When an equimolar mixture of HCl and $O_2$ was used, the maximum surface roughness of oxidised ZnS and preferential orientation of the (002) planes of ZnO were observed. At 1050°C, less ZnO was formed than at 850°C, and the properties of these ZnO crystals were similar to those of pure ZnO crystals.

For basic oxidation studies in the present research, zinc sulphide samples of widely different particle size were precipitated from solution at various pH levels and electrolyte concentrations.

## 1.6 Precipitation and ageing of Zinc sulphide

### 1.6.1 General phenomena of precipitation processes

The stages of a precipitation process are represented by A.E. Nielson (1970)(27) in Fig 5 . Precipitation starts with nucleation on impurity particles (or seeds), or with the formation of embryos. The nuclei grow into visible crystallites.

According to R.F. Strickland-Constable (1963)(28), sometimes the growth process is accompanied by the formation of new (secondary) nuclei, so that crystallites of two or more size groups are present. The crystallites may form a stable suspension or they may coagulate. When the crystallites or the coagulated clusters in a liquid become larger they tend to sediment. This is usually the last step of the process, and then the growth of the individual particles seems to have ceased. But if the system is observed for a very long time it is evident that the small crystallites redissolve and the larger ones grow further.

Figure 5

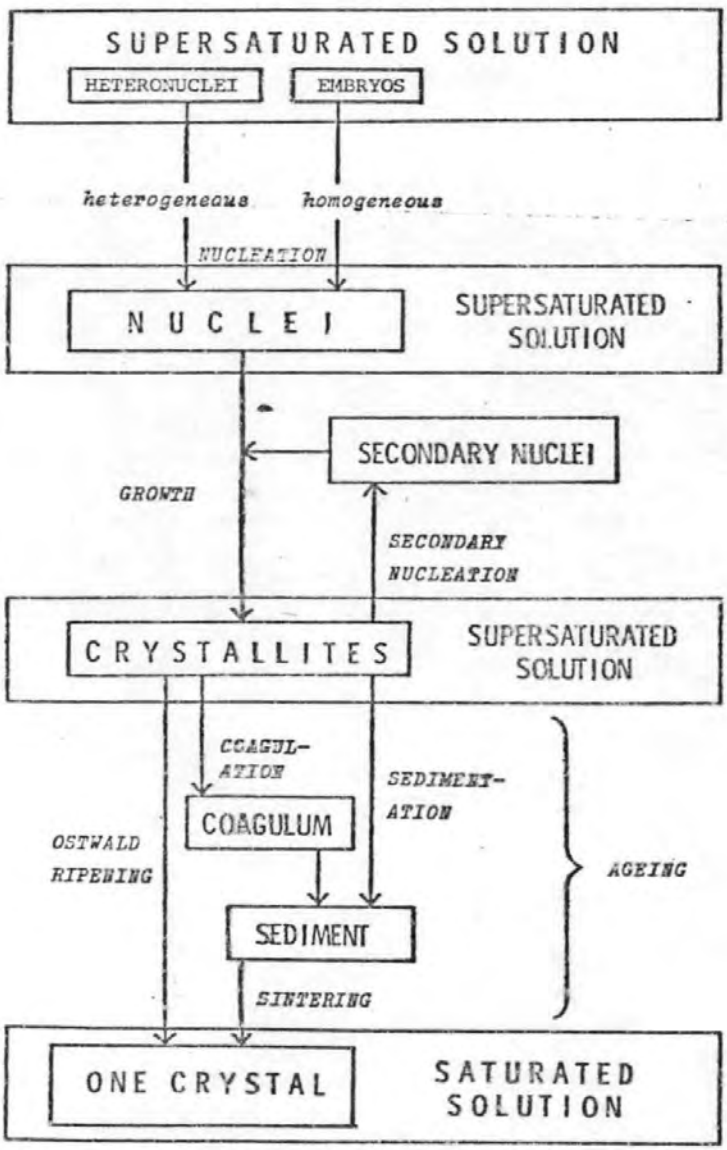


. Ways and stages of precipitation processes.

Supersaturation

Precipitation is not possible unless the solution is supersaturated. A saturated solution can be supersaturated by temperature change or by fractionation through evaporation or crystallization of the solvent. Another way of making a supersaturated solution is to mix two solutions or liquids which react chemically, e.g. electrolyte precipitation from aqueous solution.

Nucleation

Preciptiation does not start at any supersaturation because small crystals have a higher equilibrium concentration than large crystals. It follows that crystals smaller than a certain critical size will dissolve if they are brought into contact with a solution of moderate supersaturation - the critical size depending on the ratio of the concentration to the solubility whereas crystals larger than the critical size start growing - and grow more and more rapidly, as they get larger. This can happen in two ways :

Heterogeneous nucleation

Any solution which has not been extremely well cleaned contains a vast number of invisible solid particles. A hundred particles per $mm^3$ is quite normal even in filtered liquids. They may act as heteronuclei, i.e. catalysts for the initiation of precipitate crystals, the solute being adsorbed on the particles to form a layer which is larger than a face of a crystal of the critical size, and thus able to grow in the solution. This is the normal way of nucleation of a new phase.

Homogeneous nucleation

R. Baker et al (1935)(29) explained homogeneous nucleation. At a moderate supersaturation there is an appreciable number of embryos, i.e. subcritical associates of crystal-like structure in equilibrium with the solution. A small fraction of these reaches the critical size by thermal fluctuation. When this happens the chance that the associate will grow further is larger than the chance that it will dissolve again. The critically-sized embryos thus play a role similar to the activated complex of chemical reaction kinetics. Homogeneous nucleation has been observed in two types of experiments.

According to E.R. Buckle (1960)(30) and H.J.De Nordwall et al (1961)(31) the growth of the heteronuclei is limited by dividing the system into a very large number of small parts, so that only a small fraction of these contains one or more of the heteronuclei.

In the experiments of precipitation of sparingly soluble electrolytes from solution, A.E.Nielsen (1961)(27) showed that a very high supersaturation is produced very rapidly so that the number of homogeneously-nucleated particles is much larger than the number of heteronuclei present.

In the case of heterogeneous nucleation the number of particles is roughly constant during the precipitation process, and the particles are of nearly the same size. When homogeneous nucleation takes place the number of crystals increases with time. The rate of nucleation is strongly dependent on the concentration and approaches zero as soon as the concentration has decreased by a relatively small amount.

Crystal growth

Nucleation in a solution has never been observed directly because

(i) the nuclei are extremely small

(ii) they are formed at random positions, and

(iii) they are extremely unstable and immediately start to grow.

Therefore the nuclei cannot be observed until they have been developed through growth.

Crystals grow by the continued addition of one layer of molecular units on another. The units arrive at the crystal surface by diffusion, sometimes aided by convection, and are fitted to the crystal lattice. The addition of new layers to the crystal may follow at least four different patterns :

A. Growth on a perfect crystal face:

(i) Mononuclear layer fomation (Fig 6a): A.E.Nielsen(1964)(32) has described mononuclear layer formation. On a perfect crystal face very small surface embryos are unstable and dissolve, but larger surface nuclei grow. At low degrees of supersaturation this results in a very slow surface nucleation followed by a growth, which is relatively slow, but fast enough to spread the layer all over the face before the next surface nucleus is formed.

(ii) Polynuclear layer formation (Fig 6b): W.K. Burton et al (1949)(33), O.M. Todes (1949)(34) and A.E. Nielsen (1964)(32) have shown that nucleation rates increase more rapidly with concentration than growth rates. At higher concentration this will result in several nuclei being present at a time on the crystal faces. Each layer originates in more than one surface nucleus, but the layers in the final crystal are just as perfect as in the case of mononuclear layer formation.

Figure 6

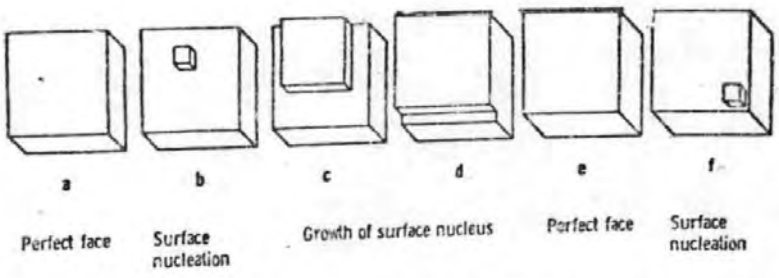


(a) 1. Series of 'snapshots' of mononuclear growth. The time interval between two surface nucleations is longer than the time it takes a new layer to spread all over the face.

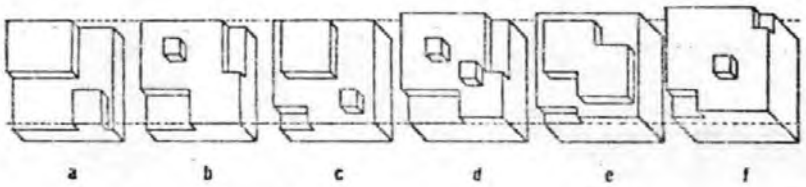


(b) Polynuclear growth. New surface nuclei are formed before the previous ones have spread. The surface is always covered with nuclei.

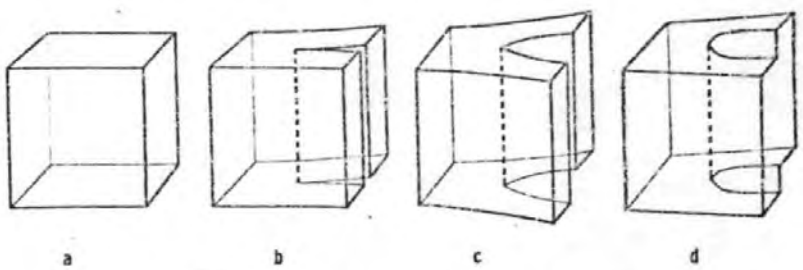


(c) Drawings illustrating the deformation of the crystal in the vicinity of a screw dislocation.

B. Growth on an imperfect crystal face

(i) Spiral step (screw dislocation) growth (Fig 6c):

Most macroscopic crystals have many lattice defects called dislocations. One type is the screw dislocation. This can be visualized as a perfect crystal cut half way through, distorted and put together again, with an imperfection only visible on two opposite faces, but not on the face from where the cut was made. When a crystal has a screw dislocation, it can grow without surface nucleation, since the step on the face where a screw dislocation ends will not disappear. According to F.C. Frank (1949)(35) and W.R. Burton et al (1951)(36) the crystal grows and acts therefore as a permanent catalyst for growth, efficient even at very small supersaturation.

(ii) Rough Surface Growth:

In precipitations from solutions of very soluble substances the interfacial tension may become so small that it does not stretch the interface into a plane. Instead the interface becomes molecularly rough. This is found in metallic systems.

Suspension Stability

Particles in a suspension act on one another by electrostatic and dispersion forces. If all the particles have appreciable electrical charges of the same sign, they will collide rarely and when colliding, they will probably part again. J.Th.G.Overbeek (1952)(37), B.Tezak et al (1954,1968)(38), J.Kratohvil et al (1960)(39) showed that if the charges are small the particles collide more readily and stick together because of the short-range dispersion forces. Substances which neutralize the charges on the particles, such as indifferent ions, may induce coagulation.

Other substances which charge the ions electrically, such as specifically adsorbed ions or ions with a high charge, stabilize the suspension and thereby prevent coagulation, and may even peptize a coagulated material.

Ageing:

The decrease of the interfacial area of a precipitate is called ageing. This process takes place through

(a) Recrystallization of the primary particles, transforming, e.g. needles, thin plates or dendrites, into a more compact shape by surface wandering of adsorbed molecular units, or by transport through the mother liquid.

(b) Transformation of a crystal from a metastable modification into a stable modification by dissolution and reprecipitation.

(c) Aggregation of primary particles followed by sintering (inter-growth) and

(d) Ostwald ripening, i.e. growth of the larger particles at the expense of the smaller ones.

Ostwald Ripening

Small particles have a higher Gibbs free energy per molecular unit than larger particles have, because of the larger interface per molecular unit. The solubility of a small particle is higher than the solubility of a large particle.

If a solution is in contact with three sizes of crystals, and in equilibrium with the middle size, the small particles will find the solution undersaturated and therefore dissolve, whereas the large particles find it supersaturated—and grow. It follows that a solution cannot be in equilibrium with a precipitate consisting of crystals of two or more sizes (O.M.Todes (1946)(40);

I.M. Lifshitz et al (1961)(41); E. Klein et al (1963)(42) and M. Kahlweit (1963)(43).

If a solution is left with a polydisperse precipitate, the concentration will sooner or later reach a value between the solubilities of the largest particles and of the smallest particles, and remain in this interval while the small particles dissolve and the larger ones grow, until eventually only one large crystal remains. During the ageing the concentration is close to the equilibrium concentration of a particle with the radius equal to the arithmetic mean value of the radii of all the particles.

1.6.2 Precipitation of Zinc sulphide

Levi and Fontana (1928)(44) reported that the particle size was essentially the same, Ca.20Å (0.002 μm) for zinc sulphide precipitated by hydrogen sulphide from normal zinc sulphate solutions alone or with additions of ammonium hydroxide, sodium hydroxide and acetic acid. They suggested that the dissimilar analytical behaviour of the precipitates was caused by differences of agglomeration rather than particle size. However, Allen and Crenshaw (1912)(4) described newly-precipitated zinc sulphide as spherical particles 0.2 - 0.5 μm in diameter.

Ortman and Piwonka (1960, 1961)(45,46), Lendvay et al (1965)(47) obtained samples with particle sizes of up to 50 μm and 100 - 200 μm by slowly precipitating zinc sulphide with hydrogen sulphide from acid solutions of a soluble zinc salt. Brown (1968)(48) showed that the pH of the surrounding solution had a marked effect on the particle size. Precipitation in strongly acidic solution resulted in the formation of aggregates of the order 1 - 5 μm which were irregular globular masses.

Production of finely-divided zinc sulphide with hydrogen sulphide from more dilute acidic zinc salt solution (0.1. - 0.2 M - $ZnSO_4$ or $ZnCl_2$) has been described recently by Shishlyanmkov (1970)(49). Some of the products had sp. surface of over 100 $m^2g^{-1}$, corresponding to average crystallite sizes below 0.0147 $\mu$m).

## 1.7 The spontaneous oxidation of more reactive zinc sulphide ores

### 1.7.1 INTRODUCTION

The chemical changes occurring in Bafq and other Zinc-lead concentrates susceptible to spontaneous atmospheric oxidation have been examined by M.Hill *et al* (1970)(2). "Bafq concentrates"is Zinc-lead concentrate of composition Zn = 44% W/W; Pb = 7% W/W; Fe = 8% W/W; the phases present in the concentrate, as determined by X-ray diffraction, are $\beta$-Zinc sulphide, lead sulphide (Galena), iron pyrites and lead sulphate. After oxidation at 70°C for 300 h, this material contained $\beta$-sulphide, lead sulphate, zinc sulphate ($ZnSO_4.7H_2O$) and iron pyrites.

The initial reactions of Bafq concentrate are, therefore, the oxidation of sphalerite and Galena to their respective sulphates :

$$ZnS + 2O_2 \rightarrow ZnSO_4 \quad \ldots\ldots\ldots\ldots \text{(i)}$$

$$PbS + 2O_2 \rightarrow PbSO_4 \quad \ldots\ldots\ldots\ldots \text{(ii)}$$

or, in the presence of moisture :

$$ZnS + 2O_2 + 7H_2O \longrightarrow ZnSO_4.7H_2O \quad \ldots\ldots\ldots \text{(iii)}$$

A sample of concentrate that had caught fire contained zinc ferrite ($ZnO.Fe_2O_3$), lead sulphate and Zinc sulphate. Oxides can be produced by the following reaction :

$$2ZnSO_4 \longrightarrow 2ZnO + 2SO_2 + O_2 \quad \ldots\ldots\ldots\ldots \text{(iv)}$$

or by direct reaction :

$$2ZnS + 3O_2 \longrightarrow 2ZnO + 2SO_2 \ldots\ldots\ldots\ldots \text{(v)}$$

In a stockpile of concentrates the heat evolved from the low temperature ($<100^{o}C$) exotherm reactions of types (i), (ii) and (iii) is sufficient to raise the temperature of the stockpile such that reactions of the type (iv) and (v) can occur. The enthalpies and free energies are listed in Table 3.

1.7.2 Kinetic studies of sulphation

(i) Effect of moisture and temperature on reaction rate

Maximum reaction rate was achieved with 3% W/W moisture. Increasing the moisture content (>3% W/W) appeared to decrease slightly the reaction rate. The 6% W/W $H_2O$ sample at $70^{o}C$ became flooded (13.1% $H_2O$) and this effectively killed the reaction. Dry concentrate did not undergo a sulphation reaction to any significant extent during the time of test. It is possible that the moisture removes the reaction products (e.g. sulphates) from the surface of the concentrate particles and hence provides a fresh surface for further attack by oxygen, thereby increasing the reaction rate. The reaction rate is increased two-fold for a $20^{o}C$ rise in temperature.

(ii) Effect of inhibitors on reaction rate

Most of the additives decreased the rate of reaction (except ammonium pentaborate, which has no effect) but did not stop the reaction. Addition of 0.05% phenol results in a three-fold reduction rate.

(iii) Reaction rates of various concentrates

The order of reactivity of various concentrates is as follows :

Bafq > Type A > Type B > Type C > Type D

TABLE 3

THERMODYNAMIC VALUES

| Compound | $\Delta Hf^{o}$ K.cal/mole | $\Delta Ff^{o}$ K.cal/mole | $S^{o}$ | $Cp^{o}$ |
|---|---|---|---|---|
| ZnS(sphalerite) | -48.5 | -47.4 | 13.8 | 10.8 |
| $ZnSO_4$ | -233.88 | -208.31 | 29.8 | 28 |
| $ZnSO_4.7H_2O$ | -735.1 | -611.9 | 92.4 | 93.7 |
| PbS(Galena) | -22.15 | -22.15 | 21.8 | 11.83 |
| $PbSO_4$ | -219.5 | -193.89 | 35.2 | 24.9 |
| $FeS_2$ (pyrite) | -42.52 | -39.84 | 12.7 | 14.8 |
| $FeS_2$(markasite) | -36.88 | - | - | - |
| $FeSO_4$ | -220.5 | -195.5 | - | - |
| $FeSO_4.7H_2O$ | -718.7 | | | |
| FeS α | -22.72 | -23.32 | 16.1 | 13.1 |
| β | -21.35 | -23.32 | - | - |
| CuS | -11.6 | -11.7 | 15.9 | 11.43 |
| $CuSO_4$ | -184.0 | -158.2 | 27.1 | 24.1 |
| $CuSO_4.5H_2O$ | -544.45 | -449.3 | 73.0 | 67.2 |
| $O_2$ | 0.00 | 0.00 | 49.003 | 7.017 |
| $H_2O$ liquid | -68.3171 | -56.6902 | 16.716 | 17.97 |
| $H_2O$ gas | -57.7976 | -54.6352 | 45.105 | 8.025 |

Typical assays of these compounds are given in Table 4.

According to M. Hill et al (1970)(2) the reasons for the greater reactivity of Bafq and Type A concentrates is not known. However, they have suggested the following :

(a) Pyrite content

The involvement of pyrite is questioned, but the above order of reactivity can be correlated roughly with decreasing pyrite content. Bafq and Type A concentrations also show variations in the pyrite content. The pyrite content in the Bafq concentrate is believed to be of the mackinawite ($FeS_{1-x}$), early stage in its oxidation.

When 10% W/W pyrite was added to Bafq concentrate the reaction rate did not increase. It is concluded that it is probably not the amount of pyrite, but possibly its degree of alteration that is important.

(b) Particle size

The fineness of Bafq concentrate contributes to its reactivity, because the finer the particle size, the greater is the surface area available for oxidation and the greater the reactivity.

(c) Flotation additives

It is considered that the addition of copper sulphate, potassium amyl xanthate and sodium cyanide to the concentrate have no significant effect on the rate of oxidation.

(iv) Reaction rates of synthetic mixtures

Very little oxidation occurs in synthetic mixtures of Zinc sulphide (50:50 mixture of $\alpha$ and $\beta$ forms), pyrite and Galena.

TABLE 4

TYPICAL ASSAYS OF CONCENTRATES

| % W/W | Bafq | Type A Tynagh | Type B New Brunswick | Type C Timmins | Type D Broken Hill |
|---|---|---|---|---|---|
| Zn | 44.2 | 23.05 | 47.7 | 51.2 | 52.6 |
| S | 31.6 | 22.4 | 32.7 | 31.9 | 31.8 |
| Pb | 7.2 | 32.55 | 3.1 | 0.41 | 1.11 |
| Ag (oz.troy/ longton) | 0.16 | 10.05 | 3.35 | 6.95 | 0.65 |
| Cl | 0.027 | 0.002 | 0.001 | 0.003 | 0.05 |
| As | 0.04 | 0.165 | 0.12 | 0.03 | 0.06 |
| Fe | 7.8 | 4.45 | 10.9 | 9.6 | 9.85 |
| $Al_2O_3$ | 0.60 | 1.64 | 0.55 | 0.67 | 0.26 |
| Mn | 0.14 | 0.07 | 0.06 | <0.01 | 0.74 |
| CaO | 0.66 | 0.18 | 0.45 | 0.13 | 0.27 |
| MgO | 0.17 | 0.02 | 0.17 | 0.12 | 0.03 |
| Insoluble | 1.28 | - | 0.52 | 2.38 | 1.63 |
| Cd | 0.15 | 0.23 | 0.08 | 0.28 | 0.17 |
| Cu | 0.12 | 0.40 | 0.20 | 0.52 | 0.12 |
| Sb | 0.008 | 0.10 | 0.03 | <0.01 | 0.025 |
| Sn | <0.002 | 0.001 | 0.05 | 0.17 | 0.001 |
| F | 0.05 | 0.04 | 0.02 | <0.01 | 0.05 |
| S as $SO_4$ | 1.32 | 0.30 | 0.83 | 0.77 | 0.17 |
| $SiO_2$ | 1.06 | 2.93 | 0.93 | 2.00 | 1.29 |
| $BaSO_4$ | <0.1 | 5.96(Bao) | ND | 0.14 | ND |
| Bi | 0.01 | 0.004 | 0.005 | 0.003 | 0.005 |
| $CO_2$ | 0.31 | - | - | <0.1 | - |
| C | Ca 1 | 4.0 | 0.3 | 0.3 | - |

Therefore, the pure minerals undergo oxidation only very slowly, compared with Bafq concentrates.

(v) Effect of Acids and Bases

The reaction rate in the presence of 0.1% W/W sulphuric acid and 0.2% W/W sodium hydroxide are analogous to and not significantly different from, that of Bafq concentrate alone.

Cause of self-heating of Bafq concentrates

From the above observations, M. Hill et al (1970)(2) came to the conclusion that the probable cause of self-heating of Bafq concentrates are as follows :

(i) The presence of highly reactive material in the ore itself.

(ii) Chemical additives and physical changes to which the ore is subjected during the flotation and subsequently handling procedures.

(i) Bafq concentrate contains a type of pyrite (mackinawite) which could possibly be a 'reactive species'.

(ii) Increasing the particle size and the presence of water in the concentrate accelerate the oxidation process.

Increasing the accessibility of oxygen to the stock-piling procedure could be a means of increasing the rate of reaction.

It was thought that bacteria may be initiating the oxidation process. An investigation by the Warren Spring Laboratories confirmed the presence of thiobacillus-ferro-oxidans in Bafq concentrates. These bacteria cannot be involved in the oxidation process because they are inactive above 50°C, and at pH 5.0, they are alive but inactive.

However, bacteriological initiation cannot be ruled out since the presence of thermophilic bacteria (capable of oxidising sulphide minerals under extremes of temperature) has not been negated.

Thus, in the spontaneous ignition of zinc ore concentrates it is probable that there are primarily low-temperature and subsequently high-temperature oxidation mechanisms operative. The latter mechanisms will be similar to those encountered in the commercial roasting of zinc concentrates, of which available thermodynamic information is now summarised.

1.8 The thermodynamic properties of the Zn-Fe-S-O system at elevated temperatures as related to Zinc Concentrate Roasting :

A compound stability diagram was constructed by R.L.Benner and H. Kenworthy (50) for the Zn-Fe-S-O system to show the phases that should be thermodynamically stable at various temperatures, oxygen pressure, and $SO_2$ pressures. Because of the complexity of the problem, the thermodynamic properties of the ternary system of Zn-S-O and of Fe-S-O were calculated first; then the thermodynamic properties of the two ternary systems were combined to give the Zn-Fe-S-O systems. The calculations were simplified by assuming the following conditions :

1. The free energy of reaction equations are linear functions of temperature.
2. Reactions regarding basic sulphates were not considered.
3. All solid phases have an activity of unity and they are completely immiscible in one another, with the exception of ZnO, $Fe_2O_3$ and $Fe_3O_4$.
4. Only two types of reactions were considered: those involving oxygen or oxygen plus $SO_2$, and those involving solid—solid ion exchanges.

1.8.1 Development of Zn-Fe-S-O compound stability diagrams

In order to show the effects of temperature and oxygen pressure on compound stability during roasting, the co-ordinates of the stability diagrams were plotted as the logarithm of oxygen pressure versus the reciprocal of absolute temperature, at a constant $SO_2$ pressure. The effect of $SO_2$ pressure was shown by constructing the diagrams at two different $SO_2$ pressures. In constructing the diagrams of the Zn-Fe-S-O systems, $SO_2$ pressures of $1 \times 10^{-1}$ and $1 \times 10^{-5}$ atmospheres were selected: the first of these was selected because roasters frequently operate in this range; the second was selected to illustrate the effect that very low $SO_2$ pressures have on the system.

1.8.2 Zn-S-O system:

Because of the interest in roasting ZnS, considerable data have been tabulated on the thermodynamic properties of the Zn-S-O system (51). Within the system, the following compounds are known to exist: ZnS, ZnO, $\alpha ZnSO_4$, $\beta ZnSO_4$, $ZnO.2ZnSO_4$, $SO_2$ and $SO_3$. However, because of the conditions found in a roaster and because of the simplifying assumptions noted previously, only the compounds of ZnS, ZnO, $\beta ZnSO_4$ and $SO_2$ were considered in this study. Table 5 gives equations for the free energy of formation of these compounds as presented in the literature. These equations were used to calculate the free energy of reaction equations 1,2,3 and 4 which are also shown in Table 5. The reaction equations were then used to establish the boundary lines between regions of stability. An example of this procedure follows :

When reaction No.1 is considered, the low temperature free energy equation is given as

$$\Delta F = -156,800 + 125.28T \ldots\ldots\ldots (i)$$

Table 5 - Free energy data for the Zn-S-O system

| Reaction | Temperature range, ° K | Cal/mole, $\Delta F°$ |
|---|---|---|
| Zn:[1] | | |
| Solid + $\frac{1}{2}$ $S_{2\,(gas)}$ + $2O_{2\,(gas)}$ ⟶ $ZnSO_4$ (sol). | 298-1,180 | -249,500 + 105.5T |
| Liquid | 1,180- | -277,000 + 128.8T |
| Gas | - | - |
| Zn:[2] | | |
| Solid + $\frac{1}{2}$ $S_{2\,(gas)}$ ⟶ $ZnS_{(solid)}$ | 298-693 | -60,565 + 22.70T |
| Liquid | 693-1,180 | -61,740 + 24.27T |
| Gas | 1,180-1,500 | -89,165 + 47.50T |
| Zn:[3] | | |
| Solid + $\frac{1}{2}$ $O_{2\,(gas)}$ ⟶ $ZnO_{(solid)}$ | 298-693 | -83,100 + 23.57T |
| Liquid | 693-1,180 | -84,480 + 25.55T |
| Gas | 1,180-1,500 | -110,140 + 47.35T |
| $\frac{1}{2}$ $S_{2\,(gas)}$ + $O_{2\,(gas)}$ ⟶ $SO_{2\,(gas)}$ (Coughlin[3]) | 298- | -86,620 + 17.31T |
| Derived reactions:[4] | | |
| $SO_2$ + $\frac{1}{2}$ $O_2$ ⟶ $SO_3$ | 298- | -22,600 + 21.36T |
| (1) $2ZnO + 2SO_2 + O_2$ ⟶ $2ZnSO_4$ | 693-1,180 | -156,800 + 125.28T |
| | 1,180-1,500 | -160,400 + 128.28T |
| (2) $ZnS + \frac{3}{2}$ $O_2$ ⟶ $ZnO + SO_2$ | 693-1,180 | -109,360 + 18.59T |
| | 1180-1500 | -107,595 + 17.16T |
| (3) $ZnS + 2O_2$ ⟶ $ZnSO_4$ | 298-693 | -188,935 + 82.2T |
| | 693-1,180 | -187,760 + 81.2T |
| (4) $3ZnSO_4 + ZnS$ ⟶ $4ZnO + 4SO_2$ | 693-1,180 | +125,700 - 169.4T |

[1] Mathewson, C. H. Zinc, The Science and Technology of the Metal, Its Alloys and Compounds. Am. Chem. Soc. Monograph Series No. 142, Reinhold Pub. Corp., New York, N.Y., 1959.

[2] Richardson, F. D., and J. H. E. Jeffes. The Thermodynamics of Substances of Interest in Iron and Steelmaking. III. Sulfides. J. Iron and Steel Institute, v. 170, 1952, pp. 165-175.

[3] Coughlin, J. P. Contributions to the Data on Theoretical Metallurgy. XII. Heats and Free Energies of Formation of Inorganic Oxides. BuMines Bull. 542, 1954, 80 pp.

[4] Derived by addition or subtraction of the proper free energy of formation equations given above.

However, the free energy equation can also be written as

$$\Delta F = -2.303RT \log_{10} Keq \ldots\ldots\ldots\ldots (ii)$$

Where Keq = equilibrium constant

Since the condensed phases are considered pure and immiscible, according to condition 3, the equilibrium constant can be expressed as :

$$Keq = (Po_2)^{-1}(Pso_2)^{-2} \ldots\ldots\ldots\ldots (iii)$$

Where $Po_2$ and $Pso_2$ are the pressure of oxygen and the pressure of $SO_2$, respectively. By substituting this expression into equations, setting the equation equal to the tabulated free energy equation, and simplifying, an expression of $\log_{10} Po_2$ can be obtained in terms of temperature and $\log_{10} Pso_2$,

$$\log_{10} Po_2 = (-34,280/T) + 27.38 - 2\log_{10} PSO_2 \ldots\ldots (iv)$$

This equation is then used to establish the boundary line between ZnO and $ZnSO_4$ at a constant $SO_2$ pressure, as shown in Fig 7. From equation 1 of Table 5 and the application of LeChatelier's principle, it can be seen that sustained oxygen pressure, greater than the equilibrium values, would force the system completely to the $ZnSO_4$ side of the reaction. Applications of similar procedures to equations 2 and 3 of Table 1 result in a complete diagram (Fig 7) with three regions of stability. The solutions of equations 1,2, 3 and 4 of Table 5, together with the material needed to construct Fig 7, are shown in Table 6. Equation 4 of Table 5 represents the point of intersection of all three boundaries, and because the $SO_2$ pressure is held constant, it gives the invariant point in Fig 7.

1.8.3 Fe-S-O system

Although the compounds of $FeS_2$, FeS, FeO, $Fe_3O_4$, $Fe_2O_3$, $FeSO_4$, $Fe_2(SO_4)_3$, $SO_2$ and $SO_3$ were known to exist, there were

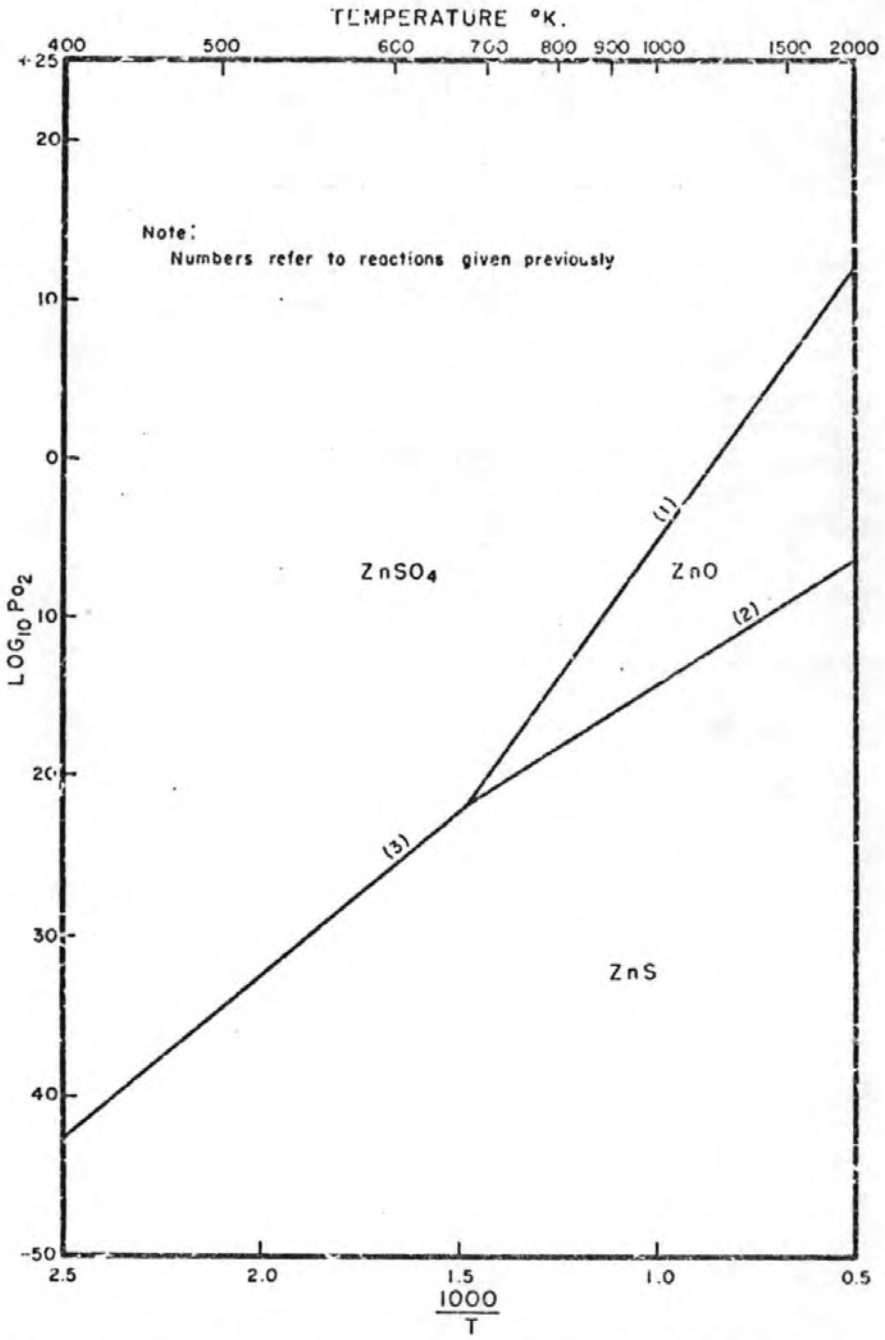


Figure 7 - Zn-S-O Compound Stability Diagram at a Constant $SO_2$ Pressure of 0.1 Atmosphere.

Table 6 Temperature and oxygen pressure data for the Zn-S-O compound stability diagram

| Reaction | Temperature, ° K | $\Delta F°$ | $P_{SO_2}$, atmospheres | $\log_{10} P_{O_2}$ |
|---|---|---|---|---|
| (1) $ZnO + SO_2 + \frac{1}{2} O_2 \rightleftharpoons ZnSO_4$ .... | 1,200 | -3,100 | 0.1 | +0.9 |
| | | | $1x10^{-5}$ | +7.5 |
| | 700 | -34,600 | 0.1 | -19.6 |
| | | | $1x10^{-5}$ | -11.5 |
| (2) $ZnS + \frac{3}{2} O_2 \rightleftharpoons ZnO + SO_2$ ..... | 1,200 | -87,100 | 0.1 | -11.2 |
| | | | $1x10^{-5}$ | -14.1 |
| | 700 | -96,300 | 0.1 | -20.7 |
| | | | $1x10^{-5}$ | -23.3 |
| (3) $ZnS + 2 O_2 \rightleftharpoons ZnSO_4$ ..... | 600 | -139,635 | 0.1 | -25.0 |
| | | | $1x10^{-5}$ | -25.0 |
| | 400 | -156,085 | 0.1 | -42.8 |
| | | | $1x10^{-5}$ | -42.8 |
| (4) $3ZnSO_4 + ZnS \rightleftharpoons 4ZnO + 4SO_2$ .. | 670 | 12,200 | 0.1 | -21.8 |
| | 482 | 12,200 | $1x10^{-6}$ | -34.2 |

probably a number of basic sulphates and other complex compounds that also exist within the system. Of the known compounds, experimentally determined free energy data exist for $FeS_2$, FeS, FeO, $Fe_3O_4$, and $Fe_2O_3$. In addition, Moore and Kelly (52) have published $\Delta H^\circ_{298}$ and $\Delta S^\circ_{298}$ values for $FeSO_4$, these values permit the estimation of the free energy of formation of $FeSO_4$ at any temperature. This estimate employs the assumption that the change in heat capacity ($\Delta Cp$) for the reaction equals zero at all temperatures and that

$$\Delta F_T = \Delta H^\circ_{298} - T\Delta S^\circ_{298} \quad \ldots\ldots\ldots\ldots \text{(v)}$$

Although this assumption is not necessarily true, the equation does give a good first approximation for the free energy of reaction at any temperature.

A free energy of formation equation for $Fe_2(SO_4)_3$ was developed from published decomposition pressures of the sulphate(53). In general the decomposition pressure measured in the sum of the partial pressures of $SO_3$, $SO_2$ and $O_2$, because the decomposition occurs in two steps. The first of these is the decomposition of the sulphate :

$$Fe_2(SO_4)_3 \rightarrow Fe_2O_3 + 3SO_3 \ldots\ldots\ldots\ldots\text{(vi)}$$

The second is the decomposition of the sulphur trioxide:

$$2SO_3 \rightleftharpoons 2SO_2 + O_2 \quad \ldots\ldots\ldots\ldots\ldots\text{(vii)}$$

By considering the thermodynamic properties and stoichiometry of the second reaction, the partial pressures of $SO_3$, $SO_2$ and $O_2$ can be calculated. By employing this procedure, Warner and Fagraham (53) derived the equation :

$$\log_{10} (P_{SO_3})^3 = 28.34 - \frac{(29,600)}{T} \quad \ldots\ldots\text{(viii)}$$

where $P_{SO_3}$ is expressed in atmospheres, and the temperature (T) is between 630° and 724°C.

Applying the relationship :

$$\Delta F = 2.303RT \log_{10}(P_{SO_3})^3 \quad \ldots\ldots\ldots\ldots (ix)$$

to equation viii, a linear free energy equation :

$$\Delta F = 135{,}400 - 129.7T \quad \ldots\ldots\ldots\ldots (x)$$

was derived for the reaction given in equation vi.

By combining this equation with the free energy of formation equations of $SO_3$ and $Fe_2O_3$(55), it was possible to calculate the free energy equation of $Fe_2(SO_4)_3$ from its elements according to the reaction

$$2Fe(\alpha) + {}^3/2\ S_2(gas) + 6O_2 = Fe_2(SO_4)_3\ (solid) \ldots\ldots (xi)$$

the value of this free energy equation is

$$\Delta F = -656{,}620 + 305.1T \quad \ldots\ldots\ldots (xii)$$

In order to determine if equation xii was a fair estimate of the free energy and to determine if it was valid over a wide range of temperature, an alternate method was used to calculate a free energy of formation equation. This method employs the approximation mentioned earlier, of

$$\Delta F_T = \Delta H^\circ_{298} - T\Delta S^\circ_{298} \quad \ldots\ldots\ldots (xiii)$$

Where $H^\circ_{298}$ and $S^\circ_{298}$ now represent the standard heat of formation and entropy change, respectively, of $Fe_2(SO_4)_3$, according to the reaction given in equation xi. Utilizing the heats of the reactions

$$2Fe(\alpha) + 3S(rh) + 6\ O_2(gas) = Fe_2(SO_4)_3(solid) \ldots\ldots (xiv)$$

$$\Delta H^\circ_{298} = -640{,}000 \text{ cal}$$

and $${}^3/2\ S_2(gas) = 3S(rh)$$

$$\Delta H^\circ_{298} = -46{,}500 \quad \ldots\ldots\ldots\ldots (xv)$$

it was possible to calculate the heat of formation for $Fe_2(SO_4)_3$

$$\Delta H^\circ_{298} = -686{,}500 \text{ cal} \quad \ldots\ldots\ldots \text{(xvi)}$$

as the reaction is shown in equation xi. It was necessary to estimate the entropy value of $Fe_2(SO_4)_3$ with a method devised by Latimer.

In this method the compound is considered to be the sum of an equivalent number of cations and anions :

$$Fe_2(SO_4)_3 = 2Fe^{3+} + 3(SO_4)^{2-} \quad \ldots\ldots\ldots \text{(xvii)}$$

The standard entropy of this compound is likewise the sum of an equivalent number of cationic and anionic entropies that have been empirically determined from the size, the charge, and the mass of the ions.

Employing the ionic entropies given in Table 7, the standard entropy of $Fe_2(SO_4)_3$ was estimated as :

$$S^\circ_{298} = 2(10.4) + 3(13.7) = 61.9 \text{ cal/degree} \quad \ldots\ldots \text{(xviii)}$$

This value was combined with the standard entropies of the elements given in Table 8 to calculate the entropy change of the reaction given in equation xi.

$$\Delta S^\circ_{298} = -326{,}9 \text{ cal/degree} \quad \ldots\ldots\ldots \text{(xix)}$$

Substituting equations xv and xix into xiii gives the estimated free energy equation

$$\Delta FT = -686{,}500 + 326.9T \quad \ldots\ldots\ldots \text{(xx)}$$

Equation xii and the free energy of formation equations for FeS, FeO, $Fe_3O_4$, $Fe_2O_3$, $FeSO_4$, $SO_2$ and $SO_3$ are listed in Table 8. The values of $FeS_2$ are not shown because it decomposes quite readily at low temperature into FeS and S. Also given in the table are the free energy of reaction equations needed to calculate the boundary lines in Fig 8.

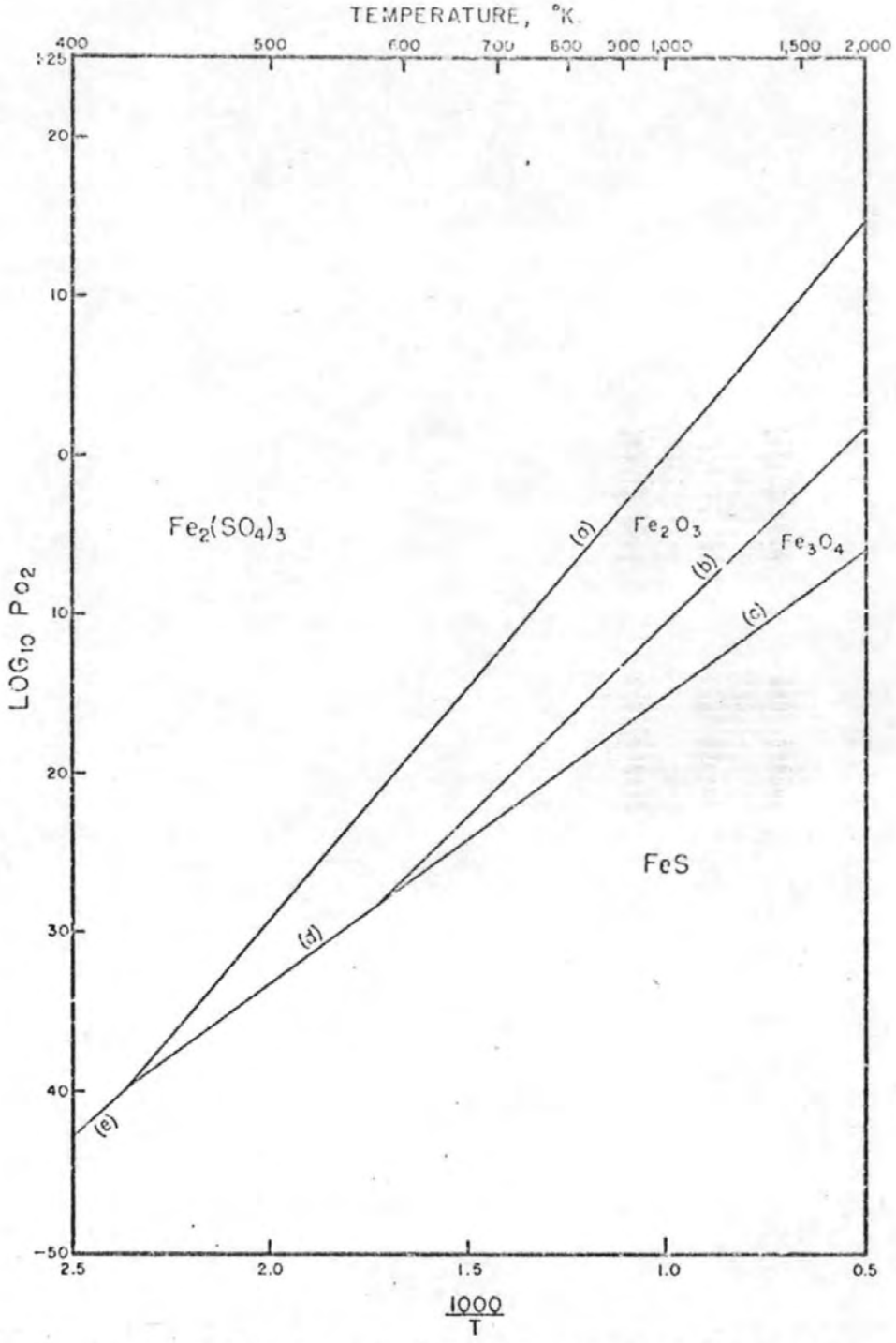


Figure 8 · Fe-S-O Compound Stability Diagram at a Constant $SO_2$ Pressure of 0.1 Atmosphere.

Table 7 - Free energy data for the Fe-S-O system

| Reaction | Temperature range, ° K | ΔF° cal/mole |
|---|---|---|
| $Fe_{(\alpha,\gamma)} + \frac{1}{2} S_{2(gas)} \rightarrow FeS_{(solid)}$[1] | 412-1,300 | -36,020 + 12.65T |
| $0.947Fe_{(\alpha,\gamma)} + \frac{1}{2} O_{2(gas)} \rightarrow Fe_{0.947}O_{(solid)}$ | 298-1,650 | -63,200 + 15.47T |
| $3Fe^{\alpha}_{\gamma} + 2O_{2(gas)} \rightarrow Fe_3O_4$ (magnetite)[2] | 298-900 | -265,660 + 76.81T |
| | 900-1,803 | -261,200 + 71.36T |
| $2Fe^{\alpha}_{\gamma} + \frac{3}{2} O_{2(gas)} \rightarrow Fe_2O_3$ (hematite)[3] | 298-950 | -195,450 + 61.38T |
| | 950-1,800 | -192,680 + 58.21T |
| $Fe_{(solid)} + \frac{1}{2} S_{2(gas)} + 2O_{2(gas)} \rightarrow FeSO_{4(solid)}$[4] | 298- | -221,300 + 106.22T |
| $2Fe_{(solid)} + \frac{3}{2} S_{2(gas)} + 6O_{2(gas)} \rightarrow Fe_2(SO_4)_{3(solid)}$[5] | 298-1,500 | -656,620 + 305.1T |
| $\frac{1}{2} S_{2(gas)} + O_{2(gas)} \rightarrow SO_{2(gas)}$[3] | 298-2,000 | -86,520 + 17.48T |
| $\frac{1}{2} S_{2(gas)} + \frac{3}{2} O_{2(gas)} \rightarrow SO_{2(gas)}$[3] | 298-1,500 | -109,550 + 39.09T |
| (a) $Fe_2O_3 + \frac{3}{2} O_2 + 3SO_2 \rightleftharpoons Fe_2(SO_4)_3$ | 298-950 | -201,610 + 188.3T |
| | 950-1,500 | -204,380 + 194.4T |
| (b) $4Fe_3O_4 + O_2 \rightleftharpoons 6Fe_2O_3$ | 298-900 | -110,060 + 61.04T |
| | 900-1,803 | -111,280 + 63.82T |
| (c) $3FeS + 5O_2 \rightleftharpoons Fe_3O_4 + 3SO_2$ | 412-900 | -417,160 + 91.30T |
| | 900-1,300 | -412,700 + 85.85T |
| (d) $2FeS + \frac{7}{2} O_2 \rightleftharpoons Fe_2O_3 + 2SO_2$ | 412-950 | -397,730 + 80.60T |
| | 950-1,300 | -394,880 + 77.40T |
| (e) $2FeS + 5O_2 + SO_2 \rightleftharpoons Fe_2(SO_4)_3$ | 412-300 | -498,060 + 262.3T |
| (f) $2FeSO_4 + SO_2 + O_2 \rightleftharpoons Fe_2(SO_4)_3$ | 298- | -137,500 + 75.2T |
| (g) $Fe_2O_3 + \frac{1}{2} O_2 + 2SO_2 \rightleftharpoons 2FeSO_4$ | 298-950 | -74,110 + 116.1T |
| | 950-1,800 | -76,960 + 119.3T |
| (h) $Fe_3O_4 + 3SO_2 + O_2 \rightleftharpoons 3FeSO_4$ | 298-900 | -138,680 + 189.41T |
| | 900-1,803 | -143,140 + 194.86T |
| (i) $FeS + 2O_2 \rightleftharpoons FeSO_4$ | 412-1,300 | -185,420 + 93.52T |
| (j) $FeS + \frac{3}{2} O_2 \rightleftharpoons FeO + SO_2$[6] | 298-1,300 | -113,700 + 20.3T |
| (k) $3FeO + \frac{1}{2} O_2 \rightleftharpoons Fe_3O_4$[6] | 298-900 | -76,060 + 30.4T |
| | 900-1,650 | -71,600 + 24.9T |
| (m) $10Fe_2O_3 + 27SO_2 \rightleftharpoons 7Fe_2(SO_4)_3 + 6FeS$ | 412-950 | -521,920 + 1,125.8T |
| (n) $7Fe_3O_4 + SO_2 \rightleftharpoons 10Fe_2O_3 + FeS$ | 412-900 | -44,380 + 71.3T |

[1] Richardson, F. D., and J. H. E. Jeffes. The Thermodynamics of Substances of Interest in Iron and Steelmaking. III. Sulfides. J. Iron and Steel Inst., v. 170, 1952, pp. 165-175.

[2] Coughlin, J. P. Contributions to the Data on Theoretical Metallurgy. XII. Heats and Free Energies of Formation of Inorganic Oxides. Bulletin 542, 1954, 80 pp.

[3] Work cited in footnote 2. Average of two equations:

$2Fe_{(\alpha)} + \frac{3}{2} O_2 \rightarrow Fe_2O_3(\beta,\gamma)$ 950-1179 - 192,800 + 58.30T

$2Fe_{(\alpha)} + \frac{3}{2} O_2 \rightarrow Fe_2O_3(\gamma)$ 1179-1800 - 192,550 + 58.72T .

[4] Moore, G. E., and K. K. Kelley. The Specific Heats at Low Temperature of Anhydrous Sulfates of Iron, Magnesium, Manganese, Potassium. J. Am. Chem. Soc., v. 64, 1942, pp. 2949-2951.

[5] Derived from equation in the text and the above free energy equations.

[6] For simplicity, $Fe_{0.947}O$ was assumed to be stoichiometric FeO.

TABLE 8. - Temperature and oxygen pressure data for the Fe-S-O compound stability diagrams

| Reaction | Temperature, ° K, | ΔF° cal | $SO_2$ pressure; atmosphere | $\log_{10} P_{O_2}$ |
|---|---|---|---|---|
| (a) $Fe_2O_3 + \frac{3}{2} O_2 + 3SO_2 \rightleftharpoons Fe_2(SO_4)_3$ | 400 | -126,290 | 0.1 | -44.01 |
| | | | $1 \times 10^{-5}$ | -36.01 |
| | 750 | -60,385 | 0.1 | -9.73 |
| | | | $1 \times 10^{-5}$ | -1.73 |
| | 1,000 | -13,310 | 0.1 | +0.06 |
| | | | $1 \times 10^{-5}$ | +8.06 |
| | 1,500 | -80,840 | 0.1 | +9.85 |
| | | | $1 \times 10^{-5}$ | +17.85 |
| (b) $4Fe_3O_4 + O_2 \rightleftharpoons 6Fe_2O_3$ | 400 | -85,640 | - | -46.8 |
| | 750 | -64,280 | - | -18.7 |
| | 1,000 | -47,460 | - | -10.3 |
| | 1,500 | -15,550 | - | -2.2 |
| (c) $3FeS + 5O_2 \rightleftharpoons Fe_3O_4 + 3SO_2$ | 400 | -380,640 | 0.1 | -46.8 |
| | | | $1 \times 10^{-5}$ | -42.2 |
| | 750 | -348,685 | 0.1 | -18.7 |
| | | | $1 \times 10^{-5}$ | -20.9 |
| | 1,000 | -326,850 | 0.1 | -10.3 |
| | | | $1 \times 10^{-5}$ | -14.8 |
| | 1,500 | -283,925 | 0.1 | -2.2 |
| | | | $1 \times 10^{-5}$ | -8.8 |
| (d) $2FeS + \frac{7}{2} O_2 \rightleftharpoons Fe_2O_3 + 2SO_2$ | 400 | -286,034 | 0.1 | -42.4 |
| | | | $1 \times 10^{-5}$ | -44.7 |
| | 750 | -243,170 | 0.1 | -20.8 |
| | | | $1 \times 10^{-5}$ | -23.1 |
| | 1,000 | -225,810 | 0.1 | -14.6 |
| | | | $1 \times 10^{-5}$ | -16.9 |
| | 1,500 | -191,875 | 0.1 | -8.5 |
| | | | $1 \times 10^{-5}$ | -10.8 |
| (e) $2FeS + 5O_2 + SO_2 \rightleftharpoons Fe_2(SO_4)_3$ | 400 | -393,140 | 0.1 | -42.6 |
| | | | $1 \times 10^{-5}$ | -41.8 |
| | 1,500 | -104,710 | 0.1 | -2.8 |
| | | | $1 \times 10^{-5}$ | -2.5 |
| (f) $2FeSO_4 + SO_2 + O_2 \rightleftharpoons Fe_2(SO_4)_3$ | 400 | -97,418 | 0.1 | -52.2 |
| | | | $1 \times 10^{-5}$ | -48.2 |
| | 1,500 | -14,739 | 0.1 | -1.1 |
| | | | $1 \times 10^{-5}$ | +2.8 |

Table 8 Temperature and oxygen pressure data for the Fe-S-O compound stability diagrams--Continued

| Reaction | Temperature, ° K | $\Delta F^\circ$ cal | $SO_2$ pressure, atmosphere | $\log_{10} P_{O_2}$ |
|---|---|---|---|---|
| (g) $Fe_2O_3 + \frac{1}{2} O_2 + 2SO_2 \rightleftharpoons 2FeSO_4$ ..... | 400 | -27,670 | 0.1 | -26.2 |
| | | | $1 \times 10^{-5}$ | -10.2 |
| | 750 | +12,965 | 0.1 | +11.5 |
| | | | $1 \times 10^{-5}$ | +27.5 |
| (h) $Fe_3O_4 + 3SO_2 + O_2 \rightleftharpoons 3FeSO_4$ ..... | 400 | -62,916 | 0.1 | -31.3 |
| | | | $1 \times 10^{-5}$ | -19.3 |
| | 750 | +3,377 | 0.1 | +3.9 |
| | | | $1 \times 10^{-5}$ | +15.9 |
| (i) $FeS + 2O_2 \rightleftharpoons FeSO_4$ ..... | 400 | -147,872 | - | -40.4 |
| | 1,500 | -45,000 | - | -3.2 |
| (j) $FeS + \frac{3}{2} O_2 \rightleftharpoons FeO + SO_2$ ..... | 400 | -32,500 | 0.1 | -12.5 |
| | | | $1 \times 10^{-5}$ | -15.1 |
| | 1,000 | -83,250 | 0.1 | -8.7 |
| | | | $1 \times 10^{-5}$ | -11.4 |
| (k) $3FeO + \frac{1}{2} O_2 \rightleftharpoons Fe_3O_4$ ..... | 400 | -63,900 | - | -69.8 |
| | 750 | -53,260 | - | -31.0 |
| | 1,000 | -46,650 | - | -20.4 |
| | 1,500 | -34,175 | - | -9.9 |
| (m) $10Fe_2O_3 + 27SO_2 \rightleftharpoons 7Fe_2(SO_4)_3 + 6FeS$. | 420 | -49,170 | 0.1 | -39.8 |
| (n) $7Fe_3O_4 + SO_2 \rightleftharpoons 10Fe_2O_3 + FeS$ ..... | 584 | -2,640 | 0.1 | -27.7 |
| | 471 | -10,800 | $1 \times 10^{-5}$ | -37.4 |

The solution to the reaction equations, in terms of $\log_{10}Po_2$ and temperature, are given in Table 9 and are shown graphically in Fig 8. It can be seen from the figure that only reactions a,b,c,d and e are stable within the temperature and atmospheric conditions for this figure. The Fe-S-O system shows two invarient points, which are given by equations m and n in Table 8.

1.8.4 Zn-Fe-S-O system

The compound stability diagrams were constructed by superimposing the Zn-S-O system onto the Fe-S-O system. The Zn-Fe-S-O diagram (resulting from the two ternary systems) was divided into areas where a zinc compound was stable with an iron compound. Reactions between the compounds were considered and with the exception of ZnO plus $Fe_2O_3$ or $Fe_3O_4$ were found to be thermodynamically unstable. The reactions between ZnO and $Fe_2O_3$ or $Fe_3O_4$ were assumed to produce $ZnFe_2O_4$ and the free energy of this reaction was assumed to be small in comparison with the equilibrium reaction between ZnO and $ZnSO_4$ (reaction 1, Table 5 and Fig 7). Thus, when the ternary systems were superimposed, line 1 was not altered. Under actual conditions, however, line 1 is probably displaced slightly to the left of its position in Figures 9 and 10. If attention is now confined to the ordinary conditons of roasting ($\log_{10}Po_2$ between -1 and -2) Fig 9 shows three regions of stability:

$ZnSO_4$ plus $Fe_2(SO_4)_3$, $ZnSO_4$ plus $Fe_2O_3$ and $ZnFe_2O_4$

These three regions have been observed by Umethu and Suzuki (56) in their investigation of recovery of zinc from $ZnFe_2O_4$.

Figures 9 and 10 can now offer a simple explanation as to why zinc metallurgists have found $ZnFe_2O_4$ to be more prevalent at higher roasting temperatures. Apparently, the higher roasting

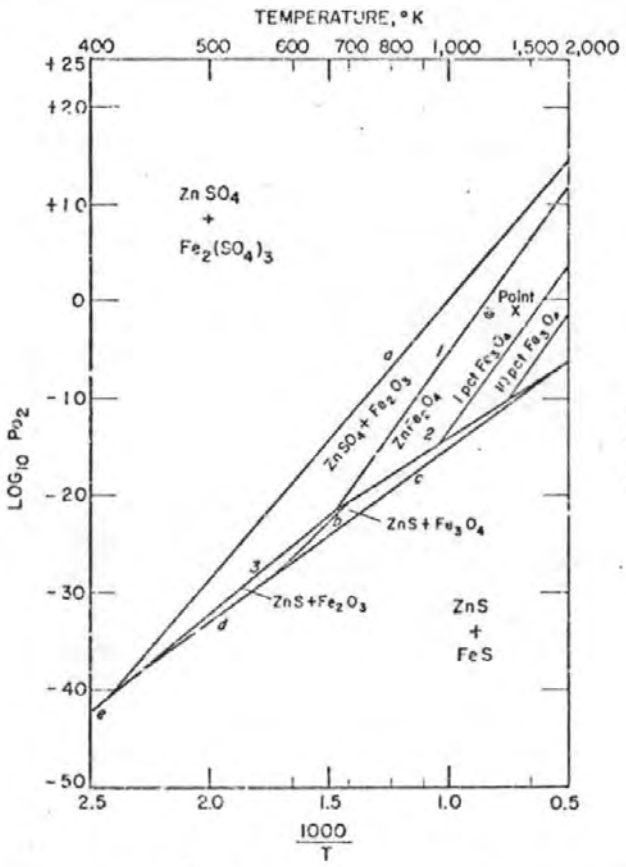


Figure 9 Zn-Fe-S-O Compound Stability Diagram at a Constant $SO_2$ Pressure of 0.1 Atmosphere.

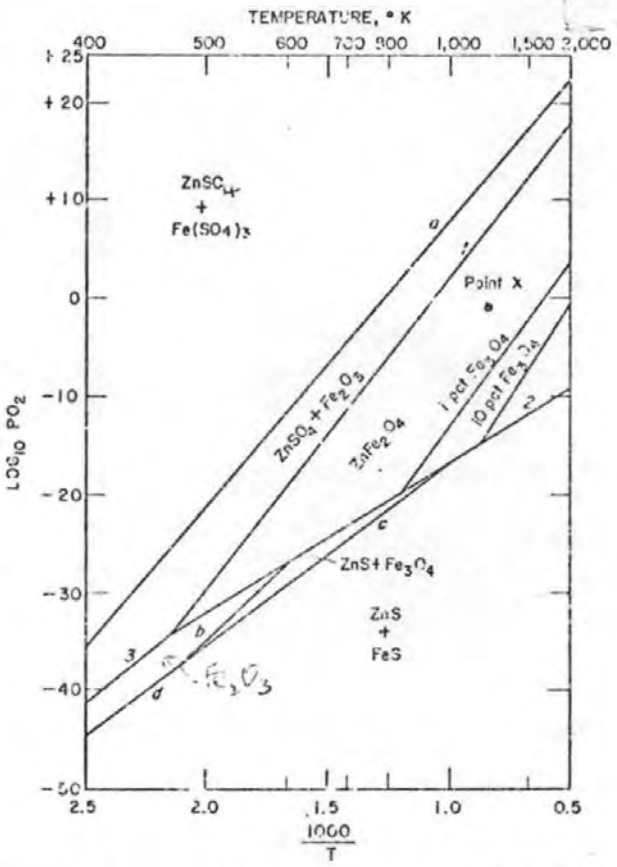


Figure 10 - Zn-Fe-S-O Compound Stability Diagram at a Constant $SO_2$ Pressure of $1X10^{-5}$ Atmospheres.

Table 9 - Standard entropy values of the constituents of $Fe_2(SO_4)_3$

| Constituent | Entropy value at 298° K, cal/degree | Source |
|---|---|---|
| $Fe_{\alpha}$ | 6.49 | Kelley[1] |
| $S_{2(gas)}$ | 54.50 | Do.[1] |
| $O_{2(gas)}$ | 49.01 | Do.[1] |
| $Fe^{+3}$ | 10.4 | Latimer[2] |
| $(SO_4)^{-2}$ | 13.7 | Do.[2] |

[1] Kelley, K. K., and E. G. King. Contributions to the Data on Theoretical Metallurgy. XIV. Entropies of the Elements and Inorganic Compounds. BuMines Bull. 592, 1959, 149 pp.

[2] Latimer, W. M. Methods of Estimating the Entropies of Solid Compounds. J. Am. Chem. Soc., v. 73, 1951, pp. 1480-1482.

temperatures are only temperatures at which ZnO and $Fe_2O_3$ can coexist with oxygen and $SO_2$ in the atmosphere; therefore, it is the only condition at which they can be present to combine to form $ZnFe_2O_4$.

General conditons for the industrial roasting of zinc concentrates are now presented.

1.9 Roasting of Zinc Concentrates:

Roasting is one of the main stages in the production of zinc. The recovery of zinc and the efficiency of subsequent treatment of roasted ore depend to a great extent on the success of roasting. The principal process of roasting is the oxidation of sulphides with oxygen from the air.

Roasting has two aims: the complete or partial removal of sulphur and the transformation of the sulphides into metal oxides.

The oxidation of metal sulphides proceeds in various ways, but they are all based on the chemical reactions occurring in the system Me-S-O. The heat evolved during oxidation depends mainly on the amount of sulphur in the raw material, on the amount of air coming into the furnace, on the amount of raw material, i.e. ore concentrate, and on many other factors.

The degree of desulphuration depends on the composition and other characteristics of the raw material, and on the conditions (temperature, gas composition, particle size etc.) which influence the mechanism of roasting.

There are different hypotheses (57) explaining the phenomena associated with the oxidation of sulphides. However the following two theories are the most important :

1. Sulphate theory

2. Oxide theory

According to the first hypothesis the following reactions occur during roasting :

$$ZnS + 2O_2 \longrightarrow ZnSO_4 \quad \ldots\ldots\ldots \text{(i)}$$

$$ZnSO_4 \rightleftharpoons ZnO + SO_3 \quad \ldots\ldots\ldots \text{(ii)}$$

$$SO_3 \rightleftharpoons SO_2 + \tfrac{1}{2}O_2 \quad \ldots\ldots\ldots\ldots \text{(iii)}$$

$$ZnO + SO_3 \rightleftharpoons ZnSO_4 \quad \ldots\ldots\ldots \text{(iv)}$$

$$ZnSO_4 + ZnS + O_2 \longrightarrow 2ZnO + 2SO_3 \ldots\ldots \text{(v)}$$

According to this the primary product of roasting is metal sulphate. Metal oxide is a secondary product which results from dissociation of the sulphate (ii) and from reaction (v) between unchanged sulphide and primary sulphate. Under certain conditions which depend on temperature, gas composition, material properties etc., the oxide can react with $SO_3$ (iv) and form metal sulphate. Therefore, at the end of the process the primary and secondary sulphate can exist.

According to the oxide theory the following reactions proceed :

$$ZnS + {}^{3}/_{2}O_2 \longrightarrow ZnO + SO_2 \quad \ldots\ldots\ldots (1)$$

$$SO_2 + \tfrac{1}{2}O_2 \rightleftharpoons SO_3 \quad \ldots\ldots\ldots\ldots (2)$$

$$ZnO + SO_3 \rightleftharpoons ZnSO_4 \quad \ldots\ldots\ldots\ldots (3)$$

$$ZnS + 2O_2 \longrightarrow ZnSO_4 \quad \ldots\ldots\ldots\ldots (4)$$

The oxide theory maintains that metal oxide is the primary product of roasting while the metal sulphate appears as a secondary product.

1.9.1 Sulphating roasting of sphalerite in a fluidised bed:

Many authors (58) have concerned themselves with the kinetics of the oxidation of sphalerite. A.A. Perfenov (1970) (59) studied the ratio of oxidation of zinc sulphide in air and gas media under the conditions of sulphating roasting. He carried out the experiments with natural sphalerite, Zn = 64.1%, S = 31.78%, Fe = 3.68%. The particle size of the mineral was 0.246 — 0.208 mm. Mathematical analysis of the curves 2,3,4 (Fig. 11) established the regularity of the isothermal process as described by the Benkhem equation:

$$\log \frac{\alpha}{1-\alpha} = \log C + \log \frac{\alpha}{Tind} \quad \ldots\ldots\ldots(1)$$

where $\alpha$ = the degree of desulphuration

and Tind = the length of the induction period

The graphically-treated data of equation (1)(Fig 12) establish that value of $\alpha$ at which the concentration of zinc oxide formed at the end of the induction period is determined ($\alpha$ = 0.2, dotted line parallel to the x-axis).

The rate of the process is determined by the length of the induction period and by the gradients of the lines; for this reason the observed rate constant K, expressed in parts of reacted sulphide per unit time, may be represented as the fraction of sulphide reacted after the induction period

$$K = \frac{\alpha}{Tind}$$

The activation energy of the process calculated is 49.9 k.cal/mole which indicates the kinetic nature of the process in the temperature interval studied. He also studied the variation of the rate of oxidation of sphalerite with concentration of oxygen in the process outside the kinetic region using 4.15 and 21% oxygen at 700°C. Mathematical analysis of the curves (Fig. 11,

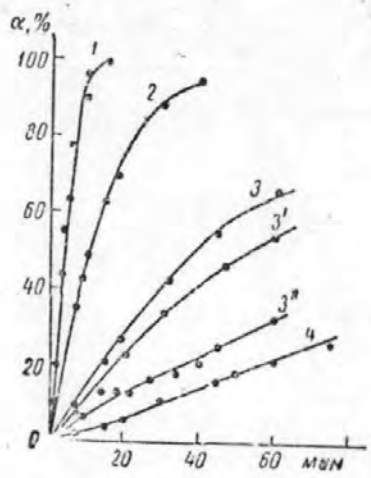


Figure 11. Kinetics of the desulphurisation of sphalerite at different temperatures and concentration of oxygen in the gaseous medium: 1 - 800°C, 21% $O_2$; 2 - 750°C, 21% $O_2$; 3 - 700°C, 21% $O_2$; 3' - 700°C, 15% $O_2$; 3" - 700°C, 4% $O_2$; 4 - 650°C, 21% $O_2$.

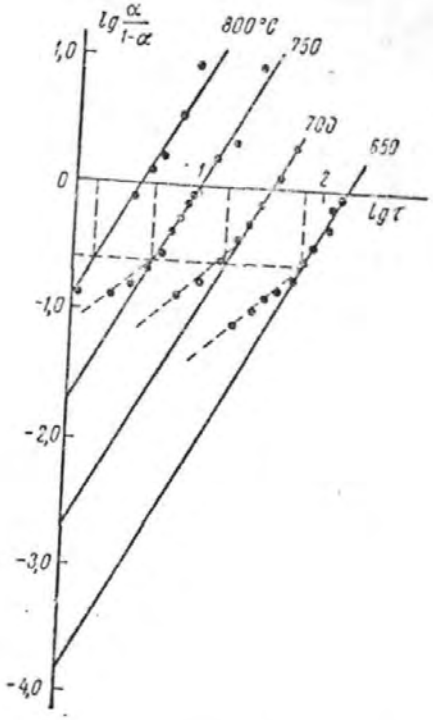


Figure 12 Change of the value of $\frac{\alpha}{1-\alpha}$ with time at different temperatures.

curves 3, 3' and 3") shows the linear variation of the value of the rate constant with the oxygen concentration. $K = \alpha C^{0.5}$, which indicates the zero order of the reaction with respect to oxygen(60).

R.Dimitrov and A.Paulin (1965)(61) carried out the experiments on synthetic ZnS (99% pure) and selected crystals of sphalerite (65.9% Zn, 32.4%S, 0.95%Fe, 0.06%Cu and 0.65%$SiO_2$) and marmatite (55.1% Zn, 11.7%Fe, 33.1%S). They did the differential thermal analysis (DTA), in order to determine the temperature range within which the experiments should be made. According to them, the oxidation of ZnS, sphalerite and marmatite proceeds at temperatures above 580, 670 and 660°C respectively (Fig 13). G.S. Frents (1964)(62) gave 560°C as the temperature of initial oxidation of ZnS and 623° and 647°C for sphalerite. The endothermic peak at 850°C was due to decompostion of zinc sulphate.

The area between the DTA curve and the zero line is given by the equation :

$$F = \int_a^c y\,dt \qquad \ldots\ldots\ldots\ldots\ldots(i)$$

where F = peak area

a = time of the start

c = end of reaction

y = the temperature difference measured

and dt = differential time.

The heat liberated during the process can be defined as :

$$Q = \int_a^c dQ \qquad \ldots\ldots\ldots\ldots(ii)$$

The peak area F is directly proportional to the quantity of heat liberated (61) in the course of the reaction :

$$m\Delta H = gKs\int_a^c y\,dt \qquad \ldots\ldots\ldots\ldots(iii)$$

Figure 13

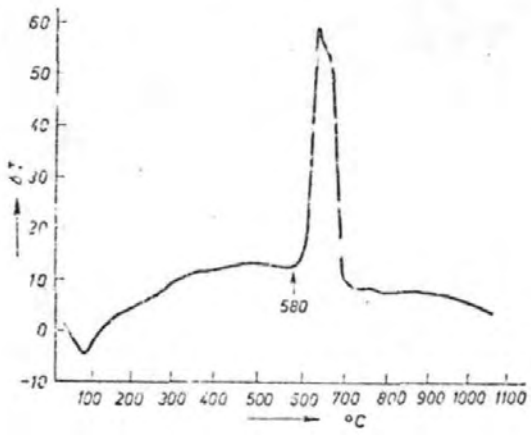


. DTA curve of ZnS

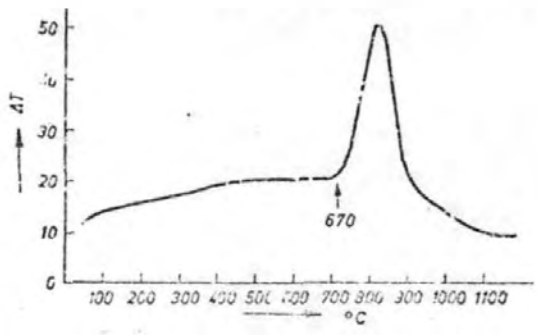


. DTA curve of sphalerite

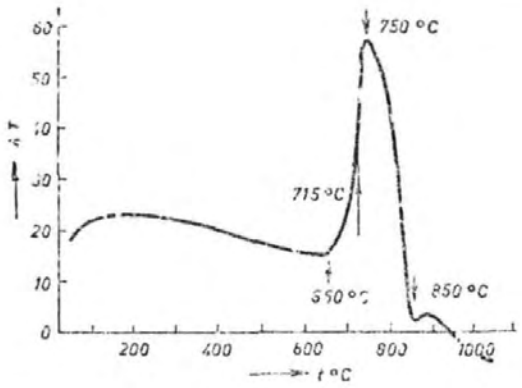


DTA curve of marmatite

where m = sample weight

$\Delta H$ = specific reaction heat

g = geometrical constant

and Ks = a constant which depends on the sample investigated

The constant gKs depends on the thermal conductivity density, and other properties of the sample, and on the geometrical shape of the sample block, heating rate, etc. All experiments must be carried out under the same conditions in order to maintain gKs at the same value so that the results can be compared.

Although a particular reaction proceeds only up to a certain degree, which depends on the experimental conditions, the peak area F, being proportional to the heat liberated, can be used as a progress of roasting (63). The length and height of the peak indicate the intensity of the process.

R. Dimitrov and A.Paulin (1965)(61) measured the peak areas and the ratio between them and the maximum area, which was constant at higher temperatures. They show the relationship between the ratio F/Fmax and the temperature of synthetic ZnS, sphalerite and marmatite (Fig 14). According to them, the point at which the curve cuts the zero line represents the initial temperature of oxidation, i.e. the temperature at which the oxidation starts, depending on the sensitivity of the apparatus; whereas the sharp deviation in the curve represents the initial temperature of intense oxidation. Then the oxidation of ZnS, sphalerite and marmatite starts at 420, 620 and 630°C respectively, while intense oxidation begins at 570, 680 and 710°C respectively.

Figure14

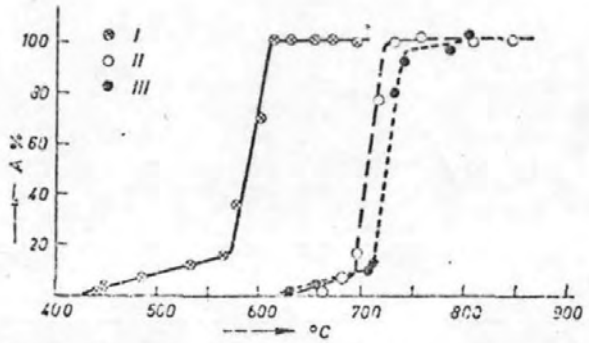


. Relationship between the ratio $r/F_{max}$ and temperature for ZnS (I), sphalerite (II) and marmatite (III). (A — progress of roasting)

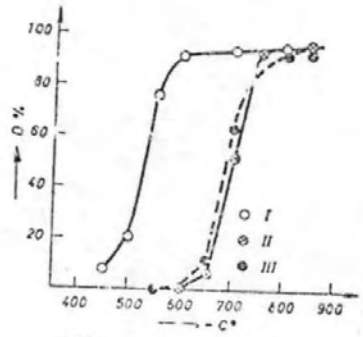


Effect of temperature on the degree of desulfuration of ZnS (I), sphalerite (II) and marmatite (III) for 30 min (D — degree of desulfuration)

Besides determining the kinetics of ZnS roasting, they tried to determine the rate constant of the overall process. Since the roasting process is composed of several reactions, a number of them can proceed simultaneously (62) :

$$ZnS + 2O_2 = ZnSO_4 \quad \ldots\ldots\ldots\ldots \text{(a)}$$

$$ZnS + {}^3/_2O_2 = ZnO + SO_2 \quad \ldots\ldots\ldots\ldots \text{(b)}$$

$$ZnSO_4 + ZnS + O_2 = 2ZnO + 2SO_2 \quad \ldots\ldots \text{(c)}$$

$$3ZnSO_4 + ZnS = 4ZnO + 4SO_2 \quad \ldots\ldots\ldots \text{(d)}$$

$$ZnO + SO_3 \rightleftharpoons ZnSO_4 \quad \ldots\ldots\ldots\ldots \text{(e)}$$

$$SO_2 + \tfrac{1}{2}O_2 \rightleftharpoons SO_3 \quad \ldots\ldots\ldots\ldots\ldots \text{(f)}$$

$$ZnS + 2ZnO = 3Zn + SO_2 \quad \ldots\ldots\ldots\ldots \text{(g)}$$

$$ZnS + ZnSO_4 = 2Zn + 2SO_2 \quad \ldots\ldots\ldots\ldots \text{(h)}$$

$$Zn + \tfrac{1}{2}O_2 = ZnO \quad \ldots\ldots\ldots\ldots\ldots \text{(i)}$$

Since the experiments were carried out with a significant excess of air, it can be assumed that the interaction between the sulphate and the sulphide more probably proceeded according to (c) than according to (d) which would also seem reasonable after consideration of free energies. Further, it can be assumed that the concentration of $SO_3$ was very low because of a strong air flow, which means that (e) should proceed only from the right to the left. Reactions (g), (h) and (i) are not probable since their free energies are positive. Thus only (a), (b) and (c) remain. The free energies dependence on temperature (64) for (a), (b), (c) and (e) were calculated to determine the temperature range within which the particular reaction predominates :

$$\Delta G_4 = -150215 + 7.95T \log T - 3.99.10^{-3}T^2 + 0.47.10^5T^{-1} + 41.64T \quad \ldots\ldots\ldots\ldots \text{(j)}$$

$$\Delta G_5 = -71205 + 6.41T\log T - 2.46.10^{-3}T^2 + 0.084.10^5T^{-1} - 20.86T \quad \ldots\ldots\ldots\ldots \text{(k)}$$

Figure 15

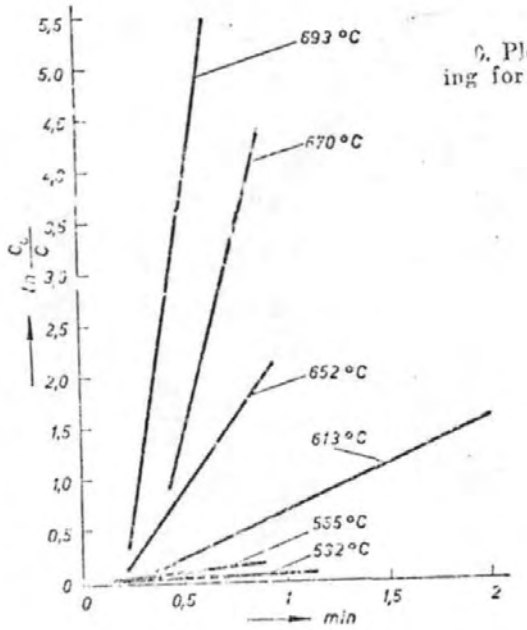


6. Plot of $ln(c/c_0)$ versus the time of roasting for ZnS in dependence on temperature

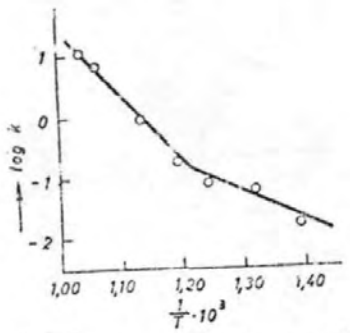


F . Plot of $ln\, k$ versus $1/T$

$$\Delta G_6 = -32205 - 1.34T \log T + 5.76.10^{-3}T^2 - 0.79.10^5 T^{-1} - 47.67T \quad \ldots\ldots\ldots\ldots (l)$$

$$\Delta G_7 = 126975 - 15.15T \log T + 190.10^{-3}T^2 - 3.15.10^5 T^{-1} - 145.2T \quad \ldots\ldots\ldots\ldots (m)$$

From Fig.16 it was seen that generally the most probable reaction is the formation of sulphate at lower temperatures.

It was assumed that the reaction

$$ZnS + {}^3/_2O_2 = ZnO + SO_2$$

is of the first order, the rate of which is proportional to the concentration:

$$v = K.C \quad \ldots\ldots\ldots\ldots (n)$$

Instead of v, put dc/dt. By differentiation:

$$\ln \frac{C}{Co} = - Kt \quad \ldots\ldots\ldots (o)$$

or $$C = Coe^{-Kt} \quad \ldots\ldots\ldots (p)$$

Equation (p) shows that $\ln({}^C/Co)$ is proportional to the time of the first order reaction, and that the rate constant K can be determined graphically from the plot of $\ln({}^C/Co)$ versus t. To verify the assumption that (b) is the first order reaction, the plot of $\ln({}^C/Co)$ and t was made for different times and temperatures as in Fig. 15. Change in the concentration of ZnS was determined indirectly by measuring the heats liberated up to a definite time. The linear form of the plot confirmed the validity of the assumption. The inclination of the straight curves indicated strong dependence of the rate constant on temperature. This relationship was more clearly given in the lnK versus ${}^1/T$ plot (Fig 15). The relationship was linear within the temperature range of $700^\circ$- $570^\circ$C whereas at lower temperatures there is a deviation from linearity. A break in the curve, in the temperature range which corresponds to the intense oxidation of ZnS may be explained by the fact that at lower temperatures only reaction (a)

Figure 16

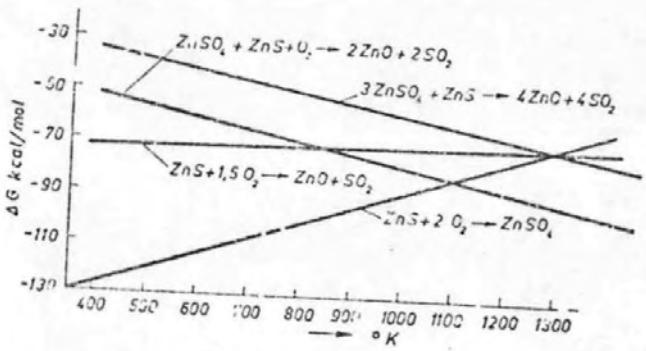


Temperature dependence of free reaction enthalpy of reactions (5), (6), (6) and (7)

proceeds on the surface of grains. After the formation of a compact sulphate layer (64), further oxidation is restrained.

The kinetics of roasting of ZnS in a fluid-solid reactor was also investigated by R. Dimitrov and A.Paulin. The degree of desulphuration :

$$D = \frac{Se.100}{So}$$

where Se = removed sulphur

So = original amount of sulphur in the sample,

in relationship to temperature and time was presented in Fig.14. They confirmed that the rate of roasting in the fluidized bed is much higher than that in the stationary layer.

They also carried out experiments with five different grain sizes at 700°C in order to determine the effect of grain size on the kinetics of ZnS oxidation.

Similarly as in the case of the stationary layer, the roasting proceeds at a lower rate when using coarse grains due to smaller active surface and hindering influence of diffusion.

They also studied the effect of air flow and its oxygen content on the kinetics of ZnS oxidation. Their results were shown in Fig.17 from which it could be seen that both of these factors accelerate the roasting. The addition of oxygen has a supplementary positive effect since it caused a more complete roasting. The enrichment of air with oxygen was more appropriate for increasing the roasting rate, since air flow cannot be increased above a certain limit without bringing along large amounts of dust.

In practice, the reactions are made more favourable kinetically by special sintering processes.

Figure 17

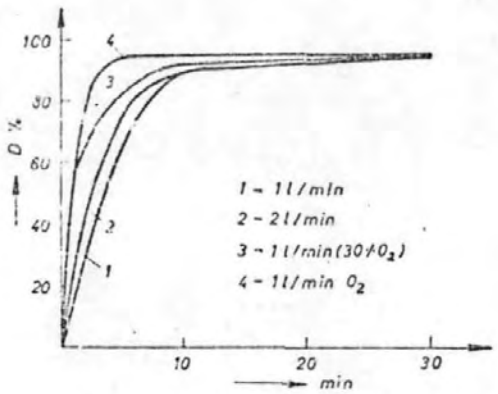


1. Effect of air flow and oxygen content of the air on the rate of desulfuration, (D = degree of desulfuration)

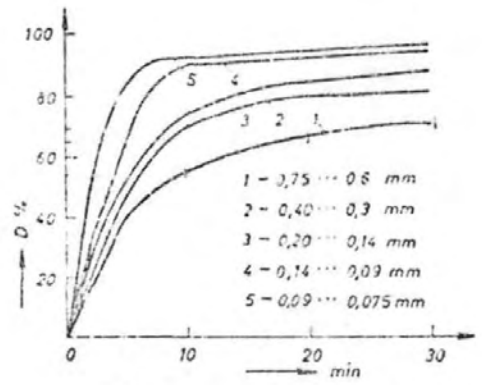


Effect of grain size on the rate of desulfuration (D = degree of desulfuration)

1.10 Sintering of Zinc Concentrates:

Zinc is produced at Avonmouth by two processes, the Vertical Retort process and the Improved Vertical, or blast furnace process. Each requires the zinc feed in oxide form, but the physical nature of this oxide differs for the two processes. The objects of the sintering operation are to desulphurize the zinc blende and to produce zinc oxide in forms most suitable for the subsequent reduction to the metallic form.

For retort smelting the zinc feed composition is simply that of a roasted mixture of concentrates, i.e. the sinter consists principally of zinc oxide, zinc ferrite and very minor quantities of gangue materials. Good desulphurization and a uniform porous texture of sinters are the objectives in this type of sintering; the sinter used in retort processes is a crushed product, so that hardness and lump sizing are irrelevant.

For the blast furnace a lump sinter feed is required, within the $\frac{1}{2}$ in - 4 in range. To supply such feed, after handling in plant systems, a minimum hardness or strength of sinter is necessary, and this dictates the use of added silica and limestone in the sinter mix. Furthermore, the incorporation of fluxes in the sinter rather than as a separate additon is advantageous.

The sintering process may be conveniently divided into four major stages, namely :

(1) Conditioning of the raw blende

(2) Mixing of the sinter machine feed

(3) Sintering of this mixed feed

(4) Separation of the sintered material into "product" and "returns" and the physical conditioning of each.

The raw blendes received are mainly flotation concentrates containing 50-60 per cent zinc and 30-33 per cent sulphur. A certain amount of agglomeration takes place in these finely-divided concentrates. These agglomerates have to be broken down to obviate imperfect sulphur elimination during sintering. The high sulphur content of the blende precludes its direct use on the sintering machines as the high fuel value would cause excessive bed temperatures with consequent slagging of the material and imperfect sulphur elimination. The sulphur content of the feed is adjusted therefore by the addition of sintered product (returns) so as to give a mixture which will combine high sulphur elimination and the requisite degree of fritting to give a good quality, cellular-structured product.

During sintering, the feed becomes fritted together and is discharged from the machine largely in lump form. This is screened on a bar screen, the undersize providing the "returns" and the oversize the product for the furnaces.

The direct and complete roasting of zinc concentrates on sintering machines had been envisaged for some years and an extensive campaign of investigations on a stationary sintering pallet had indicated its feasibility and of utilizing the flue gases for sulphuric acid manufacture. The underlying principle was the dilution of the fine zinc concentrates with sufficient inert and porous material to reduce the sulphur content to a suitable level and to render the mixture permeable to the gases. Without some such diluent, the bed became so hot during sintering that it slagged into a non-porous, partly roasted mass. This became more so, as the quantity of air

passed through the bed was restricted in order to produce a strong gas for the Acid Plant. Sinter was the obvious diluent, and in the first attempts, sufficient sinter was mixed with the concentrates to reduce the sulphur content of the mix. However the fuel value of this was found to be too great, and a hard, slaggy sinter high in sulphur content was formed. A hard seal rich in galena was formed on the grate bars, sealing them off and effectively preventing further roasting. The reason for this was the absence in the mixture of the endothermically-reacting sulphate compounds in the preroast, and equivalent fuel value being obtained with a lower sulphur content in the concentrate mix than in the preroast mix.

The determination of sulphur conditions in the charge was, however, only part of the problem. The effect of particle size, the form of the bed, the distribution of gas through the bed, and the quantity of moisture in the charge had all been investigated. This culminated in patents being granted in all countries for what has become known as the "5:1 straight sintering process", which remains essentially for producing the sinter for the Vertical Retort process. It is known familiarly as "soft" sinter in differentiation from the harder, lump sinter required by the blast furnace process.

The need for this latter type of sinter arose with the development of the blast furnace process, and initially the normal "soft" sinter was hardened by increasing the fluel value of the mix, and the inclusion of silica and lime in it.

The introduction of the blast furnace process for the simultaneous smelting of zinc and lead created problems in burden preparation. They were resolved by the adoption of the

updraught sintering method for the production of self-fluxing sinter. Since most zinc and lead raw materials are sulphides, it is usual to employ the sulphide content of the sinter mix as the fuel for sintering and to use the sinter gas for sulphuric acid production.

The increasing availability of mixed zinc-lead raw materials and the world-wide interest in a process which can treat economically such raw materials have involved the preparation of sinters from raw materials of widely differing chemical composition. During the course of experimental work on the preparation of these sinters, it became evident that the quality of the sinter was affected markedly by variations in its chemical composition. Sinter quality is usually judged by sulphur content and rattle index - low sulphur and high rattle index being desirable.

1.10.1 Factors in Zinc-Lead sinter production :

S.E. Woods and C.F. Harris (1956)(66) discussed the factors in zinc-lead sinter production. In the first place, they gave a brief outline of the physicochemical background, indicating the phases existing in different circumstances, the possibilities of partial melting, the vapourization or decomposition which was liable to take place.

The following properties of the compounds arising in the different types of sinter were relevant to the behaviour in sintering :

1. The roasted zinc concentrate of the composition of 53% Zn, 31% S, 8% Fe, 1.5% Pb, 1.5% $SiO_2$ used in soft sintering consists virtually entirely of zinc oxide and zinc ferrite.

Microscopic examination showed that above a temperature of 1380°C zinc ferrite enters into solid solution in zinc oxide and the state of sub-division of the zinc ferrite in the final sinter is related to the rate of cooling of the sinter from this temperature. At the peak temperatures attained in soft sintering, sublimation of zinc sulphide becomes an important consideration. Gaseous zinc sulphide is dissociated into zinc and sulphur. In highly-fuelled zinc sulphide sintering there is evidence of transport of zinc in some gaseous form, in that crystals of zinc oxide are found which have clearly been deposited from the gas.

2. The incorporation of silica in the sinter mix leads to the possible presence of a number of silicates. The oxidizing conditions in the sinter bed leave the iron in the final sinter predominantly as zinc ferrite, so that the iron can exist in the ferrous state only to a limited extent or perhaps transiently in the burning zone.

Willemite, $Zn_2SiO_4$, is frequently found in the sinter.

3. Lead as a constituent of the sinter necessarily implies phases which are molten, over a substantial period in the sintering process. The sulphide, sulphate, oxide, silicate and the metal itself all have melting points at least 100°C below the peak temperatures normally encountered.

4. The maximum temperature at which the sulphate is stable in the presence of air containing 1% $SO_2$ is :

$ZnSO_4$ ... 805°C

$PbSO_4$ ... 1005°C

$CaSO_4$ ... 1255°C

$BaSO_4$ ... 1575°C

Zinc sulphate is so unstable that it should not be formed, lead sulphate should also be decomposed in the sintering, but calcium sulphate is sufficiently stable for its decomposition to depend upon the particular sintering under consideration.

The change from soft sinter to hard sinter manufacture involves higher sulphur content of both output and returns. In addition, however, the peak temperature in hard sintering is lower than in soft sintering.

A thermocouple at any point in the bed will rise in the course of sintering to a temperature which is referred to as the peak temperature. The value of this peak temperature is lower in early stages of sintering, but thereafter fairly constant, until in the later stages it is influenced by the cooling effect of grate bars or radiating top surface. As the fuel content of the bed is increased, the peak temperature also rises until a range is reached in which no great change in peak temperature occurs.

In soft sintering, i.e. with zinc concentrates only, peak temperatures in the range 1450 - 1500°C are typical.

Hard sintering gives peak temperatures about 1300°C.

Temperatures attained with coke fuel are similar to those obtained with zinc sulphide.

The main effect of lime or lead additions is to reduce the peak temperature and to enhance the effect when both are present. Silica has no consistent effect; in association with high lime it diminishes the effect of the lime.

Sinter hardness:

As a physical property of sinter, hardness could be defined and measured in a variety of ways. In this instance, what is meant by hardness is simply the ability to withstand plant handling; the handling treatment at Avonmouth seems to be reflected best by measuring hardness in a tumbler or rattle test. In the test used at Avonmouth a 50 lb. sample of sinter sized - 2 in. + $\frac{1}{2}$ in. is rotated in a drum (outside diameter 16 ins. external length 16 ins.) fitted with one 2 in. lifter, for 80 seconds in which time the drum has completed 84 revolutions. The percentage of sinter remaining in an $\frac{1}{2}$-in screen is quoted as the rattle index of the sinter.

Lead volatilization and migration:

At the peak temperature in zinc-lead sintering, both PbS and PbO are volatile, and transport of the vapours takes place in the gas stream. As long as the hot zone has not reached the top (or bottom, in down-draughting) of the cake, condensation and filtration of the volatilized lead occurs, so that the net effect is a transport of lead and of heat forward from the roasting zone. When the hot zone reaches the top a copious evolution of lead compounds occurs; with continued draughting and cooling of the bed, the concentration of lead in the gas falls again. The temperatures in this type of sintering are higher than in lead sintering, so that the lead volatilization can be a more serious problem. Migration of lead can also take place by downwards movement of liquid under gravity.

In soft sintering it is advantageous to remove as much lead and cadmium as possible from the cake. In hard sintering of mixes containing substantial amounts of lead,

lead elimination is undesirable. Typical figures in soft sintering are as follows :

Downdraughting : lead volatilized 30-40% of lead charged, i.e. 2-3% of the sulphur burnt.

Updraughting: lead volatilized about 60% of lead charged, i.e. 4½% of sulphur burnt.

In hard sintering, a volatilization of lead equal to about 15% of the sulphur would be typical.

Retention of lead in the region of the grate bars occurs in downdraughting, both in static pallet experiments and on the plant. In updraughting, this type of retention does not occur but the volatilized lead is largely filtered out in plant practice, in so far as the gases are recycled.

The compositional effects shown can be summarised as follows :

With oxidised lead, the presence of silica prevents lead volatilization; however, lime neutralizes this effect of silica, but with lead sulphide additions the volatilization is high and insensitive to composition.

1.10.2 Effect of compositional variations on the quality of Zinc-lead sinter :

C.F. Harris et al (1967)(67) studied the effect of variation of the lead, lime, silica, iron, alumina and magnesia content of sinter on the quality of zinc-lead sinter. It was shown that the quality of sinter (defined by the sulphur content of sinter) and the strength (as indicated by a rattle test) were affected by compositional variations. On this basis, low sulphur and high rattle index are desirable. Usually, less than 1.0% sulphur and a minimum rattle index of 75 are required.

10.2.1 Experimental procedure:

The optimum fuel content in zinc-lead sintering is approximately 5% new sulphur in mix (69) (i.e. the sulphide sulphur content of the new materials excluding sinter returns). The fuel content is controlled by mixing the appropriate amount of returns (previously sintered material) with the new materials. The allowance for lead volatilization is normally about 10-15% of the lead in the mix, but this has to be varied with the lead content of the mix and with the temperature attained during sintering. The components of the sinter mix are used in the same size range as on the sinter plants and returns are crushed, essentially to $-\frac{1}{4}$ in. before use.

Sintering was carried out on a laboratory updraught pallet with a $10\frac{1}{2}$ in. diameter grate and a 6 in. bed depth. Ignition was effected by downdraughting a 1 in. layer of sinter mix under a gas-fired ignition box for $1\frac{1}{4}$ minutes, after which the rest of the sinter mix was placed on the pallet and updraughting was commenced. The apparatus was shown diagrammatically set up for ignition and for updraughting in Fig.18. The sinter mix was contained in a packing of soft sinter fines (fines produced from the sintering of zinc concentrates for retort smelting) during sintering in order to reduce edge effects. The packing was held in position by formers, the former between the packing and the sinter mix being removed before updraughting was commenced.

During sintering, bed pressures were noted at 1 minute intervals and bed temperatures are recorded by use of two sheathed platinum/platinum rhodium thermocouples placed 2 and 4 inches above the grate. The waste gas temperature was

Figure 18

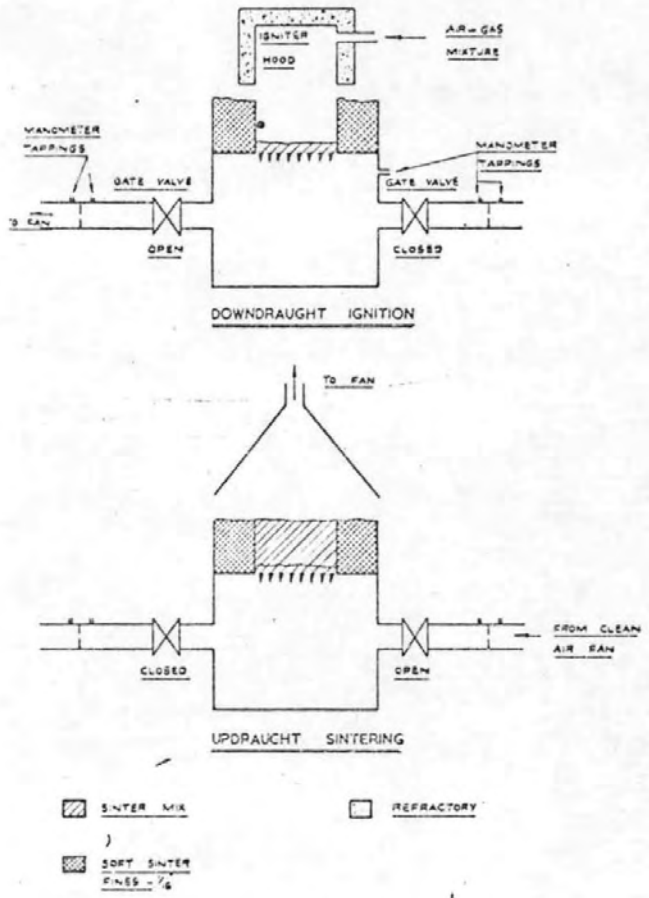


b Schematic layout of laboratory updraught sinter pallet

also recorded in order to determine when the draughting was stopped.

After sintering, the cake was broken in a standard manner by placing it on two 1 inch thick bars at 4 inch spacing and breaking with a 1 inch thick centrally-placed lever. The broken cake was allowed to fall about 2 ft. to the floor and the proportion remaining above 1 inch in size was determined.

10.2.2 Effect of lime, silica and lead variations on sinter quality:

Sinter for the zinc-lead blast furnaces was normally self-fluxing, but variations required in slag composition had meant that sinters had to be produced at times with different lime and silica levels. The work involved two lead levels to give an indication of the effect of lead. During this work the iron level was held constant at 7½%.

There was no difference in rattle index attributable to the change in lead level. The effect of increasing the silica level was to increase rattle index linearly at both lead levels (20% and 30%). The rattle index also increased with the lime content at the lower level, the relationship being quadratic and tending to flatten at the higher lime levels. The lime effect was not significant at the higher lead level.

The total sulphur content of sinter made under each experimental condition was measured as sulphate. The sulphur contents of the sinters containing 30% lead were higher than for those containing 20% lead. The total sulphur content was increased with both lime and silica additions.

The peak temperature reached in a sinter bed depends on the way that the hot zone moves through the bed (69), and on some limiting processes of heat consumption such as fusion and/or an endothermic chemical reaction.

It was shown that increasing the lead, lime and silica content of sinter resulted in depression of the peak bed temperature. The effect of lead and silica could be attributable to the greater proportion of readily fusible material in the sinter mix. The effect of lime was difficult to explain.

10.2. 3 Effect of iron variation on sinter quality:

Tests were made using zinc concentrates with a low iron content and deriving the iron from additions of commercial iron sulphide (essentially FeS) in one case and from additions of iron oxide derived from pyrites roasting (essentially $Fe_2O_3$) in the other. The lead, lime and silica levels were 15, 8 and $5\frac{1}{2}\%$ respectively.

It was clear that the rattle index of sinter declined with increasing iron content, but that this effect was more marked when iron oxide was used as the source of iron than when iron sulphide was used. No effect of iron was found on either total sulphur content or on sulphate sulphur content of sinter. This was in accordance with neither ferric sulphate nor ferrous sulphate being stable at sintering temperatures.

The values for the peak bed temperatures obtained are particularly interesting; when iron was added as oxide, the bed temperature declined with increasing amounts of iron, but when iron was added as sulphide, the bed temperatures tended to rise with increasing iron content.

10.2.4 Effect of alumina variations on sinter quality:

Alumina was relatively minor component of zinc-lead sinter, with a typical level of 0.5%. It can have an effect on the properties of blast-furnace slag. It was clear that the sinter with the highest rattle index was made at the higher alumina level using ball clay (impure aluminium silicate). Also, sinter with the lowest rattle index was made at the higher alumina level by using alumina. The sinter with the higher alumina and lower lime content had the lowest sulphur content. The peak bed temperatures were not significantly different. The effect on rattle index was clearly attributable to the form in which alumina was added. Alumina in the form of ball clay rather than fairly pure $Al_2O_3$ was probably more easily assimilated into the glassy material which binds sinter together. For that matter, it seemed that silica in the form of ball clay may also be more easily assimilated into the binding material than sand.

10.2.5 Effect of magnesia:

Magnesia, like alumina, is normally a minor constituent of sinter and has a typical level of about 0.5%. Some ores and concentrates contributed more magnesia than normal to sinter and a further contribution could be made from some limestones. In the course of operation it was found that relatively small increments in the magnesia content of sinter were associated with a significant decline in rattle index. The use of dolomite appeared to produce an even more pronounced effect than the use of magnesia; the latter had no effect on either sulphur content or peak temperature.

## 1.11 Objectives of the present research:

The research comprises a physicochemical study of roasting and sintering processes for zinc sulphide ores. Conditions under which the sulphides are oxidised to metal oxides or sulphates are to be compared to determine the relative effects of time of heating and composition of surrounding gases, whether in static or dynamic environment. To elucidate the mechanisms and kinetics of the oxidation processes, information is required also about the surface area, crystallite and aggregate sizes of the materials and the influence of any impurities.

Thus, for basic oxidation studies it will be necessary to prepare finely-divided zinc sulphide samples of widely different specific surfaces. This will involve precipitation from solution at various pH levels and in the presence of different concentrations of electrolytes. The behaviour of the pure zinc sulphides on oxidation is to be compared with samples having added impurities, particularly other metal sulphides (such as those of lead, iron and copper) normally present in zinc ores.

There will be attempts to correlate the basic researches with problems arising with the industrial roasting and sintering of natural ores such as spontaneous ignition (during shipment, storage and processing) and their poor sintering behaviour and incomplete sulphur removal at higher temperatures. Improvements obtained by the use of lime and silica additives in the production of sinters will also be investigated.

## Chapter 2

## EXPERIMENTAL TECHNIQUES

### 2.1 X-ray diffraction identification of phases

#### 2.1.1. Theory of X-ray diffraction

A crystal consists of a regular three-dimensional arrangement of atoms in space. Points having identical surroundings in the structure are called lattice points, and a collection of such points in space forms the crystal lattice. The arrangement is such that a straight line drawn through any two adjacent lattice points of the network and continued will intersect at equal intervals the same succession of points. If neighbouring lattice points are joined together one obtains the unit cell, i.e. the repeating unit of the structure. In general the shape of the unit cell is a parallelepiped, but in some cases, depending on the symmetry of the crystal, it can have more regular shape e.g. a rectangular box, or in the extreme case a cube. The shape of the unit cell is completely described by the length of its three edges or axes and the angles between them. By convention, the axes are named x,y,z or a,b,c and the angles $\alpha$, $\beta$, $\gamma$; the angle between y and z is $\alpha$ etc.

Crystals are classified into seven classes depending on their symmetry. The unit cell dimensions of a crystal obey certain relationships according to the crystal class. These relationships are represented as :

| Crystal class | Conditions limiting Cell dimensions | Minimum symmetry |
|---|---|---|
| Triclinic | $a \neq b \neq c$; $\alpha \neq \beta \neq \gamma \neq 90^\circ$ | - |
| Monoclinic | $a \neq b \neq c$; $\alpha = \gamma = 90^\circ \neq \beta$ | One two-fold axis or one plane of symmetry. |

| Crystal class | Conditions limiting Cell dimensions | Minimum symmetry |
|---|---|---|
| Orthorhombic | $a \neq b \neq c$; $\alpha = \beta = \gamma = 90^\circ$ | Two perpendicular two-fold axes or two perpendicular planes of symmetry |
| Tetragonal | $a = b \neq c$; $\alpha = \beta = \gamma = 90^\circ$ | One four-fold axis |
| Hexagonal | $a = b \neq c$; $\alpha = \beta = 90^\circ$; $\gamma = 120^\circ$ | One six-fold axis |
| Trigonal | $a = b = c$; $\alpha = \beta = \gamma \neq 90^\circ$ | One three-fold axis |
| Cubic | $a = b = c$; $\alpha = \beta = \gamma = 90^\circ$ | Four three-fold axis |

It is possible to draw various sets of parallel planes through the lattice points of a crystal. Each set of planes is identified by a set of three integers, namely, the Miller indices, h, k, l, corresponding to the three axes a, b, c, respectively.

The index, h, is the reciprocal of the fractional value of the intercept made by the set of planes on the a-axis and so on.

When an incident beam of X-rays impinges on a crystal, they are scattered by the atoms. Since the scattered radiation results from the acceleration and deceleration of electrons set in motion by the X-rays, it has the same wave-length as the incident X-rays. This fact plus the regularity of the pattern of atoms in a crystal permits the crystal lettice to act as a three-dimensional diffraction grating. The diffracted beam which emerges, in phase, from a particular set of lattice planes obeys Bragg's law

$$\lambda = 2d \sin \theta$$

where $\lambda$ = wavelength of X-rays

$d$ = interplanar spacing

and $\theta$ = angle of incidence

= angle of diffraction

d is related to the unit cell dimensions of the crystal and the Miller indices of the set of planes. Hence the measurement of Bragg angles can lead to the determination of lattice parameters.

There are a large number of lattice planes in each set when the crystal is large; so the diffracted beam appears at a sharp angle in the case of a large crystal. However, with appreciably small crystals, diffraction takes place over a range of Bragg angle. With aggregates of small crystallites, broadening occurs, of which the extent serves as a measure of crystallite size.

If a single crystal of a substance is rotated in a beam of monochromatic X-rays, the diffraction pattern forms a series of spots on a photgraphic film. However, if the sample is in the form of a crystalline powder or a sintered compact, the crystallites of which show random orientation, the diffracted beams lie along the surfaces of a set of coaxial cones.

The pattern can be recorded in two ways :

(1) By a photographic method

(2) Using an X-ray diffractometer with attached counter and ratemeter.

2.1.2 Debye-Scherrer Powder Diffraction Camera

A Debye-Scherrer camera of 9 cm-diameter was used for the photographic method, the film being mounted according to the Van Arkel method.

The specimen was prepared by loosely filling a glass capillary tube about 0.5 mm in diameter and 1 cm in length with the crystalline powder; and sealing both ends of the capillary tube with an adhesive. The sample was mounted vertically along the camera axis and the necessary alignments were made by means of two push-pull screws set at right angles to each other. The specimen was rotated about the camera axis bringing each set of

lattice planes of every crystallite to a diffracting position several times during an exposure. The camera was evacuated by having it continuously pumped for several hours during exposures in order to minimise the scattering of X-rays by air. The powder camera was used in conjunction with the Raymax 60 generating unit.

Kodirex X-ray films were used in the powder camera. After exposure the film was developed for 5 minutes at 20°C in Kodak D-196 developer, rinsed with water, fixed in Kodak FX40 fixer, washed in running water for ½ an hour and hung up to dry. The fixing time was twice the time required for the milkiness on the film to disappear. This was usually about 5-6 minutes. The films were examined and measured on an illuminated screen fitted with a scale. The intensities of the powder diffraction lines were visually compared.

2.1.3 The Counter Diffractometer

The counter diffractometer gives a direct, simple and accurate measurement of Bragg angles of the various "reflections" in the powder diffraction patterns.

A Solus-Schall X-ray diffractometer fitted with a Geiger counter and connected to a Panax ratemeter and an Elliot chart recorder was used. The diffractometer works on the focussing principle described by Bragg and Brentano. The diameter of the diffractometer is 50 cm.

The sample for examination was prepared by pouring a suspension of the crystalline powder in acetone onto a glass slide. On evaporation of the organic liquid, the powder remained adhered to the slide. Sometimes it was necessary to mix an adhesive with the suspension. The glass slide containing the

sample was mounted vertically at the centre of the diffractometer and rotated at half the speed of the detector. The X-rays generated in a sealed tube unit, passed through a collimator diaphragm. The intensity of the diffracted radiation as a function of the diffracting angle, $\theta$, was given by the chart recorder coupled to the associated rate meter. The full chart deflection could be made equal to 2,000, 10,000 and 40,000 counts per minute to accommodate the traces of the peaks. To give reasonable smooth traces, a time constant of 25 seconds was used for the highest scale (2,000 c.p.m) and 5 seconds for the other two scales. Since the peaks are recorded at different times by the diffractometer, it is necessary to have a stable incident beam of X-radiation. Hence the sealed off tube type generator with a copper target was used with the diffractometer. It was necessary to use nickel filter to remove the $K_\beta$ component, for obtaining monchromatic radiation. The tube was operated at a rating of 30 kV and 10 mA. The Elliot chart recorder could be operated at either 3 inches per hour or at 30 inches per hour and records the line intensities. Both the specimen and the counter could be rotated in a clockwise or anti-clockwise direction by means of a geared electric motor having three available speeds of 1/3, 1 and 2 angular degrees per minute. In order to obtain the intensity of a particular peak, the mean background level on either side of the peak was subtracted from the maximum peak height. The breadth of the peak was measured at half-maximum intensity.

2.1.4 X-ray Line-Broadening

X-ray diffraction is useful not only for identifying chemical constituents in various samples, but also for determining average sizes and shapes of crystallites. A narrow sharp peak indicates relatively coarse material, and a low, broad peak indicates fine crystallites ultimately transitional to an amorphous phase. The X-ray diffraction line broadening technique is ordinarily used for measurements in the size range 15 to 2,000Å (0.00015 to 0.02 micron) or approximately the range covered by the electron microscope. Though the electron microscope gives the advantage of direct observation of size, the x- ray method is faster and statistically more valid because it measures a far greater number of crystallites.

2.1.4 (a) Theory of X-ray Line-Broadening

The Bragg equation, $\sin\theta = \frac{n\lambda}{2d}$

specifies a definite angle for a diffraction maximum to occur, $\theta$ being the angle between lattice plane in a crystal, and the incident X-ray beam. The incident beam is diffracted in phase from planes, i.e. the difference in the path length of the diffracted beam is an integral multiple of one wavelength.

In large crystals containing numerous parallel atomic planes the value of $\theta$ is precise, and the diffraction maximum is sharp.

In small crystals or crystallites the number of atomic planes is reduced, and a small deviation from the ideal $\theta$ angle becomes tolerable to in-phase diffraction. The diffraction therefore no longer produces a sharp maximum. The normally sharp diffraction peak broadens; the amount of broadening is related to the size of the crystallite. This relation was quantitatively

defined by Scherrer (1915)(70) with the equation :

$$D = \frac{K\lambda}{\beta \cos \theta},$$

where $K$ = constant ($\sim$ unity)

$\lambda$ = wavelength of the radiation

$\theta$ = Bragg angle

$Vm$ = mean crystallite volume

$D$ = a linear dimension

$= 3\sqrt{Vm}$

$\beta$ = line width (in terms of $2\theta$)

$\beta$ is estimated either from the recorder trace as the peak width at half the peak maximum after substraction of the background radiation, or using the sealer and printout to give optimum statistical accuracy. This formula can be used experimentally only when there is no significant instrumental line broadening. As it is not possible to correct by simple subtraction the contribution of the instrumental broadening, the method due to Jones (1938)(71) is used (in cases where such broadening is significant).

The observed integral breadths of the lines are first corrected for the fact that they are produced by the $\alpha_1\alpha_2$ - doublet of the copper X-radiation using the graph of $b/\beta_o$ against $\Delta/B_o$, where $B_o$ is the observed line broadening, b is the corrected width for the sharp, S-line of calcite ($14^o43'$) (taken as a standard for a large perfect crystal), $\Delta$ is the doublet separation measured in the same unit.

The correction curve is reproduced in Appendix 1(a) and can be used to calculate the intrinsic broadening due to the single radiation, $K - \alpha$. The symbols shown in the Appendix have the following meanings :

| Radiation | Observed Breadth | Instrumental Breadth | Intrinsic Broadening |
|---|---|---|---|
| K $-\alpha_1$ | B | C | $\beta$ |
| K $-\alpha_{doublet}$ | $B_o$ | $C_o$ | $\beta_o$ |

The angular separation, $\Delta$, of the K $-\alpha_1$, and K $-\alpha_2$ radiations is calculated using the expression, whose derivation is given in Appendix 2

$$\Delta = \frac{360}{\lambda} \cdot \frac{\lambda\alpha_2 - \lambda\alpha_1}{\lambda_{average}} + \tan\theta_{average} = C \tan\theta$$

The value of C for copper K$\alpha$ radiation is 0.285.

There is a further correction required to account adequately for instrumental broadening as given by the curve in Appendix 1(b).

The curve of $\beta/_B$ against $C/_B$ was derived by Jones (1938) using the function :

$$1/(1 + K^2 x^2)$$

where K = a constant

x = the angular distance from the top of the peak.

This function describes the intensity distribution across the diffraction line obtained under ideal conditions of no instrumental broadening. The evidence available so far (Jones, 1938, 1950) suggests that the function is the best one to describe the intrinsic diffraction profile where a Gaussian distribution of crystallite sizes (or even distribution of strains) is present. In applying Jones's method of correction it was assumed that there was such a distribution of crystallite sizes or strains in the material.

## 2.2 Electron Microscopy and Diffraction

Comprehensive accounts of the theory and practice of electron microscopy and diffraction are given by Hirsch et al (1965)(72), Kay (1965)(73) and Zworykin et al (1945)(74).

2.2.1 Theory of Electron Microscopy and Diffraction

A beam of electrons possesses wave properties similar to those of a beam of electromagnetic radiation, the wavelength being given by the de Broglie relationship

$$\lambda = \frac{h}{p} = \frac{h}{mv} \quad \ldots\ldots\ldots\ldots\ldots\ldots \text{(i)}$$

where $\lambda$ = wavelength

$h$ = planck's constant

$m$ = mass of an electron

$v$ = velocity of electron

and $p$ = momentum of the electron

If the accelerating potential difference is $V$, the energy E of an electron is given by :

$$E = \tfrac{1}{2} mv^2 = Ve \quad \ldots\ldots\ldots\ldots\ldots\ldots \text{(ii)}$$

where $e$ = electron charge

Eliminating v from equation (i) and (ii),

$$\lambda = \frac{h}{\sqrt{2mev}} \quad \ldots\ldots\ldots\ldots\ldots\ldots \text{(iii)}$$

A relativity correction has to be applied to this equation to account for the variation in electron mass with velocity, which itself depends on the voltage. In practice, however, the wavelength, if required, is determined by recording the diffraction pattern of a substance with known unit cell dimensions. This enables a single factor, the camera constant, $L\lambda$, to be calculated, where L is the effective camera length. If the same instrument, is used at the same accelerating voltage, then $L\lambda$ remains constant. At an accelerating voltage of 100 kilovolts, the wavelength of an electronic beam is 0.037Å.

In view of the fact that electrons beams possess wave properties they can be used in a magnifying instrument with electromagnetic fields as lenses, just as light waves are used

Figure 19

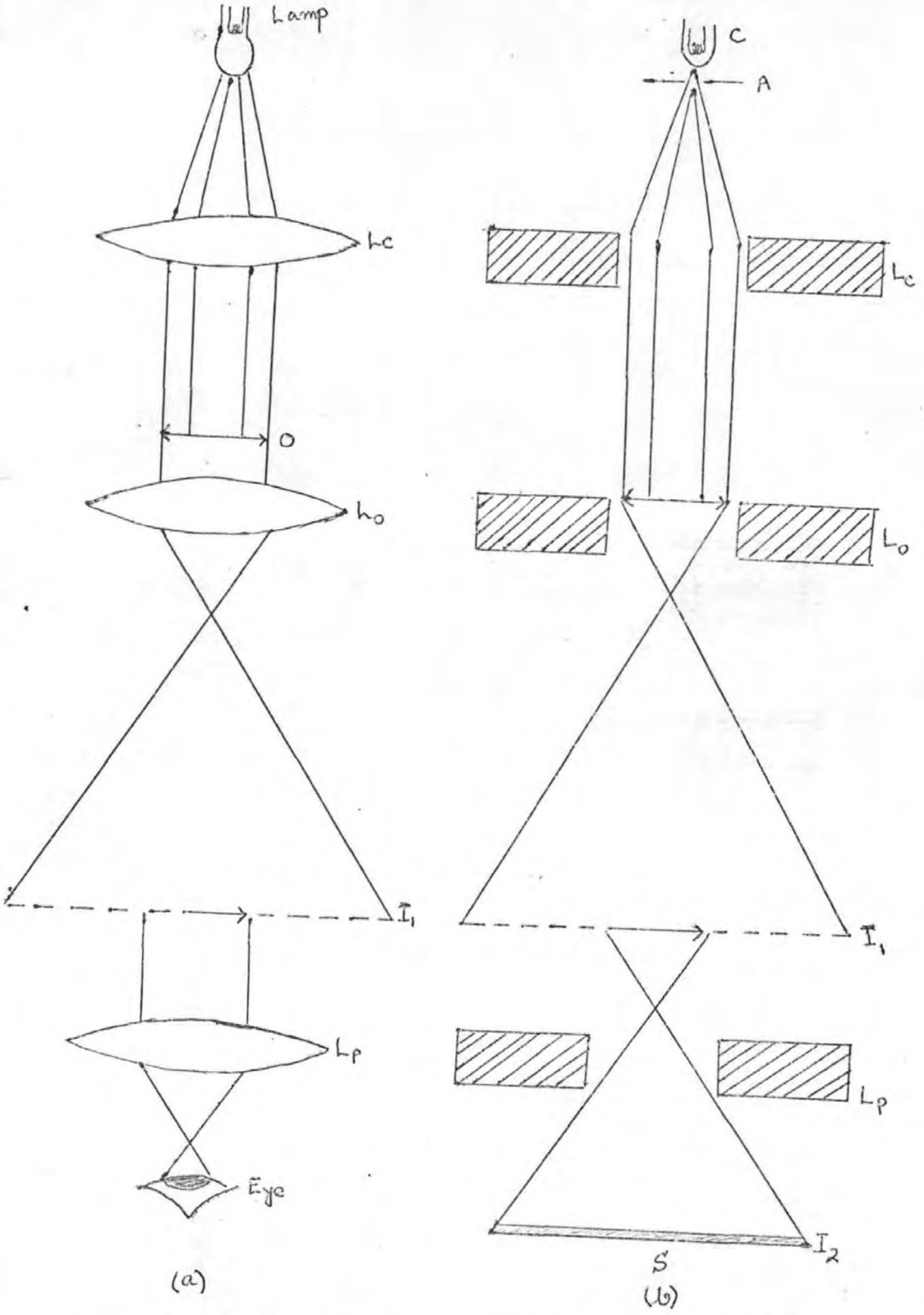


Diagramatic analogy between (a) optical and (b) electron microscopes

in the Optical microscope with glass lenses. The theoretical limit of resolution of a microscope is half the wavelength of the radiation used. For the electron microscope this is about 0.02 Å, whilst for an optical microscope it is about 2000 Å. The shorter wavelength of electrons enables a much greater resolution to be achieved on the electron microscope, although this is still very far from the theoretical limit.

The construction of an electron microscope, in principle, is similar to that of the optical microscope, Fig. 19. It consists of a cathode, C, which provides a source of illuminating electrons. A high voltage applied between C and the anode A, accelerates the electrons, which pass through a small hole in A. The condenser lens, Lc, converges the electron beam onto the specimen, O, situated in the magnetic field of the objective lens, Lo. An image, $I_1$, is formed due to magnification by the objective lens. This is followed by further magnification by the the projector lens, Lp, to form a final image, $I_2$ on a screen, S. The microscope, used in this work, consists of two or more lenses, namely a diffraction lens and an intermediate lens, placed between the objective and the projector. The intermediate lens enables a high overall magnification to be reached without the magnification of the individual lenses having to be excessively large. It also helps to keep the length of the instrument short and to attain easily a continuously varying magnification within wide limits.

The energy of electrons is reduced when they are scattered readily on collision with gas molecules. Hence the instrument is operated at a sufficiently low pressure (about $10^{-6}$ mm Hg). Focussing is achieved by the variation of the strengths of the magnetic fields by changing the currents

generating them. A phosphor screen is provided at the end of the tube to align and select a suitable part of the image, and the magnified image can also be recorded on a 35 mm photographic film held in a camera within the instrument.

Electron diffraction by a crystal is similar in principle to that of X-ray diffraction, but there are some important differences. Because of their electrical charge, electrons are heavily scattered by solid materials, and therefore the depth of the penetration of the electrons is relatively small. Hence only very thin crystals can be used in contrast to X-rays which penetrate deeply. The diffraction pattern of a single crystal consists of 'reflections' from a plane of reciprocal lattice points. For a polycrystalline specimen in random orientation, the diffraction pattern consists of concentric powder rings, provided the sample is sufficiently thin.

2.2.2 The Apparatus

The Philips EM 100B model electron microscope.

(Van Dorsten, Nienwdorf and Verhoeff (1950)(75).

The instrument has a resolution of 25Å, under normal operating conditions. The pumping system of the instrument consists of a prevacuum rotary pump, a mercury diffusion pump and an oil diffusion pump. The magnification is varied by adjusting the currents to the electromagnetic lenses. There are also control knobs provided for focussing and for moving the sample holder so that different regions of the grid can be observed.

An image of a section of the sample is thrown on the fluorescent screen directly in front of the observer. When a

micrograph of the image on the screen is required, the camera is lowered into position and the shutter opened. The exposure is adjusted according to the brightness of the image and varies upto several seconds. The magnification is determined by reading a scale and referring to standard Tables. When a diffraction micrograph is required an exclusive area of the sample is selected by means of diffraction selection diaphragms; the diffraction lens is switched on and the intermediate lens switched off. Diffraction micrographs require longer exposures because of their lower intensity, whilst transmission micrographs are exposed up to a few seconds according to the brightness of the image. The microscope was usually operated at 80 KV.

Films of carbon and metal were prepared in a "speedivac" High Vacuum Coating unit 12 E6 model, manufactured by Edwards High Vacuum Ltd. The unit consists of a glass work chamber, evacuated by an oil diffusion pump backed by a rotary pump. Inside the chamber electrical leads are fitted for striking an arc across carbon electrodes and for the vapour deposition of metal films from a filament. The pressure at the low vacuum in the work area inside the chamber was registered by a Pirani gauge and that at high vacuum by a Penning gauge. The ultimate vacuum obtainable with this unit was $3 \times 10^{-5}$ torr. The electrical supplies to the carbon electrodes and tungsten filaments were provided by a 10V, 60A source, the current being regulated as necessary by means of controls.

2.2.3 Preparation of samples

Samples of the crystalline powders for microscopic examination were made by dispersing the particles on a carbon film supported on a copper grid. The thickness of the carbon film was approximately 200Å. The copper grid had a diameter of 3 mm and a mesh of square windows, each 100 μm across. The grid was handled always by a pair of forceps with a fine grip.

The substrate used for depositing the carbon film was freshly cleared high quality mica available from "Mica and Miconite Supplies Ltd." The dimensions of the mica plates were 2 x 1 inches. A thin film of carbon was deposited on to the mica substrate placed inside the work chamber by striking an electric arc between two spectrographically pure carbon electrode. The arc voltage was 10 volts and the current 60 amperes. The arc was struck in about 8 intermittent bursts, in order to avoid overheating the carbon electrodes. Each burst was approximately of three seconds duration. The pressure inside the chamber was in the order of $3 \times 10^{-5}$ torr. The carbon film was floated off on distilled water by carefully dipping the mica substrate at an angle of about $45^{\circ}$. This operation stripped the carbon film off the mica due to the surface tension of the water. It was facilitated by trimming the mica sheet around its edges after deposition of the film and contaminating the mica sheet by breathing heavily onto it before deposition.

A section of the floating carbon film was picked up by a copper grid. The grid carrying the film was transferred to a vertical cylindrical holder and held in position with a cylindrical cap. The latter had an open end, thus exposing the

grid. Micro-crystalline samples, for direct transmission were prepared by suspending the powder in distilled water or an inert organic solvent. The particles were well dispersed by means of an ultrasonic dispersion unit. A drop of the suspension was placed on the copper grid carrying the film, and evaporated to dryness under an infra-red lamp. Finally the sample was transferred into a microscope grid holder, which was inserted in the instrument.

2.2.4 The Replica Technique and Shadow Casting

The principle of the replica technique involves the transfer of a surface topography of a solid body to a thin film which may be observed by transmission electron microscopy. The details of a surface may be sharpened by shadowing with a heavy metal which absorbs electrons strongly. Where the surface detail was of particular interest, carbon replicas with a shadow casting of palladium metal were prepared as follows :

A small amount of a polystyrene polymer was melted on a glass slide, which was held over a bunsen burner until the polymer was melted. The appropriate surface of the sintered sample was pressed into the clear melt and allowed to cool, when it solidified. The solidified polymer was immersed in dilute hydrochloric acid in order to dissolve out the sintered sample. The surface of the sintered sample thus transferred its features and impressions on to the solidified polymer, which was fixed inside the vacuum unit before a carbon film was deposited on it, as described above. The film replica so produced was then shadowed, i.e. coated with a film of palladium placed inside a helical tungsten filament. On passing a heavy current through the filament, the thin

palladium metal wire evaporated into the film at an angle of 15° to the horizontal and struck the film replica obliquely.

In this manner, the surface structure was highlighted. The polymer was dissolved away, using 1:2 dichloroethylene. The film was picked up on a copper grid, dried under an infra-red lamp and then the specimen was ready for examination, under the electron microscope.

2.2.5 Optical Microscopy

The determination of particle sizes of specimen was carried out by a Polarising Photomicroscope (manufactured by Carl Zeiss Ober Kochen/West Germany). This is the only method in which direct observation can be made of the particle size (B.S. 3406, 1963). Examination of the samples under reflected light, using a high-power objective (magnification x 16) gave an approximate estimation of single crystallite and aggregate sizes and shapes. A graticule (as described in B.S. 3625,1963) was mounted in the eye-piece (magnification x 10). The magnified image formed by the high-power objective in the plane of the graticule was viewed through the eye-piece. The total magnification obtained was x 160. A colour film has been used in order to see the internal reflections of the crystals.

To see the microstructure of the surface of the sintered cake we have also used the photomicrographic camera with Ikophot M (manufactured by Carl Zeiss Ober Kochen/West Germany).

2.3 Surface Area Measurement by Gas Sorption

When a highly disperse solid is exposed in a closed space to a gas or vapour at some definite pressure, the solid begins to adsorb the gas. This is made manifest by a gradual reduction in the pressure of the gas and by an increase in the weight of the solid. The amount of gas adsorbed on a solid

depends on, inter alia, the specific surface, i.e. the surface area per unit mass, of the solid. The mean particle size of a specimen can be calculated from its specific surface.

2.3.1 BET Procedure

The specific surface of a solid can be determined from nitrogen adsorption data by the well known and widely used method due to Brunauer, Emmett and Teller (1938)(76). The BET equation is usually expressed in the linear form

$$\frac{P}{X(Po - P)} = \frac{C - 1}{X_m C} \cdot \frac{P}{Po} + \frac{1}{X_m C}$$

where P = pressure of adsorbate vapour in equilibrium with adsorbent.

Po= saturated vapour pressure of vapour adsorbed

X = amount of vapour adsorbed ($g.g^{-1}$ or $cm^3.g^{-1}$)

C = a constant, related to the heat of adsorption

Xm= capacity of filled monolayer ($g.g^{-1}$ or $cm^3.g^{-1}$)

In the literature of the subject there are recorded very many adsorption isotherms, measured on a wide variety of solids; nevertheless the majority of those isotherms, which result from physical adsorption, may be grouped for convenience into five classes - the five typed of the classification originally proposed by Brunauer, Deming, Deming and Teller (1940)(77) (BDDT), nowadays commonly referred to as the Bruauer, Emmett and Teller (BET) classification (Fig 20). Of these only type 11 and IV can be used to calculate the specific surface of the adsorbing solid and only type IV for making an estimate of pore size distribution. The type IV isotherm also possesses a hysteresis loop, the lower branch of which represents measurements obtained by progressive addition of vapour to the system and the upper branch by progressive withdrawal. Hysteresis effects of an analogous kind are liable to be encountered with isotherms of other types.

Figure 20

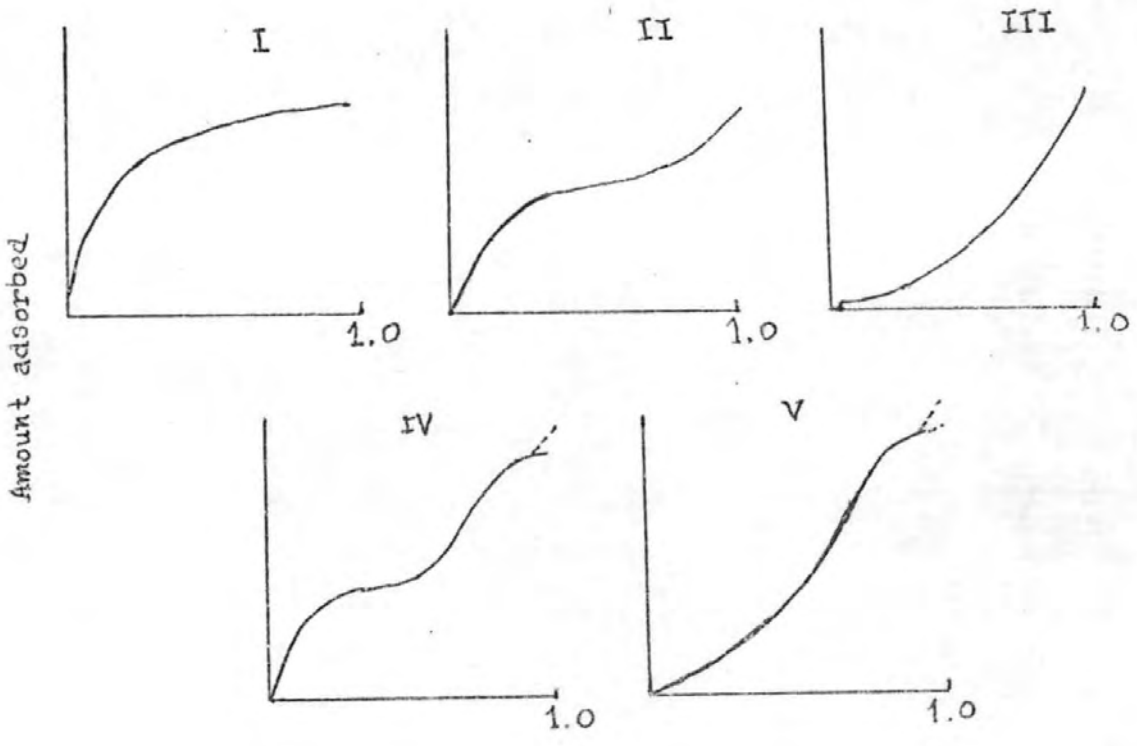


Five types of adsorption isotherm in the B.E.T. classification

However, type II isotherms give best agreement with the BET equation over limited ranges of relative vapour pressure (Gregg 1961, P.31). Thus a plot of P/X(Po-P) against P/Po results in a straight line of slope $\frac{c - 1}{X_m C}$ and intercept 1/XmC. Elimination of C from these two expressions gives Xm. The region of relative vapour pressure P/Po over which a straight line is obtained is not very great. For a type II isotherm, the value of P/Po varies between the limits 0.05 to about 0.3. The adsorbate vapour can be measured either gravimetrically or volumetrically (tensiometrically). (Gregg and Sing, 1967 P.310)(78).

The specific surface, S, is related to Xm by the equation :

$$S = \frac{Xm}{M} N.Am$$

where M = molecular weight or adsorbate,

N = Avogadro number,

Am = cross-sectional area of an adsorbate molecule in a completed monolayer.

The value of the monolayer capacity, Xm, and the specific surface, S, were calculated from the BET plots drawn graphically by hand or from computer programmes (P.O'Neill and Miss. D. Harris - see Appendix 3) checked by line-plotters. If the specific surface (S) of a powder is known the average crystallite diameter, $\ell$, can be easily determined, assuming that all the particles are spherical

$$S = \frac{4\pi(\ell/2)^2 n}{4/3\pi(\ell/2)^3 n\rho} = \frac{6}{\rho\ell}$$

where n = number of particles per gram of solid

$\rho$ = the density of the solid (adsorbed)

The assumption that all the particles are cubic leads to the same expression; similar relationships can be derived for plate and needle-shaped crystals.

2.3.2 The Apparatus

The sorption balance used in this work is based on one designed by Gregg (1946,1955)(79). The balance arms are made of glass and supported on saphire needles set into a glass cradle. One arm of the balance supports buckets for the sample and counterweights, the other arm either a solenoid or magnet enclosed in glass and surrounded by an external solenoid. The whole assembly is enclosed in glass and connected to a system of evacuation pumps, gauges and gas reservoirs. The balance used for low temperature nitrogen adsorption as described by Glasson (1956)(80) and B.S. 4359 Part 1 (1969)(81) is shown in Fig.21.

The current in the external solenoid is varied to obtain the null point, which is observed by noting the position of a horizontal metal pointer attached to the balance arm against a similar fixed point. The instrument is calibrated by measuring the current required to observe the null-point for known loadings on the balance pan.

2.3.3 The measurement of sorption isotherms

The samples for which surface areas were to be measured, were placed in turn, in the bucket and outgassed to remove physically adsorbed vapour; this was undertaken at 200°C to remove possible moisture (Glasson 1964(82)). The adsorbate was nitrogen gas and the coolant boiling liquid oxygen, so that the isotherms were measured at -183°C. The weight of the sample was determined *in vacuo* and aliquots of nitrogen gas were introduced into the system. Simultaneous readings of sample weight and nitrogen gas pressure were taken after equilibrium was reached. A final reading was recorded at just

Figure 21

The gas sorption balance

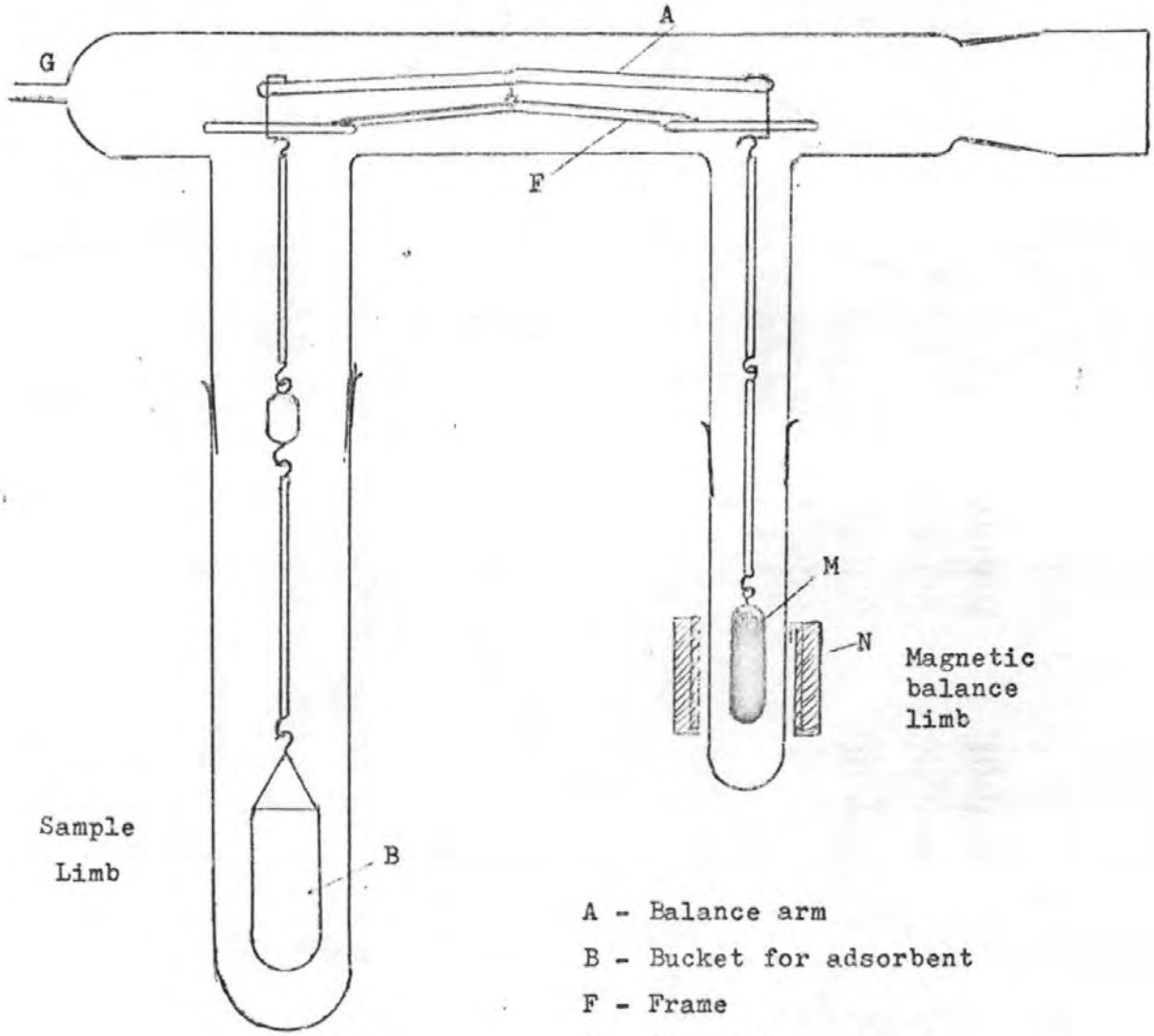


A - Balance arm

B - Bucket for adsorbent

F - Frame

G - Connection to gas handling system

M - Permanent magnet or solenoid

N - Solenoid

below one atmosphere pressure of nitrogen. To obtain the desorption branch of the isotherm, increments of the nitrogen vapour were pumped away and the change in weight of the sample again followed. All the weight changes had to be corrected for buoyancies of the samples and their containers. These were determined from experiments using materials of known X-ray density and negligible surface area.

The quarter-milligram sensitivity of the older types of vacuum balance (80) gave an accuracy of $\pm 0.1\ m^2g^{-1}$ on 10g samples, leading to possible errors of over 3% where $S < 3m^2g^{-1}$. Thus, a Sartorious Electrono Vacuum microbalance (87) proved more versatile, since it maintained an accuracy better than 3% for the less active samples, using the medium and lower sensitivity ranges for samples from 1-3 $m^2g^{-1}$ and 0.1 - $1m^2g^{-1}$ respectively. The microbalance was advantageous also where only small amounts of material were available from precipitations in more dilute solutions.

The remaining details of the technique are basically similar to those described in 1956 in the original paper involving use of a vacuum balance for low-temperature surface area determination (80). Thus, the liquid-oxygen bath remained constant within the $\pm$ 0.2° and at least 1 hr was allowed for the sample to attain a constant temperature. In practice, the sample is generally up to about 1° warmer than the liquid oxygen outside the balance limb (as indicated by internal and external thermocouples). The sample shows a temperature constancy similar to that of the bath ($\pm$ 0.2°) and dependent to some extent on the sizes of the sample containers and hangdown tubes ( up to 30 mm diameter), depth of immersion in the liquid oxygen (over 15 cm) and possibly on the surrounding nitrogen gas pressure.

By standardising the equipment and improving the heat insulation at the top of the Dewar flask, the sample temperature is kept within $\pm$ 0.1°, thereby minimising the variation in the s.v.p. of the nitrogen to preserve an accuracy of better than 3% in the surface area determination.

The oxygen isotherms, which extended to a relative pressure P/Po, near unity, exhibiting little or no hysteresis at P/Po $<$ 0.3; an example of one of the more active of the zinc sulphide samples is illustrated in Fig. 21a.

From these and the nitrogen isotherms, S could be calculated by the BET procedure (76) by use of values of 14.1Å$^2$ and 17.0Å$^2$ for the cross-sectional areas, Am of oxygen and of nitrogen; this gave agreement within Ca 5% in the values of S obtained from both series of isotherms. The older graphical and newer computer (with line-plotter) methods agreed within $\pm$ 1% for values of S from each individual isotherm.

## 2.4 Thermometric Analysis

There are a number of analytical techniques which come under the title of thermometric analysis. Of these, perhaps, two are most widely applied. One, thermogravimetric analysis (T.G.A.) is a technique whereby the weight of a sample can be followed over a period of time while its temperature is being changed; usually it is increased at a constant rate. It is particularly suited for measuring the loss of weight on the decomposition of a solid to a solid residue and to a gas, and gives an indication of the thermal stability of a compound in inert and in reactive atmospheres. The second widely-used method of thermometric analysis is that of differential thermal analysis (D.T.A,).

Fig 21a

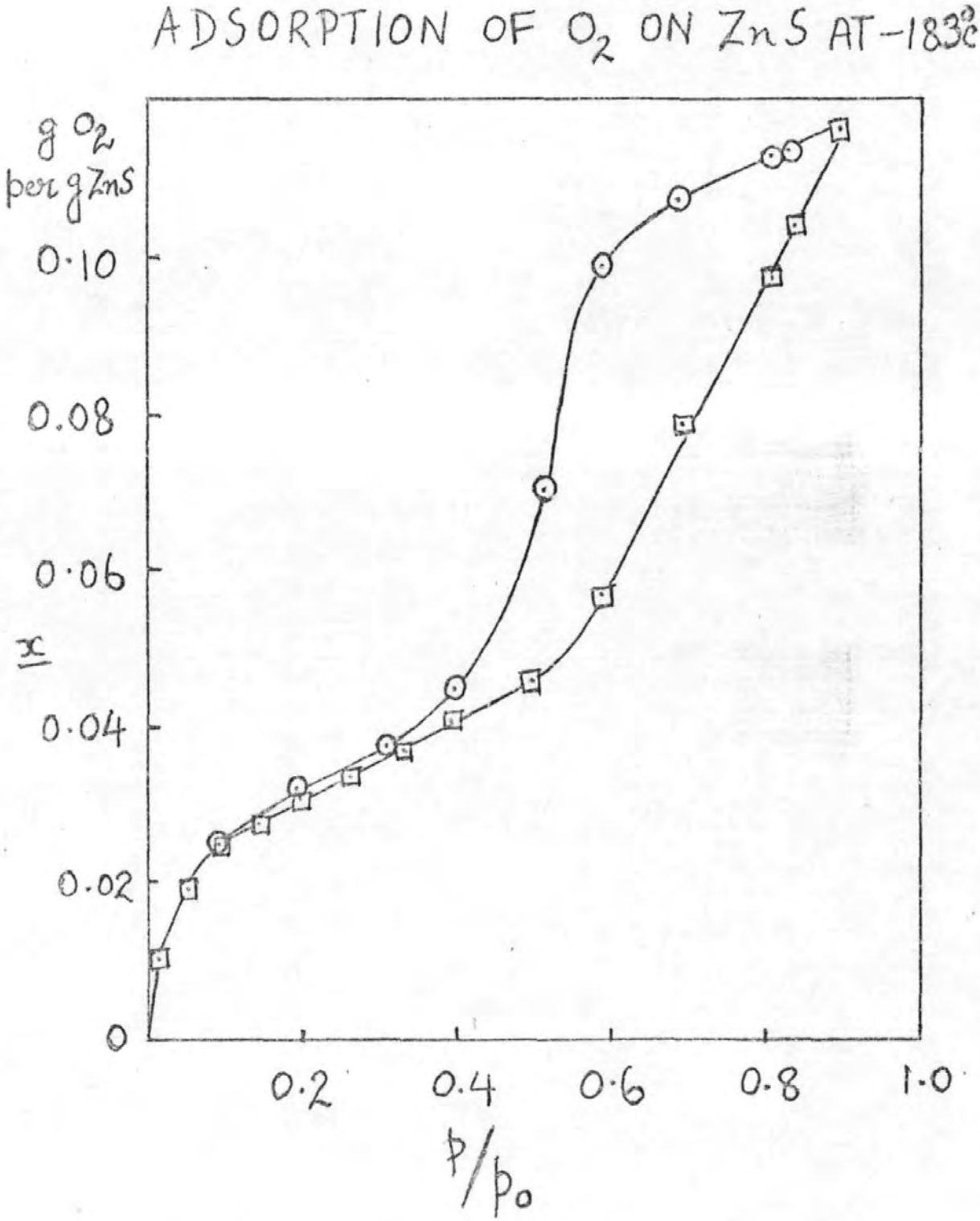
ADSORPTION OF $O_2$ ON ZnS AT -183°C
g $O_2$ per g ZnS
0·10
0.08
0·06
x
0·04
0.02
0
0.2
0.4
0·6
0.8
1·0
p/p₀

2.4.1 Thermal Balance

The thermal balance usually consists of a modified single or double pan analytical balance (Gregg and Winsor, 1945(83)). In the present investigation, a Stanton-Redcroft Model A.49, balance was used, which could detect a weight change of $10^{-4}$g. One pan of the balance was furnished, on its underside, with a hook carrying a length of nichrome wire. The wire passed through a hole in the balance shelf and supported a sample bucket, made of silica which was suspended in an electric furnace. The temperature in the vicinity of the sample was measured using a chromel-alumel thermocouple placed close to the sample bucket and attached to a millivolt meter. The general arrangement is shown in Fig 22. 1 g. of the powder under test was accurately weighed into an alumina crucible attached to the balance and the weight noted. The thermal programmer was set to give a linear rise ($20^{\circ}$/min) from the ambient to the set temperature for the run, and the weight of the crucible recorded at known intervals of time. In the present work the reacting gas was air. The weight loss of the specimen was plotted against the corresponding time to provide oxidation rates.

2.4.2 Differential Thermal Analysis

Differential thermal analysis (D.T.A.) was first applied by Houldsworth and Cobb (1922)(84). Thermocouples embedded in the test and inert materials were connected in opposition so that any appreciable E.M.F. set up during the heating resulted from the evolution or adsorption of heat in the test sample; the temperatures at which such changes occurred were noted.

This is a technique by which phase transitions or chemical reactions can be followed by observation of the heat absorbed or liberated.

Figure 22

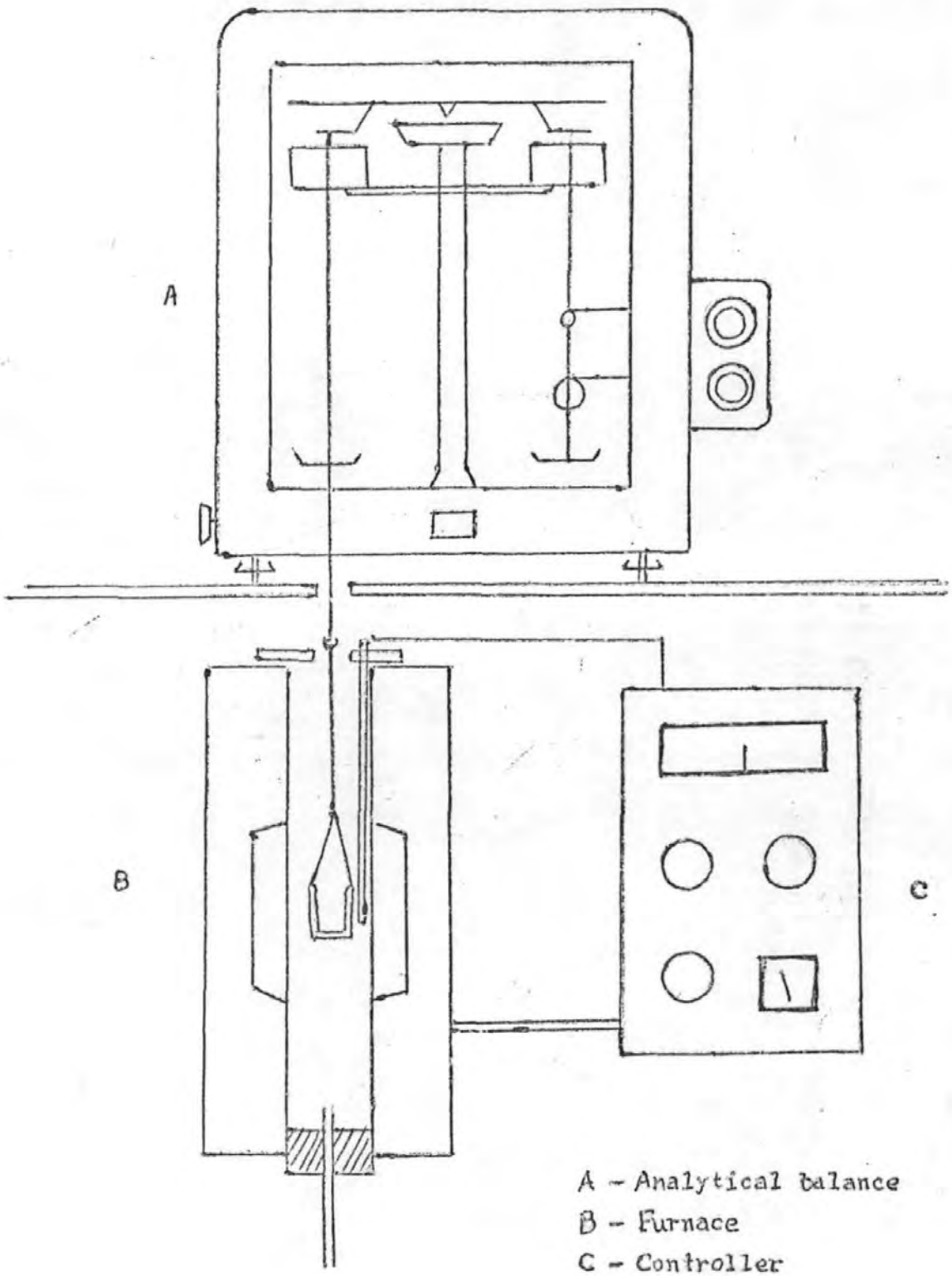


THERMAL GRAVIMETRIC ANALYSIS APPARATUS

D.T.A. equipment was designed by Grimshaw, Heaton and Roberts (85). In our apparatus, Fig 23, one set of thermocouple junctions, is inserted into an inert material, such as aluminium oxide $Al_2O_3$ which does not change in any manner through the temperature range studied. The other set of thermocouples is placed in the sample under test. A weighed amount of sample is taken each time. The sample is rested on quartz wool and the top of the sample is covered with a piece of quartz wool each time.

With constant heating, controlled by (Stanton-Redcroft) heat controller, any transition or thermally-induced reaction in the sample is recorded automatically in the X-Y chart recorder as a peak or dip.

An endothermic process will cause the thermocouple junction in the sample to lag behind the junction temperature in the inert material, and hence develope a voltage; an exothermic event will cause a voltage of opposite sign. It is customary to plot exotherms upward, endotherms downwards.

Figure 23 shows schematically the essential parts of the D.T.A. apparatus, which includes provision for bathing the sample with a controlled atmosphere; the gas can be made to flow at a desired rate (measured by means of a flow meter) through the bed of particulate sample, thereby flushing away any gaseous product of decomposition.

Figure 23

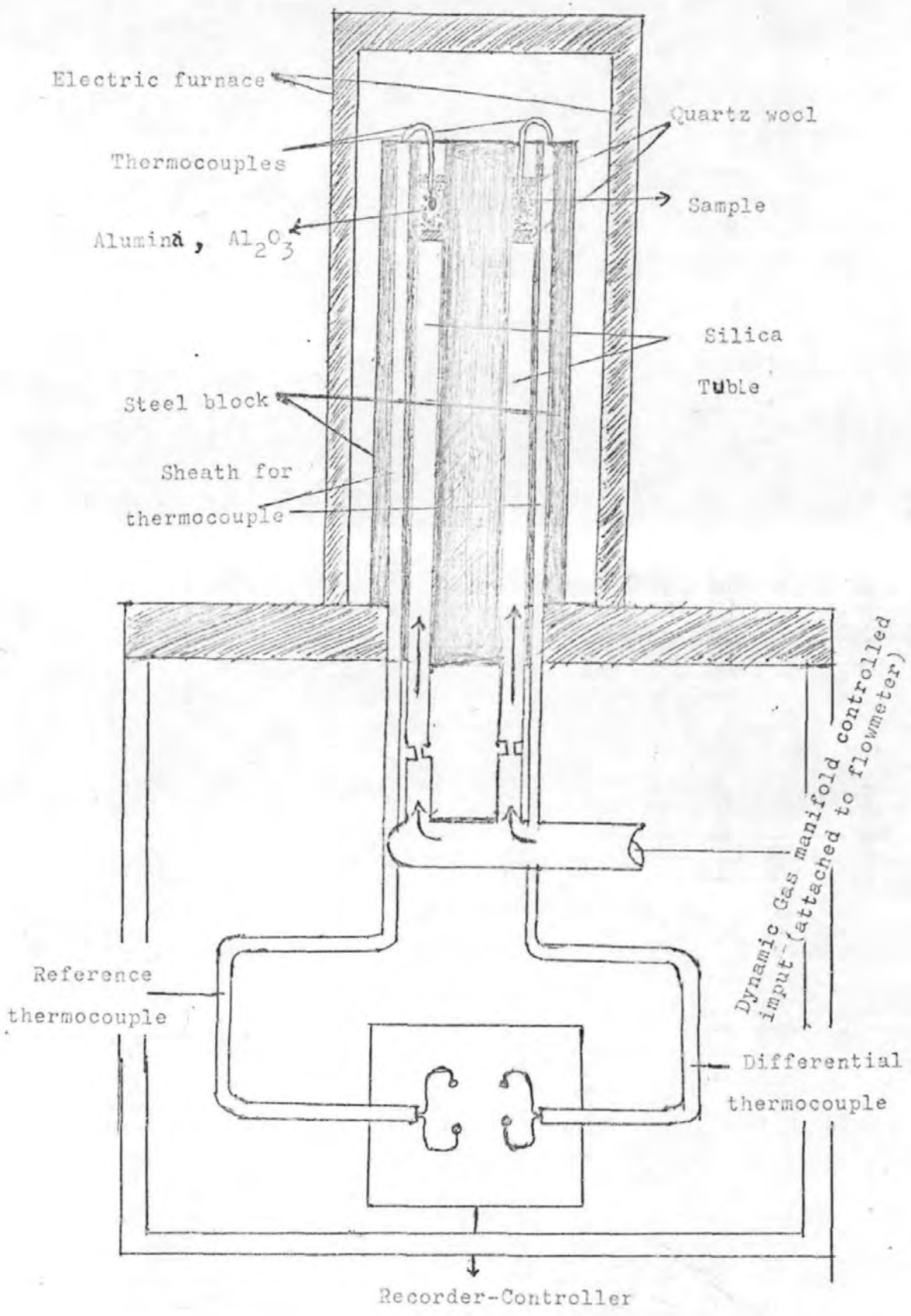


D.T.A. APPARATUS

## Chapter 3

### PRECIPITATION AND AGEING OF ZINC SULPHIDE

For basic oxidation studies, finely-divided zinc sulphide samples of widely different specific surfaces were precipitated from solution at various pH levels and in the presence of different concentrations of electrolytes.

Samples of Zinc sulphide were precipitated in acidic media by passing hydrogen sulphide at a flow rate of 5 l/h through a gas-dispersion tube into solutions (50 - 500 ml) of M.-, 0.25M- and 0.1M- $ZnSO_4$ or $ZnCl_2$ at 20° or 85°. After 1h, the precipitates were filtered off, washed twice with 50 ml-portions of acetone to remove immediately most of the water left in contact with them, thereby arresting any further ageing, cf. treatment of calcareous materials (D.R. Glasson, 1960)(86). The last traces of acetone and water were removed by outgassing the samples at 200° *in vacuo* on an electrical sorption balance (Gregg, 1946 and Sartorius-Werke, 1965)(87) before measurement of their surface areas by the BET method from adsorption isotherms of nitrogen determined at -183°.

Zinc sulphide samples were precipitated in alkaline media by adding stoicheiometric amounts of M-$ZnSO_4$ or $ZnCl_2$ to M- or 0.1M-$Na_2S$. The specific surfaces of the zinc sulphide precipitates were practically independent of the standard rate of addition (5 ml per minute) of one reactant to the rapidly-stirred solution (50-500 ml) of the other; only if the rate of addition were considerably increased (and/or the rate of stirring considerably decreased) did the specific surface decrease appreciably, since the concentration of the additive at the time of precipitation would then be increased,

cf. precipitation of calcium carbonate from solution (D.R.Glasson 1960)(86). These samples were filtered off after 1 hour and washed with acetone to remove most of the remaining water and thus prevent possible ageing, before drying and examination on the sorption balance in the same way as the samples precipitated in the acidic media.

A few zinc sulphide samples were precipitated in the acidic or alkaline media in the presence of 50 g. dissolved sodium chloride. Additional zinc sulphide samples were prepared in less acidic and less alkaline conditions. M-$Na_2S$ was added to 0.1M-$ZnSO_4$, giving precipitation at pH values increasing from about 5 to 7. Zinc oxide was dissolved in 3M-$NH_4OH$ (providing a Zn concentration of 0.1M-, D.R. Glasson and S.A.A.Jayaweera, 1968)(88) and then treated with hydrogen sulphide, giving precipitation at pH values decreasing from about 11 to 9.

The zinc sulphide samples were X-rayed using a Solus-Schall diffractometer (Cu$K\alpha$-radiation) with Geiger counter and rate meter. Certain samples were examined further for morphology and aggregate sizes by optical and electron-microscopes (Philips EM-100).

## 3.1 RESULTS

In Fig.24, the variations in specific surface, S, and average crystallite size are shown for zinc sulphide samples aged for different lengths of time in acidic or alkaline media at lower electroleye concentrations (ca.0.1M). The average crystallite sizes have been calculated (for a cubic habit) from the specific surface measurments and the density of the zinc sulphide (4.09 g $cm^{-3}$) obtainable from the X-ray diffraction pattern, blende (sphalerite) form of ZnS, except for those precipitated in less acidic media by the addition of M-$Na_2S$ to 0.1M-$ZnSO_4$) which contained some basic

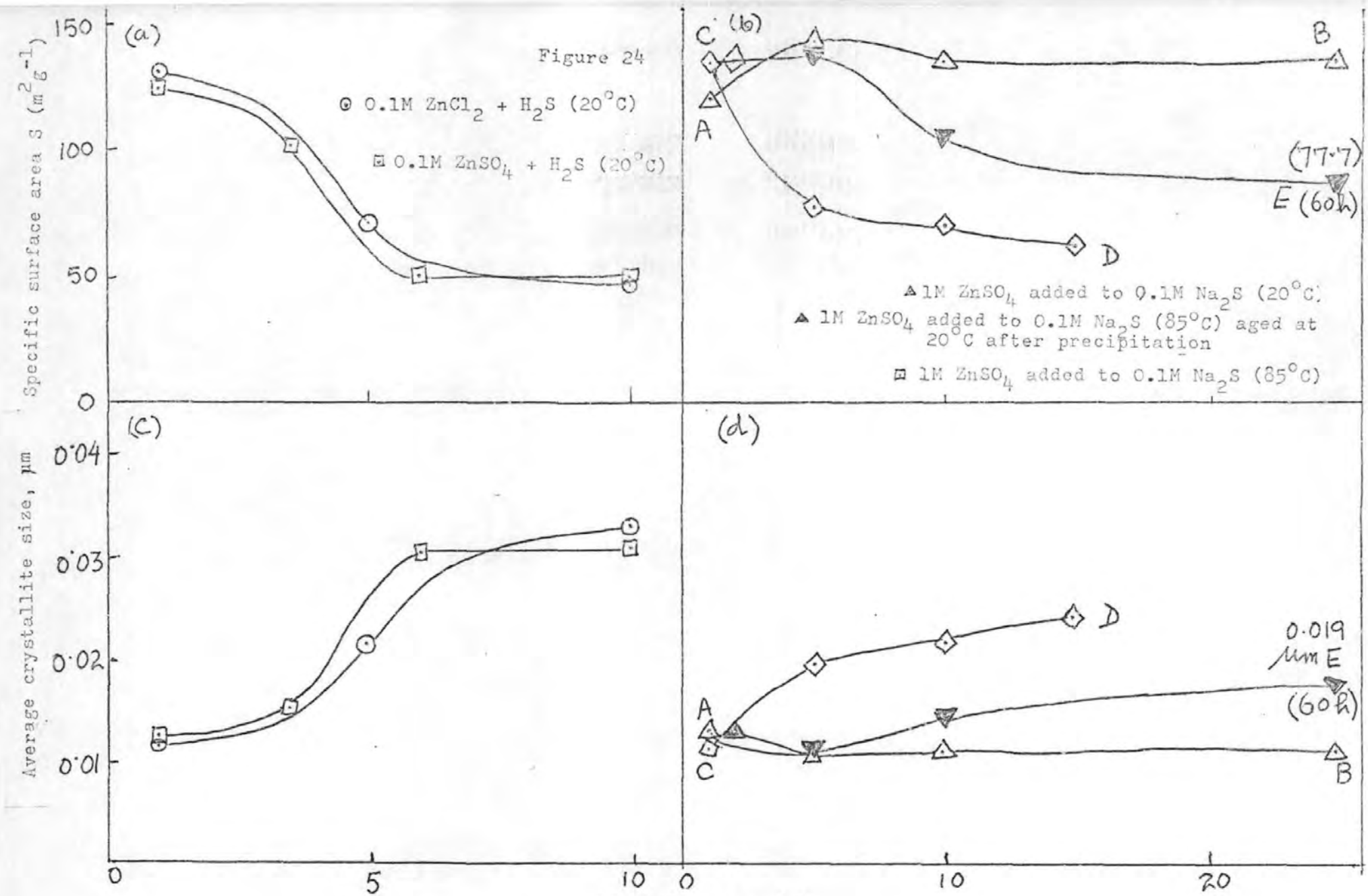


Precipitation and ageing of zinc sulphide in acidic or alkaline condition.

zinc salt. The half-peak widths of the 111, 200 and 220 "reflections" of the cubic-F (Zinc blende) crystal lattice were measured from some of the X-ray diffractometer traces. This also afforded approximate estimates of the average crystallite sizes (D.R. Glasson, 1964)(89) using the Jones method (F.W. Jones, 1938) for calculating intrinsic line-broadening.

The specific surfaces and average crystallite sizes of the zinc sulphide samples newly-precipitated in acidic or alkaline media at higher electrolyte concentrations (0.25 to 1M) are summarised in Table 10, where they are compared with those for samples precipitated at lower electrolyte concentrations (ca.0.1M).

Electron-micrographs are presented in Figs. 25-30 showing differences in morphology and aggregate sizes when the zinc sulphide samples are precipitated and aged in acidic and in alkaline media.

## 3.2 DISCUSSION

The pH conditions have a considerable effect on crystallite and aggregate size largely because they affect the solubility and hence the supersaturation ratio of the zinc sulphide; greater supersaturation ratio causes nucleation to predominate over crystal growth, giving smaller crystallites. The ageing of the precipitates proceeds by Ostwald ripening supplemented by coagulation, especially in the presence of higher concentration of surrounding electrolytes.

### 3.2.1 Precipitation and ageing at lower electrolyte concentration

When zinc sulphide is precipitated by hydrogen sulphide from 0.1M-$ZnSO_4$ or $ZnCl_2$, the pH progressively decreases from about 5 to 1. The average crystallite sizes of the products (calculated from specific surface measurements) are about 100 Å (0.01 μm) as shown in Fig 24. Subsequently, these sizes increase to about 300Å (0.03 μm) as the zinc sulphide ages for a total of 10 h at 20°,

TABLE 10

Zinc sulphide samples precipitated at different electrolyte concentrations

| Precipitation conditions (aged 1 h) | Surface area S $m^2 g^{-1}$ | Average crystallite size ($\mu$ m) calculated from | |
|---|---|---|---|
| | | S | x-ray peaks |
| Alkaline media | | | |
| 1M-$ZnSO_4$ added to 500 ml 0.1M-$Na_2S$ | 116.4 | 0.0126 | 0.0030 |
| 1M-$ZnSO_4$ added to 50 ml 1M-$Na_2S$ | 94.0 | 0.0157 | 0.0030 |
| Acidic media | | | |
| 500 ml 0.1M-$ZnSO_4$ + $H_2S$ | 122.8 | 0.0120 | 0.0050 |
| 50 ml 1M-$ZnSO_4$ + $H_2S$ | 54.0 | 0.0270 | 0.0680 |
| 500 ml 0.1M-$ZnSO_4$ + 50g NaCl + $H_2S$ | 80.0 | 0.0184 | 0.0039 |
| 500 ml 0.1M-$ZnCl_2$ + $H_2S$ | 129.4 | 0.0114 | 0.0044 |
| 500 ml 0.25M-$ZnCl_2$ + $H_2S$ | 59.8 | 0.0245 | 0.0039 |
| 500 ml 0.25M-$ZnCl_2$ + 50 g NaCl + $H_2S$ | 60.6 | 0.0242 | 0.0044 |

FIGURE 25

(a)

0.1M $ZnSO_4$ + $H_2S$ (1h ageing)

Magnification: x 20,000

(b)

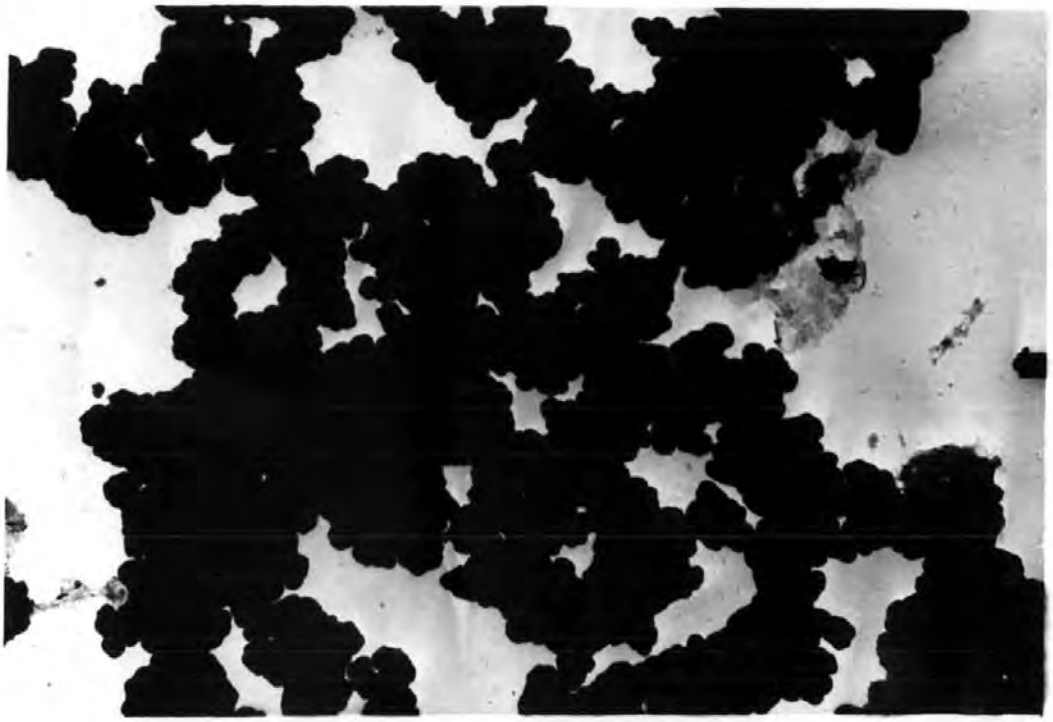

0.1M $ZnCl_2$ + $H_2S$ (1h ageing)

Magnification: x 20,000

FIGURE 26

(a)

0.1M $ZnSO_4$ + $H_2S$ (10h ageing)

Magnification: x 20,000

(b)

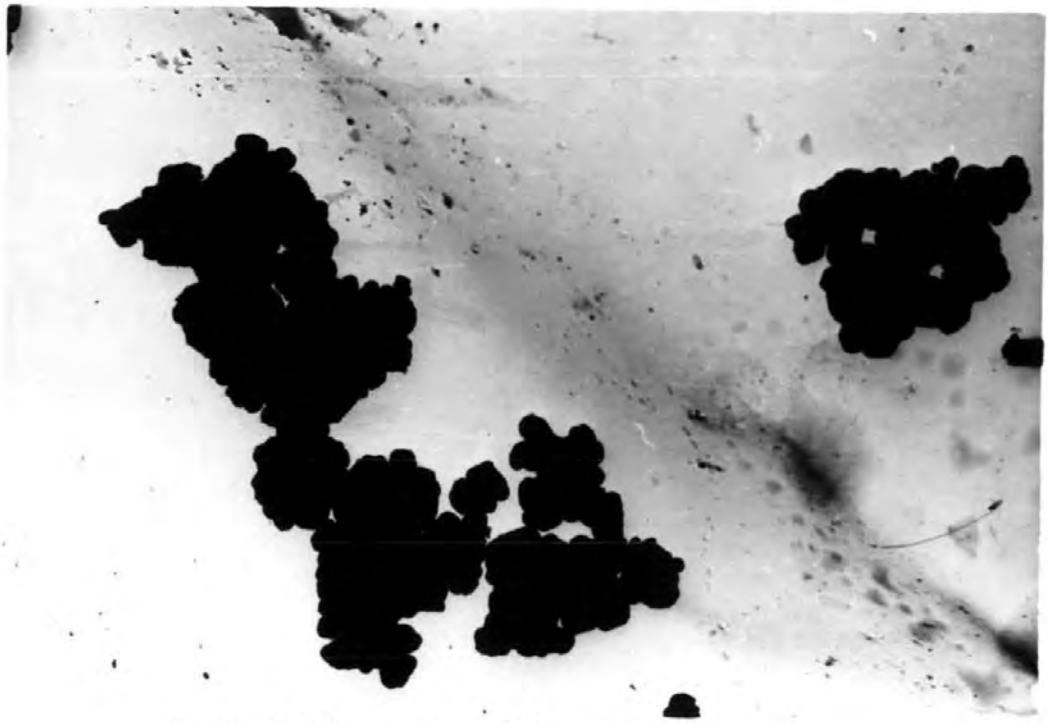

0.1M $ZnCl_2$ + $H_2S$ (10h ageing)

Magnification: x 20,000

FIGURE 27

(a)

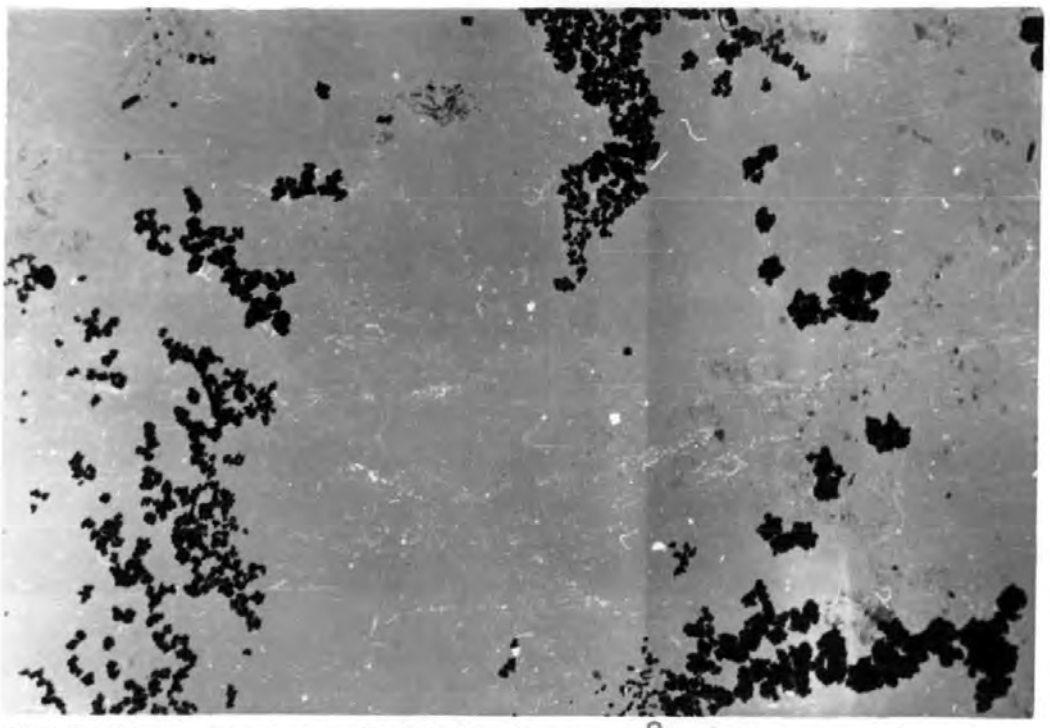

1M $ZnSO_4$ added to 0.1M $Na_2S$ at 20°C (1h ageing)

Magnification: x 20,000

(b)

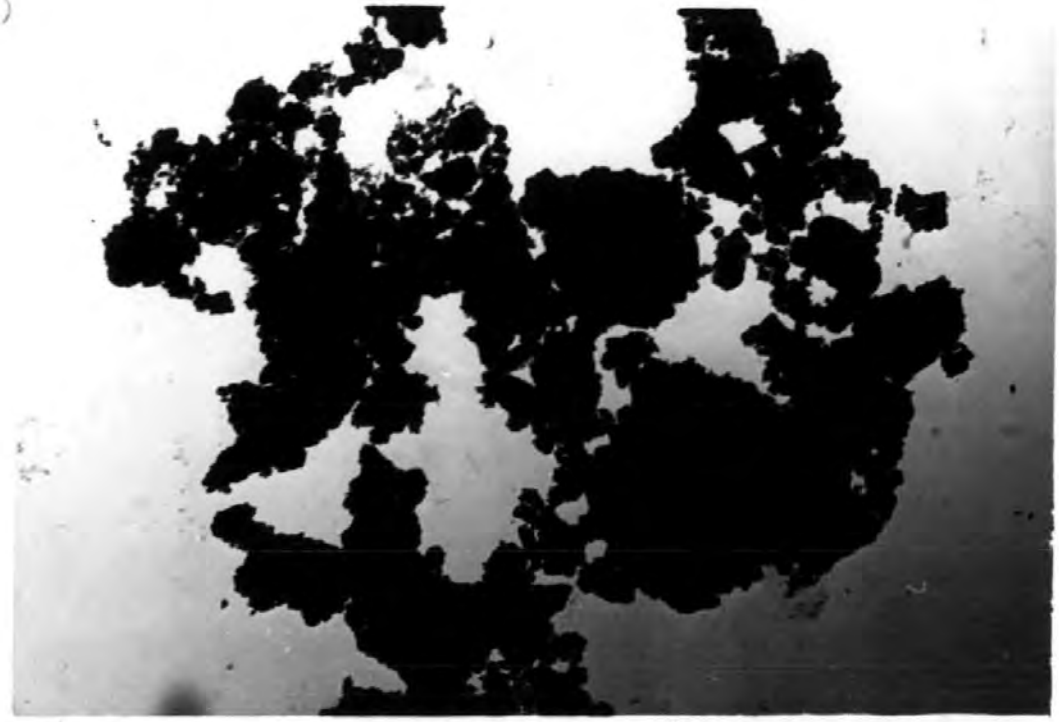

1M $ZnSO_4$ added to 0.1M $Na_2S$ at 20°C (10h ageing)

Magnification: x 20,000

FIGURE 28

(a)

0.25 $ZnCl_2$ + $H_2S$ + 50g NaCl (1h ageing)

Magnification: x 20,000

(b)

1M $ZnCl_2$ added to 0.1M $Na_2S$ at 20°C (1h ageing)

Magnification: x 20,000

FIGURE 29

(a)

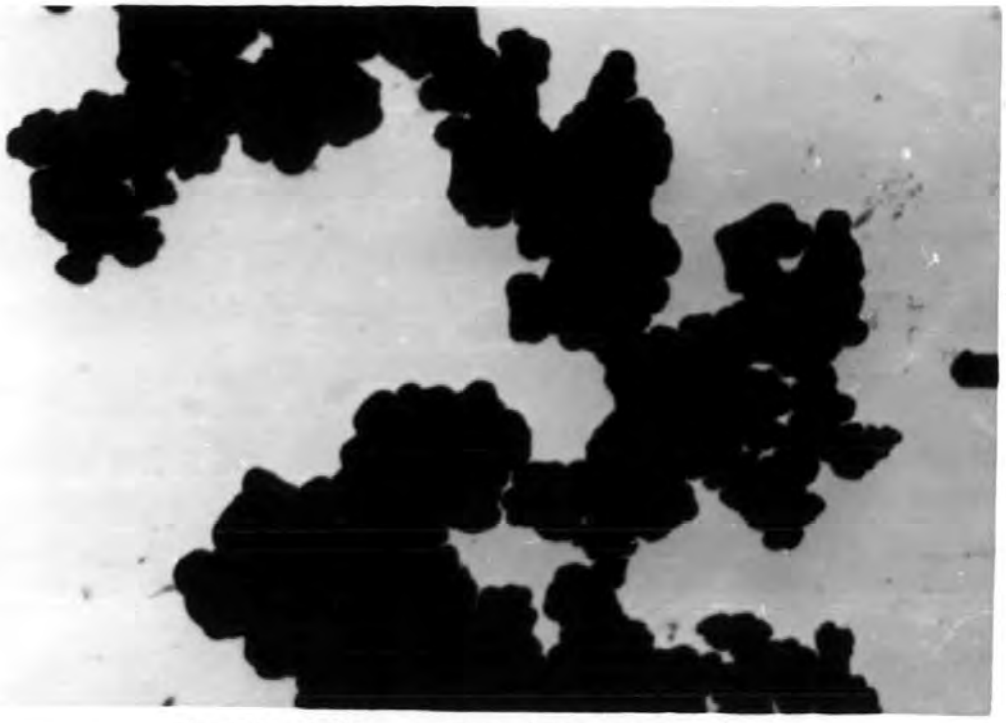

0.25M $ZnCl_2$ + $H_2S$ (1h ageing)

Magnification: x 20,000

(b)

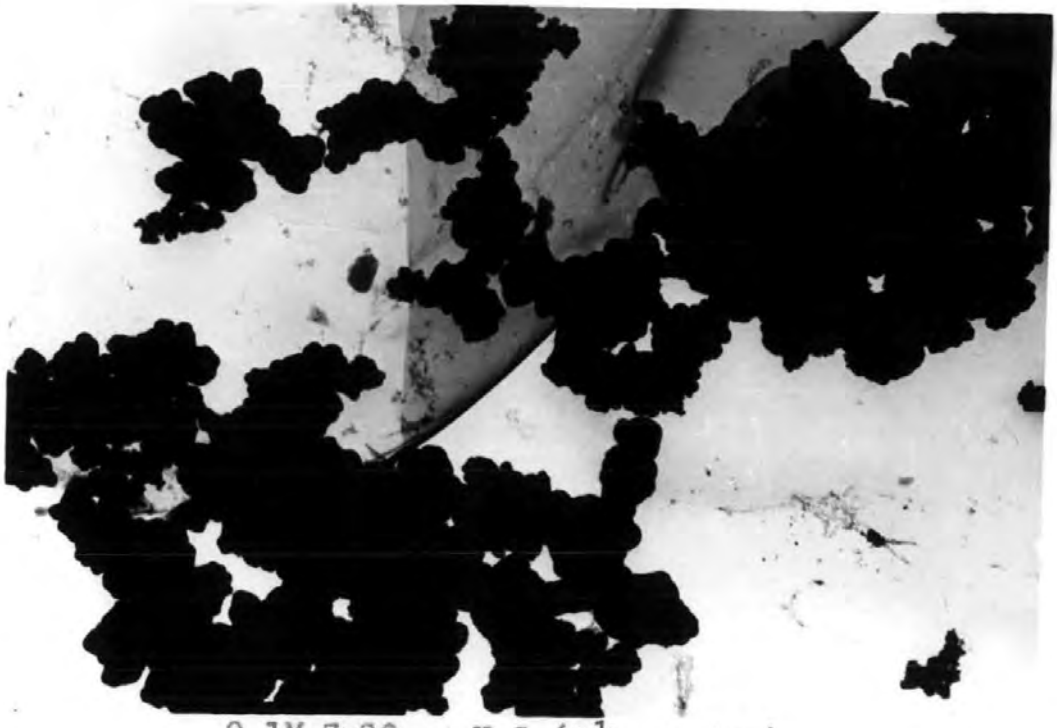

0.1M $ZnSO_4$ + $H_2S$ ($3\frac{1}{2}$h ageing)

Magnification: x 20,000

FIGURE 30

(a)

1M $ZnSO_4$ added to 0.1M $Na_2S$ at 85°C (10h ageing)

Magnification: x 20,000

(b)

1M $Na_2S$ added to 1M $ZnSO_4$ at 20°C (1h ageing)

Magnification: x 20,000

finally acquiring a comparatively slow crystallite growth rate. The close similarity of the specific surface (and average crystallite size) curves indicates that at electrolyte concentrations below 0.1M- the greater coagulating effect of the divalent sulphate ion compared with the univalent chloride ion is not prominent in promoting crystallite growth.

Similar specific surfaces and average crystallite sizes are given initially when zinc sulphide is precipitated in alkaline conditions, viz. from zinc sulphate solutions added to 0.1M-$Na_2S$ at $20^0$, Fig 24, curves AB. Subsequently, the specific surface somewhat increases ( and the average crystallite size decreases), before the material ages much more slowly than in acidic media. The initial increase may arise from removal of strains or defects in the newly-formed zinc sulphide as it recrystalises to its normal lattice structure. This effect has been found previously with some newly-hydrated limes and magnesias (D.R. Glasson, 1960 and 1964)(86, 82).

The zinc sulphide precipitated at $85^0$ initially has a greater specific surface (and smaller average crystallite size) than that prepared at $20^0$, points A and C in Fig 24(b) and (d). Evidently, the nucleation is much faster at the higher temperature, which produces a larger number of smaller crystallites and more than compensates for the loss of surface caused by the increased rate of crystal growth. Thus, the zinc sulphide precipitated and aged at $85^0$ (curve CD) subsequently has a much smaller specific surface (and larger crystallite size) than that prepared and aged at $20^0$ (curve AB). As expected, the sample precipitated at $85^0$ ages afterwards at $20^0$ more slowly than it does at $85^0$, curves CE and CD.

However, this ageing at 20° is faster than that of the sample initially prepared at 20° , curves CE and AB. This is in accord with the sample precipitated as 85° having initially a larger number of smaller crystallites (below a critical size) which redissolve and deposit on the larger crystallites in the Ostwald ripening process (A.E. Neilsen, 1964)(32).

Average crystallite size values of the same order (as those from specific surfaces) have been obtained from X-ray line-(or peak-) broadening measurements. They are smaller but show the same general trends in variation as the materials are aged. Thus, in acidic media these average crystallite sizes vary from 0.0050 to 0.0088 μm with 0.1M.$ZnSO_4$ and 0.0044 to 0.0088 μm with $ZnCl_2$. In alkaline media, the initial sizes and subsequent increases on ageing are somewhat smaller, viz. 0.0030 to 0.0054 μm and 0.0028 to 0.0044 μm for zinc sulphate added to 0.1M-$Na_2S$ at 20° and 85° respectively; also 0.0028 to 0.0031 μm for the sample precipitated at 85° and aged at 20°.

In comparing the values of the average crystallite sizes determined from specific surfaces and X-ray line-(peak-) broadening, there are 2 - 4-fold and 5 - 6-fold differences in acidic and alkaline media respectively. These are ascribed to differences in porosity, crystal strain and defects and especially crystallite size distribution. Variations due to porosity and crystal strain are comparatively small, since the nitrogen adsorption isotherms showed little hysteresis and the precipitation processes did not involve interconversion of solid material, only the more stable (cubic) form of zinc sulphide being obtained. The calculation of average crystallite sizes from specific surfaces assumes no

particular crystallite size distribution, whereas that from X-ray measurements assumes a Gaussian distribution. Nevertheless, the X-ray measurements again indicate that the samples precipitated and aged in alkaline media (compared with acidic media) generally have the smaller crystallite sizes.

3.2.2. Morphology and aggregate sizes

In addition to differences in crystallite sizes, the samples vary also in morphology and aggregate sizes. This is illustrated in Figs.25-30 where the samples precipitated from acidic media appear to have smaller ranges of aggregate sizes than those from alkaline media, (a) and (b) for $ZnSO_4$ (0.1-0.2 $\mu$m and 0.1-1 $\mu$m) and (c) and (d) for $ZnCl_2$ (0.1-0.5 $\mu$m and 0.1-2 $\mu$m). In the latter case, the formation (and presence) of sodium chloride during the alkaline precipitation affects the crystal habit, causing the aggregates to have a plate-like morphology, (d); many of them are larger than those obtained in the corresponding precipitation from 0.1M-$ZnSO_4$ in (b); the crystallites are about twice as large ($S$ = 56.3 $m^2g^{-1}$; average crystallite size, 0.0261 $\mu$m, compared with 116.4 $m^2g^{-1}$, 0.0126 $\mu$m).

3.2.3 Precipitation in less acidic and alkaline media

Smaller-sized zinc sulphide crystallites are obtained also in less alkaline conditions from zinc oxide dissolved in 3N-$NH_4OH$ and treated with hydrogen sulphide, giving precipitation at pH values decreasing from about 11 to 9. Even after 15 h. ageing at 20°, the specific surface is 124 $m^2g^{-1}$ and average crystallite size 0.0119 $\mu$m (or 0.0064 $\mu$m from X-ray peak-broadening). Much larger crystallite sizes are given in less acidic media when M-$Na_2S$ is added to 0.1M-$ZnSO_4$, with precipitation at pH values increasing from about 5 to 7. The precipitation is accompanied by

hydrolysis of the zinc salt, the newly-formed product having a specific surface of only 14.9 $m^2 g^{-1}$ and an average crystallite size as large as 0.0987 μm.

3.2.4 Precipitation and ageing at higher electrolyte concentrations

The specific surfaces and corresponding average crystallite sizes of the zinc sulphide samples precipitated in alkaline media are not changed considerably when the concentration of the sodium sulphide is increased from 0.1 to 1M, Table 10. The changes are more considerable in acidic media when the concentration of zinc sulphate or zinc chloride are increased from 0.1 to 1M or 0.25M respectively (Table 10). Addition of sodium chloride to 0.1M-$ZnSO_4$ also causes decreases in specific surface and increases in corresponding average crystallite size, but it does not cause further changes of this type when added to 0.25M-$ZnCl_2$. However, the presence of higher concentrations of chloride ions seems to change the crystallite size distributions, since the average crystallite sizes calculated from X-ray (line-) peak-broadening given abnormally lower values. Nevertheless, the aggregate sizes (Figs. 25 - 30 increase somewhat from submicron sizes at the lower electrolyte concentrations, viz. 0.1-0.2 μm for 0.1M-$ZnSO_4$ + $H_2S$, 0.1-0.5 um for 0.1M-$ZnCl_2$ + $H_2S$ compared with 0.2-5 μm for 0.25M-$ZnCl_2$ + $H_2S$ alone or in the presence of sodium chloride.

## Chapter 4

### Oxidation of pure Zinc Sulphide

The experiments were carried out on synthetic ZnS, i.e. $\alpha$-ZnS, Wurtzite (BDH) and $\beta$-ZnS, Zinc blende prepared by introducting $H_2S$ into a solution of 0.1M-$ZnSO_4$ (90).

### 4.1 Thermogravimetric Analysis (TGA)

The roastings were done on a thermogravimetric balance. About 1g of the sample was taken each time separately in a porcelain crucible and a platinum crucible and introduced into the even-temperature zone of the reaction furnace. The temperature was controlled to within $\pm$ 5°C of the operating temperature by means of a temperature controller. The experiments were conducted at different temperatures ranging from 530° - 850°C for $\alpha$- and $\beta$-ZnS. At the end of the experiment, the crucible was taken out of the furnace and the oxidised sample was analyzed for zinc sulphate and zinc oxide.

#### 4.1.1 Chemical Analysis

The roasted sample (about 1g) was treated with hot water and filtered. The filtrate contained zinc sulphate. The residue was treated with ammonium hydroxide and ammonium chloride at room temperature. This dissolved out zinc oxide. The zinc content of the filtrate in each case was determined with the disodium salt of ethylenediamine tetra-acetic acid (EDTA), using Erichrome black-T as indicator (91).

#### 4.1.2 Differential Thermal Analysis (DTA)

In our apparatus as described previously in Chapter 2, one set of thermocouple junctions is inserted into an inert material, such as aluminium oxide, $Al_2O_3$, which does not change in any manner through the temperature range studied (0° - 1000°C). The other set of thermocouples is placed in the sample under test. A weighed

amount of sample (about 0.1g) is taken each time. The sample is rested on a piece of quartz wool and the top of the sample is covered with a piece of quartz wool each time. With constant heating, 10°C/min, controlled by the Stanton-Rederoft heat controller, any transition or thermally-induced reaction in the sample is recorded automatically in the x - y chart recorder as a peak or dip. There was a provision for bathing the sample with a controlled atmosphere; the gas can be made to flow at a disired rate by means of a flowmeter (e.g. 80 $cm^3$/min).

4.2 Results and Discussion: TGA

The results obtained for roasting $\alpha$- and $\beta$-ZnS, using porcelain and platinum crucibles at the temperature range 520° to 850°C are given in Table 11 and 12.

The relative amounts of products formed at the end of roasting are given in Figures 31-34.

When pure zinc sulphide is roasted, the main reaction products are zinc oxide, zinc sulphate, sulphur dioxide and sulphur trioxide. It is also possible that a basic sulphate ($ZnO.2ZnSO_4$) is formed. Actually, the basic sulphate has been identified in the roasted sample particularly at temperatures $\geq$650°C for $\beta$-ZnS and $\geq$700°C for $\alpha$-ZnS by X-ray diffraction.

4.2.1 Formation of zinc sulphate, basic sulphate and oxide

Under equilibrium conditions, basic sulphate could possibly be formed above 700°C. It was not possible to estimate separately the basic sulphate formed in the presence of both oxide and sulphate.

In some of the isothermal oxidations for different time intervals, the amount of zinc sulphate formed reached a maximum value during the early stages and with further roasting the amount formed decreased, e.g. Figures 35-36 and Table 13.

TABLE 11

α-ZnS Calcined for 40 minutes

| Temp °C | Zinc % (in terms of total zinc in the product) | | | % Conversion of ZnS | Mol. ratio ZnO : $ZnSO_4$ |
|---|---|---|---|---|---|
| | as ZnS | $ZnSO_4$ | ZnO | | |
| (a) with porcelain crucibles | | | | | |
| 530° | 93.7 | 0.30 | 6 | 6.3 | 23 |
| 550° | 87.6 | 0.36 | 12 | 12.4 | 33 |
| 600° | 67.4 | 0.6 | 32 | 32.6 | 53 |
| 650° | 41.2 | 0.8 | 58 | 58.8 | 73 |
| 700° | 21.4 | 0.6 | 78 | 78.6 | 130 |
| 750° | 7.6 | 0.4 | 92 | 92.4 | 230 |
| 800° | 3.8 | 0.2 | 96 | 96.2 | 480 |
| 850° | 1.9 | 0.1 | 98 | 98.1 | 980 |
| 900° | | - | | | ∞ |
| (b) with platinum crucibles | | | | | |
| 520° | 94 | 2 | 4 | 6 | 2 |
| 550° | 86 | 7 | 7 | 14 | 1 |
| 620° | 50 | 30 | 20 | 50 | 0.7 |
| 650° | 23.5 | 26.5 | 50 | 76.5 | 1.9 |
| 700° | 16 | 20 | 64 | 84 | 3.2 |
| 750° | 5 | 15 | 80 | 95 | 5.3 |
| 800° | 5 | 7 | 88 | 95 | 12.6 |
| 850° | 7.5 | 0.5 | 92 | 92.5 | 18.4 |

TABLE 12

β-ZnS Calcined for 30 minutes

| Temp°C | Zinc % (in terms of total zinc in the product) | | | % Conversion of ZnS | Mol. ratio ZnO : $ZnSO_4$ |
|---|---|---|---|---|---|
| | as ZnS | $ZnSO_4$ | ZnO | | |
| (a) with porcelain crucibles | | | | | |
| 520° | 90 | 1 | 9 | 10 | 9 |
| 550° | ca 75 | | 24 | ca 25 | |
| 580° | ca 58 | | 41 | ca 42 | |
| 600° | ca 21 | | 78 | ca 79 | |
| 620° | 11.2 | 0.8 | 88 | 88.8 | 110 |
| 650° | ca 10 | | 90 | ca 90 | |
| 700° | ca 4 | | 96 | ca 96 | |
| 750° | ca 3 | | 97 | ca 97 | |
| 800° | 1.9 | 0.1 | 98 | 98.1 | 980 |
| 850° | | - | | | α |
| (b) with platinum crucibles | | | | | |
| 520° | 90 | 5 | 5 | 10 | 1 |
| 550° | 78 | 9 | 13 | 22 | 1.4 |
| 620° | 9.5 | 36.5 | 54 | 90.5 | 1.5 |
| 650° | 10 | 15 | 75 | 90 | 5 |
| 700° | 8.5 | 7.5 | 84 | 91.5 | 11.2 |
| 725° | 10 | 5 | 85 | 90 | 17 |
| 750° | 7 | 3 | 90 | 93 | 30 |
| 800° | 7.5 | 0.5 | 92 | 92.5 | 184 |
| 850° | | - | | | α |

Figure 31

OXIDATION OF PURE ZINC SULPHIDE IN PORCELAIN CRUCIBLE

(1 g sample taken each time; zinc present in each constituent expressed as percentage of the total zinc in the roast).

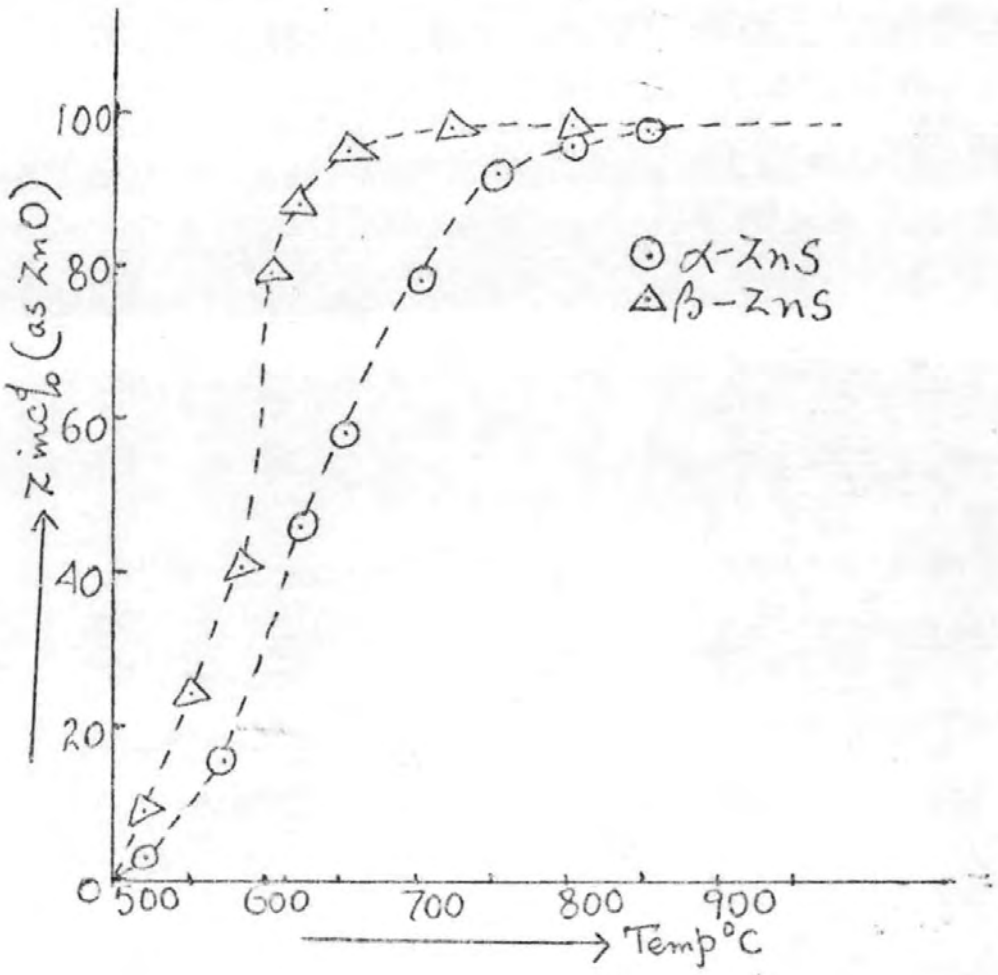

Figure 32

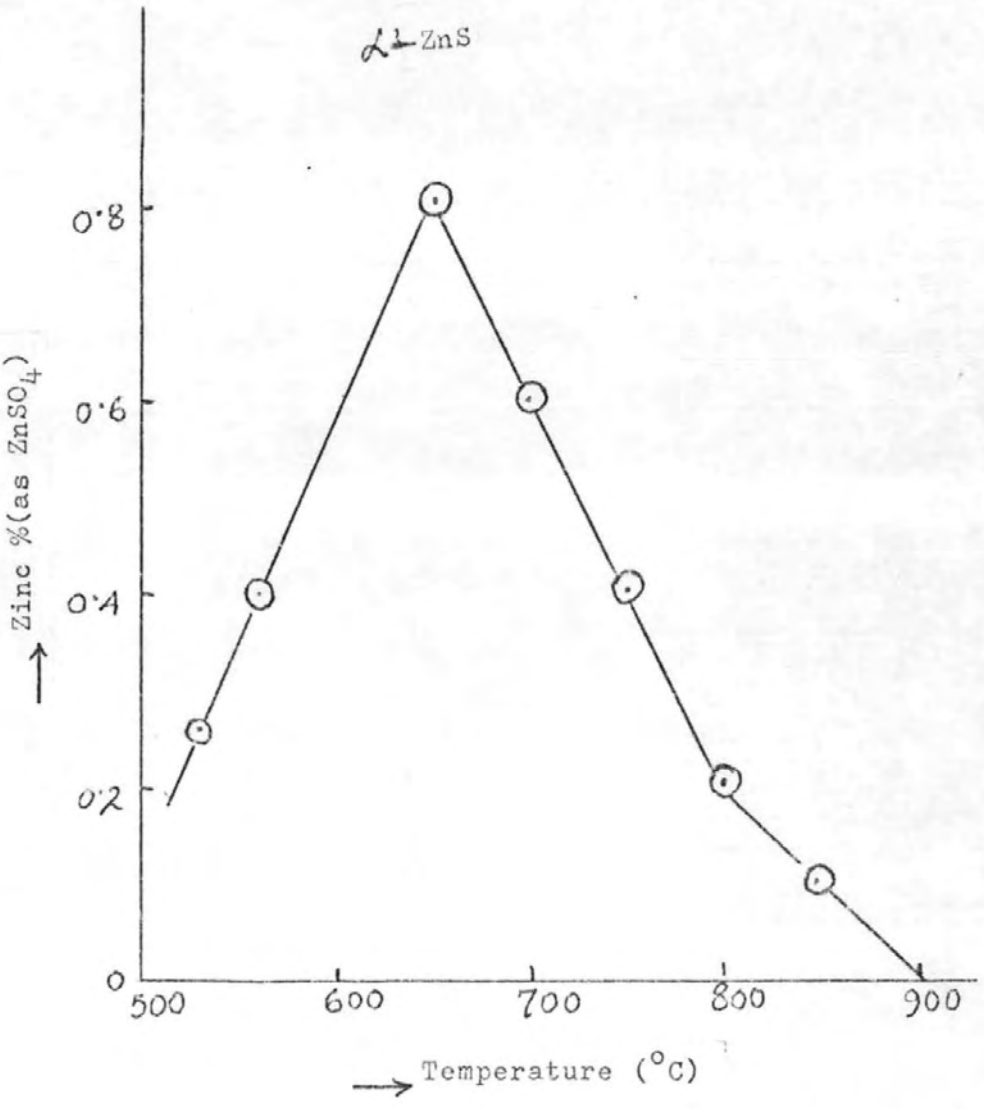
α-ZnS
0·8
0·6
0·4
0·2
0
Zinc %(as $ZnSO_4$)
500
600
700
800
900
Temperature (°C)

OXIDATION OF PURE ZINC SULPHIDE IN PLATINUM CRUCIBLE

(1 g sample taken each time; zinc present in each constituent expressed as percentage of the total zinc in the roast).

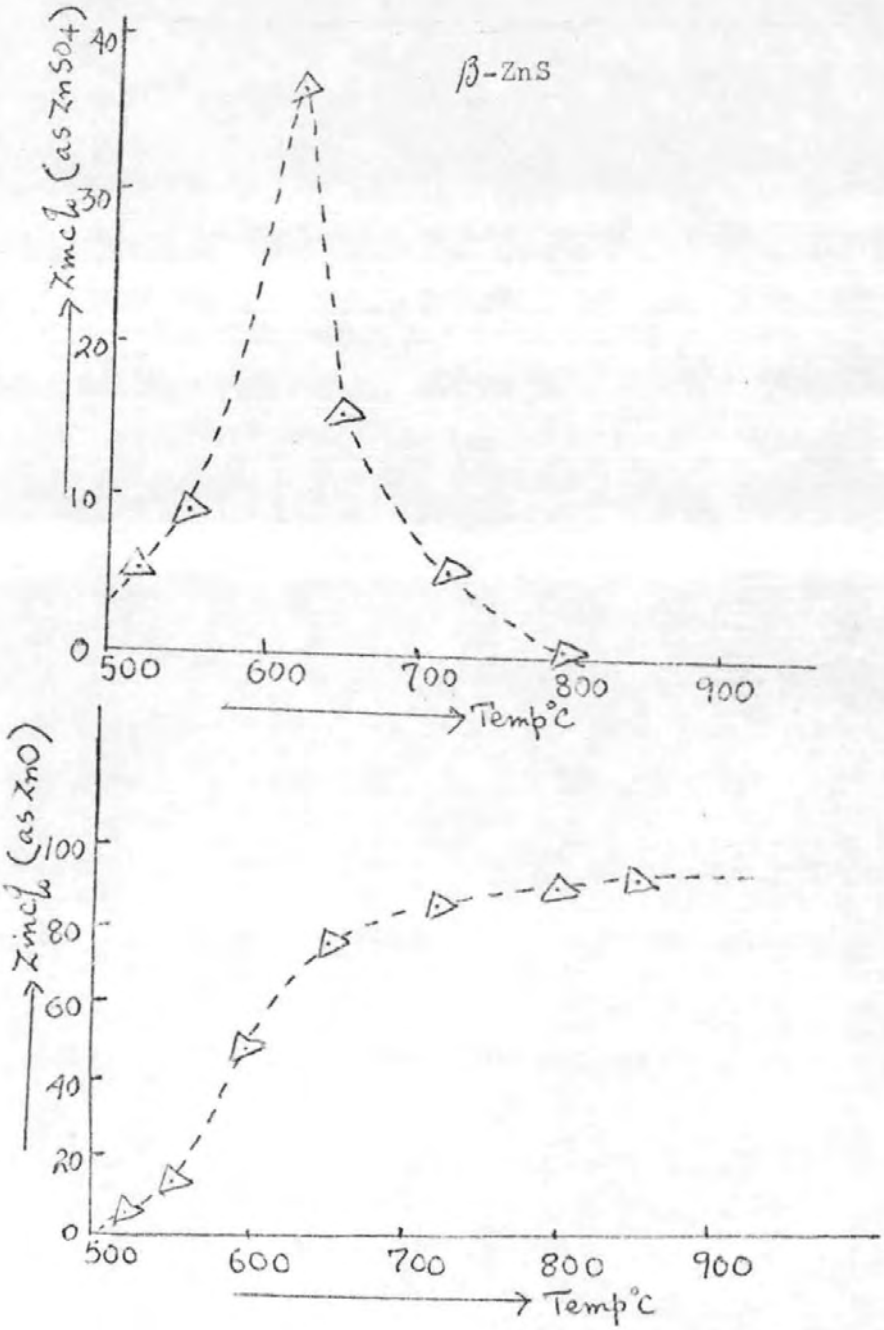


Figure 33

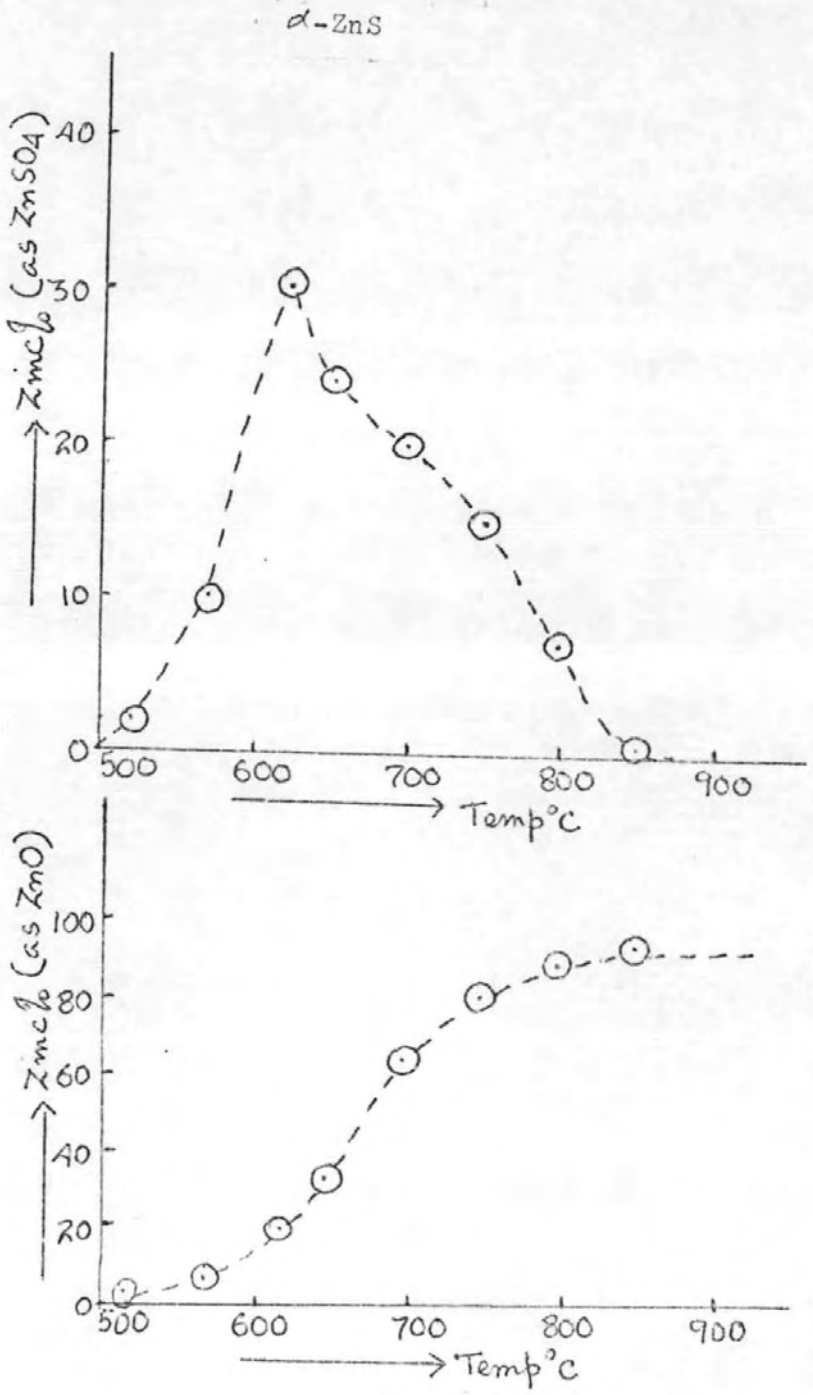
α-ZnS
Zinc % (as ZnSO4)
0
10
20
30
40
500
600
700
800
900
Temp°C
Zinc % (as ZnO)
0
20
40
60
80
100
500
600
700
800
900
Temp°C

Figure 34

OXIDATION OF PURE ZINC SULPHIDE
(α-ZnS) AT ISOTHERMAL TEMPERATURES

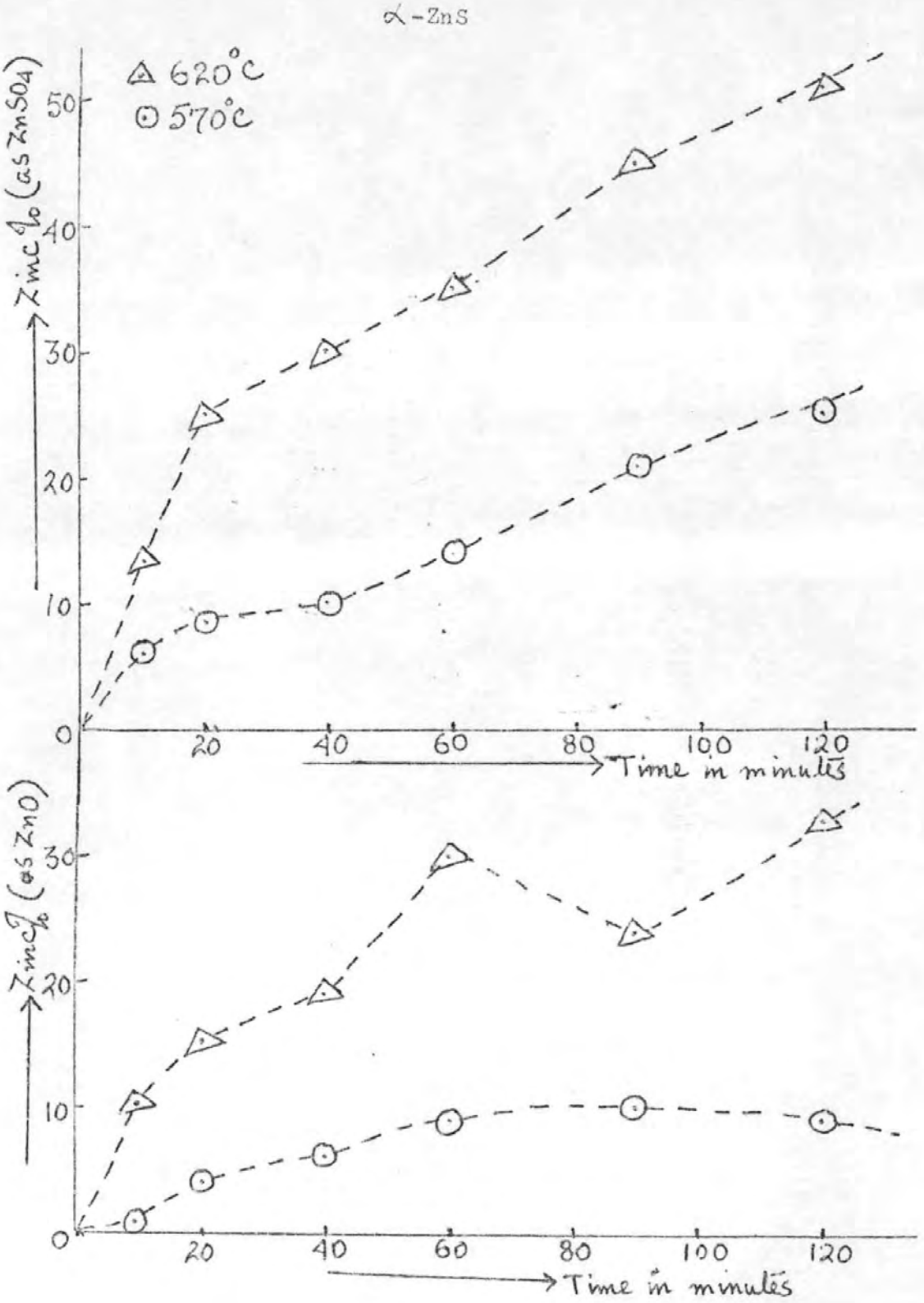


Figure 35

Figure 36

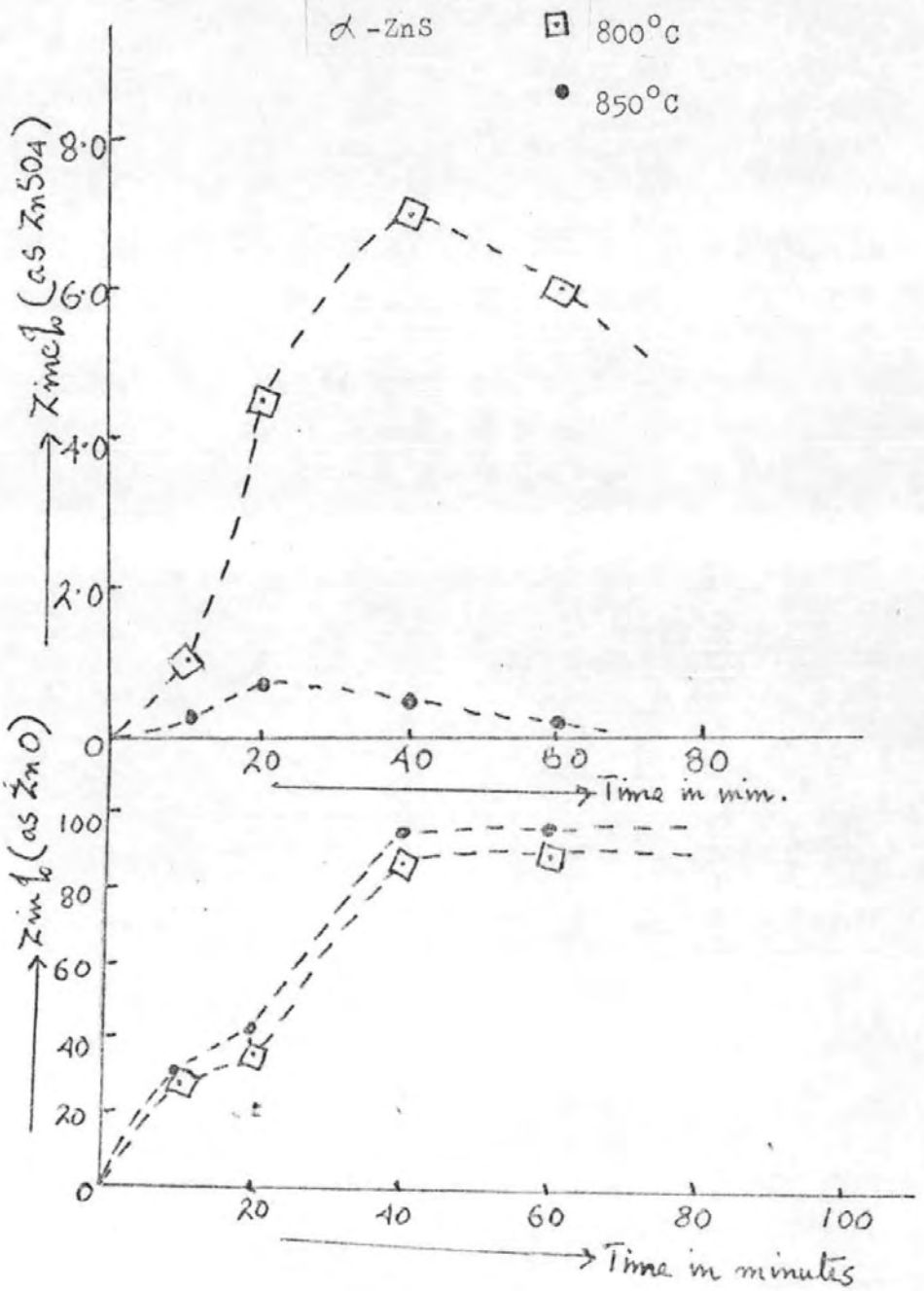
α-ZnS
800°C
850°C
Zinc % (as ZnSO4)
8·0
6·0
4·0
2·0
0
20
40
60
80
Time in min.
Zinc % (as ZnO)
100
80
60
40
20
0
20
40
60
80
100
Time in minutes

TABLE 13

$\alpha$- ZnS Calcined for different time intervals

| Temp °C | Time of oxidation | Zinc % (in terms of total zinc in the product) | | % Conversion of ZnS | Ratio $\frac{ZnO}{ZnSO_4}$ |
|---|---|---|---|---|---|
| | | as $ZnSO_4$ | ZnO | | |
| With platinum crucibles | | | | | |
| 570° | 20 min | 9 | 4 | 13 | 0.44 |
| " | 40 " | 10 | 6 | 16 | 0.60 |
| " | 60 " | 14 | 9 | 23 | 0.64 |
| 620° | 20 " | 25 | 15 | 40 | 0.60 |
| " | 40 " | 30 | 19 | 49 | 0.63 |
| " | 60 " | 35 | 30 | 65 | 0.86 |
| 800° | 20 " | 4.5 | 36 | 40.5 | 8.0 |
| " | 40 " | 7 | 88 | 95 | 12.6 |
| " | 60 " | 6 | 90 | 96 | 15.0 |

This is attributed to the fact that the $SO_2$ and $SO_3$ contents of the furnace gases decrease, whereas the oxygen pressure increases considerably towards the end of roasting and this results in high values of $Po_2/P_{(total)}$; at high values of $Po_2/P_{(total)}$ zinc sulphate decomposes.

Besides, at these temperatures the thermodynamics are favourable for the decomposition of zinc sulphate to oxide by interaction with zinc sulphate and ZnS (93).

4.2.2 Kinetics of Oxidation of Zinc Sulphide in a stationary layer

The process of sulphide oxidation is heterogeneous and exothermic. One might expect here the existence, under suitable conditions, of one of three modes of oxidation: Kinetic, diffusion or intermediate, depending on the ratio of the values of the rate constant of the crystallo-chemical conversion K and the coefficient of back-diffusion of gases D through the solid reaction products.

At low temperature, when the reaction rate is low in comparison with the rate of diffusion (Kinetic region), the overall reaction rate is determined by the true kinetics at the surface and grows exponentially with temperature in agreement with the Arrhenius law (92). However, this growth continues only until the reaction rate becomes comparable with the diffusion rate. The process subsequently transfers to the diffusion region where its rate is determined entirely by the diffusion rate and grows only extremely slightly with temperature. With such a dependence of the rate of heat emission on temperature and under specific conditions of heat removal, three stationary heat modes are possible; the intermediate one is unstable, the upper corresponds to the diffusion region and the lower is in the kinetic region. The abrupt transfer from the lower to the upper stationary heat mode leads to ignition at the surface of the zinc sulphide.

The rates of oxidation of zinc sulphide, W, expressed as Zn% (as ZnO) at 530° - 850°C are plotted in Figure 31. The graph has two branches differing markedly from each other; the lower corresponding to the kinetic region and the upper to the diffusion region.

The oxidation rate of zinc sulphide changes with temperature according to an exponential law. In this case, the graph (Fig 37) of the dependence of lnW on 1/T undergoes an inflection and can be divided provisionally into three sections a,b,c. The apparent activation energy for $\alpha$-ZnS in section "a" of the graph is 55.9 K Cal/mole (for $\beta$-ZnS 42.K Cal/mole), in section "b" 20 K Cal/mole (for $\beta$-ZnS 18 K Cal/mole) and finally in section "c" the activation energy of the process is 2 K Cal/mole (for $\beta$-ZnS 1.32 K Cal/mole). The values are in good agreement with the earlier works (94).

4.2.3 Reactivity of ZnO with Sulphur trioxide

Zinc sulphide samples (about 1g) were oxidised using both porcelain and platinum crucibles, for 40 minutes in the case of $\alpha$-ZnS and 30 minutes for $\beta$-ZnS at a series of temperatures between 520° and 850°C. The results of the thermogravimetric investigations are given in Figures 38-40. With platinum crucibles at temperatures of 520°, 550° 580° and 620°C, the weight of the samples increases with time and this is connected with the formation of sulphate.

The velocity of the process decreases apparently with time, because of the hindered diffusion of oxygen through the oxidised layer.

In the temperature range 650° to 850°C, the sulphate formation is accompanied by another process, that of desulphuration. The continuous thermogravimetric curves (Fig. 39-40) give an overall picture and reflect the faster increase of the second process in comparison with the first. The total weight change decreases with time and at temperature $\geq$ 700°C, it assumes a negative value. The dependence of the weight change on the temperature is shown in Fig. 39-40.

Figure 37

ACTIVATION ENERGY CURVE

Plot of lnW versus $^{1}/_{T}$ for pure zinc sulphide

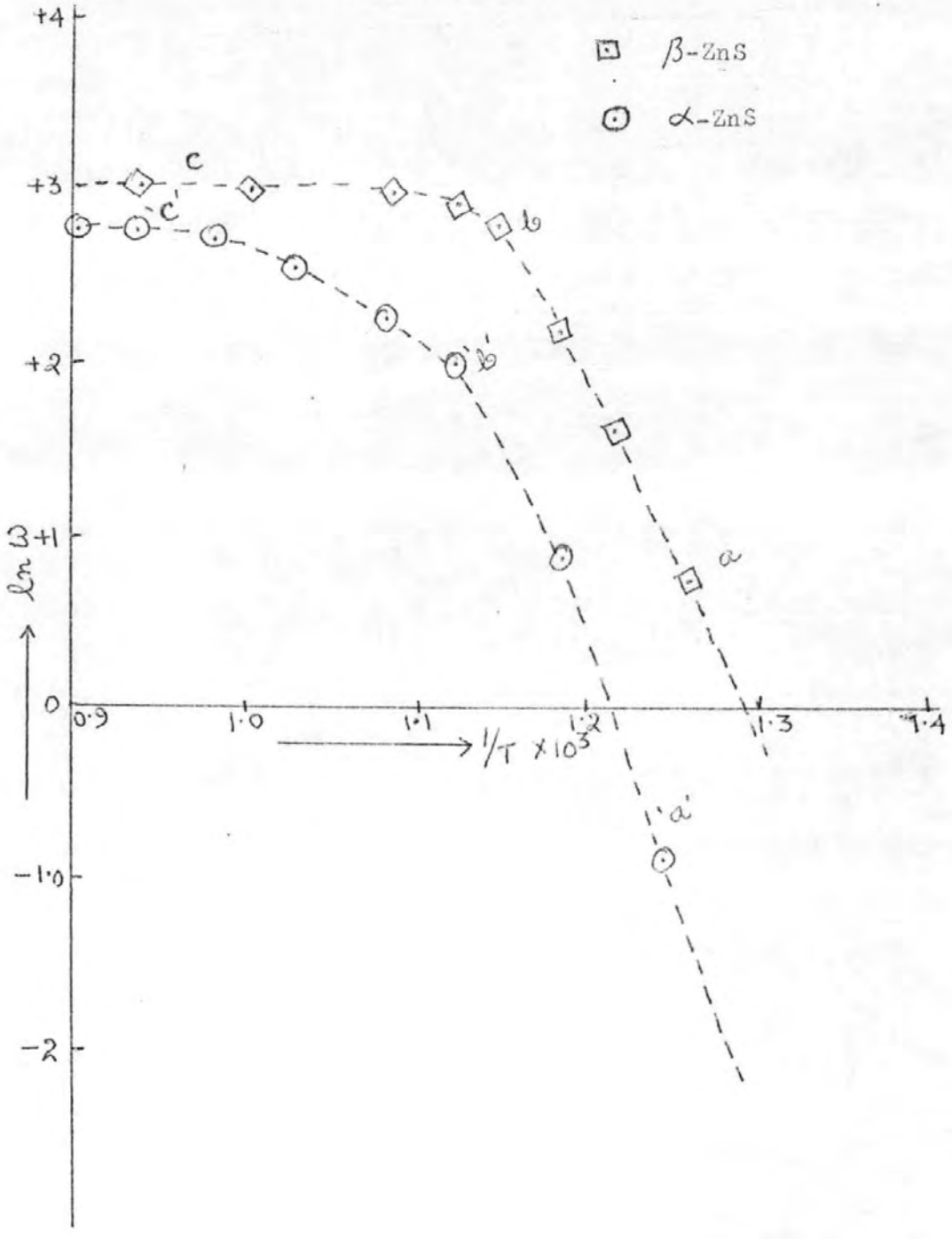

Figure 38

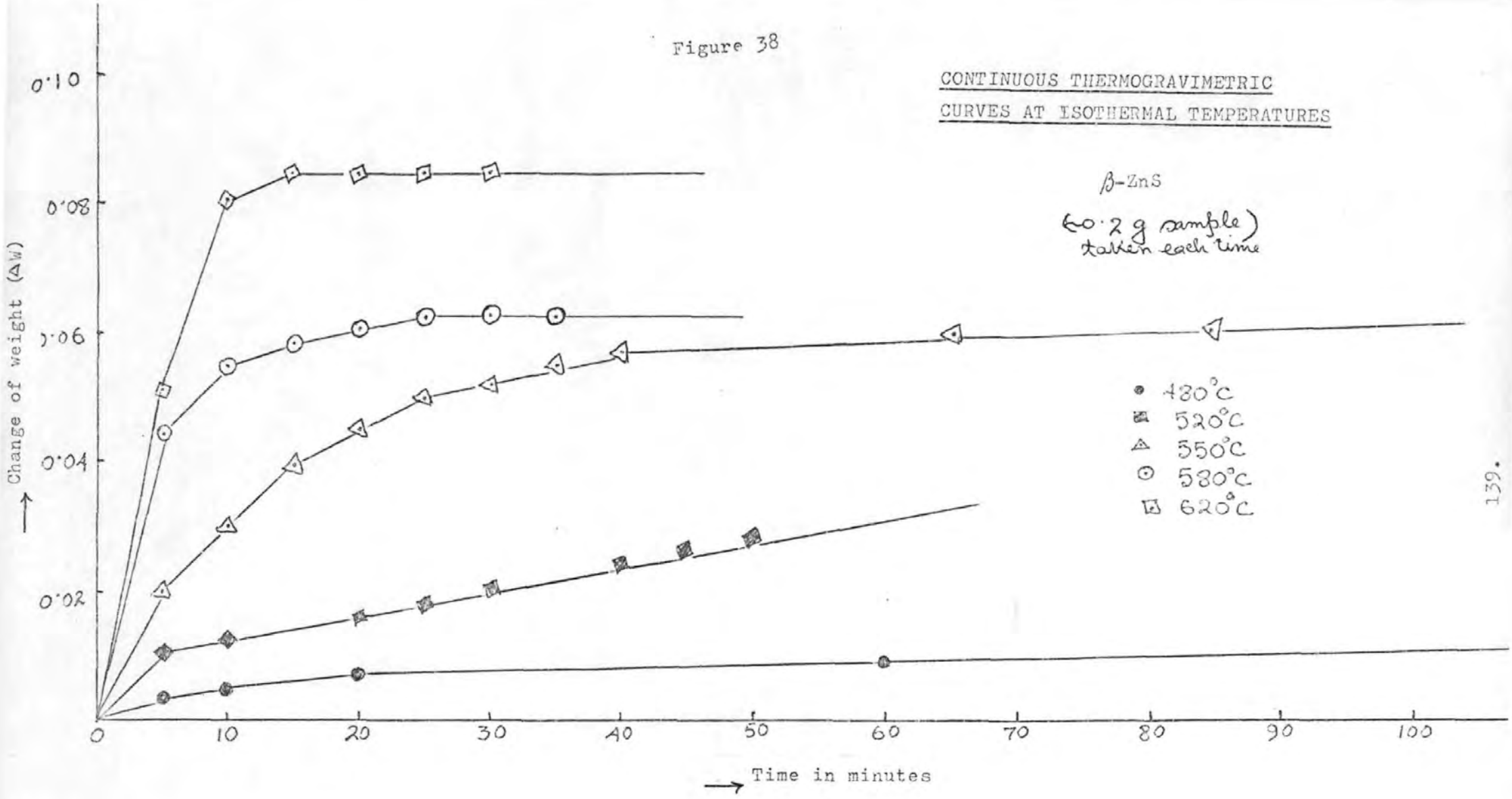
CONTINUOUS THERMOGRAVIMETRIC
CURVES AT ISOTHERMAL TEMPERATURES
β-ZnS
(~0·2 g sample)
taken each time
480°C
520°C
550°C
580°C
620°C
Change of weight (ΔW)
0·10
0·08
0·06
0·04
0·02
0
10
20
30
40
50
60
70
80
90
100
Time in minutes

Figure 39

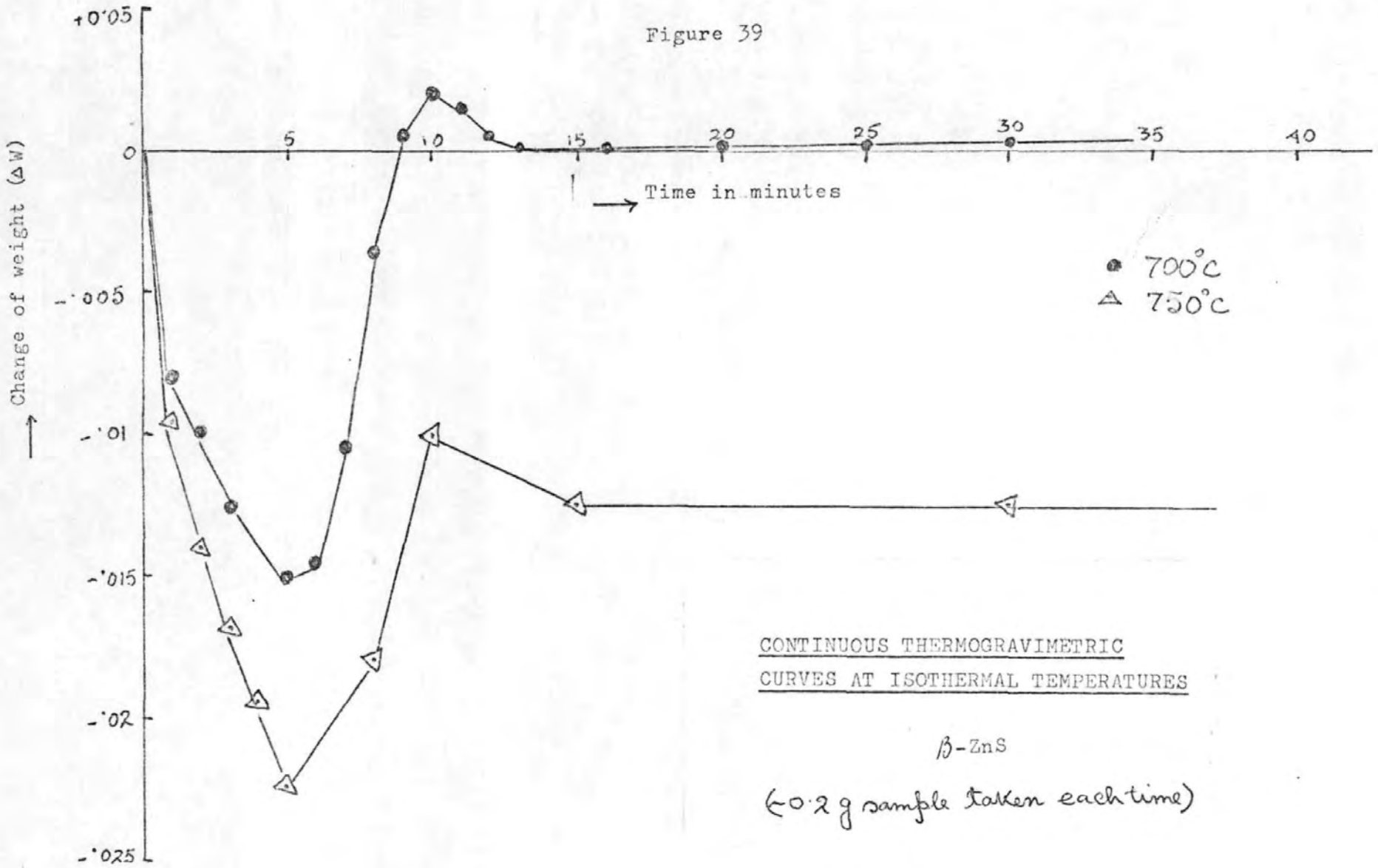


CONTINUOUS THERMOGRAVIMETRIC CURVES AT ISOTHERMAL TEMPERATURES

β-ZnS

(~0·2 g sample taken each time)

Figure 40

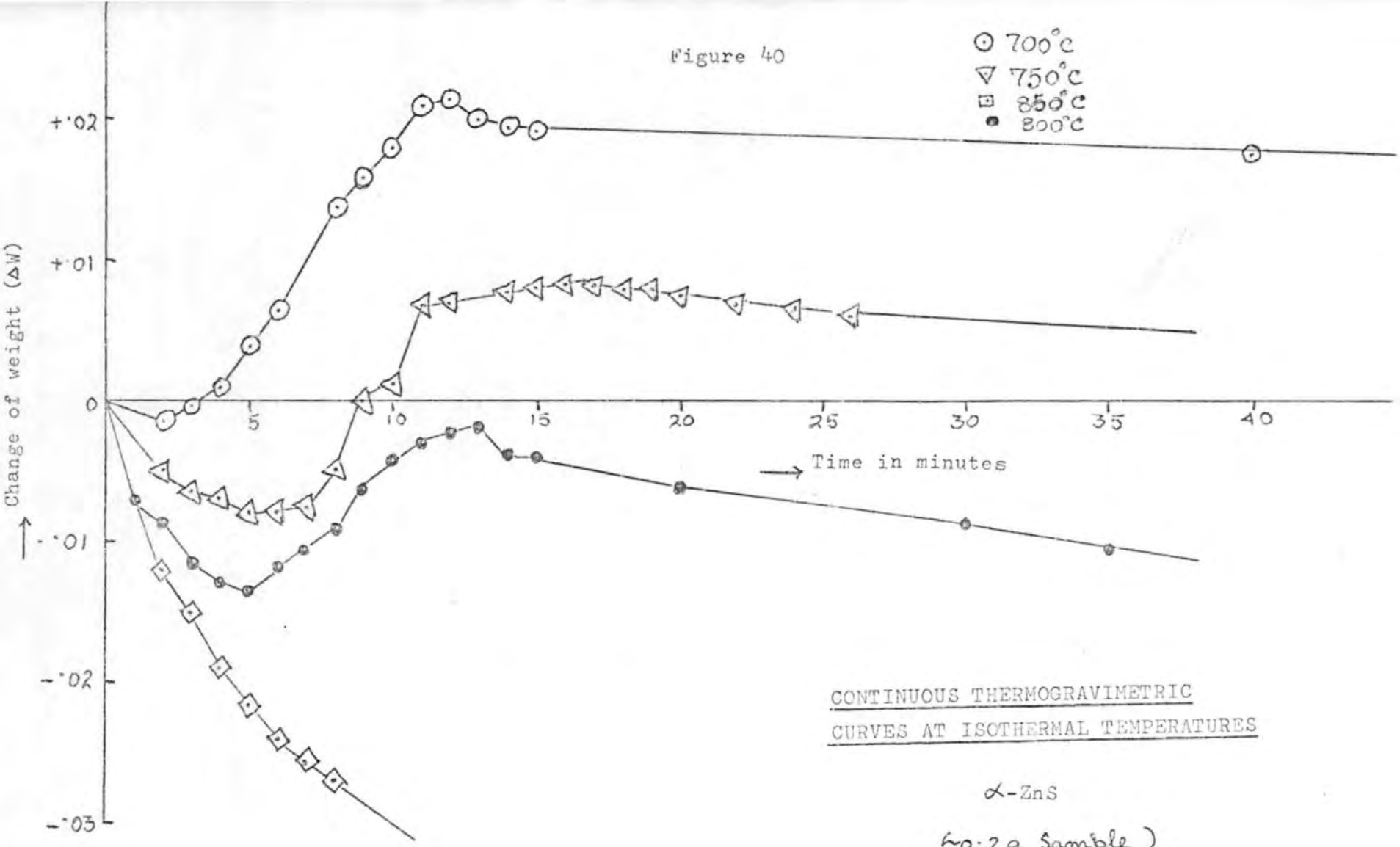


CONTINUOUS THERMOGRAVIMETRIC CURVES AT ISOTHERMAL TEMPERATURES

α-ZnS

(~0·2 g Sample taken each time)

At higher temperatures the thermogravimetric curves (Figs 39-40)have a specific form. At first, desulphuration is very pronounced, the weight reduction passes through a minimum; then there is a slow increase of weight on account of sulphate formation. This form of the thermogravimetric curve shows that the rate of sulphate formation and desulphuration vary differently with time due to the increased amount of $SO_3$gas in the furnace atmosphere in the presence of catalysts like platinum.

At first the desulphuration predominates, the weight reduction passes through a minimum and then there is a slow increase of weight on account of sulphate formation.

The variation of the composition of the phases was investigated with temperature (Figs.33-34, Tables 11 and 12).

The amount of zinc sulphate increases rapidly with temperature reaching a maximum at 620°C for $\alpha$-ZnS and $\beta$-ZnS (95). Above these temperatures, the sulphate percentage decreases up to 850°C. This is in accordance with variations in the X-ray intensities for the sulphate line (or peak) in Figure 41. To aid the interpretation of the results, the thermogravimetric runs of synthetic ZnS($\alpha$ and $\beta$) using porcelain and platinum crucible were interrupted in many experiments at desired temperatures for certain times and the materials in the crucibles were identified by chemical, spectral and X-ray analysis. It was seen that the thermograms as obtained in the two types of crucibles differ greatly. When porcelain crucibles were used, there was a continuous decrease in weight of residual material from 520° to 850°C, the examination of the material showed it to be comprised predominantly of zinc sulphide and zinc oxide, with the latter increasing in proportion with increase in temperature. Only very small amounts of zinc sulphate (maximum of about 1%) were found.

Figure 41

VARIATIONS IN THE X-RAY INTENSITES FOR THE ZINC SULPHATE LINE (OR PEAK) AT DIFFERENT TEMPERATURS

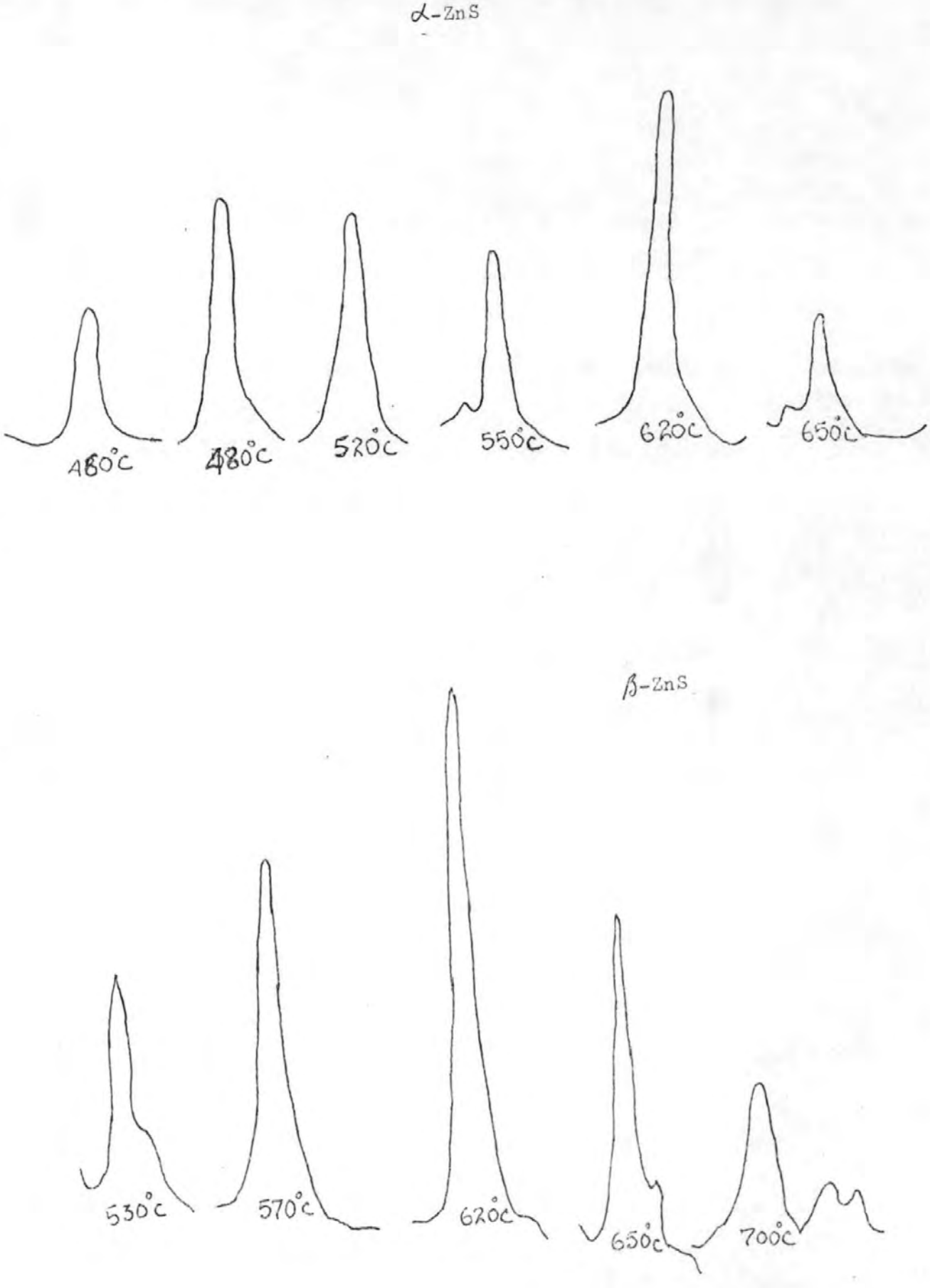

In contrast, when platinum crucibles were used at lower temperatures, 520° - 700°C, there was a significant increase in the weight of oxidised material with respect to amount of zinc sulphide taken. Beyond 620°C, the percentage of ZnO increased at the expense of both ZnS and $ZnSO_4$, cf Tables 11 and 12. The results could be explained as follows : The formation of oxide on heating the sulphide in air occurs via the reactions :

$$ZnS + {}^{3}/_{2}\,O_2 \longrightarrow ZnO + SO_2 \quad \ldots\ldots\ldots (1)$$

$$SO_2 + \tfrac{1}{2}\,O_2 \rightleftharpoons SO_3 \quad \ldots\ldots\ldots\ldots\ldots (2)$$

$$ZnO + SO_3 \rightleftharpoons ZnSO_4 \quad \ldots\ldots\ldots\ldots (3)$$

(at moderate temperatures up to 620°C for synthetic ZnS)

and

$$ZnSO_4 \longrightarrow ZnO + SO_3 \quad \ldots\ldots\ldots\ldots\ldots (4)$$

$$ZnS + ZnSO_4 \longrightarrow 2\,ZnO + 2\,SO_2 \quad \ldots\ldots\ldots (5)$$

(at higher temperatures, i.e. above 620°C for synthetic ZnS via the formation of the phase $ZnO.2\,ZnSO_4$).

In the presence of platinum, there is relatively more conversion of zinc sulphide to zinc sulphate, as shown by the much lower molecular ratios of $ZnO:ZnSO_4$ in the products (cf Table 11), nevertheless, the overall oxidation rates for $\alpha$-ZnS are generally similar, being somewhat faster in the presence of platinum at about 550° - 700°C.

This is the temperature range over which the molecular ratio $ZnO:ZnSO_4$ reaches a minimum at about 620°C, when there is molecularly more sulphate present than oxide. This is ascribed to the catalytic effect of the platinum on the formation of $SO_3$, viz. $2\,SO_2 + O_2 \longrightarrow 2\,SO_3$, becoming more appreciable at these temperatures. This promotes the formation of zinc sulphate and provides a sufficient partial pressure of sulphur trioxide to

prevent the zinc sulphate from decomposing until abnormally higher temperatures are reached. Hence, the amounts of zinc sulphate are correspondingly larger even up to 850°C.

The oxidation rates for $\beta$-ZnS are correspondingly much greater than for $\alpha$-ZnS, cf Tables 12 and 13; as expected from the much larger specific surface of the $\beta$-ZnS. Again, without platinum crucibles, very little zinc ($<1\%$) is converted to sulphate. With platinum crucibles, much larger amounts of sulphate are formed comparable in % and molecular $ZnO:ZnSO_4$ ratio with those from $\alpha$-ZnS. The much larger specific surface of the $\beta$-ZnS only appears to be very influential in giving a considerably greater oxidation rate in the initial stages. Then it favours production of zinc sulphate, cf results at 520°C in Tables 12 and 13, which would be formed mainly near the surface of the material by the nucleation and surface reaction, before the advancing interface reaction develops inwards to give too deep a layer of product for free access of oxygen. The formation of zinc oxide (requiring less oxygen than for zinc sulphate) is favoured as the oxidation proceeds. The molecular ratios $ZnO:ZnSO_4$ increase progressively as shown in Table 13.

This evidence for the reaction of ZnO and $SO_3$ at low temperature is of importance to the understanding of zinc sulphate formation in the dust-collecting equipment usually associated with zinc roasters (96). The roaster gas carries off fine dust, much of which may be unreacted zinc sulphide. The temperature in dust-collecting equipment drops from the roaster temperature (about 800°C) through the range of temperature studied, to ambient temperature. Such dusts are known to contain far larger amounts of zinc sulphate than the primary calcine. Thus, it is confirmed that this sulphate

is formed by reaction of ZnO dust with $SO_3$ (or $SO_2$ plus $O_2$) in the partly-cooled gases, after the finely divided ZnS has been converted to ZnO.

In an effort to obtain some information on the kinetics of the reaction, further tests were made. The results of these tests are shown in Figs.35-36. The reduction in the rate of sulphation with increased time probably results from the constantly diminishing surface area of ZnO as the reaction proceeds, so that the rate of the reaction is controlled by diffusion of $SO_3$ through the continually thickening layer of reaction product. It is proposed that the diffusion of gaseous $SO_3$ through pores and cracks in the newly-formed outer $ZnSO_4$ coating is the slow step. Further data on the effect of the partial pressure of $SO_3$ and $O_2$ on the rate of sulphation, and the physical structure of the $ZnSO_4$ layer are required before the rate-controlling mechanism can be rigorously established.

4.3 Differential Thermal Analysis (DTA)

Powdered synthetic zinc sulphides ($\alpha$ and $\beta$) were investigated.

The work was done with small weights (about 0.1g) in order to eliminate possible overheating of the sample due to strong exothermic reactions and to decrease the amount of $SO_2$ which attacks the thermocouple wires. The use of protective coverings for the thermocouple heads has decreased seriously the sensitivity and accuracy of the measurements. Furthermore, with high sample weights, oxygen diffusion into the sample interior influences the reaction rate. Oxidation was performed with air or oxygen-enriched air at different flow rates. The DTA thermograms showed that the oxidation commences at a low rate which gradually increases to a maximum depending on the sulphide properties and the extent of the reaction interface. After the maximum it gradually decreases.

4.3.1 DTA Curve of $\alpha$-ZnS and $\beta$-ZnS

The thermograms in Figs.42-51 represent the development of the oxidation of synthetic ZnS at different rate of flow of air.

Effect of air flow and oxygen content of the air on the kinetics of the oxidation

The effect of different air flows 0,10,20,40 and 80 $cm^3$/min was investigated. The intensity of the oxidation, as indicated by the height and the breadth of the peaks, increased with air flow, since gaseous products were then removed more readily and back-reactions were minimised. In the case of $\beta$-ZnS (cubic), it can be seen that there are two exothermic peaks throughout the air flows studied (Table 14)

As the flow rate of air increases, the heights of the two peaks increase and they merge gradually into a single peak, particularly at higher flow rates (> 80 $cm^3$/min). The first peak (i.e. the one at the lower temperature) is larger than the second peak.

In the case of $\alpha$-ZnS (hexagonal), only two exothermic peaks can be seen when the flow of air is 20 $cm^3$/min, but at other flow rates, only one peak is observed. The first exothermic peak at 620°C is smaller than the second exothermic peak at 650°C.

These observations can be explained in the following manner: The first exothermic peak is caused by the nucleation of zinc sulphide and the development of the reaction across the surface of the particles.

The second exothermic peak is due to the penetration of oxygen through the newly-formed zinc oxide layer, promoting further oxidation by an advancing interface mechanism inwards from the outside of each particle.

TABLE 14

D.T.A. Curve of pure ZnS

| Sample | Flow rate | Exothermic peaks | |
|---|---|---|---|
| | | Initial Oxidation Temp °C. | Intense Oxidation Temp °C. |
| β-ZnS | 10 $cm^3$/min, air | 550 | 620 |
| " | 20 $cm^3$/min " | 485 | 570 and 620 |
| " | 40 $cm^3$/min " | 520 | 570 and 590 |
| " | 80 $cm^3$/min " | 520 | 547 and 558 |
| " | 80 $cm^3$/min, $O_2$-enriched air | 520 | 554 |
| α-ZnS | 0 | 550 | 675 |
| " | 20 $cm^3$/min, air | 540 | 620 and 650 |
| " | 40 $cm^3$/min " | 543 | 610 |
| " | 80 $cm^3$/min " | 520 | 610 |
| " | 80 $cm^3$/min, $O_2$-enriched air | 583 | 610 |

Figure 42

D.T.A. Curve of $\beta$- ZnS

Flow of air : 10 cm $^3$/min

Rate of heating : 10°C/min

Wt. of sample : 0.1 g

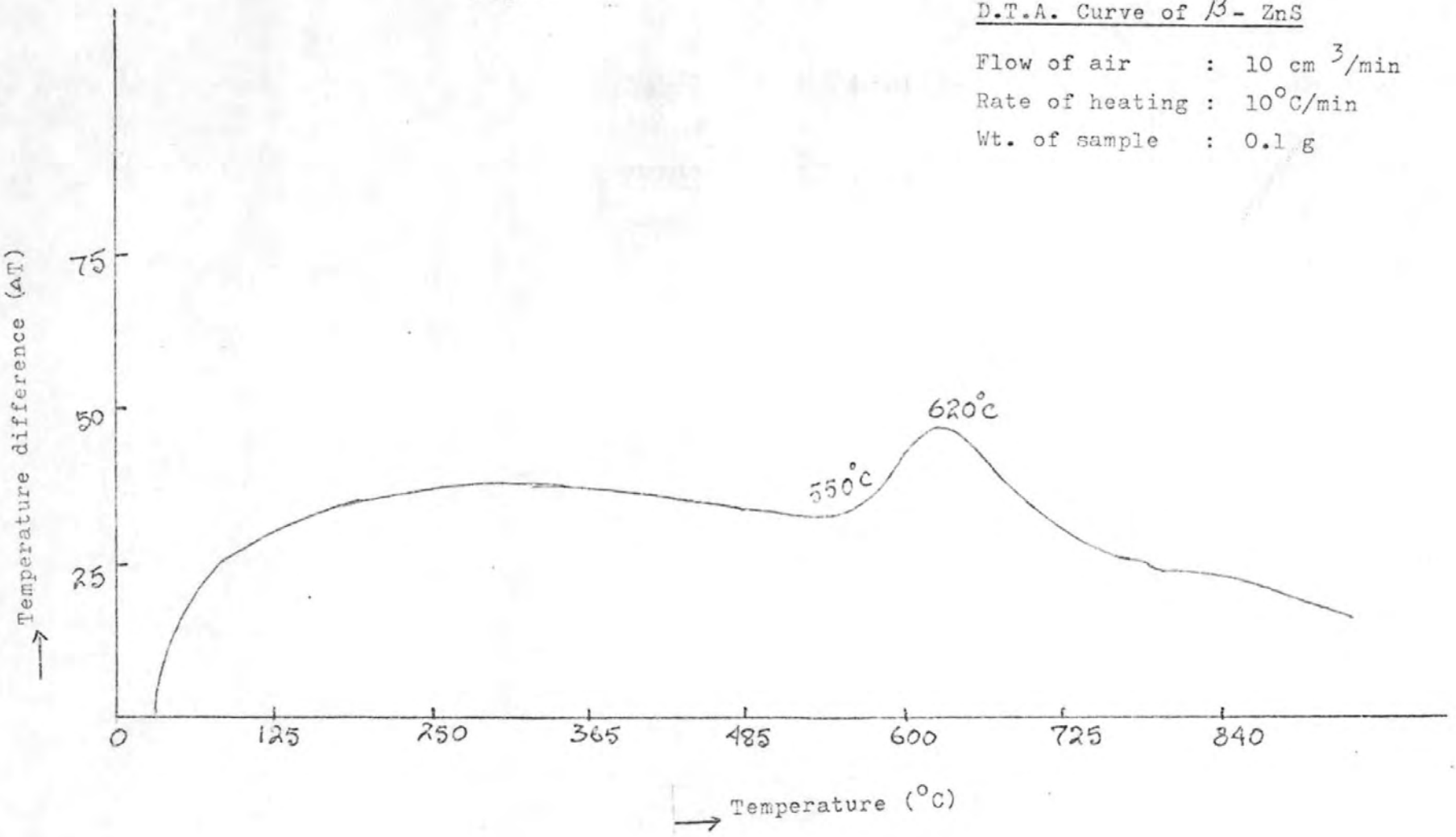

Figure 43

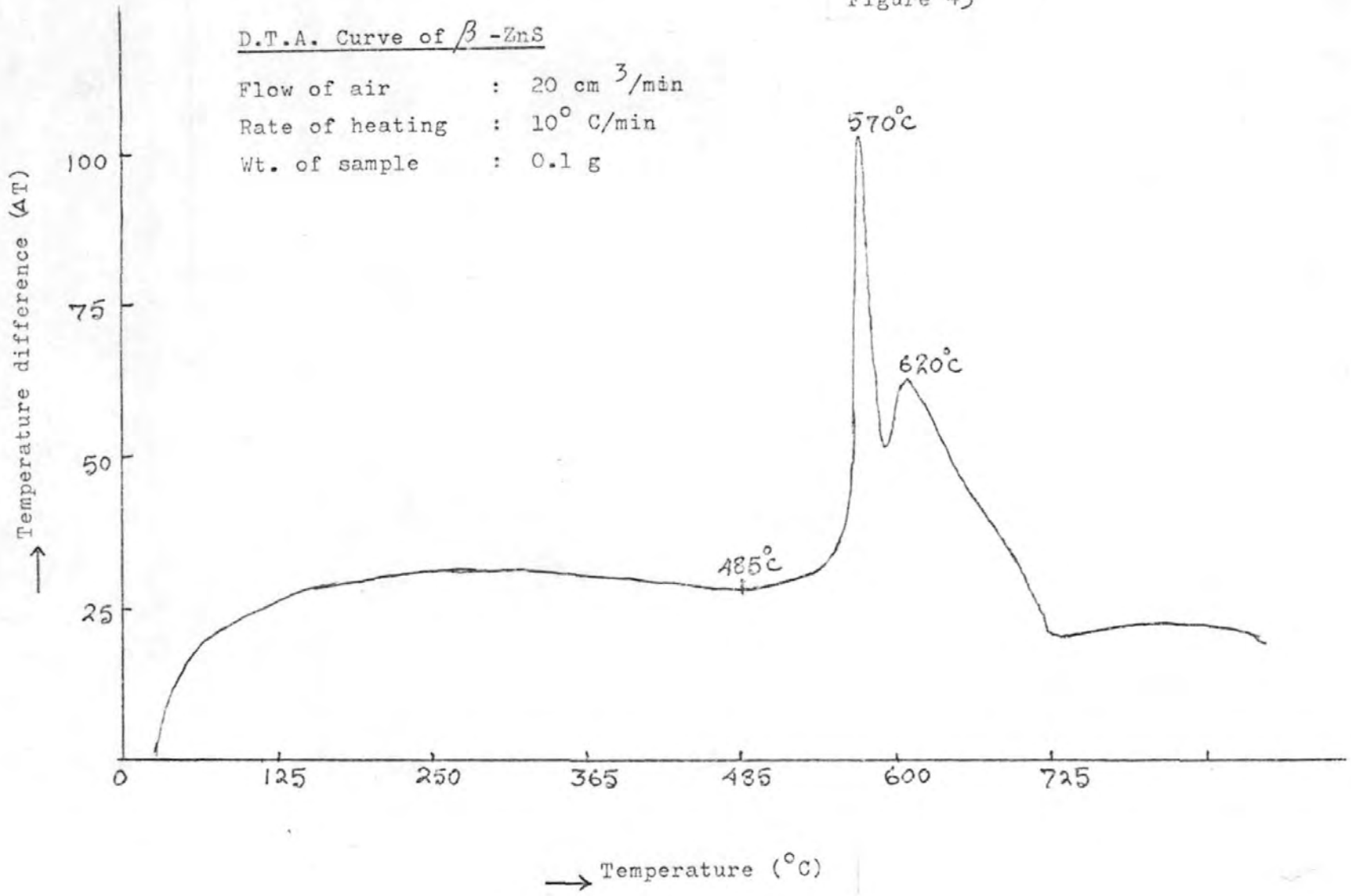
D.T.A. Curve of β -ZnS
Flow of air : 20 cm 3/min
Rate of heating : 10° C/min
Wt. of sample : 0.1 g
570°C
620°C
485°C
100
75
50
25
Temperature difference (ΔT)
0
125
250
365
485
600
725
Temperature (°C)

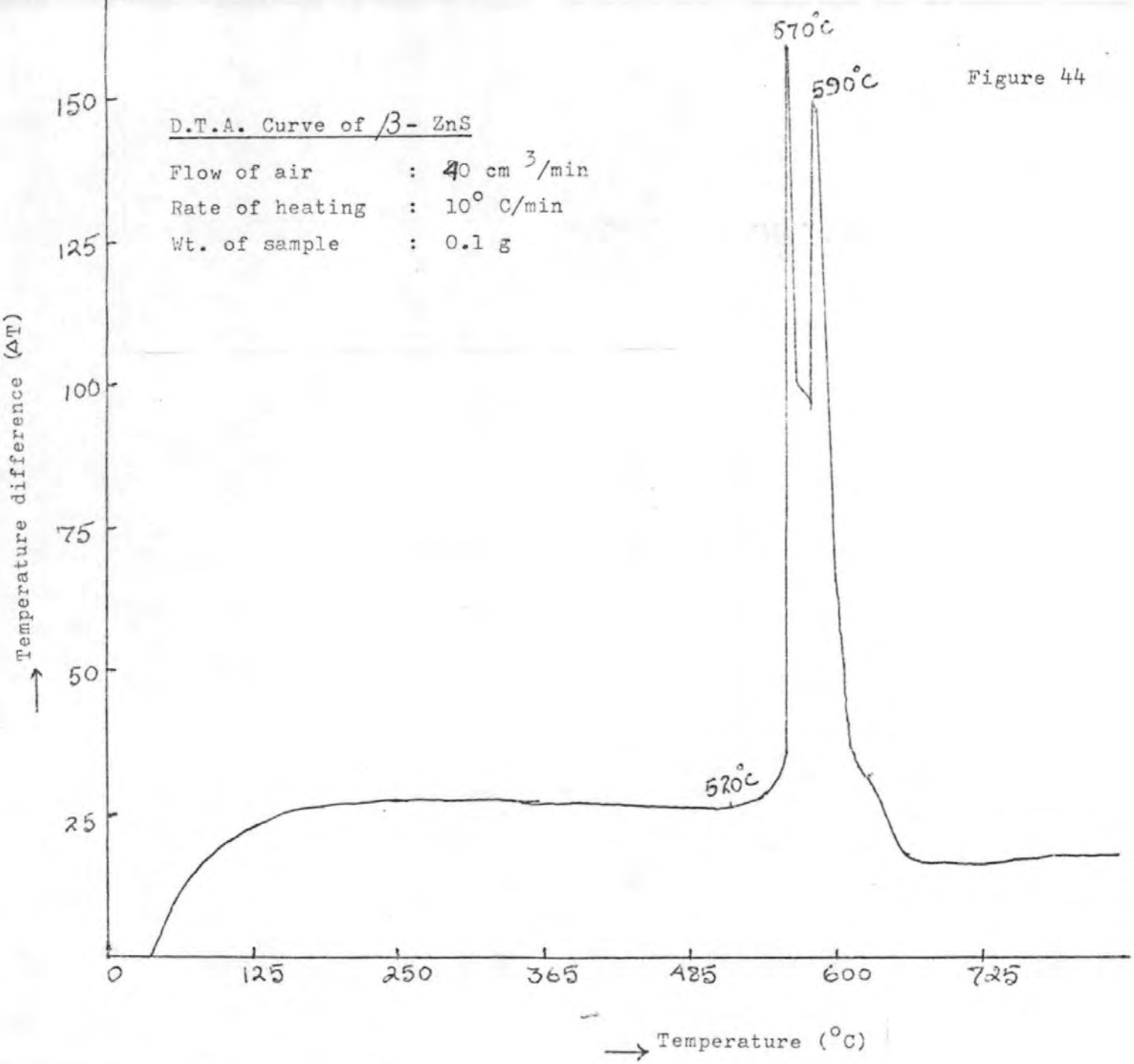
D.T.A. Curve of β- ZnS
Flow of air : 40 cm 3/min
Rate of heating : 10° C/min
Wt. of sample : 0.1 g
570°C
590°C
520°C
150
125
100
75
50
25
Temperature difference (ΔT)
0
125
250
365
485
600
725
Temperature (°C)

Figure 44

Figure 45

D.T.A. Curve of β-ZnS

Flow of air : 80 cm $^3$/min

Rate of heating : 10°C/min

Wt. of sample : 0.1 g

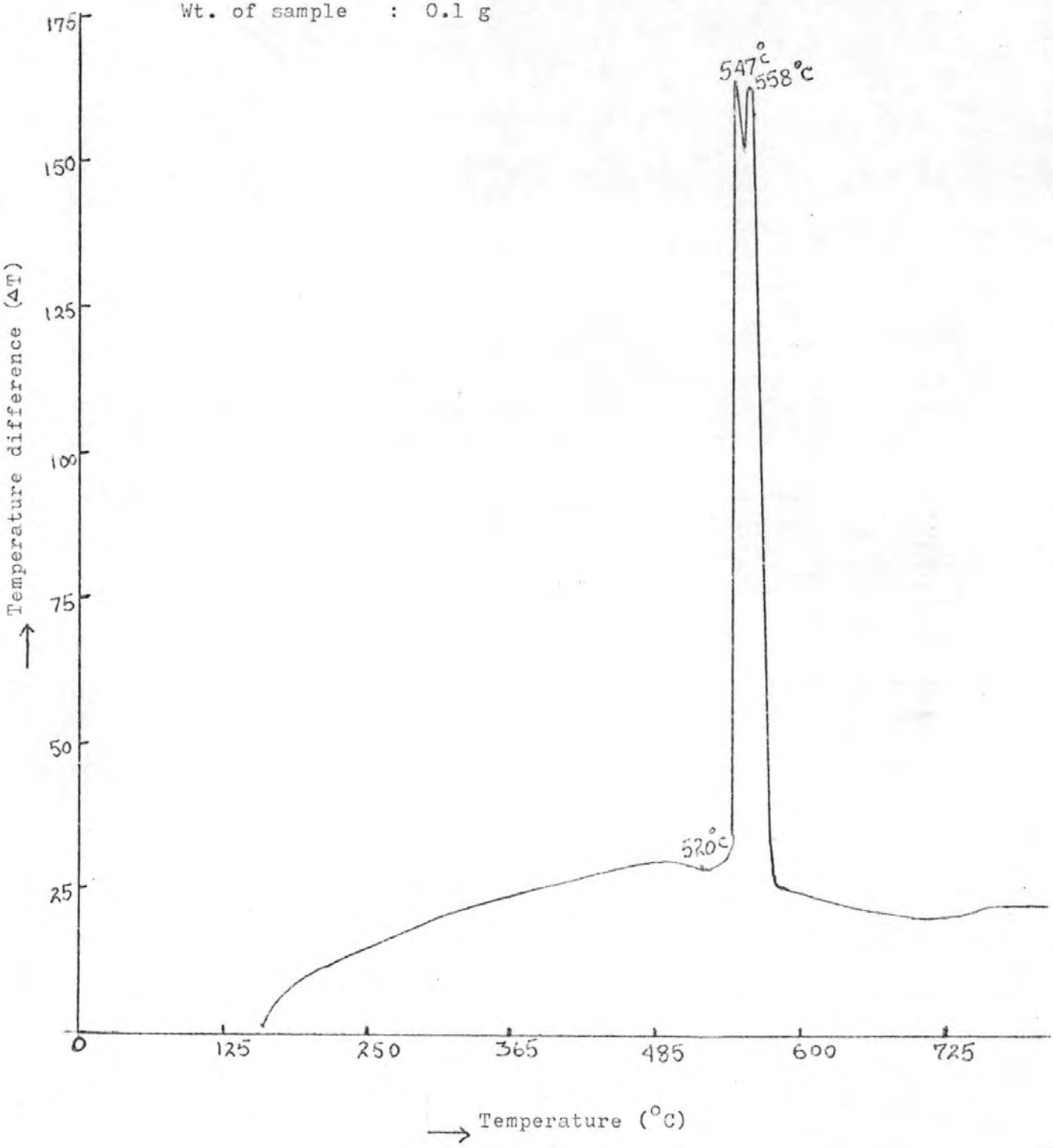

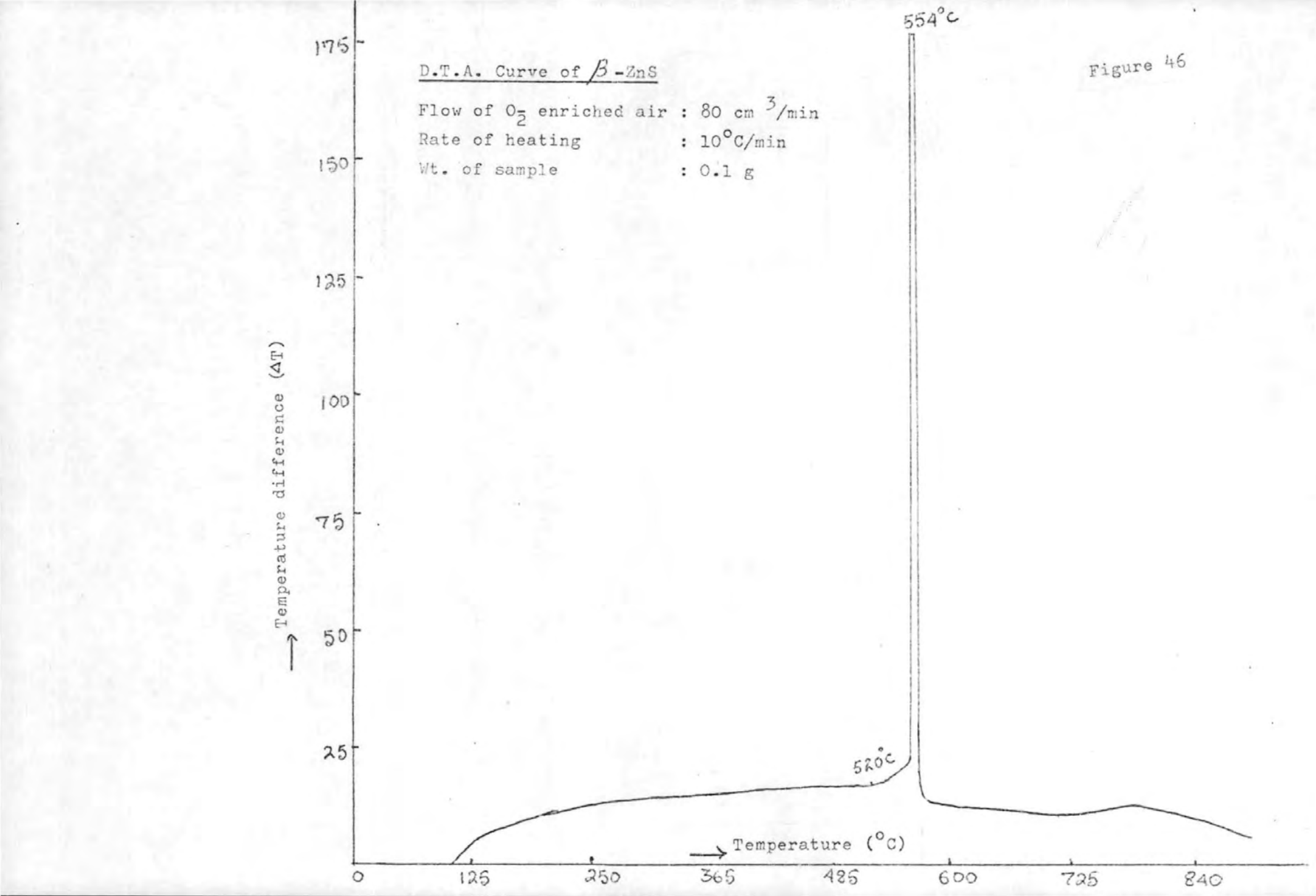
D.T.A. Curve of β-ZnS
Flow of $O_2$ enriched air : 80 cm $^3$/min
Rate of heating : 10°C/min
Wt. of sample : 0.1 g
554°C
520°C
175
150
125
100
75
50
25
Temperature difference (ΔT)
Temperature (°C)
0
125
250
365
485
600
725
840

Figure 46

Figure 47

D.T.A. Curve of $\alpha$-ZnS in static bed

Rate of heating : 10°C/min

Wt. of sample : 0.1 g

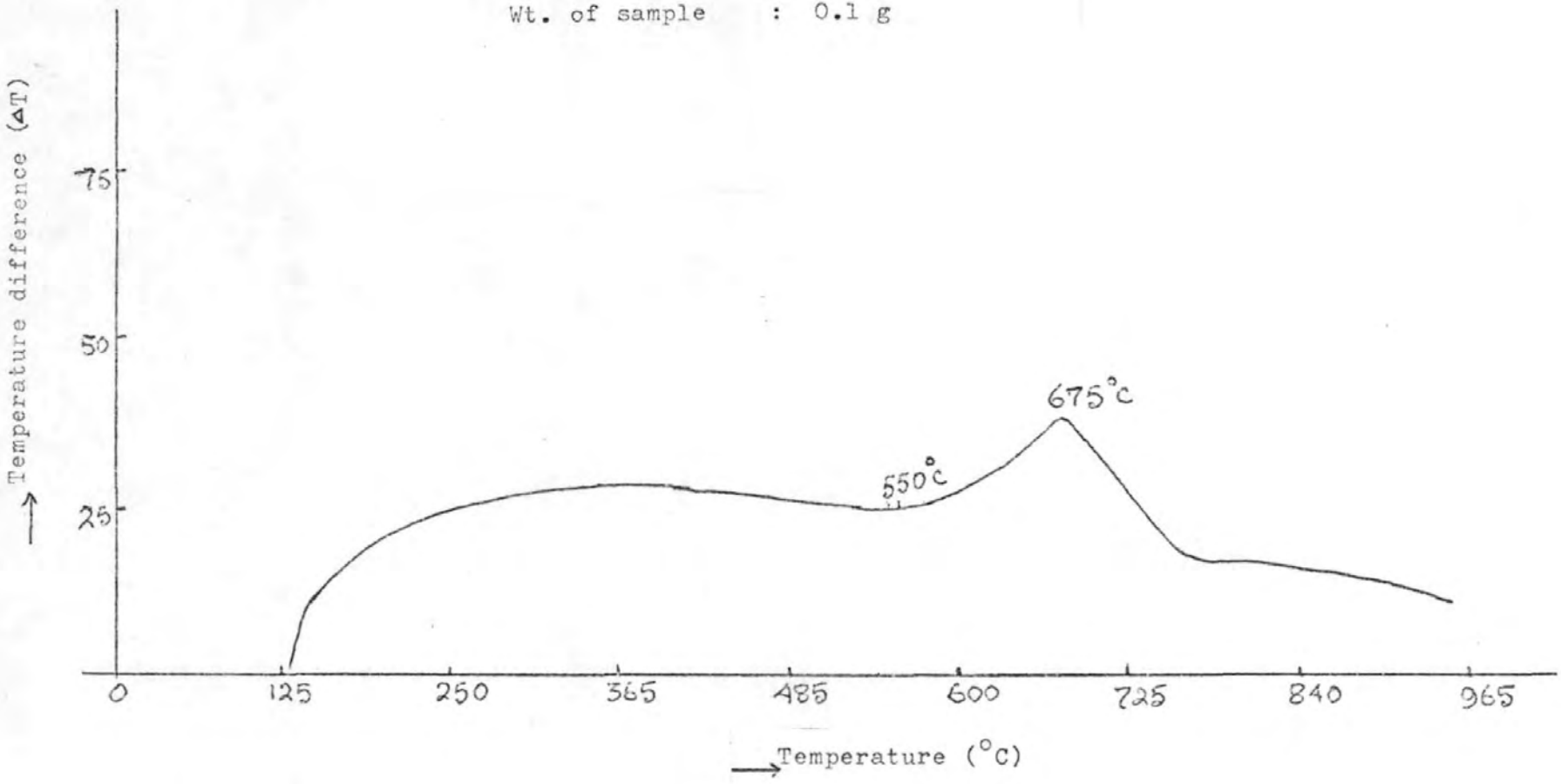

D.T.A. Curve of $\alpha$- ZnS

Figure 48

Flow of air : 20 cm $^3$/min

Rate of heating: 10°C/min

Wt. of sample : 0.1 g

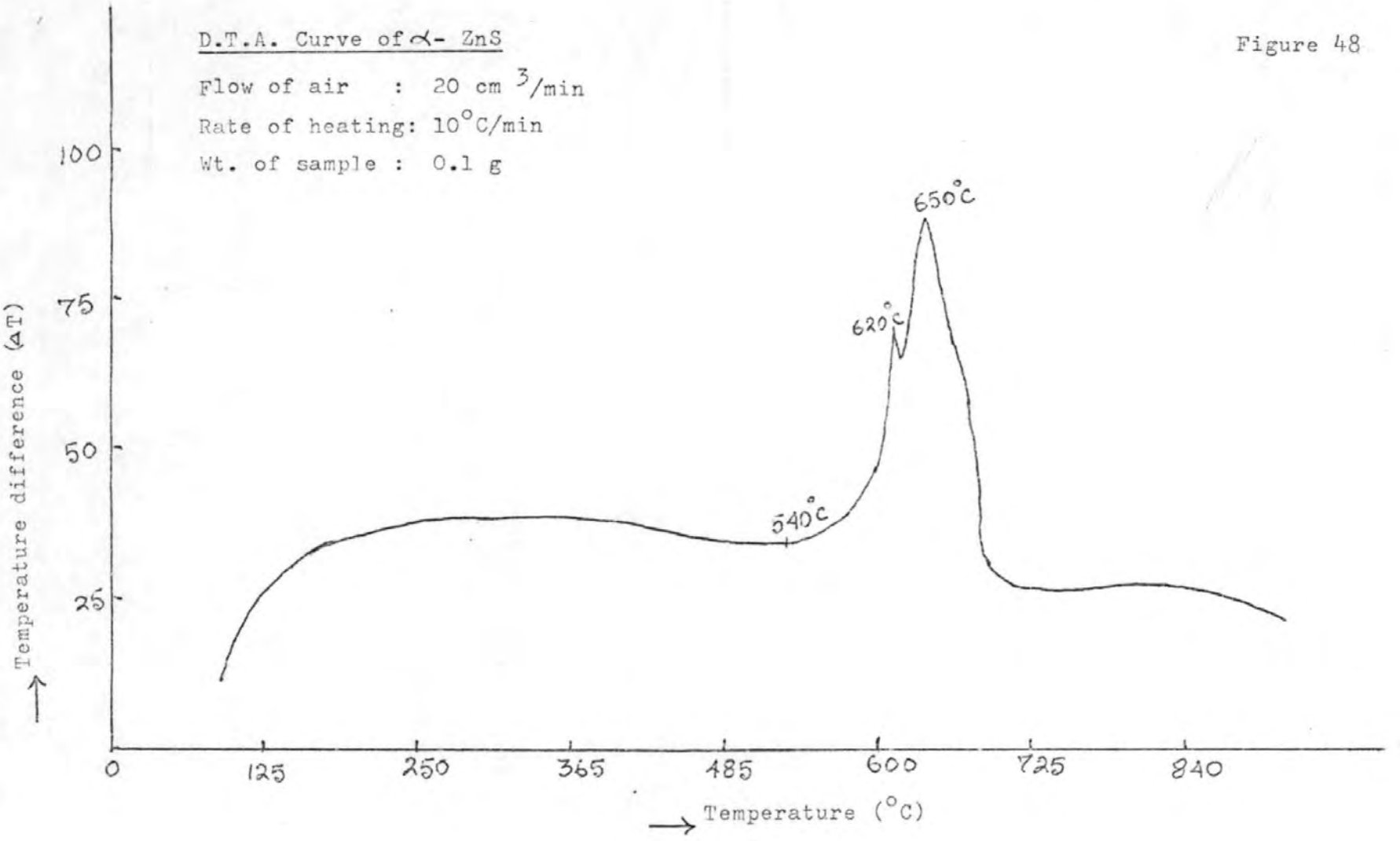

Figure 49

D.T.A. Curve of $\alpha$ - ZnS

Flow of air : 40 cm $^3$/min

Rate of heating: 10°C/min

Wt. of sample : 0.1 g

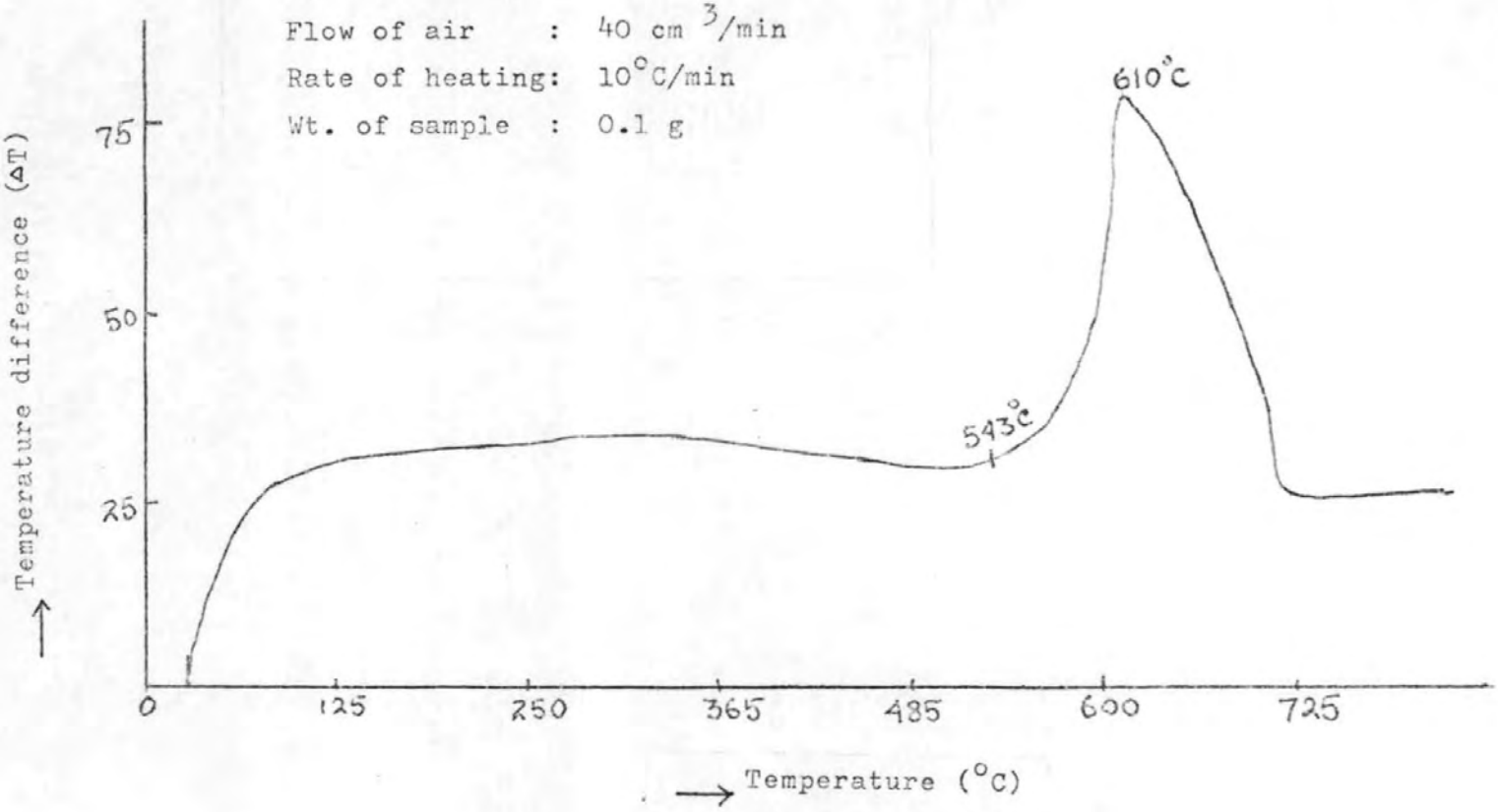

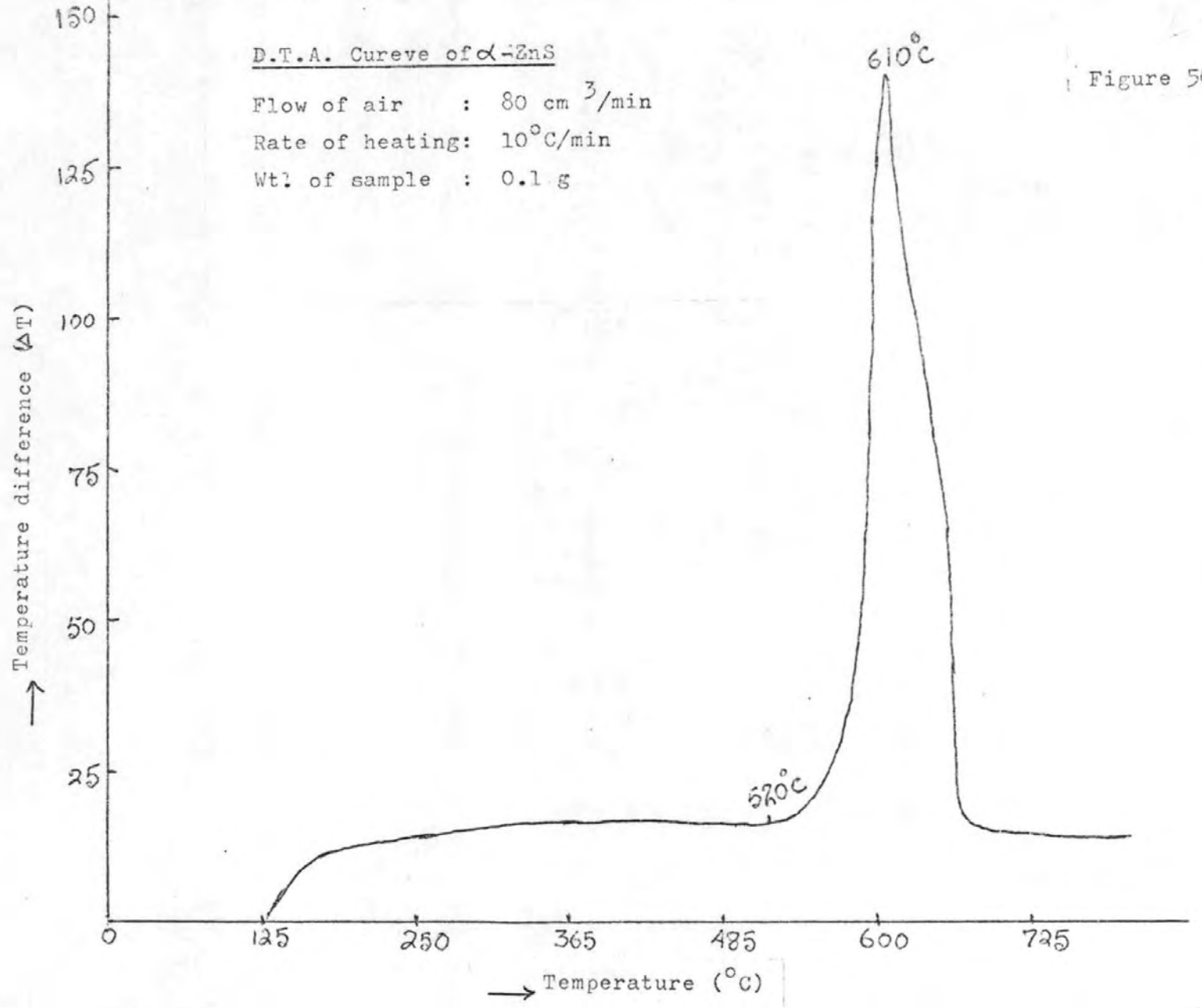
D.T.A. Cureve of α-ZnS
Flow of air : 80 cm 3/min
Rate of heating: 10°C/min
Wt. of sample : 0.1 g
610°C
520°C
150
125
100
75
50
25
0
125
250
365
485
600
725
Temperature difference (ΔT)
Temperature (°C)

Figure 50

Figure 51

D.T.A. Curves of $\alpha$-ZnS

Flow of $O_2$ enriched air : 80 $cm^3$/min
Rate of heating : 10°C/min
Wt. of sample : 0.1 g

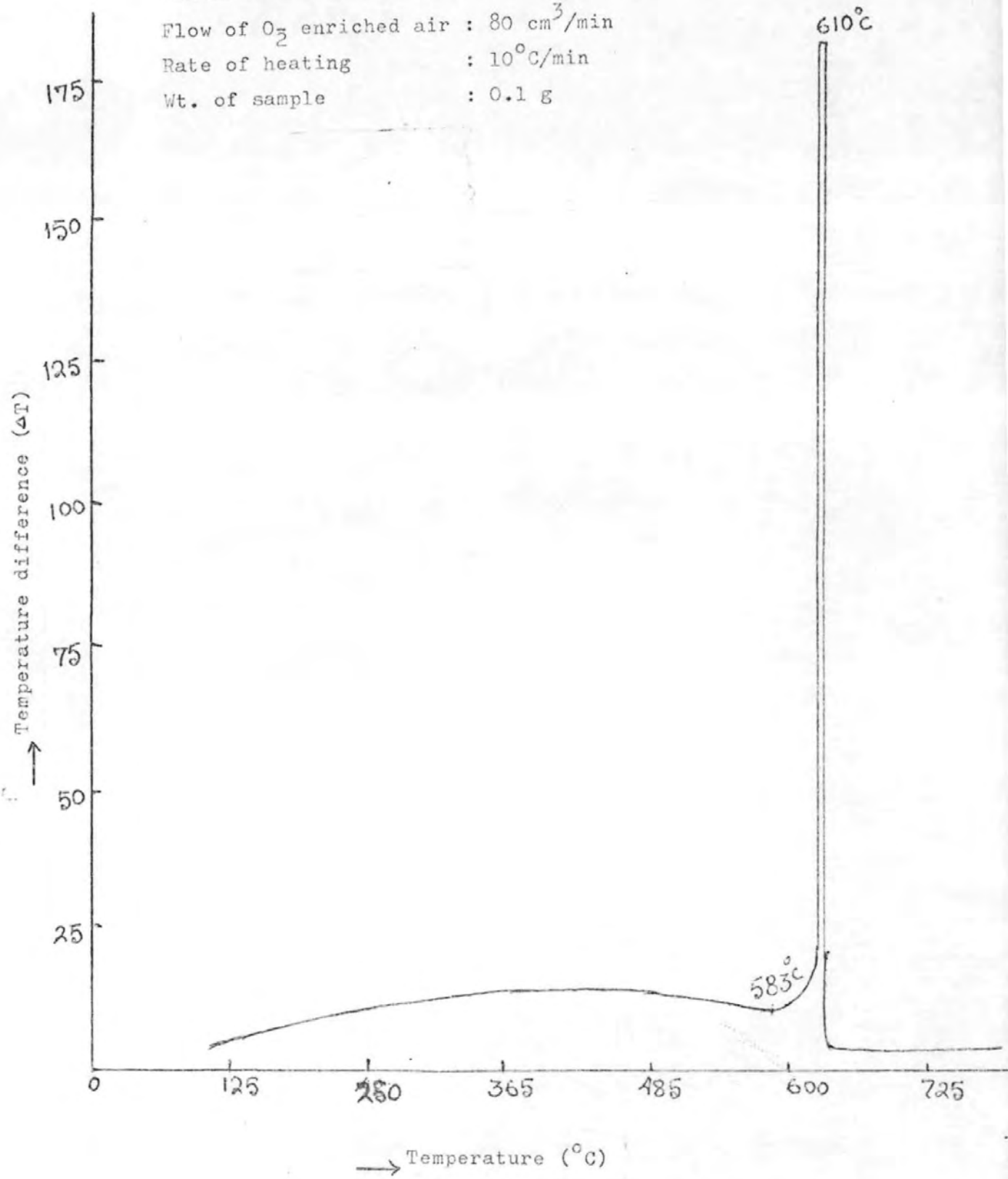

The $\beta$-ZnS would nucleate more rapidly, especially at temperatures of about 600°C, because of its much higher surface area (about 9 times specific surface of $\alpha$-ZnS) and poorer crystallinity than that of $\alpha$-ZnS ($\beta$-ZnS was prepared and aged at room temperature, compared with the $\alpha$-ZnS having been sintered at temperature above 600°C).

These factors will facilitate also development of more extensive surface reaction in the $\beta$-ZnS, giving an initial exothermic peak which is larger and located at a lower temperature than for $\alpha$-ZnS.

For the same reasons, the subsequent oxidation by advancing interface mechanism will proceed more readily for $\beta$-ZnS.

Since the particles of $\beta$-ZnS are generally smaller than those of the $\alpha$-ZnS, the oxidation of the $\beta$-ZnS will be completed in a much shorter time. Thus, the second exothermic peak for $\beta$-ZnS will be higher and narrower than that of $\alpha$-ZnS will occur over a correspondingly lower temperature range.

These observations were not made by previous investigators (61), as they used too excessive flows of air in their DTA studies. So they obtained always one exothermic peak instead of two in their DTA curves.

To determine the phases occuring during roasting at 570°C and 620°C, the samples oxidised at these temperatures were analysed chemically and by X-ray diffraction. In all cases, the presence of $ZnSO_4$ and ZnO along with unchanged ZnS was established.

The exothermic peaks at 570°C and 620°C represent the formation of zinc sulphate and oxide.

The dissociation of the zinc sulphate at higher temperatures should give an endothermic peak. This was not prominent in these experiments, but was observed at about 715°C for oxidation of zinc concentrates where larger amounts of zinc sulphate had been formed at lower temperatures.

The thermograms (Figures 46 and 51) show that the oxidation of samples with oxygen-enriched air proceed more intensely than with air. The peaks are shifted to lower temperatures and there is a narrowing of the temperature ranges of exothermic reactions.

4.4. Effect of sintering on zinc sulphide oxidation

In reactions of the type :

Solid A + Gas I $\longrightarrow$ Solid B + Gas II

as $2\ ZnS + 3\ O_2 \longrightarrow 2\ ZnO + 2\ SO_2$

and Solid A + Gas I $\longrightarrow$ Solid B

as $ZnS + 2\ O_2 \longrightarrow ZnSO_4$ ,

the rates are influenced by sintering of the solid materials. The sintering process reduces the internal porosity and total surface area. Consequently, the rates tend to be lowered because of reduction of the reaction interface. Formation of layers of solid products around the reactant particles impedes diffusion of the gases and reduces the reaction rates further, again to an extent dependent on degree of sintering.

Separate portions (about 7g) of synthetic $\alpha$- and $\beta$- zinc sulphides were calcined (A) for fixed times of 5 h at different temperatures, (B) for various times at each of a number of fixed temperatures in air in an electrical furnace.

The specific surface, S, of the cooled products was calculated by the B.E.T. procedure from sorption isotherms of nitrogen (and occasionally oxygen) at -183°C determined gravimetrically on the sorption balance. Where necessary, the products were analysed thermally and zinc oxide and sulphate contents determined as described previously. The initial $\alpha$- and $\beta$- zinc sulphide samples had widely different specific surfaces (5.7 and 46.4 $m^2 g^{-1}$), but their oxygen adsorption isotherms were both of type II (B.E.T. classification),

exhibiting little or no hysteresis at relative pressures below 0.3 similar to the more reactive zinc sulphides described in Chapter 3.

From these, and the corresponding nitrogen isotherms, the values obtained for the specific surface, S, likewise gave agreement within ca 5%. This applied also to the partly and completely oxidised samples. The variations in S with oxidation conditions are shown in Figures 52 to 53.

4.2.1 α-Zinc sulphide oxidation

Oxidation of α- zinc sulphide at lower temperature results in small increases in surface. Thus, at 500°C 26.5% of the zinc sulphide oxidises in 5 h. with increase in specific surface from 5.7 to 7.0 $m^2g^{-1}$ (Fig.52). This indicates that some of the crystallites of oxidised product split off from the initial zinc sulphide crystallites, because of differences in molecular volume and any differences in crystal lattice type between the zinc sulphide (α- hexagonal, β- cubic), zinc oxide (hexagonal) or zinc sulphate (orthorhombic).

From X-ray density data, it is calculated that there are volume decreases of about 40% when the two forms of zinc sulphide ($\underline{d}$ = 4.09) are converted to zinc oxide ($\underline{d}$ = 5.68) and volume increases of about 75% when zinc sulphate is formed ($\underline{d}$ = 3.88).

At higher temperatures, above 600°C, there is loss of surface on oxidation of the zinc sulphide indicating sintering. This is demonstrated further by comparing the actual surface areas, $S^1$, of the products when 1g samples of zinc sulphide are oxidised. Zinc oxide is the main oxidation product (cf section 4.1), less than 1% of the ZnS being converted to zinc sulphate in the series of 5h calcinations.

Progressive changes in surface area have been calculated to a first approximation on the basis that there is no sintering of

Figure 52

PURE ZINC SULPHIDE CALCINED FOR 5 HOURS

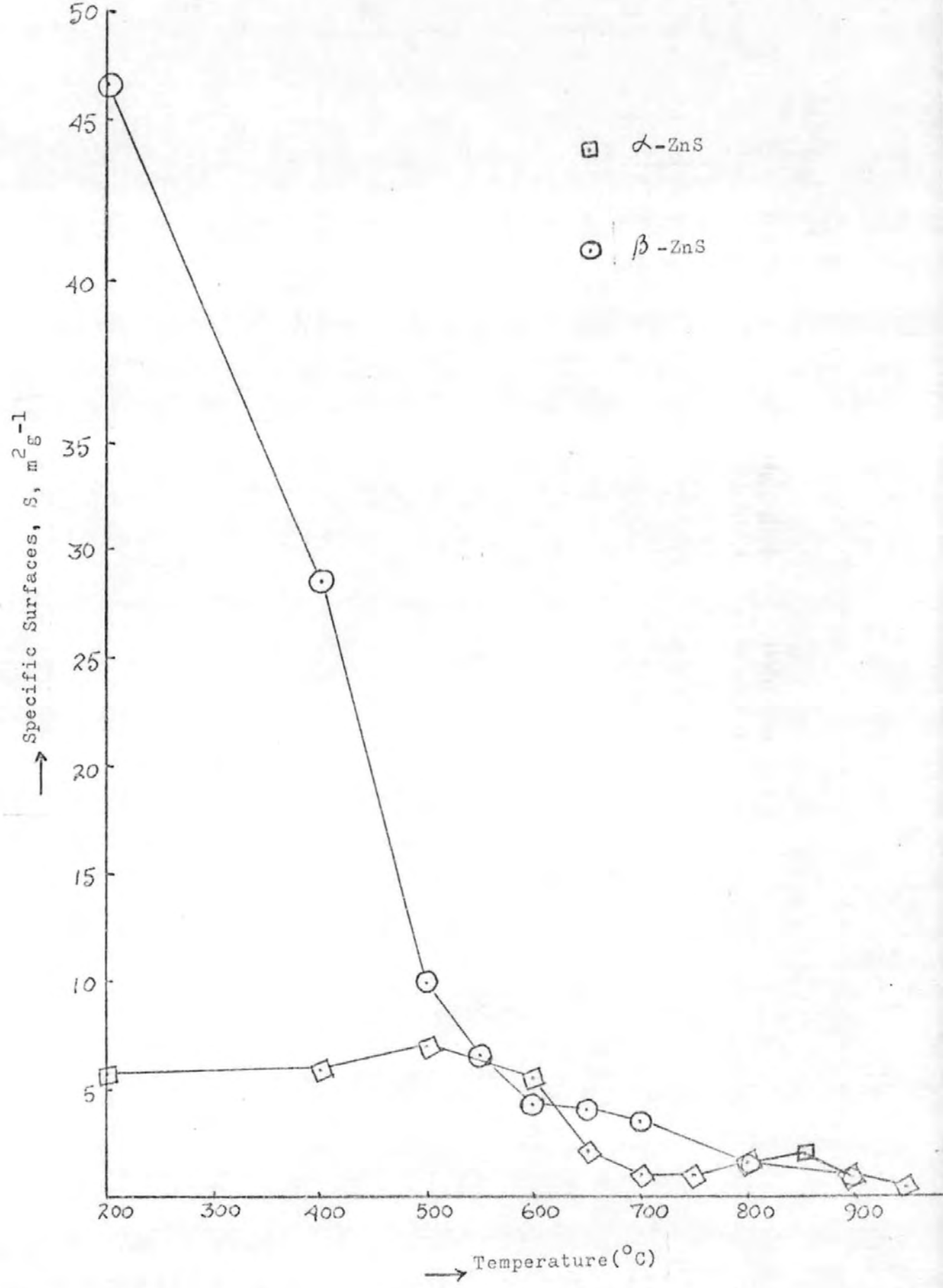

Figure 53

α-Zinc sulphide calcined for different time intervals

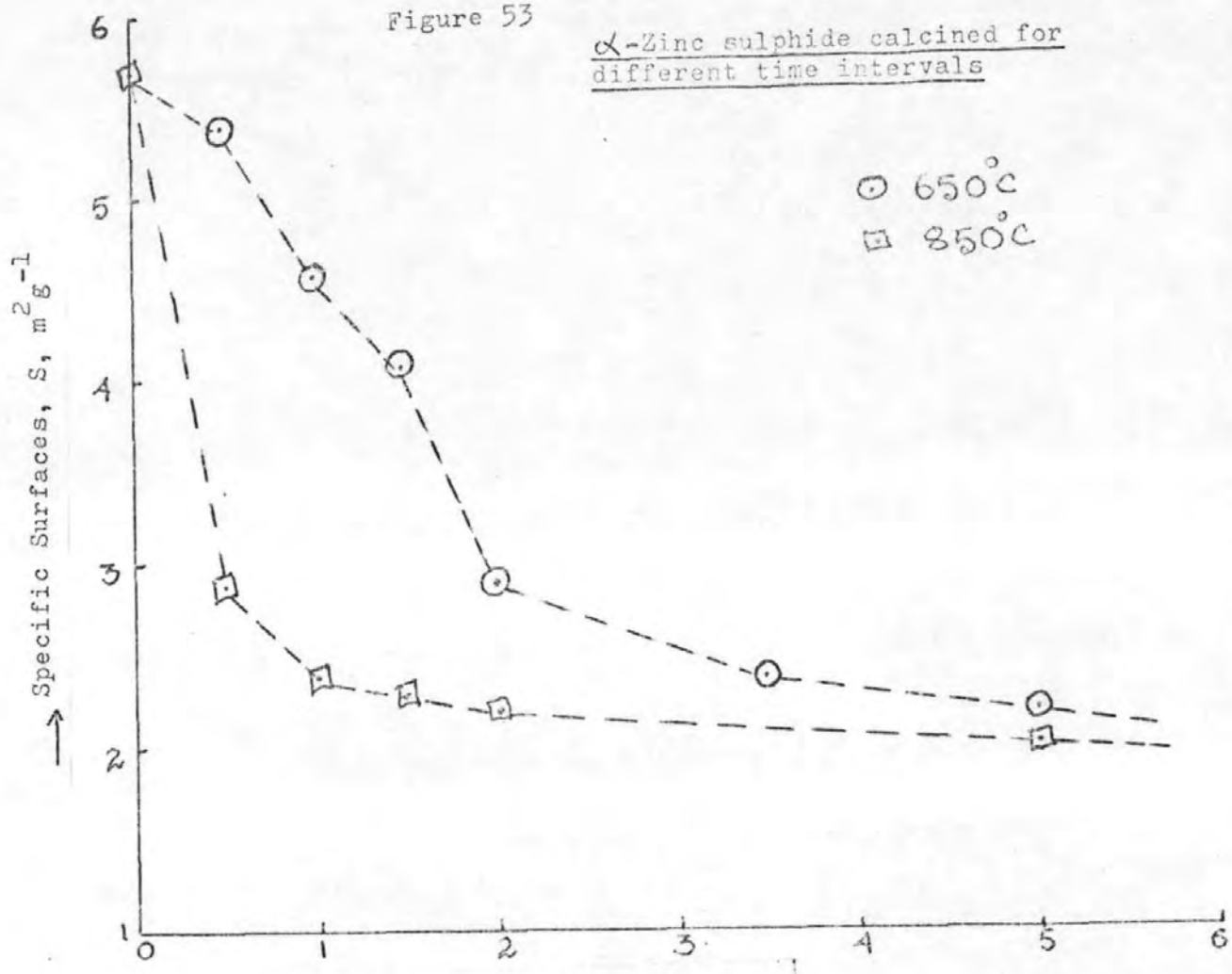


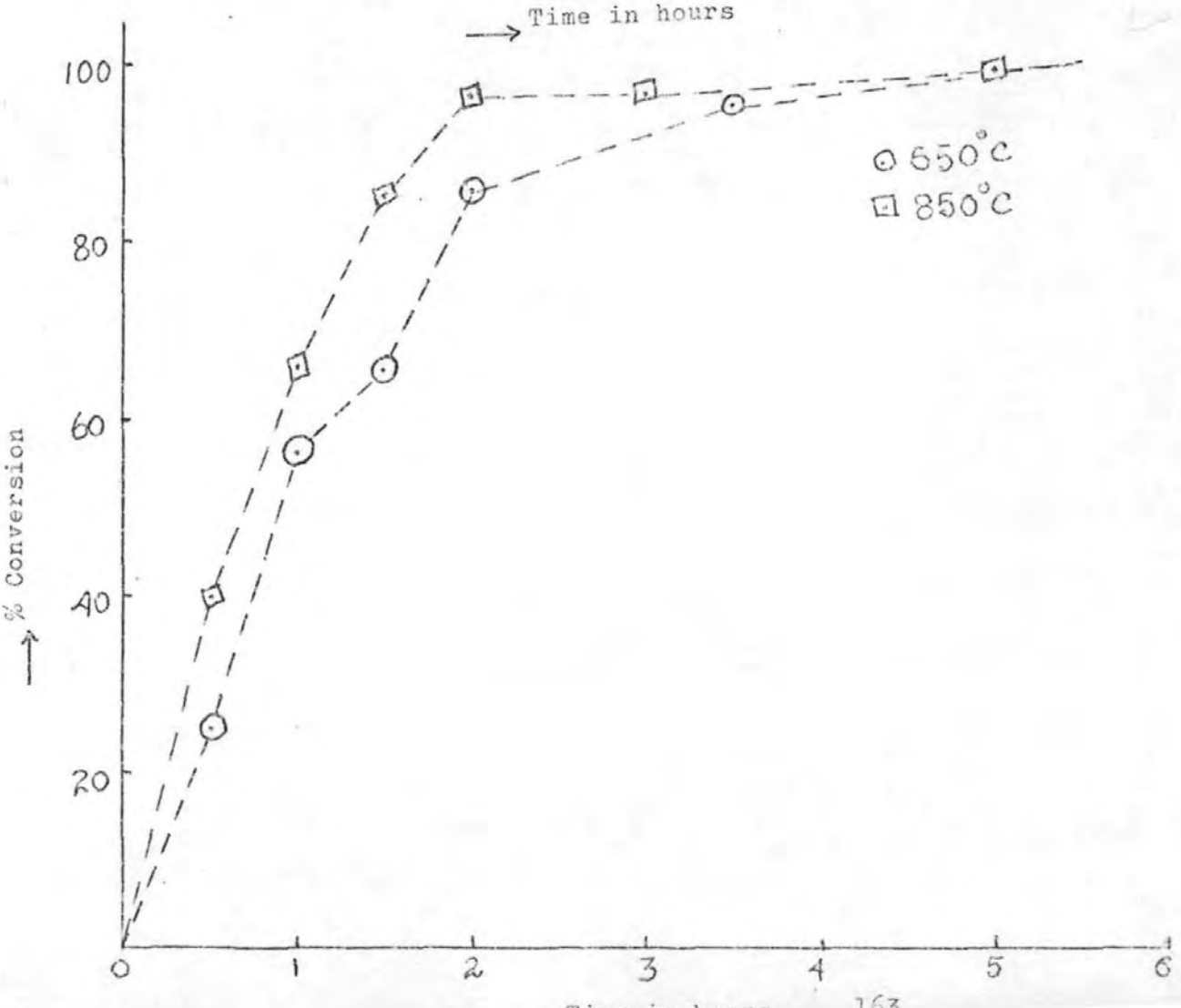

the products, but that they form stable layers around each initial zinc sulphide particle, with the oxidation proceeding inwards from the outside of each sulphide particle by an advancing interface mechanism.

Since zinc sulphide changes its volume 0.6-fold when it forms zinc oxide, the oxidation of $\underline{x}$g of a 1g sample of zinc suphide would cause a proportionate volume change of $\left[(1 - x) + 0.6x\right] = \left[1 - 0.4x\right]$. If development is approximately the same in each direction, the proportionate change in surface, $S^1/S$, would be $\left[1 - 0.4x\right]^{2/3}$. The calculated values for $S^1/S$ are compared in Figs.54-56b and Tables 15 and 16 and are larger than the experimental value where sintering of the products is appreciable.

The changes in the number of crystallites, approximately $(S^1 expt/S^1 cala)^3$, as the result of the products splitting off at lower temperatures and sintering at higher temperatures are shown in Figs.56a & b where they are compared with the average crystallite sizes of the samples. This again illustrates extensive sintering at the higher temperatures.

Sintering of the zinc oxide is expected to become appreciable at temperatures above about 500°C; the minimum temperature to initiate sintering by surface diffusion (one-third of the m.p. in degrees absolute, 2250K) is 750K (477°C). Sintering becomes extensive at temperatures above 850°C when crystal lattice diffusion becomes operative, i.e. at temperatures above the Tammann temperature, Tm, (half of the m.p. in degrees absolute) which is 1125K (852°C).

Evidently sintering of the zinc oxide is accelerated between 500°C and 850°C by the presence of small amounts of low melting zinc sulphate (m.p. with decomposition 600°C). This is more noticeable between 500°C and 700°C when the surface area falls to a minimum

TABLE 15 — $\alpha$-ZnS calcined for 5 hours

| Temp. °C | Surface area $S_m^2 g^{-1}$ | x (fraction converted to ZnO) | actual surface areas $m^2 g^{-1}$ | | multiple change in number of crystallites $(S'expt/S'calc)^3$ | number of initial ZnS crystallites per ZnO crystal | average crystallite size of product, $\mu m$ |
|---|---|---|---|---|---|---|---|
| | | | S'expt | S'calc | | | |
| 0°(200°) | 5.7 | - | 5.7 | 5.7 | 1 | | 0.26 |
| 400° | 5.9 | ~ small | 5.9 | 5.7 | 1.11 | | 0.25 |
| 500° | 7.0 | 0.265 | 6.7 | 5.3 | 2.02 | | 0.20 |
| 600° | 5.4 | 0.937 | 4.6 | 4.2 | 1.21 | | 0.20 |
| 650° | 2.2 | > 0.967 | 1.8 | 4.1 | 0.09 | 11 | 0.48 |
| 700° | 1.1 | ca 1.00 | 0.92 | 4.0 | 0.011 | 89 | 0.96 |
| 750° | 1.2 | " | 1.0 | 4.0 | 0.016 | 64 | 0.88 |
| 800° | 1.7 | " | 1.4 | 4.0 | 0.043 | 23 | 0.63 |
| 850° | 2.0 | " | 1.7 | 4.0 | 0.077 | 13 | 0.53 |
| 900° | 1.0 | " | 0.8 | 4.0 | 0.008 | 125 | 1.06 |
| 950° | 0.5 | " | 0.4 | 4.0 | 0.001 | 1000 | 2.12 |

TABLE 16

β-ZnS calcined for 5 hours

| Temp. °C | Surface area $Sm^2g^{-1}$ | x (fraction converted to ZnO) | actual surface areas $m^2g^{-1}$ | | multiple change in number of crystallites $(S'expt/S'calc)^3$ | number of initial ZnS crystallites per ZnO crystal | average crystallite size of product, μm |
|---|---|---|---|---|---|---|---|
| | | | S'expt | S'calc | | | |
| 0°(200°) | 46.4 | 0 | 46.4 | 46.4 | 1 | 1 | 0.032 |
| 400° | 28.5 | 0.261 | 27.2 | 43.2 | $2.48 \times 10^{-1}$ | 4 | 0.048 |
| 500° | 10.0 | 0.582 | 9.0 | 38.9 | $1.24 \times 10^{-2}$ | 81 | 0.12 |
| 550° | 6.5 | 0.900 | 5.5 | 34.4 | $4.09 \times 10^{-3}$ | 240 | 0.17 |
| 600° | 4.2 | 0.964 | 3.5 | 33.5 | $1.14 \times 10^{-3}$ | 880 | 0.25 |
| 650° | 4.1 | ca 1.00 | 3.4 | 33.3 | $1.07 \times 10^{-3}$ | 940 | 0.26 |
| 700° | 3.4 | " | 2.8 | 33.2 | $6.0 \times 10^{-4}$ | 1670 | 0.31 |
| 800° | 1.7 | " | 1.4 | 33.1 | $7.5 \times 10^{-5}$ | 13000 | 0.63 |
| 900° | 1.0 | " | 0.8 | 33.0 | $1.4 \times 10^{-5}$ | 70000 | 1.06 |

Figure 54

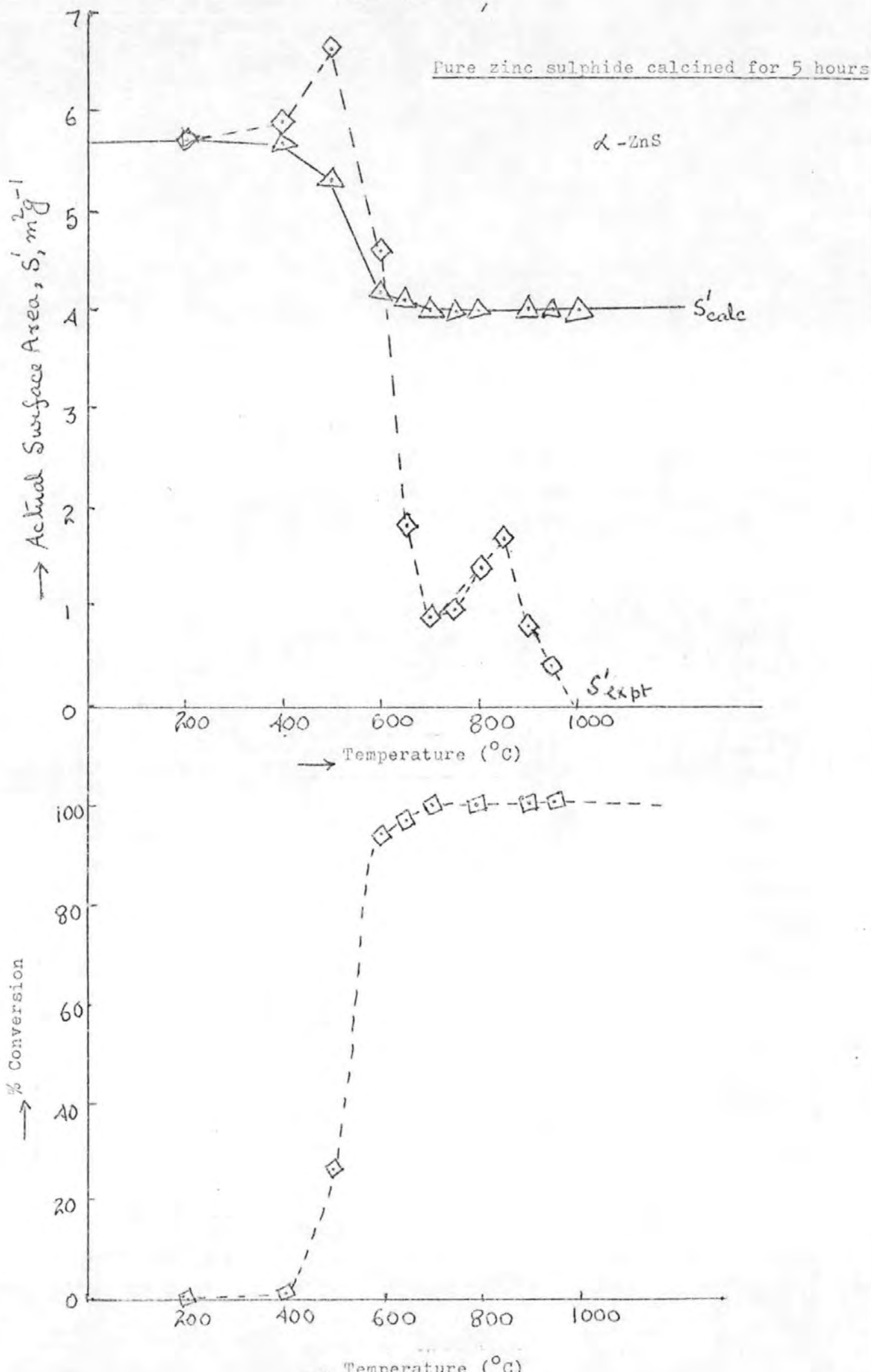
Pure zinc sulphide calcined for 5 hours
α-ZnS
S'calc
S'expt
→ Actual Surface Area, S', m²g⁻¹
→ Temperature (°C)
→ % Conversion
→ Temperature (°C)

Figure 55

Pure zinc sulphide calcined for 5 hours

$\beta$-ZnS

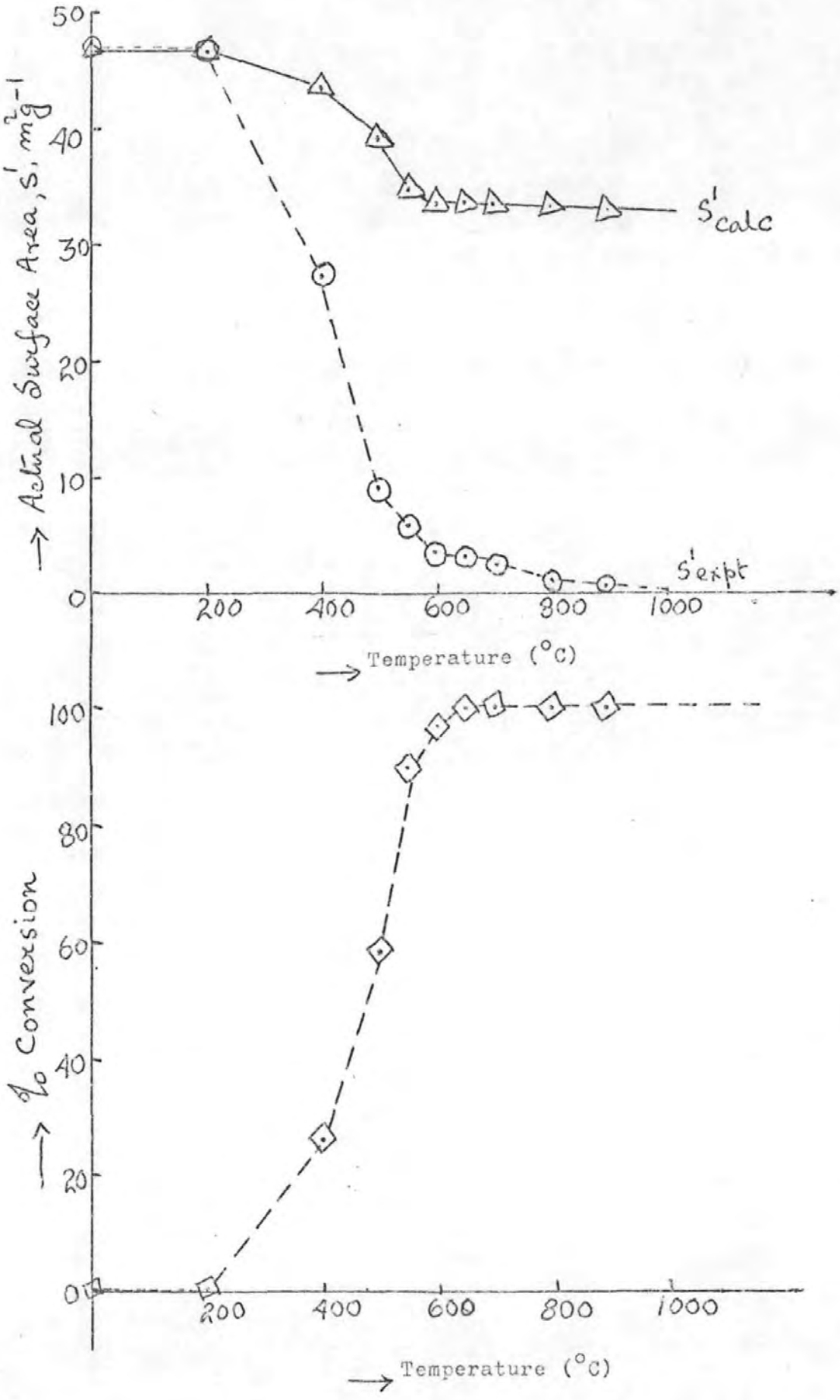

Pure zinc sulphide calcined for 5 hours

Fig 56a

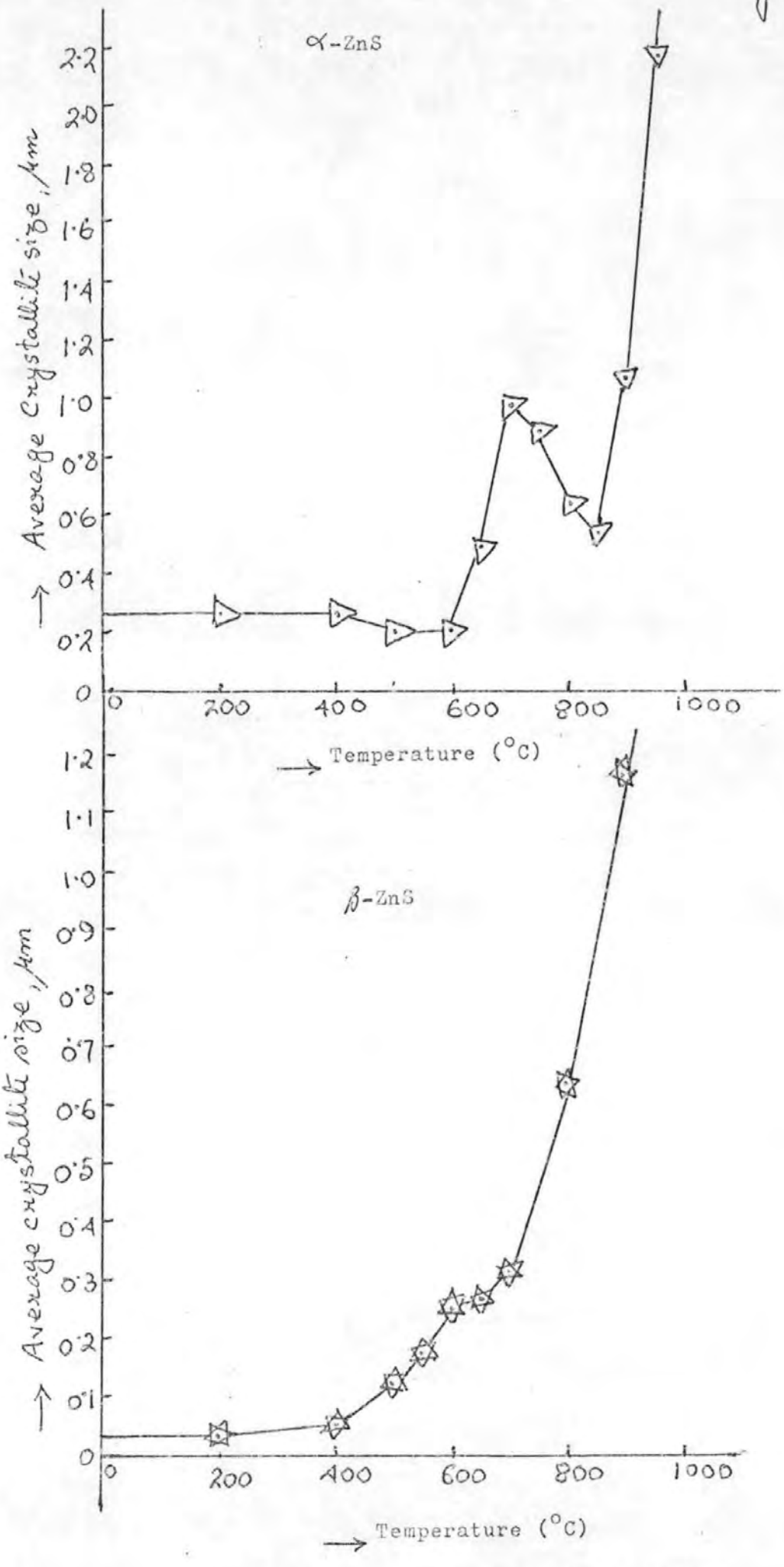


PURE ZINC SULPHIDE CALCINED FOR 5 HOURS

Fig 56b

Pure zinc sulphide calcined for 5 hours

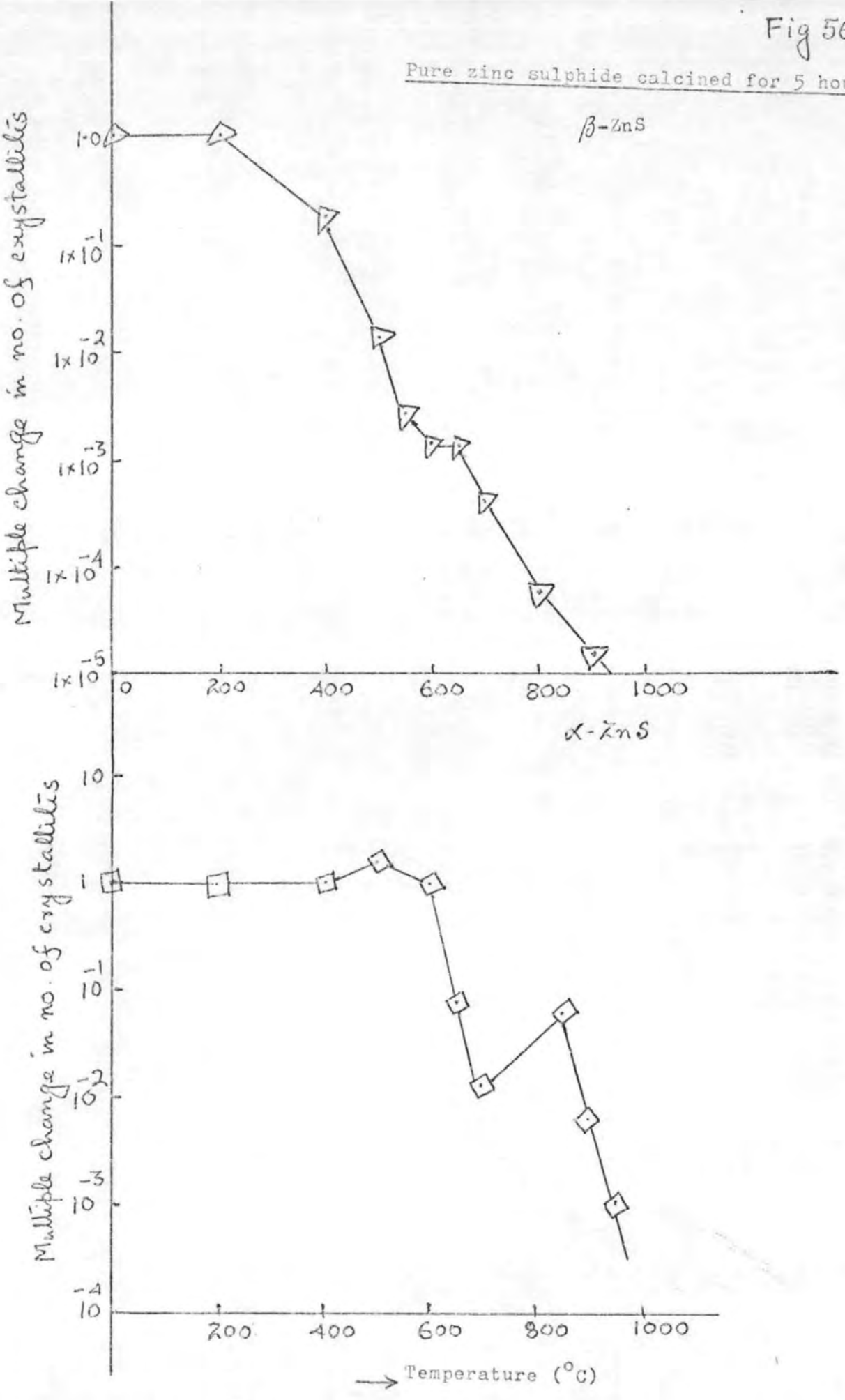

value (in Figs 54 and 55).

The amount of zinc sulphate becomes very small and progressively less as the tmperature rises from 700°C to 850°C, above which zinc oxide is the exclusive product.

The effect of sulphate on the sintering is further shown when the $\alpha$- zinc sulphide is oxidised in a platinum crucible at 550°C. For reasons discussed in section 4.1, the platinum enhances formation of zinc sulphate, so that in 5 h. at this temperature 60% of the zinc sulphide is converted to zinc sulphate, and only 40% to zinc oxide. The specific surface of the product is only $1.9 m^2 g^{-1}$ compared with about $6 m^2 g^{-1}$ indicated for this temperature in Fig.52 where only about 1% of the zinc sulphide has been converted to sulphate (and platinum is absent).

Further information regarding the oxidation process is obtained from the data in Figs.56-59 and Tables 17 & 18 for the calcination of $\alpha$-zinc sulphide at 650° and 850°C for different lengths of time. There is quite appreciable sintering throughout the oxidations as evidenced by the experimental surface area, $S^1$, being much lower than those calculated (on the basis of no sintering) Figure 4ab. The numbers of crystallites progressively decrease and their average sizes increase (Figs. 56-57).

The oxidation rates, Figure 60, approximately correspond to parabolic kinetics following short induction periods. This is consistent with nucleation and initial reaction on the surface of the zinc sulphide particles, followed by the coating of the particles with stable zinc oxide layers which may merge with those on adjoining particles as sintering proceeds. Subsequently, the reaction rate is controlled by a diffusion mechanism, typified by parabolic kinetics.

TABLE 17 — α-ZnS calcined for different time intervals at 650°C

| Time in hours | Surface area $S_m^2 g^{-1}$ | x (fraction converted to ZnO) | actual surface areas $m^2 g^{-1}$ | | multiple change in number of crystallites $(S'expt/S'calc)^3$ | number of initial ZnS crystallites per crystal product | average crystallite size of product, μm |
|---|---|---|---|---|---|---|---|
| | | | S'expt | S'calc | | | |
| 0 | 5.7 | - | 5.7 | 5.7 | 1 | 1 | 0.26 |
| ½ | 5.4 | 0.244 | 5.2 | 5.3 | 0.95 | 1 | 0.26 |
| 1 | 4.6 | 0.553 | 4.2 | 4.9 | 0.63 | 1.5 | 0.27 |
| 1½ | 4.1 | 0.663 | 3.7 | 4.6 | 0.52 | 2 | 0.29 |
| 2 | 2.9 | 0.858 | 2.5 | 4.3 | 0.20 | 5 | 0.39 |
| 3½ | 2.4 | 0.967 | 2.0 | 4.1 | 0.12 | 8 | 0.45 |
| 5 | 2.2 | ca 1.00 | 1.8 | 4.0 | 0.09 | 11 | 0.48 |

TABLE 18

α-ZnS calcined for different time intervals at 850°C

| Time in hours | surface area, $Sm^2g^{-1}$ | x (fraction converted to ZnO) | actual surface areas, S'expt | actual surface areas, S'calc | multiple change in number of crystallites $(S'expt/S'calc)^3$ | number of initial ZnS crystallites per crystal of product | average crystallite size of product um |
|---|---|---|---|---|---|---|---|
| 0 | 5.7 | - | 5.7 | 5.7 | 1 | 1 | 0.26 |
| ½ | 2.9 | 0.399 | 2.7 | 5.1 | 0.15 | 7 | 0.46 |
| 1 | 2.4 | 0.635 | 2.15 | 4.7 | 0.096 | 10.5 | 0.51 |
| 1½ | 2.3 | 0.853 | 1.98 | 4.32 | 0.096 | 10.5 | 0.49 |
| 2 | 2.2 | 0.968 | 1.85 | 4.10 | 0.091 | 11 | 0.48 |
| 3 | 2.1 | 0.969 | 1.80 | 4.10 | 0.084 | 12 | 0.51 |
| 5 | 2.0 | ca 1.00 | 1.77 | 4.00 | 0.077 | 13 | 0.53 |

Figure 56 α-Zinc sulphide calcined at 650°C for different time intervals.

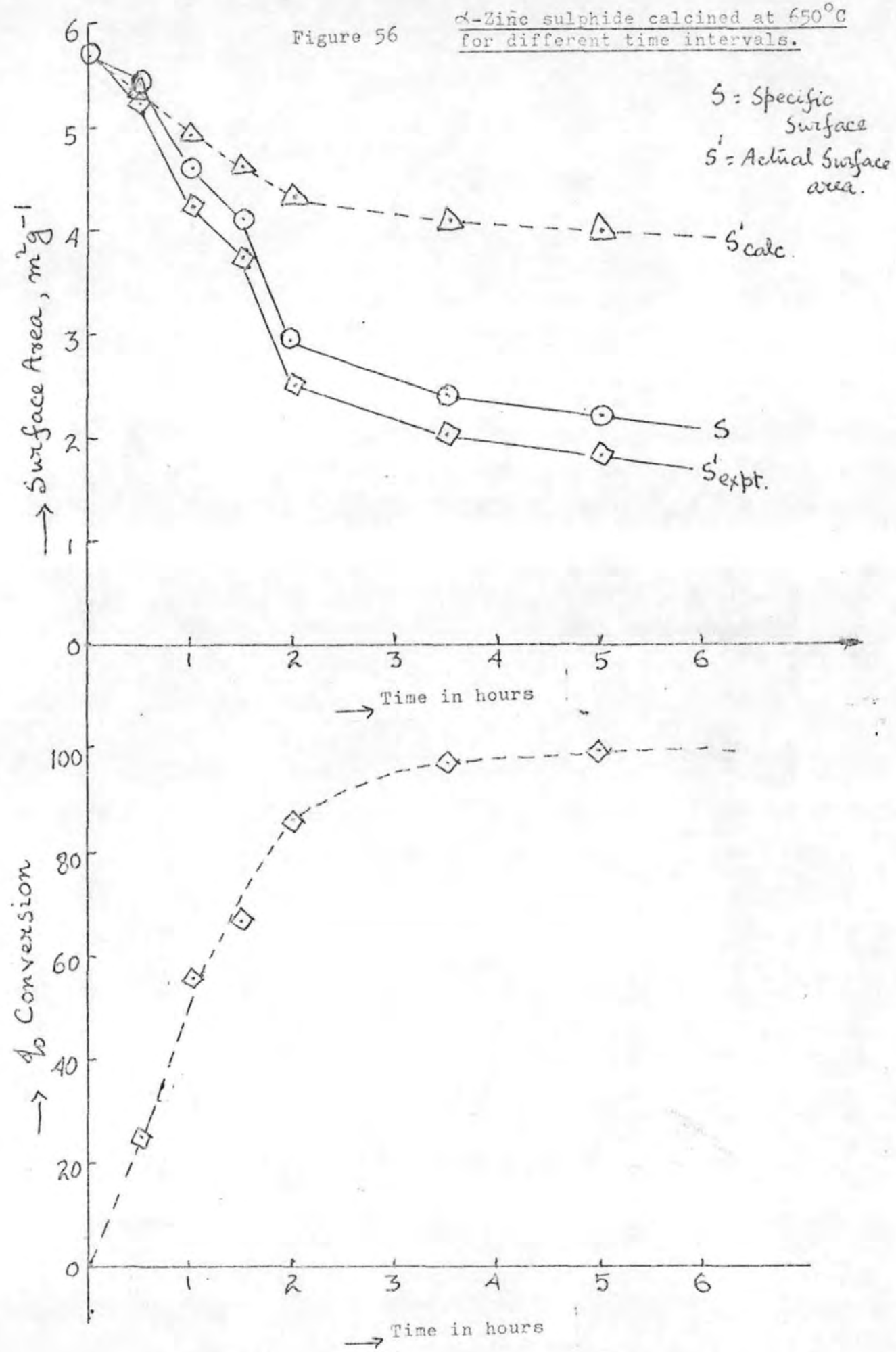

α-Zinc sulphide calcined at 850°C
for different time intervals

Figure 57

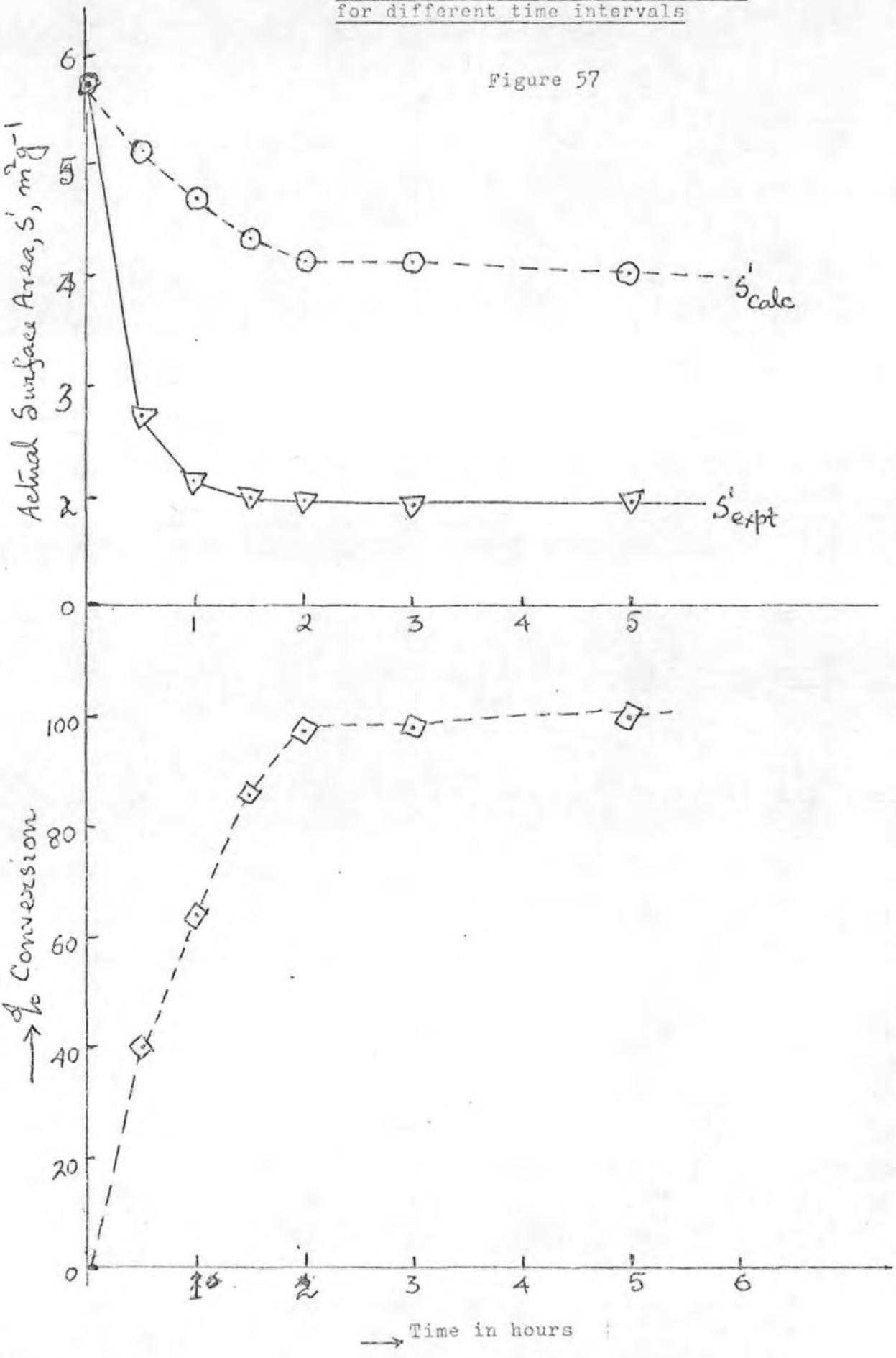

Figure 58 α-Zinc sulphide calcined at 650°C for different time intervals

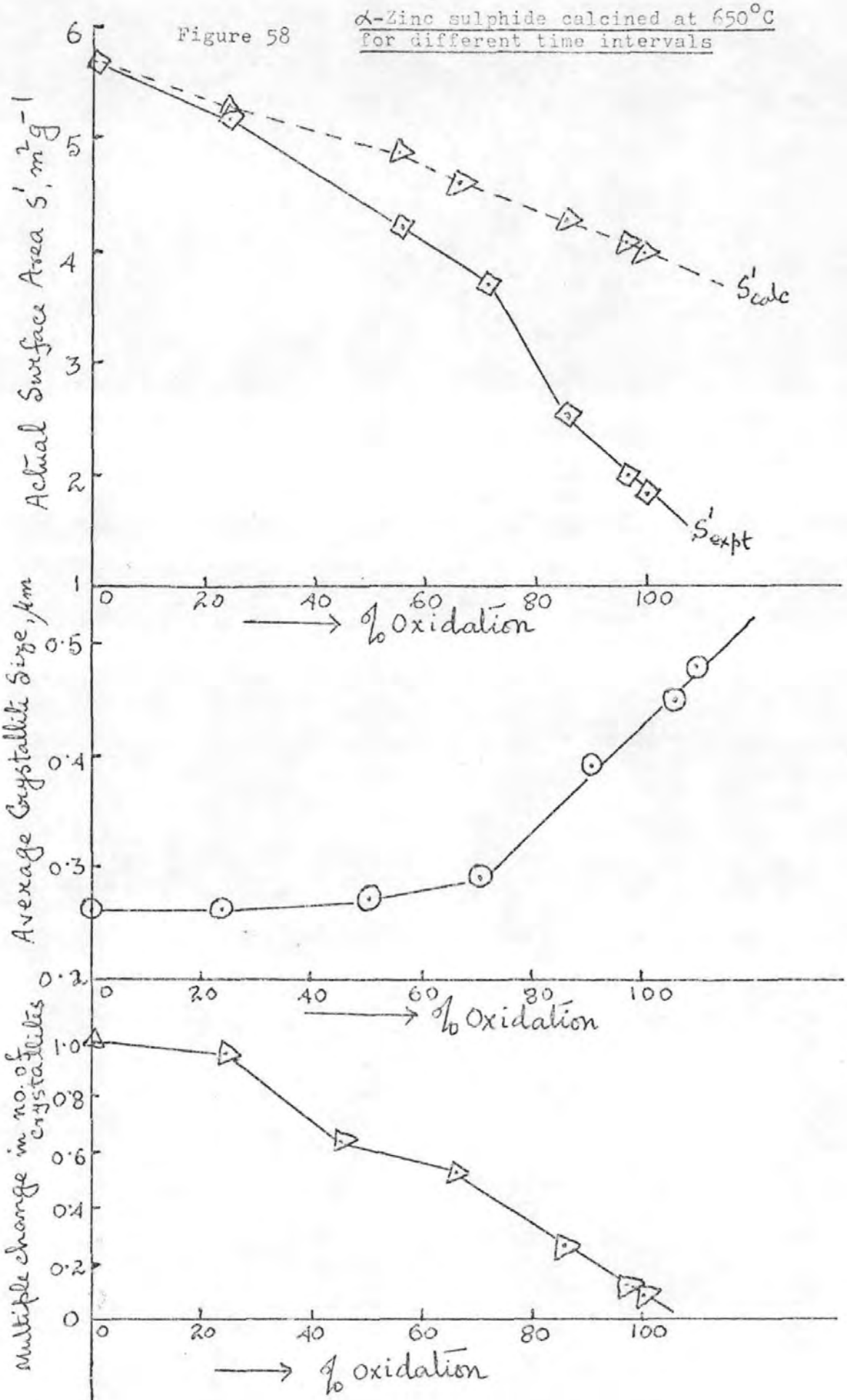

α-Zinc sulphide calcined at 850°C for different time intervals

Figure 59

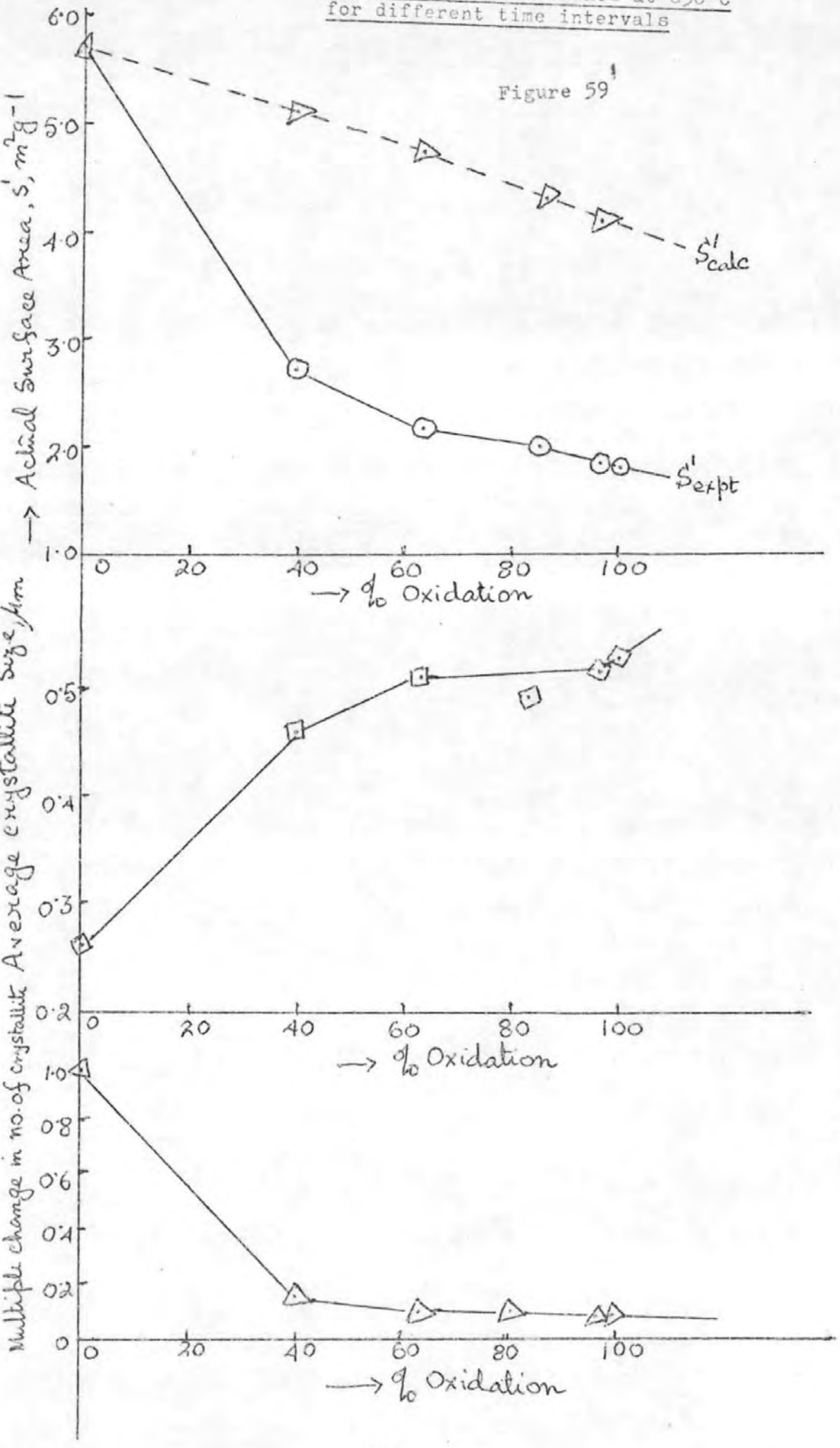

α-Zinc sulphide calcined for different time intervals

## TEST OF KINETICS AT 650° AND 850°C

Figure 60

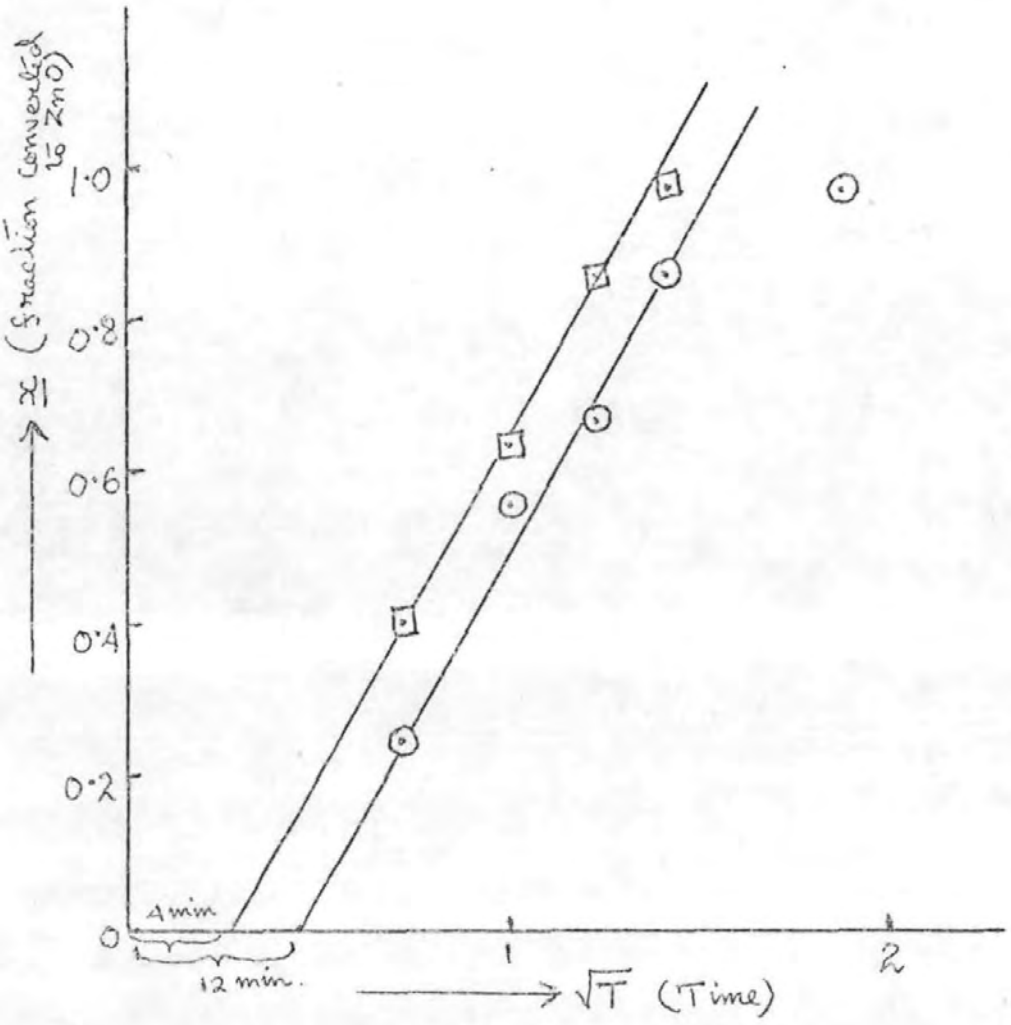

4.4.2 $\beta$-Zinc sulphide oxidation

In the oxidation of $\beta$-ZnS there is also extensive sintering of the products. This is shown by considerable decreases in surface area (Figure 52 and Table 16 ) even at lower temperatures, viz.400° - 500°C, when about 25 - 60% of the zinc sulphide has been oxidised. It may be difficult at the lower temperatures for the zinc oxide to immediately form stable layers around the zinc sulphide crystallites partly on account of their poor crystallinity and partly because the $\beta$- zinc sulphide has a cubic lattice compared with the hexagonal lattice of the zinc oxide. In contrast, $\alpha$-zinc sulphide and zinc oxide both have hexagonal lattices with approximately the same axial ratios (C/a = 1.64 and 1.60 respectively).

Thus, some sintering of the zinc sulphide may occur by surface diffusion in the earlier stages of the oxidation at lower temperatures (one-third of m.p. of ZnS in degrees absolute is 708K or 435°C).

At higher temperatures, above 550°C, the $\beta$-ZnS is almost completely oxidised to zinc oxide within the 5 h calcination time, and the products have specific surfaces and average crystallite sizes comparable with those obtained from the coarser $\alpha$-ZnS. Again, the products are mainly zinc oxide, with less than 1% of the zinc sulphide being converted to sulphate. The effect of this sulphate on the sintering of the zinc oxide is hardly noticeable against the considerable decrease (possibly at 600° ?) in surface during each calcination.

4.4.3 Crystallite and aggregate sizes of the oxide products

The average crystallite sizes (equivalent spherical diameters) of the zinc oxide products are presented in Figs.56a and b and Tables 15&16 calculated from the specific surfaces. Those for the oxidation of $\alpha$-zinc sulphide, are compared with the sizes of their aggregates shown by electron micrographs in Figures 61 to 66(1).

For the 5 hours calcination at 650°C oxidation of the zinc sulphide to zinc oxide is practically complete. The zinc oxide consists of aggregates with their larger (hexagonal) crystallites of about 0.5 - 1 μm visible at edges. This is in accordance with the average crystallite size from surface area being 0.48 μm (Figure 61). At 700°C aggregates are generally 2-3 μm size. A few portions of crystallites distinguishable at edges of some aggregates suggest average crystallite sizes of about 1 μm. Edges of smaller aggregates somewhat rounded, denoting onset of sintering (Figure 63).

At 750°C growth of acicular crystals of ZnO are observed. The crystals are about 0.2 to 0.5 μm thick and up to several microns in length.

Replicas of the shorter (and broken longer) crystals are shown in Fig.66(). The major crystals have thickness of 0.1-0.2 μm. At 800°C acicular crystals are merging to form blocks with rounded edges (Figure 62). Above 850°C (to 1100°C) when crystal lattice diffusion becomes appreciable, progressively larger aggregates are formed with rounded edges (Figures 63-65 cf average crystallite sizes calculated from specific surfaces of about 0.5, 1 and 2 μm at 850°, 900° and 950°C respectively.

The sintering above 850°C was sufficiently extensive to impede the oxidation rate, so that it was not much greater at 850°C than at 650°C. For zinc sulphide compacts, the rate was lower at 950°C than at 900°C (96), cf negative temperature coefficients occasionally found in oxidation of metals such as Nb (96a).

The sintering process reduces the internal porosity and total surface area and consequently the reaction rates are lowered. This was confirmed by the fact that when compacts of zinc sulphide presintered under nitrogen at 1050°C for 2 hours were used in the roasting experiments, the reaction rates are lowered.

FIGURE 61

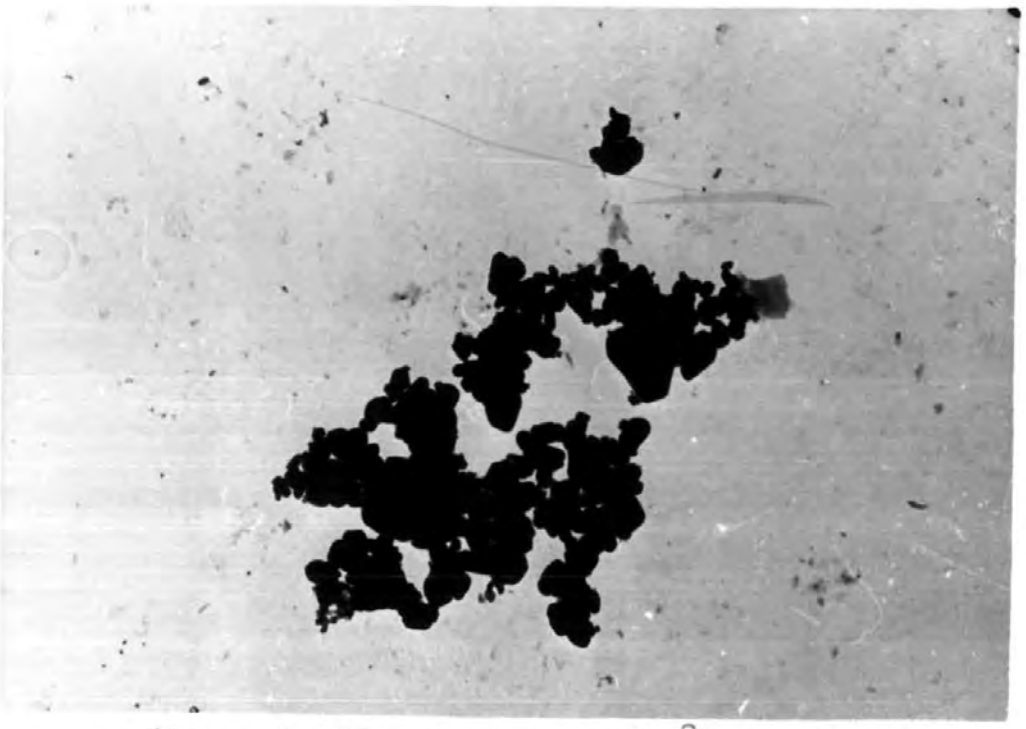

- Zinc sulphide roasted at 625°C for 5 hours

Magnification: x 13,000

FIGURE 62

(a)

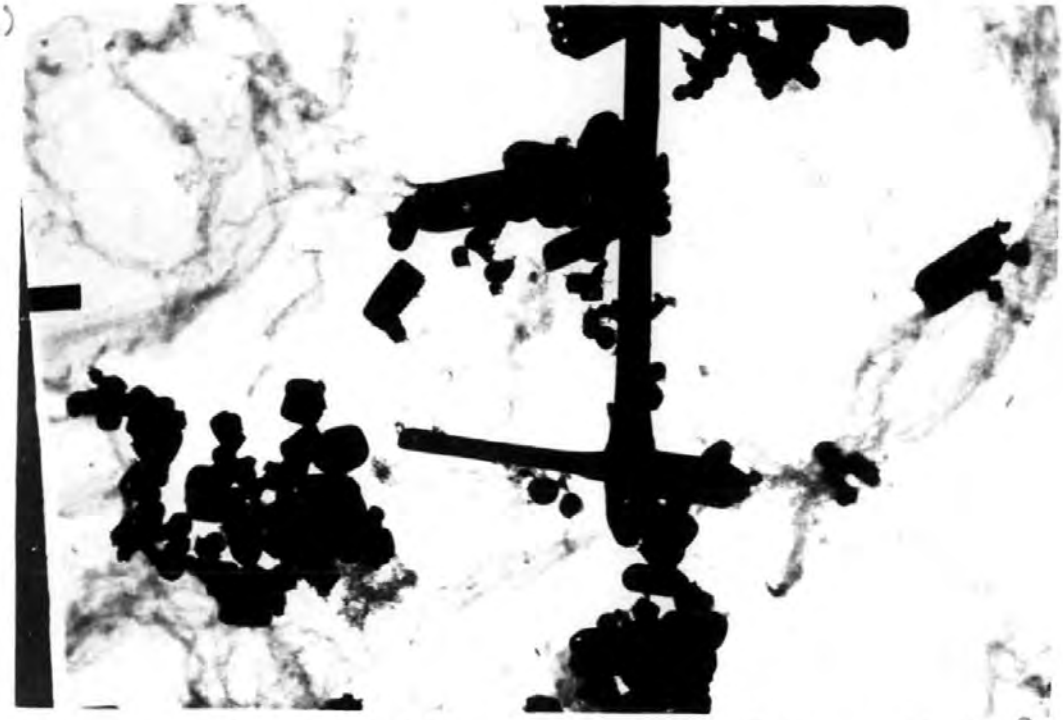

- Zinc sulphide calcined for 5 hours at 750°C

Magnification: x 13,000

(b)

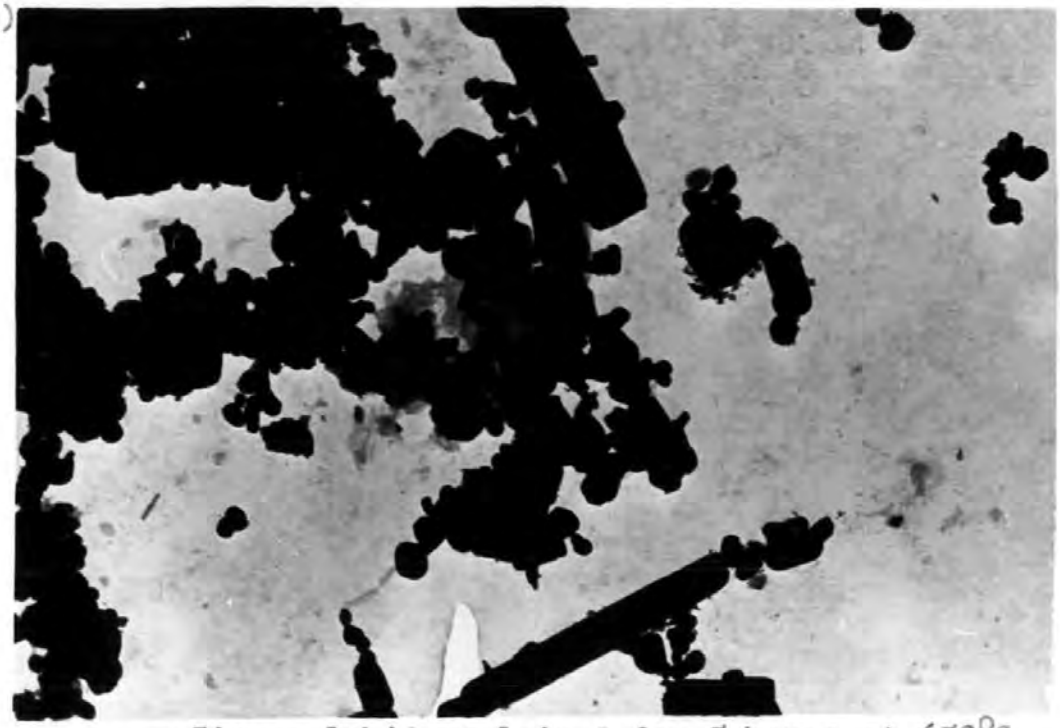

- Zinc sulphide calcined for 5 hours at 650°C

Magnification: x 13,000

FIGURE 63

(a)

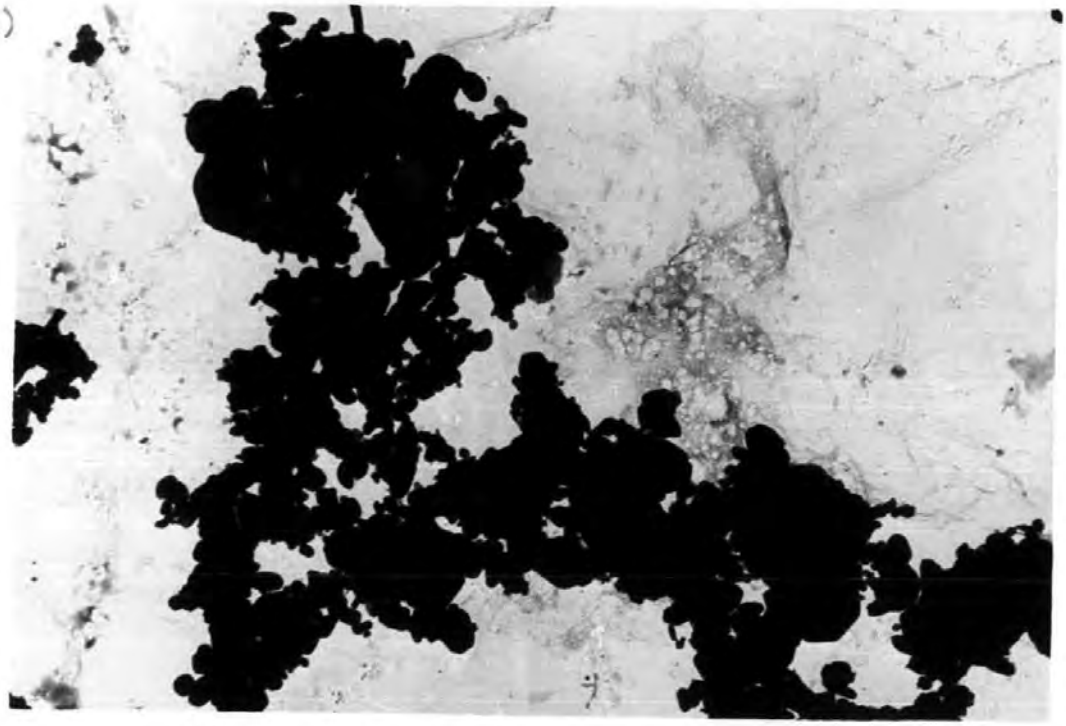

- Zinc sulphide calcined for 5 hours at 700°C

Magnification: x 13,000

(b)

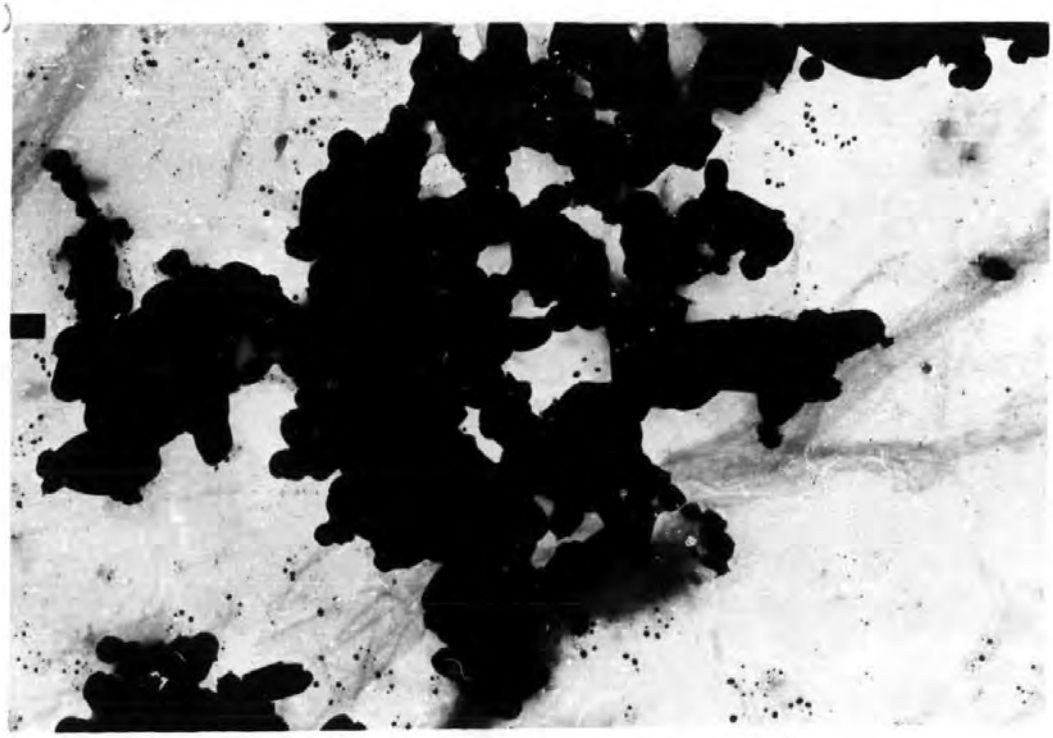

- ZnS calcined for 5 hours at 800°C

Magnification: x 13,000

FIGURE 64

(a)

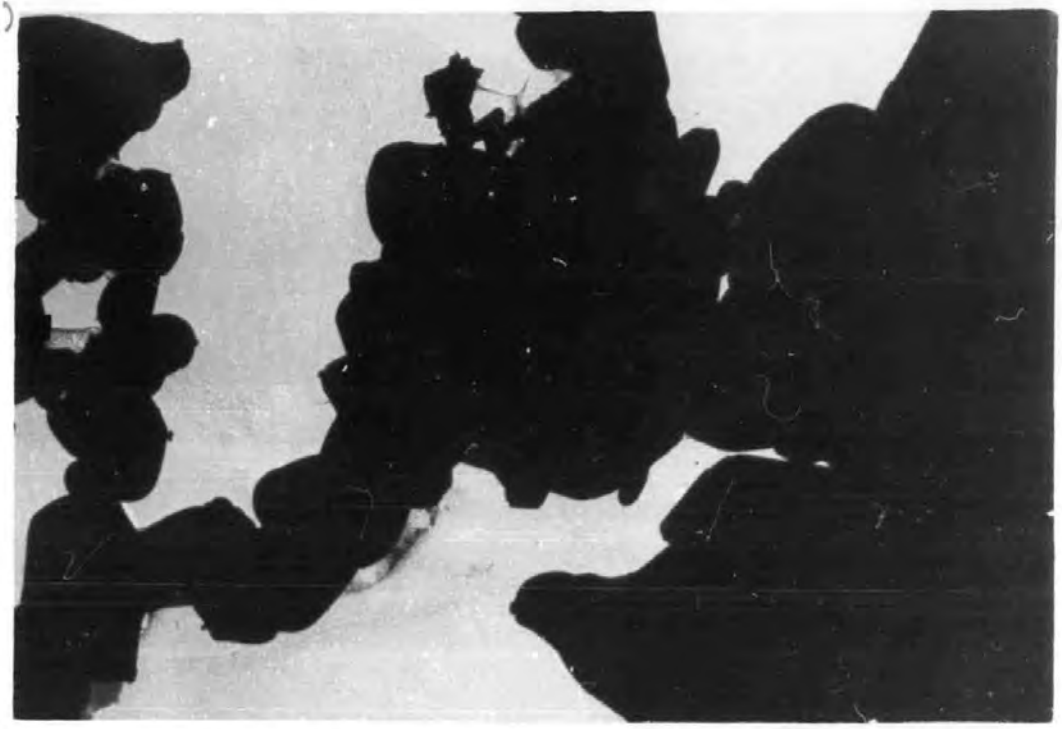

- Zinc sulphide oxidised at 1,100°C for 5 hours

Magnification: x 13,000

(b)

- Zinc sulphide oxidised at 950°C for 5 hours

Magnification: x 13,000

FIGURE 65

(a)

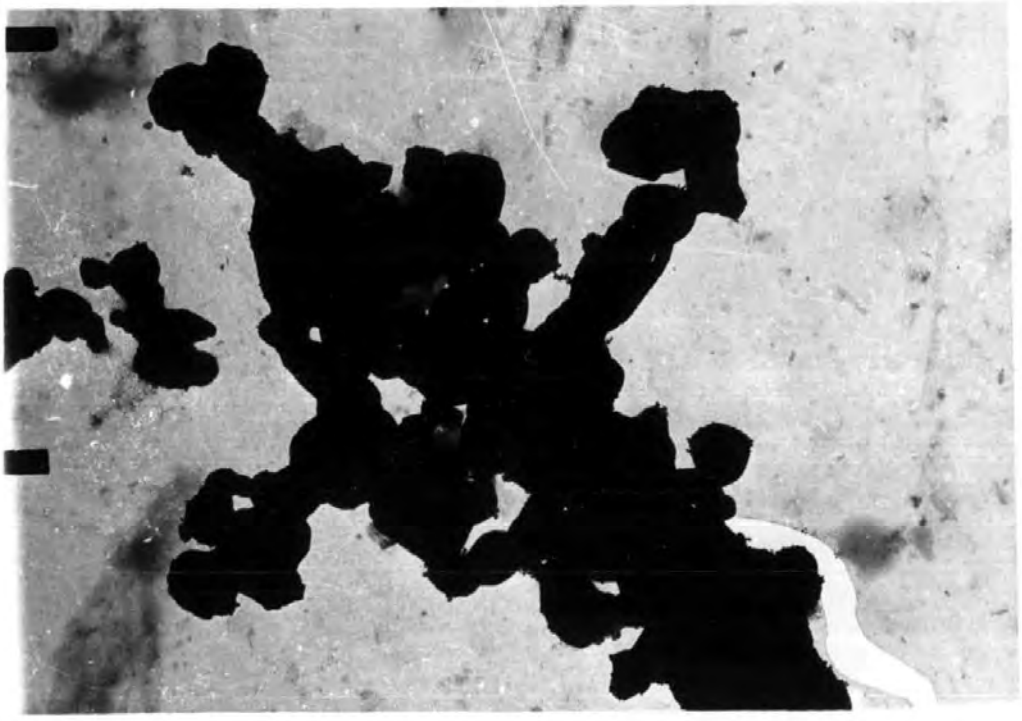

- Zinc sulphide calcined at 1,000°C for 5 hours

Magnification x 13,000

(b)

- Zinc sulphide calcined at 1,050°C for 5 hours

Magnification: x 13,000

FIGURE 66

(a)

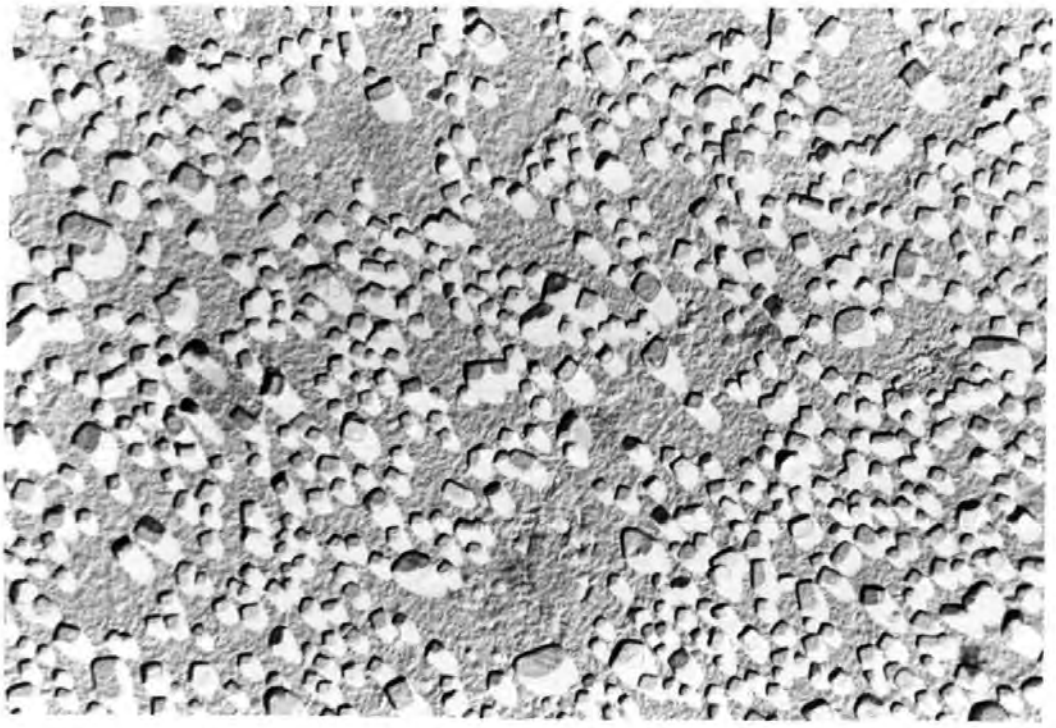

- Zinc sulphide calcined at 750°C for 5 hours

Magnification: x 23,000

(b)

- Zinc sulphide calcined at 700°C for 5 hours

Magnification: x 23,000

## Chapter 5

### Roasting of zinc concentrates

Five zinc concentrates were investigated, namely, New Brunswick, Broken Hill, Heathsteele, Silvermines and Buchan's River. Their compositions are given in Table 19. The zinc concentrates were analysed by X-ray diffraction. They contain mainly $\beta$-ZnS (cubic), zinc blende and iron pyrites, $FeS_2$.

For comparison, experiments were carried out on synthetic mixtures of zinc sulphide- iron sulphide ($FeS_2$) and zinc sulphide - iron oxide ($Fe_2O_3$).

### 5.1 Thermogravimetric Analysis (TGA)

The roastings were performed on a thermogravimetric balance. The zinc concentrates were ground and screened. The~200 mesh fraction of the zinc concentrates was used.

About 1g of the sample was taken each time separately in a porcelain crucible and introduced into the even-temperature zone of the reaction furnace. The temperature was controlled to within $\pm$ 5°C, at the operating temperature by means of a temperature controller. The experiments were conducted at different temperatures ranging from 650° - 900°C.

At the end of each experiment, the crucible was taken out of the furnace and the roasted sample was analysed as described in Chapter 4 for zinc sulphate and zinc oxide.

The formation of zinc ferrite has been identified by X-ray diffraction.

### 5.2 Differential thermal analysis (DTA)

By this technique phase transitions or chemical reactions can be followed by observation of the heat absorbed or liberated. A weighed amount of sample (0.1g) was taken each time. The sample was heated at a constant rate of 10°C/min at the temperature range 0°-1000°C using a temperature controller as described in Chapter 4.

TABLE 19

TYPICAL ASSAYS OF CONCENTRATES

| % W/W | Buchan's River | Silvermines | Heathsteele | Broken Hill | New Brunswick |
|---|---|---|---|---|---|
| Zn | 56.00 | 52.17 | 48.75 | 52.6 | 47.7 |
| S | 30.8 | 32.7 | 34.0 | 31.8 | 32.7 |
| Pb | 3.97 | 2.56 | 1.8 | 1.11 | 3.1 |
| Ag troy oz/longton | 5.11 | 1.17 | 4.08 | 0.65 | 3.35 |
| Au " | - | - | - | - | - |
| $Cl_2$ | 0.0003 | 0.01 | 0.002 | 0.05 | 0.001 |
| As | 0.03 | 0.11 | 0.06 | 0.06 | 0.12 |
| Fe | 2.55 | 5.8 | 11.9 | 9.85 | 10.9 |
| $Al_2O_3$ | 0.45 | 0.72 | 0.08 | 0.26 | 0.55 |
| Mn | 0.02 | 0.05 | 0.02 | 0.74 | 0.06 |
| CaO | 0.1 | 0.56 | 0.09 | 0.27 | 0.45 |
| MgO | 0.1 | 0.25 | 0.08 | 0.03 | 0.17 |
| Insol.Res. | 3.8 | - | - | 1.63 | 0.52 |
| Cd | 0.22 | 0.25 | 0.1 | 0.17 | 0.08 |
| Cu | 0.75 | 0.1 | 1.26 | 0.12 | 0.20 |
| Bi | 0.008 | 0.005 | 0.024 | 0.003 | 0.005 |
| Sb | 0.02 | 0.01 | 0.01 | 0.025 | 0.03 |
| Sn | 0.001 | 0.001 | 0.031 | 0.001 | 0.05 |
| $F_2$ | <0.01 | 0.02 | 0.01 | 0.05 | 0.02 |
| $SasSO_4$ | <0.1 | 0.30 | 0.21 | 0.17 | 0.83 |
| $CO_2$ | <0.1 | 0.7 | - | <0.1 | - |
| Co | 0.002 | <0.001 | 0.016 | 0.025 | - |
| Free C | - | 0.4 | - | - | 0.3 |
| Ni | <0.001 | 0.01 | - | - | - |
| $SiO_2$ | 1.2 | 1.78 | 0.44 | 1.29 | 0.93 |
| $BaSO_4$ | 2.5 | 0.65 | - | - | - |
| $(FeAl)_2O_3$ | 0.1 | 0.1 | - | - | - |
| In | - | - | 0.034 | - | - |

5.3 Results and Discussion :

Thermogravimetric Analysis (TGA)

The results obtained for roasting zinc concentrates at each of a series of fixed temperatures between 650° and 850°C for 40 minutes are given in Table 20.

The relative amounts of products formed at the end of roasting are given in Figure 67. The main reaction products are zinc oxide, zinc sulphate, ferric oxide, little zinc ferrite, $ZnFe_2O_4$ and $\beta$-ZnS.

A number of experiments at constant temperatures ranging from 700° - 850°C have been made to show the formation of zinc sulphate and zinc oxide with different time intervals in Table 21-24 (Figure 73-94).

5.3.1 Formation of sulphate on zinc concentrates roasting

Continuous isothermal experiments have been performed using about 1g sample each time at a series of temperatures between 650° and 900°C. The dependence of the weight change on the temperature is shown in Figs.68-70. The thermogravimetric curves (Figs. 68-70) at these temperatures have a specific form. At first the oxidation is very pronounced, the loss of weight passes through a minimum, then there is a slow increase of weight on account of sulphate formation. This form of the thermogravimetric curves shows that the rates of sulphate formation and oxidation to zinc oxide vary differently with time due to the increased amount of $SO_3$ gas in the furnace atmosphere in the presence of catalysts like $Fe_2O_3$. The variation of the composition of the phases with temperature was investigated (Table 21-24 and Figs.73-94). The amount of zinc sulphate increases rapidly with temperature, reaching a maximum value at 750°C before decreasing to the minimum value recorded at 850°C.

Figure 67 shows that the maximum degree of sulphation of zinc concentrates roasted at 750°C is related to the proportion of ZnS and $FeS_2$ in the initial concentrate. The degree of sulphation follows

TABLE 20

Zinc Concentrates roasted for 40 minutes

| Concentrate | Temp. °C | Zinc % (in terms of total zinc in the product) | | |
|---|---|---|---|---|
| | | as $ZnSO_4$ | ZnO | $ZnFe_2O_4$ + ZnS |
| Heathsteele | 650° | 20.2 | 54.0 | 25.8 |
| " | 700° | 23.0 | 54.5 | 22.5 |
| " | 750° | 26.0 | 55.0 | 18.0 |
| " | 800° | 23.5 | 62.5 | 14.0 |
| " | 850° | 0.5 | 69.0 | 31.5 |
| Buchan's River | 650° | 13.0 | 72.0 | 15.0 |
| " | 700° | 16.5 | 73.5 | 10.0 |
| " | 750° | 19.0 | 76.5 | 4.5 |
| " | 800° | 15.5 | 81.0 | 3.5 |
| " | 850° | 4.5 | 85.0 | 10.5 |
| Broken Hill | 650° | 11.0 | 55.0 | 34.0 |
| " | 700° | 13.8 | 56.0 | 30.2 |
| " | 750° | 15.5 | 58.0 | 26.5 |
| " | 800° | 10.8 | 64.5 | 24.7 |
| " | 850° | 1.0 | 71.0 | 28.0 |
| New Brunswick | 650° | 10.5 | 64.0 | 25.5 |
| " | 700° | 13.0 | 65.0 | 22.0 |
| " | 750° | 15.5 | 66.0 | 18.5 |
| " | 800° | 8.0 | 72.0 | 20.0 |
| " | 850° | 0.5 | 79.0 | 20.5 |
| Silvermines | 650° | 3.5 | 73.0 | 23.5 |
| " | 700° | 9.5 | 75.5 | 15.0 |
| " | 750° | 12.0 | 78.5 | 9.5 |
| " | 800° | 7.5 | 82.0 | 10.5 |
| " | 850° | 2.5 | 88.0 | 9.5 |

Figure 67

ZINC CONCENTRATES ROASTED FOR 40 MINUTES AT DIFFERENT TEMPERATURES

(1 g sample taken each time; zinc present in each constituent expressed as percentage of the total zinc in the roast).

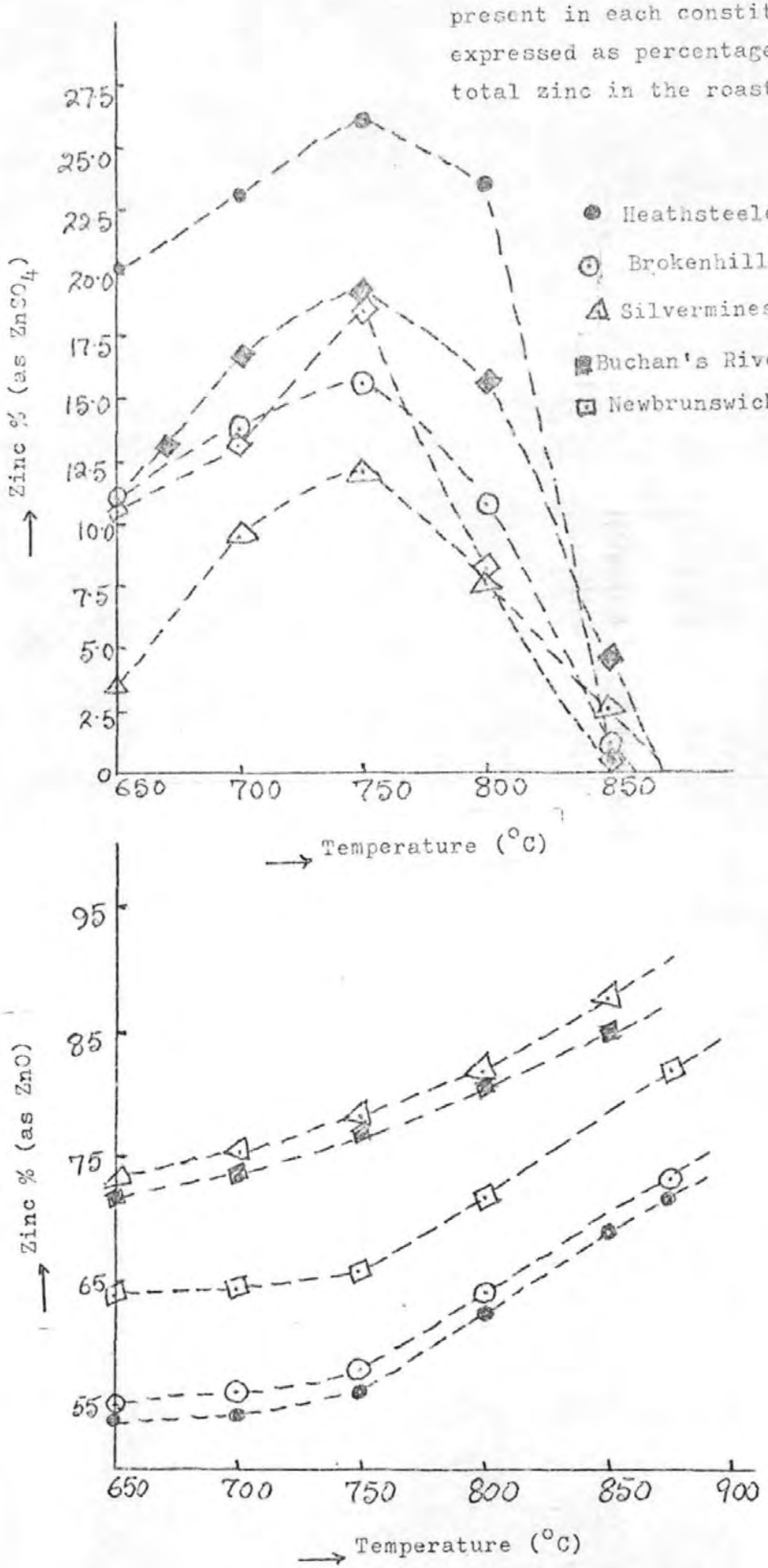

Figure 68

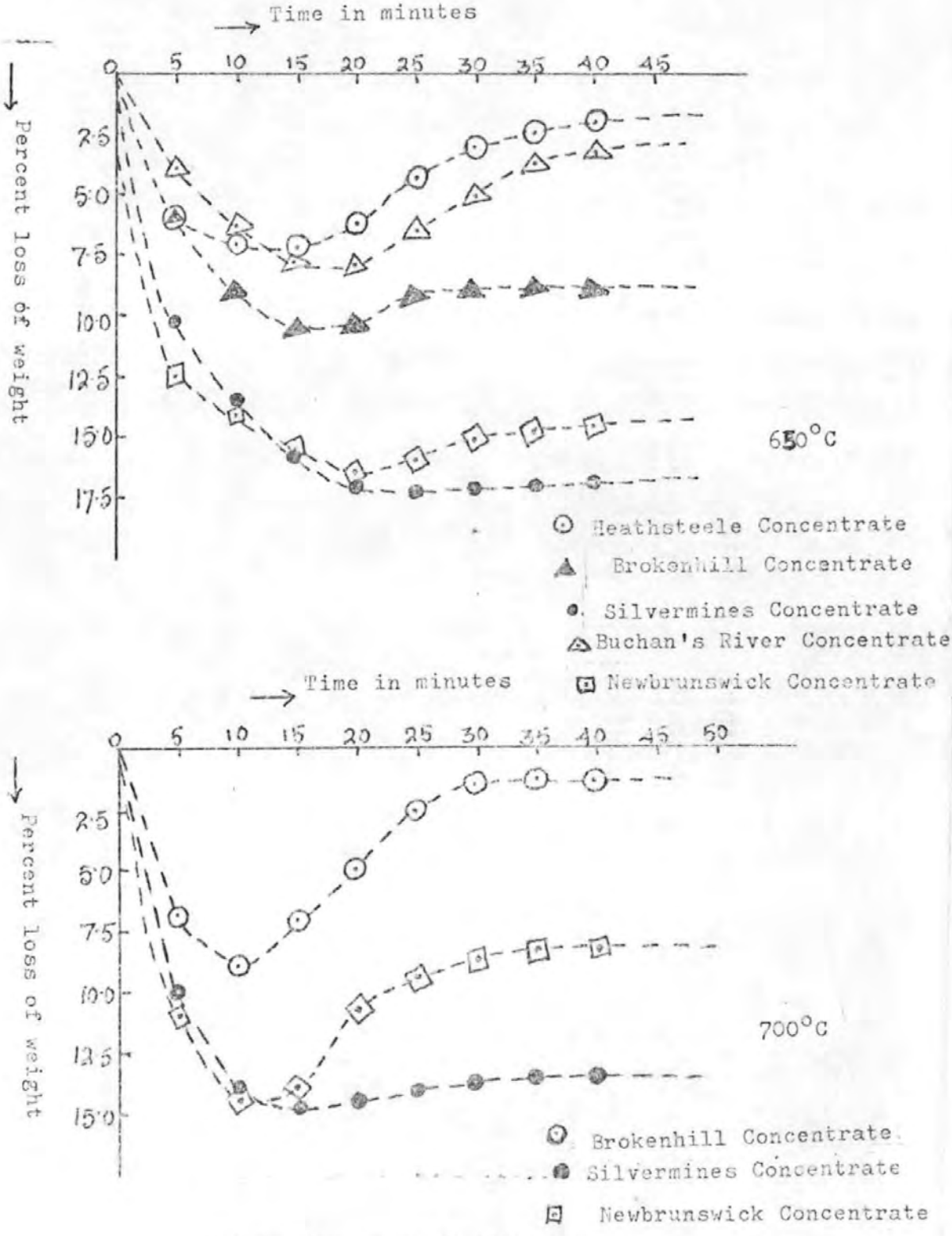


CONTINUOUS THERMOGRAVIMETRIC CURVES AT ISOTHERMAL TEMPERATURES

Figure 69

CONTINUOUS THERMOGRAVIMETRIC
CURVES AT ISOTHERMAL TEMPERATURES

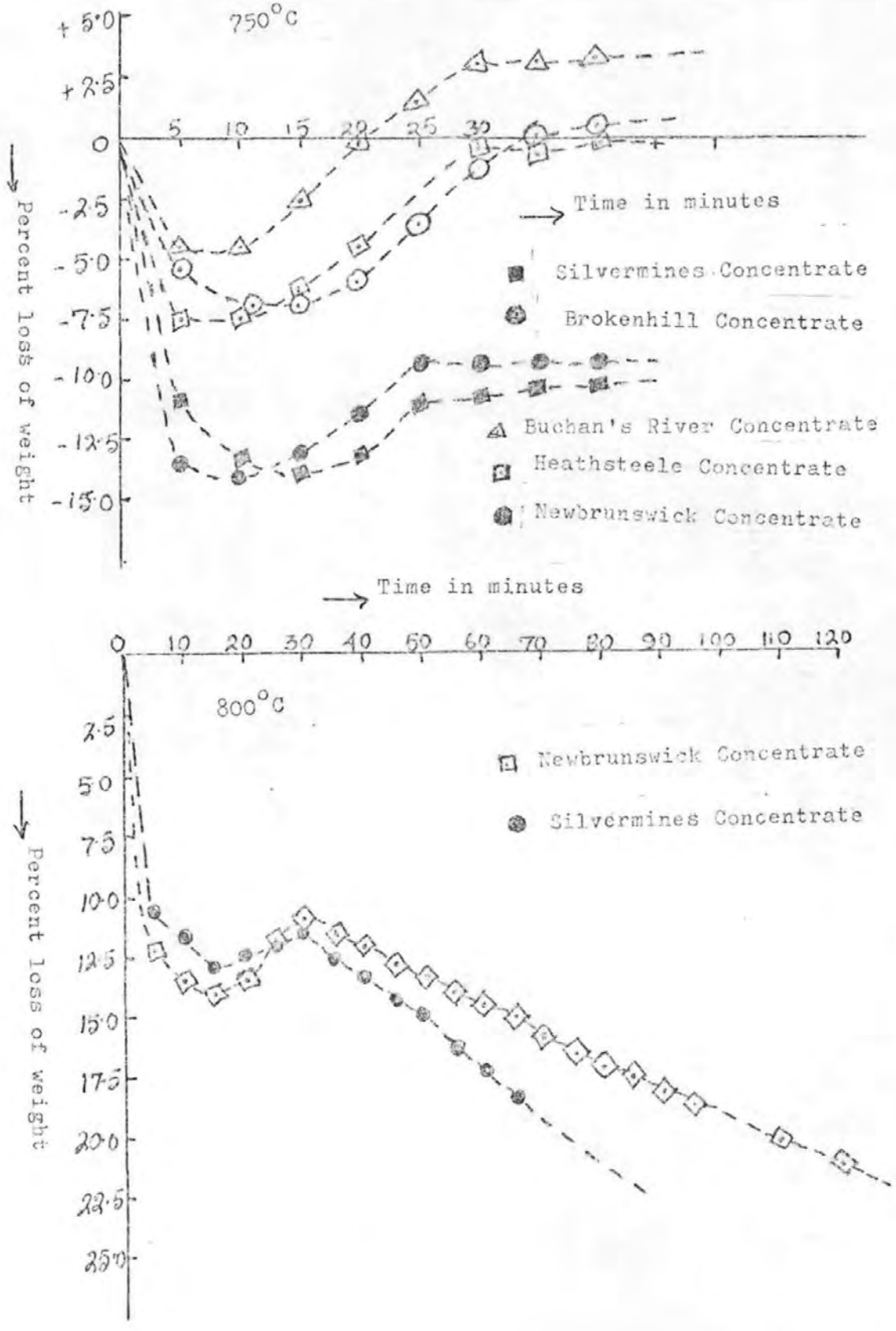

Figure 70

CONTINUOUS THERMOGRAVIMETRIC CURVES AT ISOTHERMAL TEMPERATURES

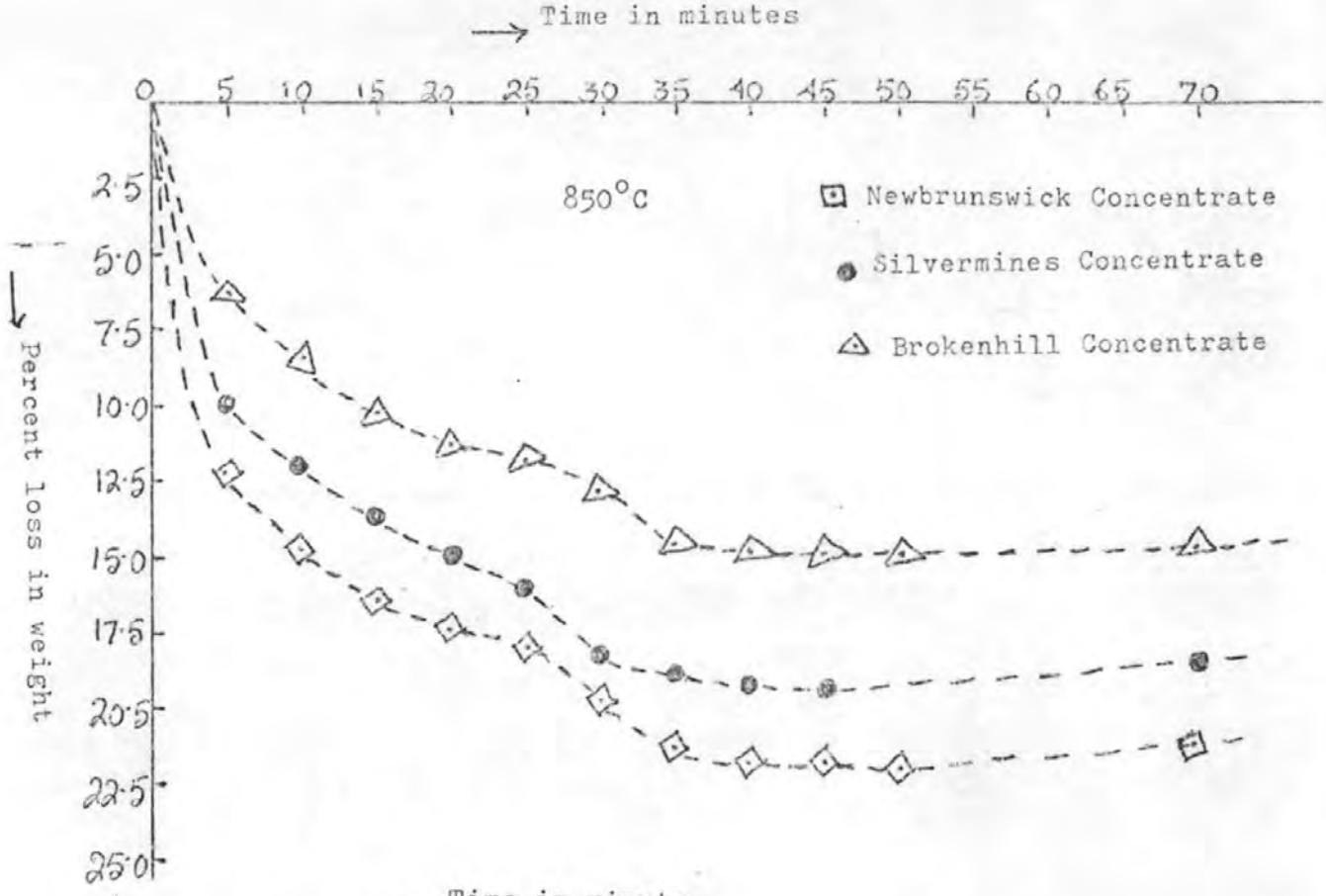


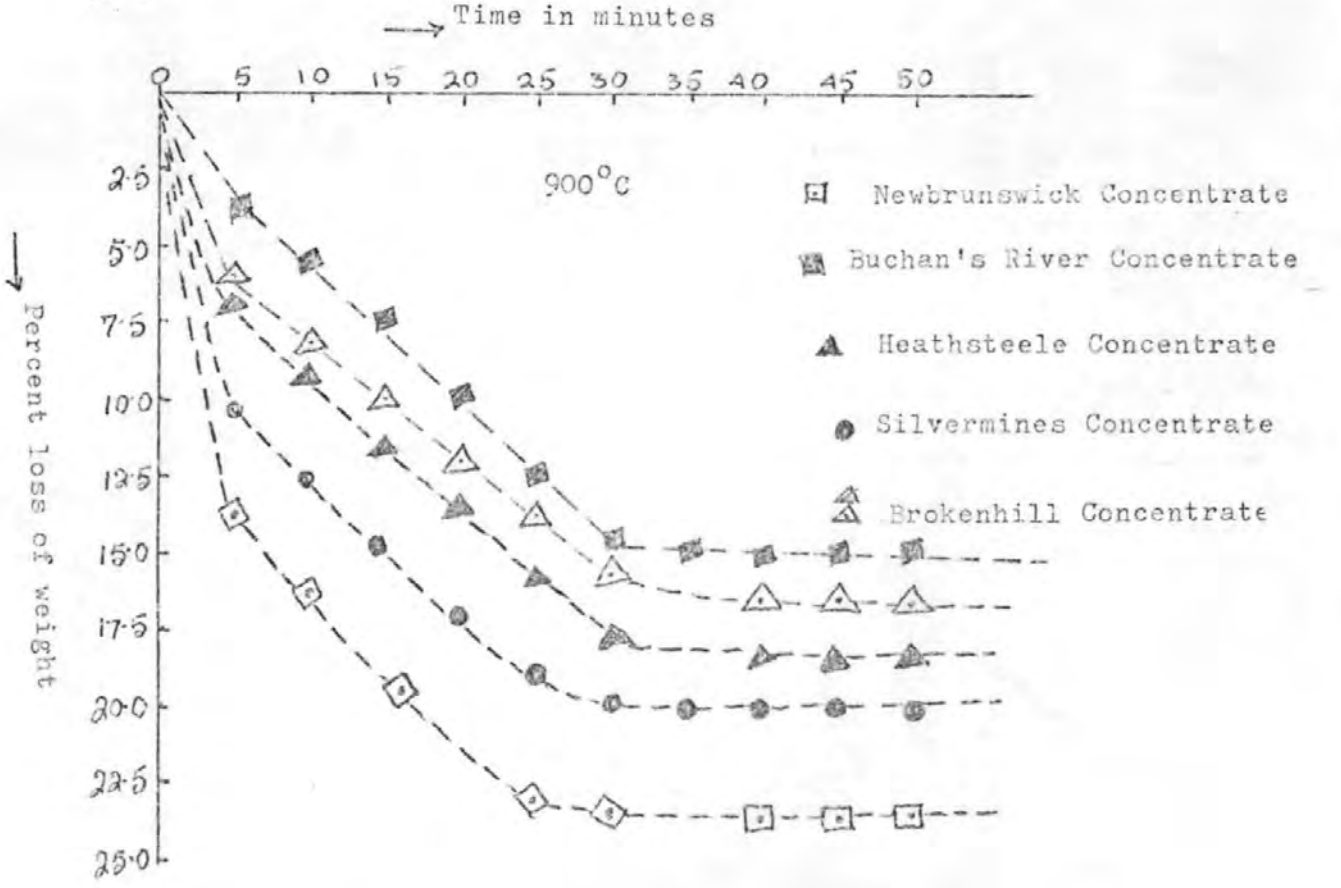

TABLE 21

Zinc Concentrates roasted at isothermal temperatures for different time intervals

| Concentrate | Temp°C | Time | Zinc % (in terms of total zinc in the product) | | |
|---|---|---|---|---|---|
| | | | as $ZnSO_4$ | ZnO | ZnS + $ZnFe_2O_4$ |
| New Brunswick | 700°C | 20min | 8.5 | 51.0 | 40.5 |
| " | " | 40 " | 13.0 | 65.0 | 22.0 |
| " | " | 60 " | 16.3 | 66.0 | 17.7 |
| Broken Hill | " | 20 " | 7.0 | 42.0 | 51.0 |
| " | " | 40 " | 13.0 | 56.0 | 31.0 |
| " | " | 60 " | 15.0 | 56.5 | 28.5 |
| Heathsteele | " | 20 " | 10.75 | 38.0 | 51.25 |
| " | " | 40 " | 23.0 | 52.0 | 25.0 |
| " | " | 60 " | 23.0 | 52.0 | 25.0 |
| Silvermines | " | 20 " | 6.25 | 57.0 | 36.75 |
| " | " | 40 " | 9.5 | 75.0 | 15.5 |
| " | " | 60 " | 10.75 | 75.0 | 14.25 |
| Buchan's River | " | 20 " | 5.5 | 53.0 | 41.5 |
| " | " | 40 " | 16.95 | 77.0 | 6.25 |
| " | " | 60 " | " | " | 6.25 |

TABLE 22

Zinc Concentrates roasted at isothermal temperatures for different time intervals

| Concentrate | Temp °C | Time | Zinc % (in terms of total zinc in the product) | | |
|---|---|---|---|---|---|
| | | | as $ZnSO_4$ | ZnO | ZnS + $ZnFe_2O_4$ |
| Heathsteele | 750°C | 10min | 2.75 | 21.5 | 75.75 |
| " | " | 20 " | 9.25 | 40.0 | 50.75 |
| " | " | 40 " | 26.5 | 56.0 | 17.5 |
| " | " | 60 " | 11.0 | 67.0 | 22.0 |
| Broken Hill | " | 10 " | 1.5 | 28.0 | 70.5 |
| " | " | 20 " | 3.5 | 43.0 | 53.5 |
| " | " | 40 " | 15.5 | 58.0 | 26.5 |
| " | " | 60 " | 14.0 | 55.0 | 31.0 |
| New Brunswick | " | 10 " | 2.0 | 29.0 | 69.0 |
| " | " | 20 " | 7.0 | 55.0 | 38.0 |
| " | " | 40 " | 18.5 | 66.0 | 15.5 |
| " | " | 60 " | 14.0 | 67.0 | 19.0 |
| Silvermines | " | 10 " | 2.7 | 27.0 | 70.3 |
| " | " | 20 " | 7.0 | 61.0 | 32.0 |
| " | " | 40 " | 11.75 | 78.0 | 10.25 |
| " | " | 60 " | 10.4 | 74.0 | 15.6 |
| Buchan's River | " | 10 " | 1.75 | 30.0 | 68.25 |
| " | " | 20 " | 10.75 | 57.0 | 32.25 |
| " | " | 40 " | 19.0 | 76.0 | 5.0 |
| " | " | 60 " | 15.5 | 75.0 | 9.5 |

TABLE 23

Zinc Concentrates roasted at isothermal temperatures for different time intervals

| Concentrate | Temp °C | Time | Zinc % (in terms of total zinc in the product) | | |
|---|---|---|---|---|---|
| | | | as $ZnSO_4$ | ZnO | ZnS + $ZnFe_2O_4$ |
| Heathsteele | 800°C | 10min | 3.0 | 35.0 | 62.0 |
| " | " | 20 " | 8.8 | 45.0 | 46.2 |
| " | " | 40 " | 23.0 | 63.0 | 14.0 |
| " | " | 60 " | 4.5 | 65.0 | 30.5 |
| " | " | 120 " | 0.5 | 65.0 | 34.5 |
| Broken Hill | " | 10 " | 1.25 | 27.0 | 71.75 |
| " | " | 20 " | 2.75 | 60.0 | 37.25 |
| " | " | 40 " | 10.75 | 64.0 | 25.25 |
| " | " | 60 " | 1.25 | 65.0 | 33.75 |
| " | " | 120 " | 0.5 | 65.0 | 34.5 |
| New Brunswick | " | 10 " | 3.5 | 35.0 | 61.5 |
| " | " | 20 " | 6.3 | 60.0 | 33.7 |
| " | " | 40 " | 8.0 | 71.0 | 21.0 |
| " | " | 60 " | 6.0 | 74.0 | 20.0 |
| " | " | 120 " | 0.5 | 82.0 | 17.5 |
| Silvermines | " | 10 " | 3.0 | 39.0 | 58.0 |
| " | " | 20 " | 6.0 | 62.0 | 32.0 |
| " | " | 40 " | 7.5 | 80.0 | 12.5 |
| " | " | 60 " | 7.0 | 82.0 | 11.0 |
| " | " | 120 " | 3.0 | 84.0 | 13.0 |
| Buchan's River | " | 10 " | 3.0 | 37.0 | 60.0 |
| " | " | 20 " | 6.5 | 63.0 | 30.5 |
| " | " | 40 " | 15.5 | 80.0 | 14.5 |
| " | " | 60 " | 1.0 | 80.0 | 19.0 |
| " | " | 120 " | 0.25 | 80.0 | 19.75 |

TABLE-24

Zinc Concentrates roasted at isothermal temperatures for different time intervals

| Concentrate | Temp°C | Time | Zinc % (in terms of total zinc in the product) | | |
|---|---|---|---|---|---|
| | | | as $ZnSO_4$ | ZnO | $ZnS + ZnFe_2O_4$ |
| Heathsteele | 850°C | 10min | 1.3 | 24.0 | 74.7 |
| " | " | 20 " | 2.0 | 53.0 | 45.0 |
| " | " | 40 " | 0.5 | 63.0 | 36.0 |
| " | " | 60 " | 0.05 | 63.0 | 36.95 |
| Broken Hill | " | 10 " | 0.85 | 20.0 | 79.15 |
| " | " | 20 " | 1.65 | 43.0 | 55.35 |
| " | " | 40 " | 1.00 | 64.0 | 35.0 |
| " | " | 60 " | 0.6 | 65.0 | 34.4 |
| New Brunswick | " | 10 " | 1.2 | 36.0 | 62.8 |
| " | " | 20 " | 3.15 | 62.0 | 34.85 |
| " | " | 40 " | 0.5 | 81.0 | 18.5 |
| " | " | 60 " | 0.35 | 83.0 | 16.65 |
| " | " | 120 " | 0.20 | 86.0 | 13.8 |
| Silvermines | " | 10 " | 2.25 | 34.0 | 63.75 |
| " | " | 20 " | 4.15 | 66.0 | 29.85 |
| " | " | 40 " | 2.5 | 88.0 | 9.5 |
| " | " | 60 " | 1.5 | 88.0 | 10.5 |
| Buchan's River | " | 10 " | 1.1 | 30.0 | 68.9 |
| " | " | 20 " | 4.5 | 63.0 | 32.5 |
| " | " | 40 " | 3.0 | 82.0 | 15.0 |
| " | " | 60 " | 1.0 | 82.0 | 17.0 |

TABLE 24a

Synthetic mixture roasted for 40 minutes

| Synthetic mixture | Temp °C | Zinc % (in terms of total zinc in the product) | | |
|---|---|---|---|---|
| | | as $ZnSO_4$ | ZnO | ZnS + $ZnFe_2O_4$ |
| 75% α-ZnS + 25% $FeS_2$ | 700° | 1.7 | 84 | 14.3 |
| " | 750° | 4.0 | 86 | 10.0 |
| " | 800° | 0.4 | 87 | 12.6 |
| " | 850° | 0.2 | 87 | 12.8 |
| 50% α-ZnS + 50% $FeS_2$ | 700° | 8.2 | 64 | 27.8 |
| " | 750° | 9.0 | 68 | 23.0 |
| " | 800° | 1.1 | 74 | 24.9 |
| " | 850° | 0.8 | 71 | 28.2 |
| 25% α-ZnS + 75% $FeS_2$ | 750° | 22.0 | 37 | 41 |
| 50% $Fe_2O_3$ + 50% α-ZnS | 750° | 6.0 | 43 | 51 |
| 75% $Fe_2O_3$ + 25% α-ZnS | 750° | 22.0 | 20 | 58 |

Figure 71

SYNTHETIC MIXTURE ($\alpha$-ZnS + $FeS_2$) ROASTED FOR 40 MINUTES AT DIFFERENT TEMPERATURES

(1 g sample taken each time; zinc present in each constituent expressed as percentage of the total zinc in the roast).

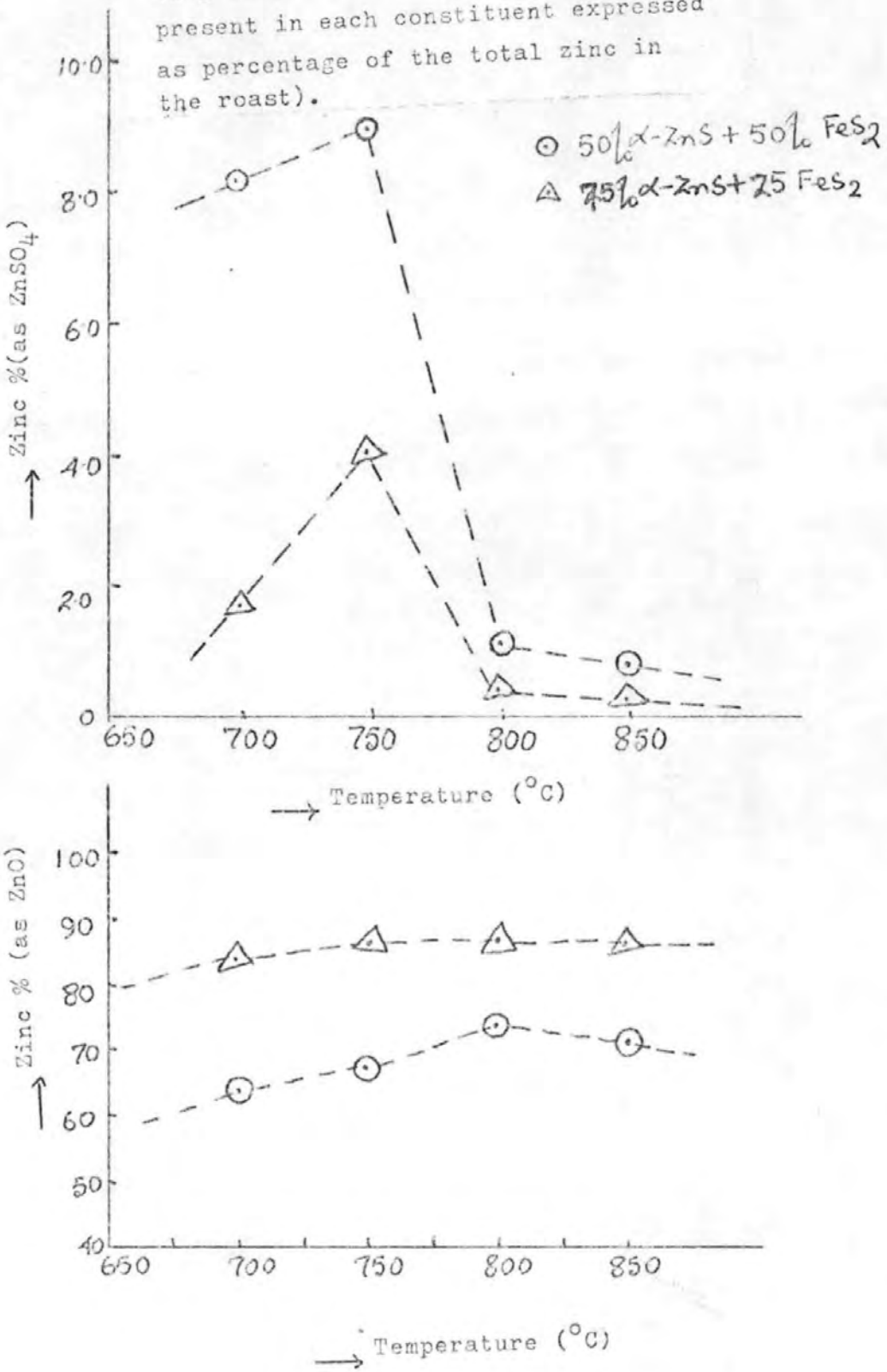

Figure 72

ROASTING BEHAVIOUR OF SYNTHETIC MIXTURE ($\alpha$-ZnS + $Fe_2O_3$) AT ISOTHERMAL TEMPERATURES

(1 g sample taken each time; zinc present in each constituent expressed as percentage of the total zinc in the roast).

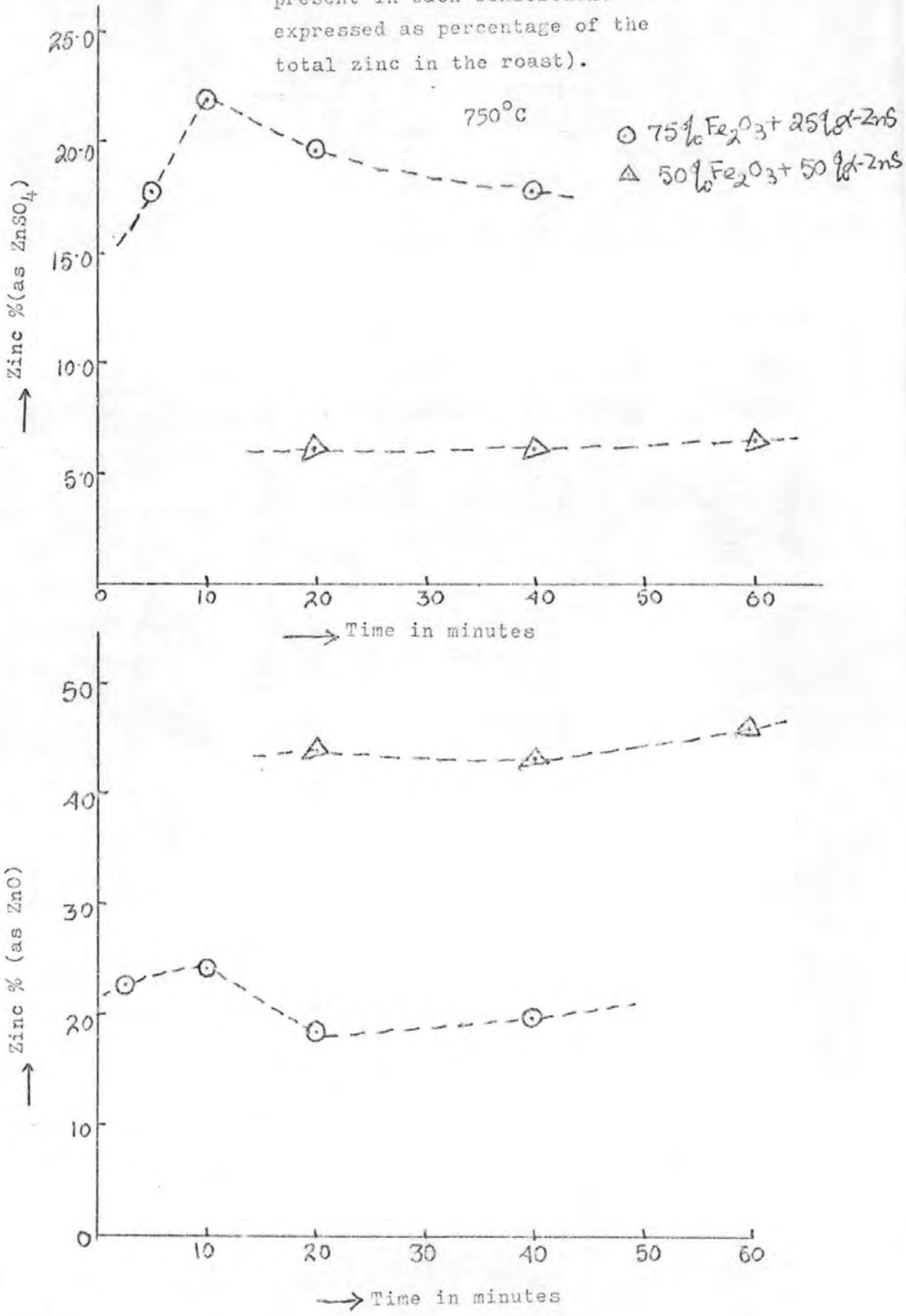

ROASTING BEHAVIOUR OF ZINC CONCENTRATES AT ISOTHERMAL TEMPERATURES

(1 g sample taken each time; zinc present in each constituent expressed as percentage of the total zinc in the roast).

Silvermines Concentrate

700°C

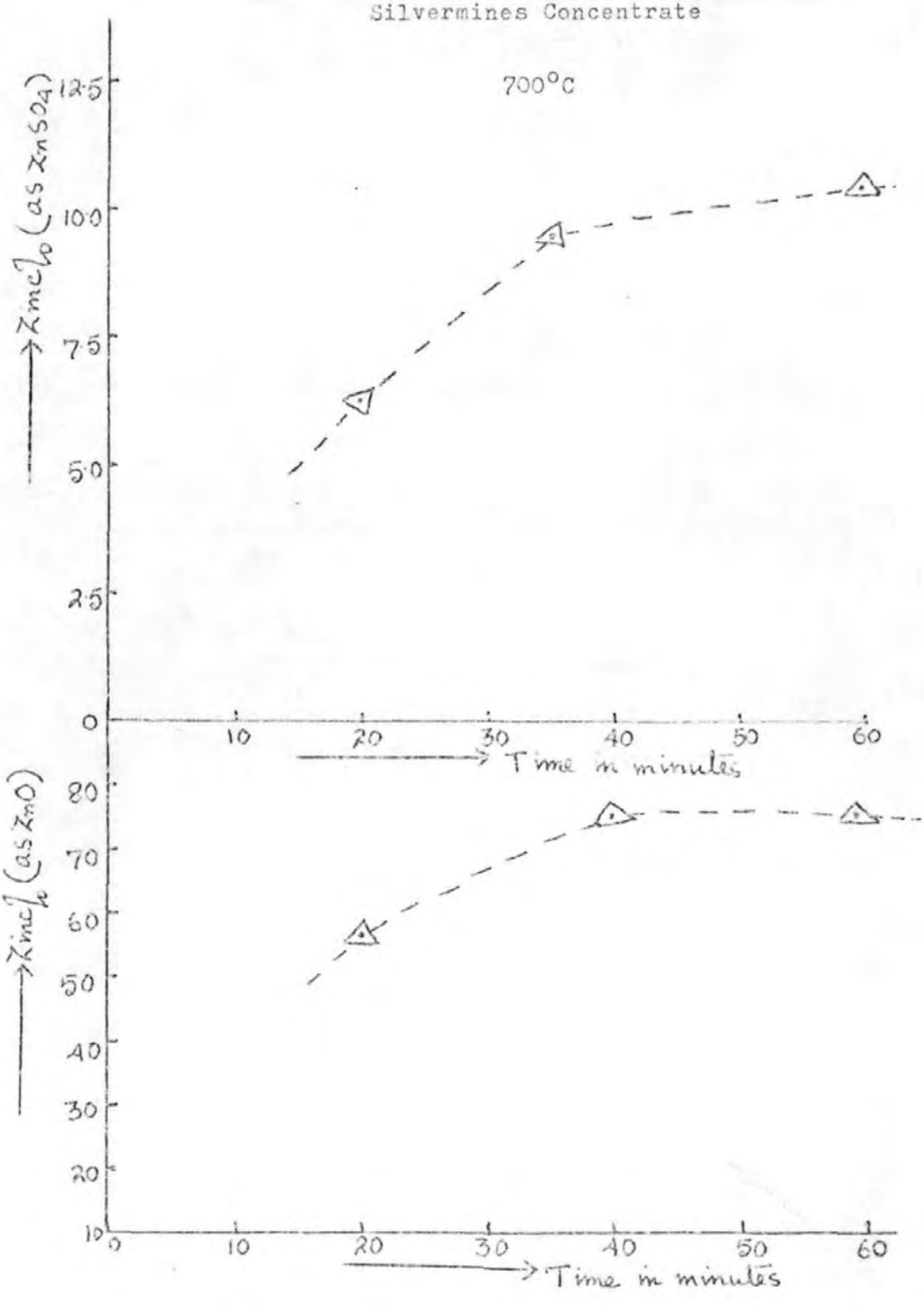


Figure 73

Figure 74

Silvermines Concentrate

750°C

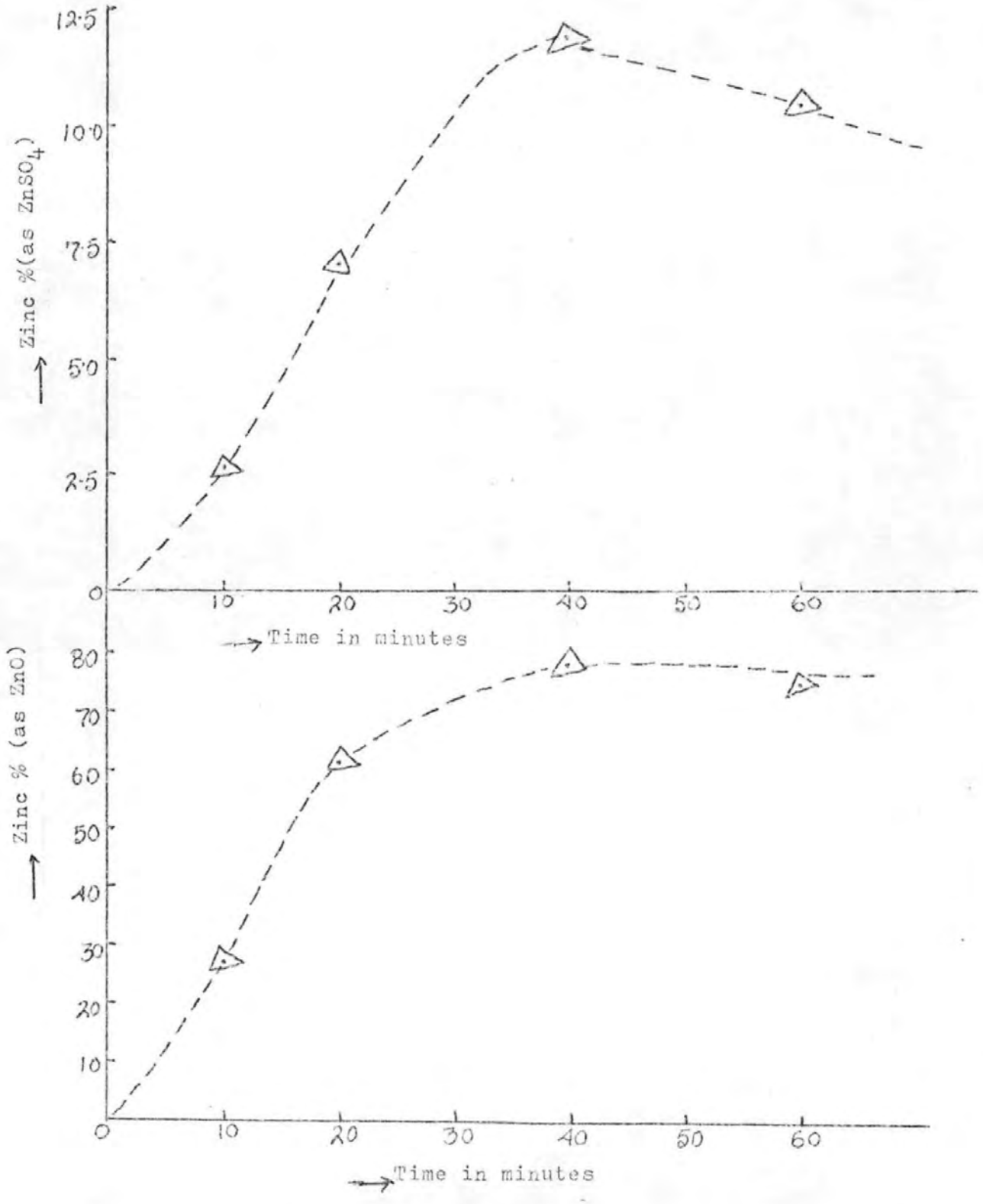

Figure 75

Silvermines Concentrate

800°C

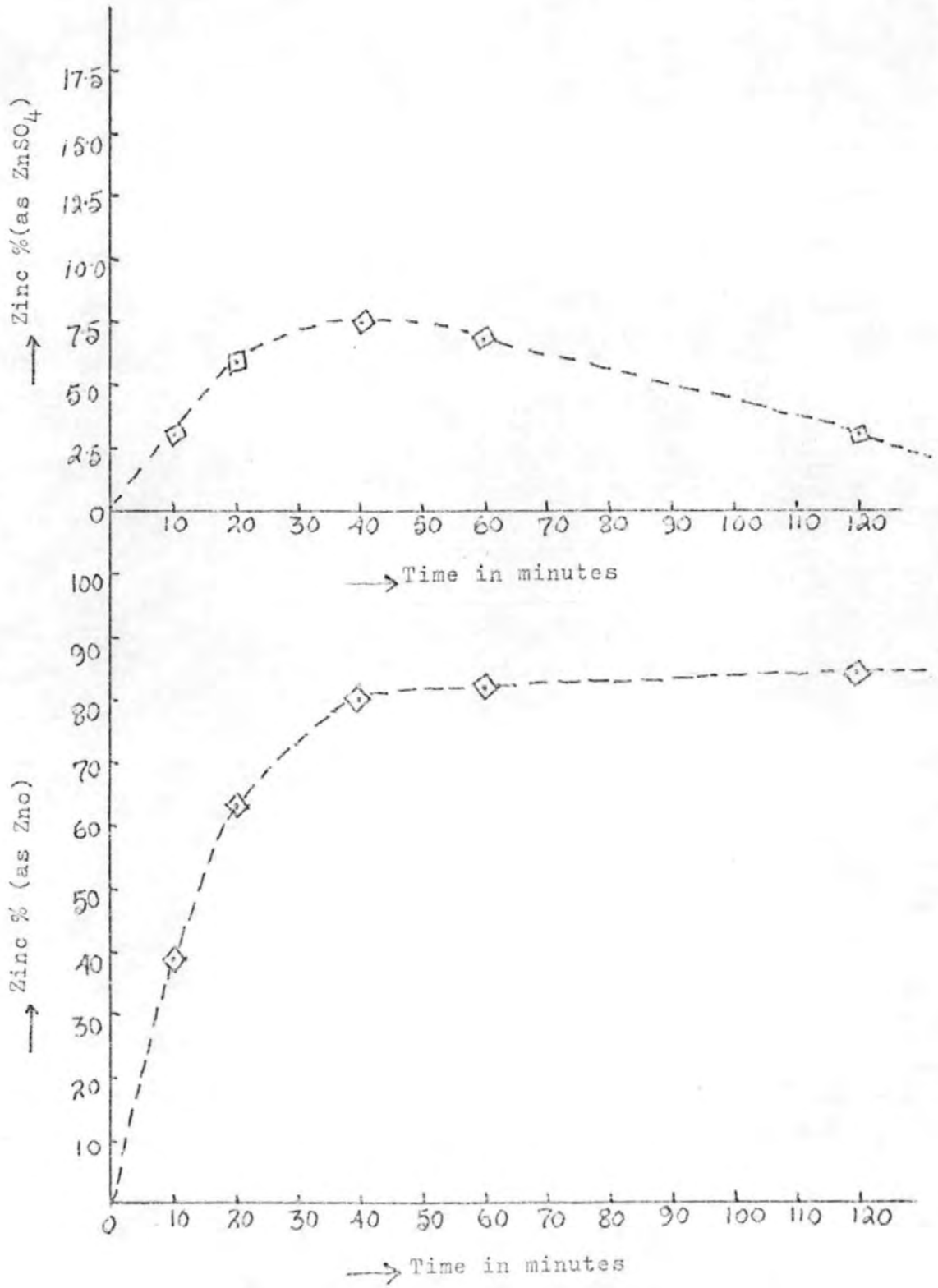

Figure 76

Silvermines Concentrate

850°C

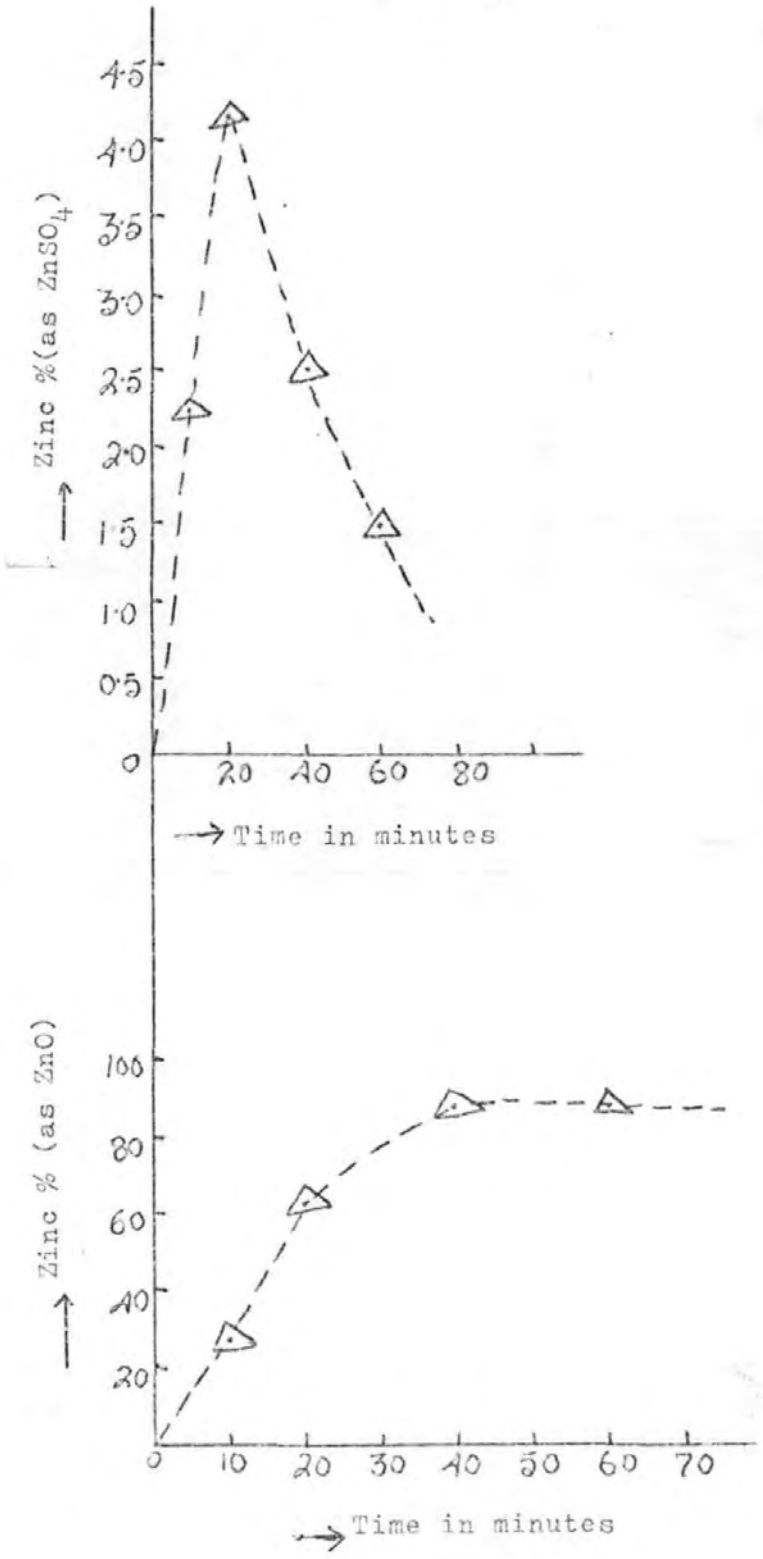

ROASTING BEHAVIOUR OF ZINC CONCENTRATES AT ISOTHERMAL TEMPERATURES

(1 g sample taken each time; zinc present in each constituent expressed as percentage of the total zinc in the roast).

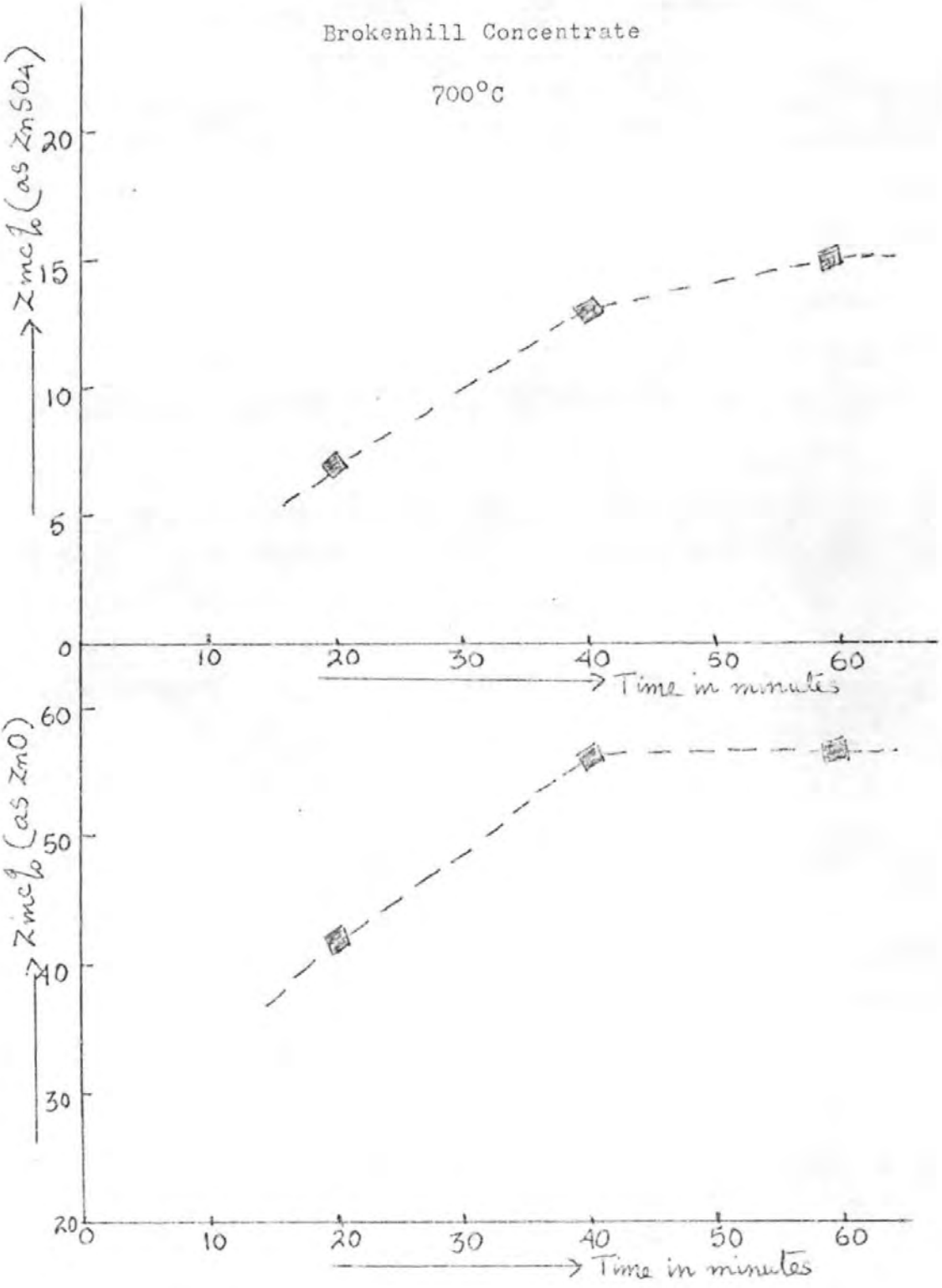


Figure 77

ROASTING BEHAVIOUR OF ZINC CONCENTRATES AT ISOTHERMAL TEMPERATURES

(1 g sample taken each time; zinc present in each constituent expressed as percentage of the total zinc in the roast).

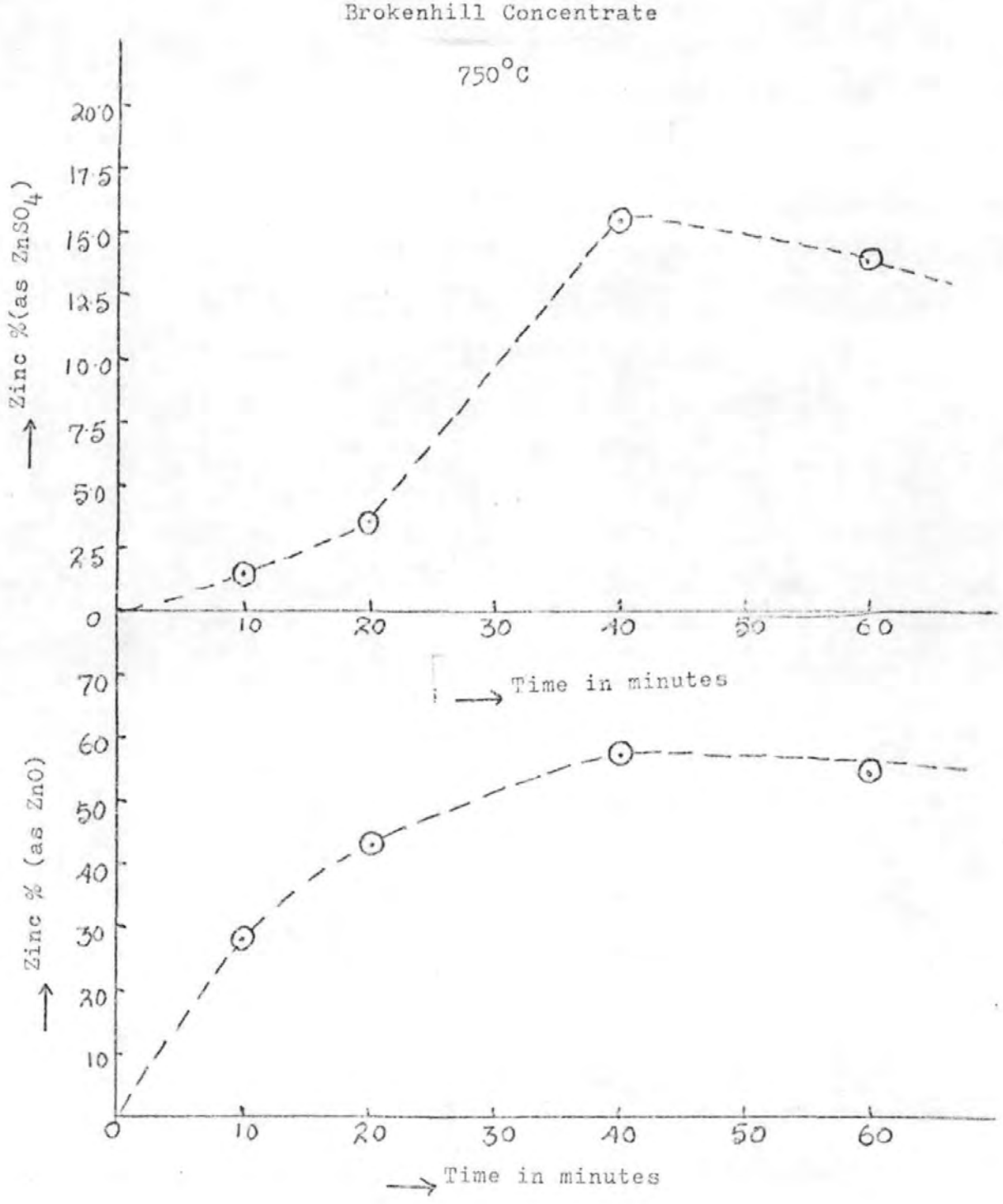


Figure 78

ROASTING BEHAVIOUR OF ZINC CONCENTRATES AT ISOTHERMAL TEMPERATURES

(1 g sample taken each time; zinc present in each constituent expressed as percentage of the total zinc in the roast).

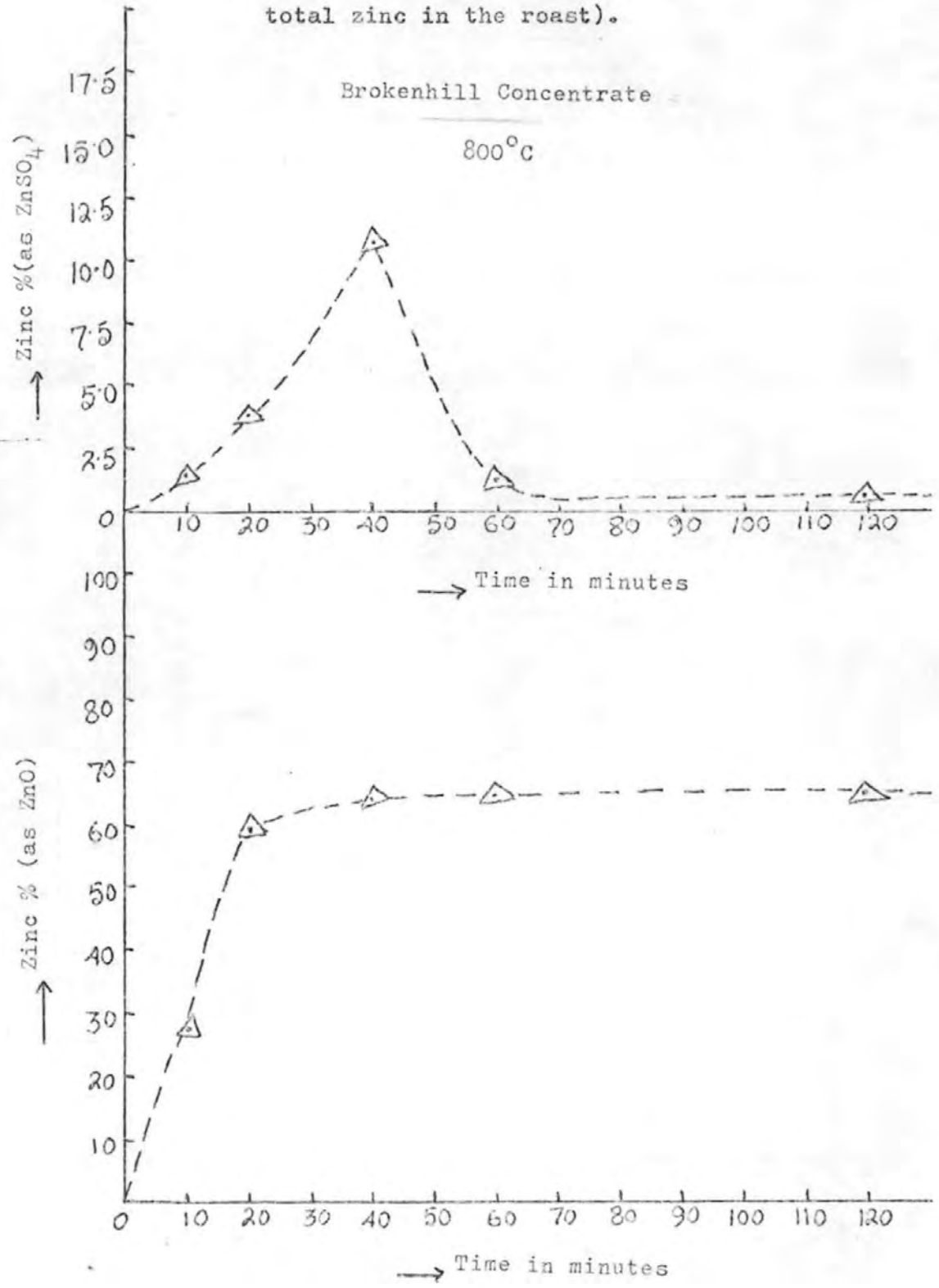


Figure 79

ROASTING BEHAVIOUR OF ZINC CONCENTRATES AT ISOTHERMAL TEMPERATURES

(1 g sample taken each time; zinc present in each constituent expressed as percentage of the total zinc in the roast).

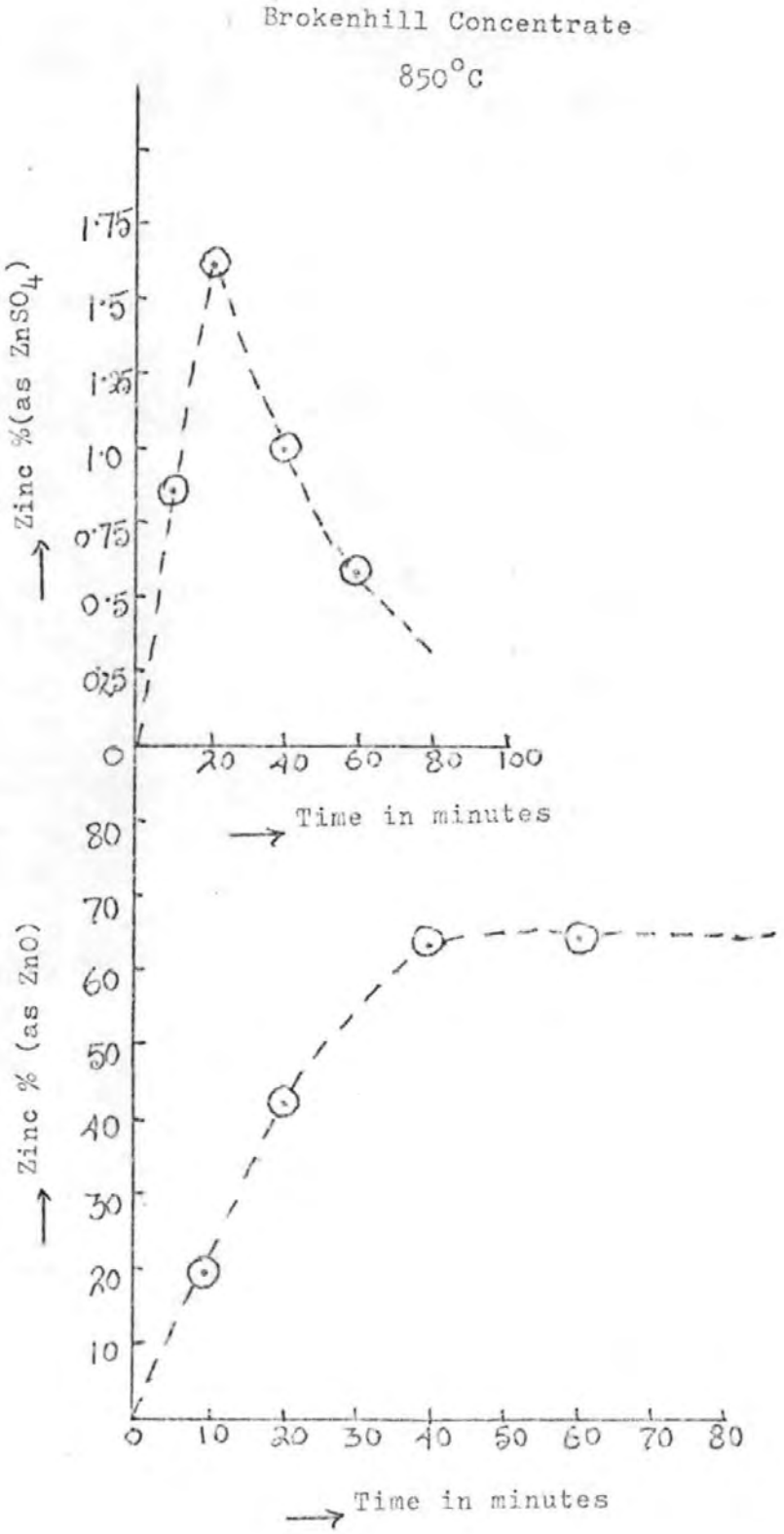


Figure 80

Buchan's River Concentrate

750°C

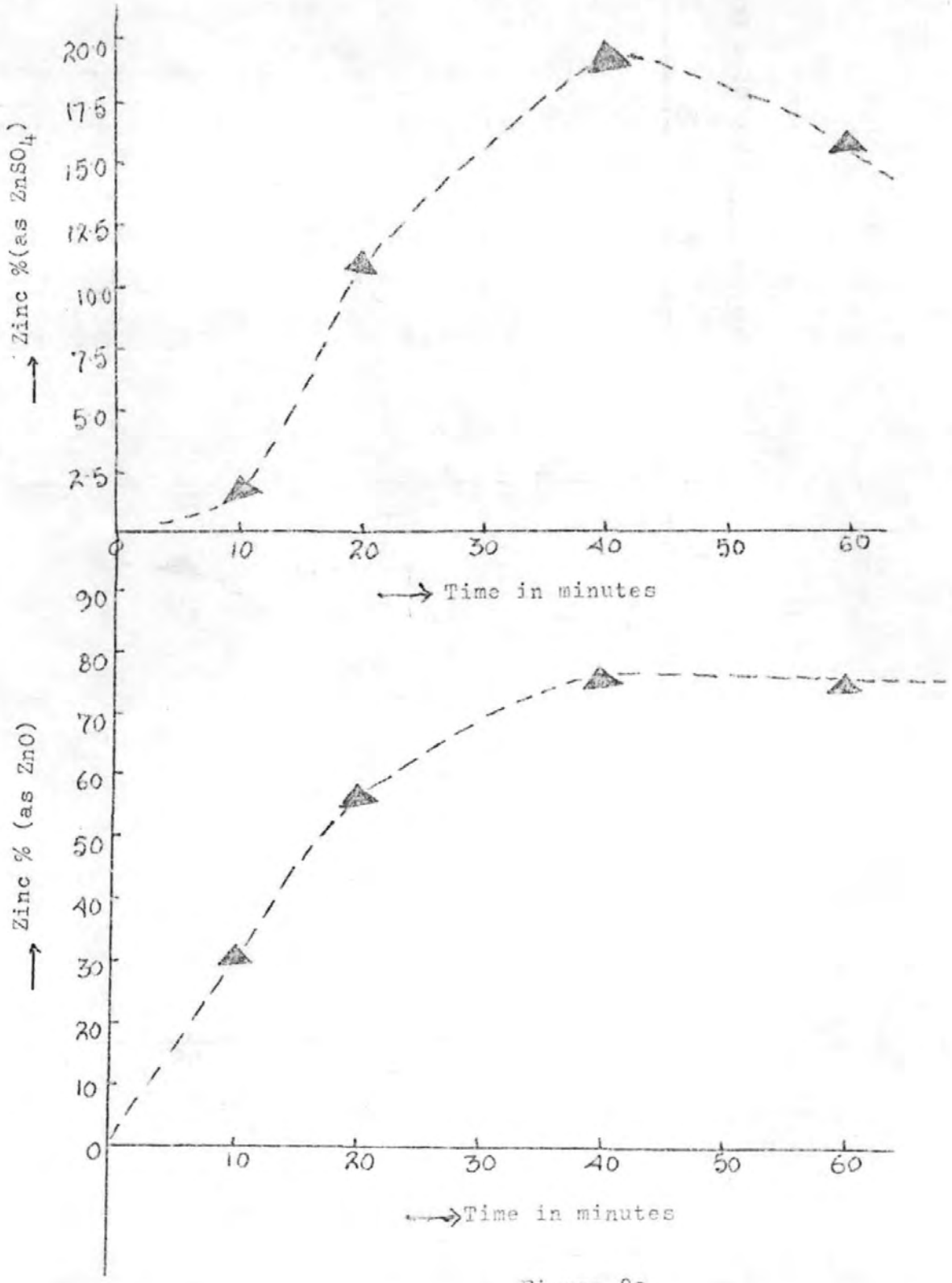


Figure 82

Figure 83

Buchan's River Concentrate

800°C

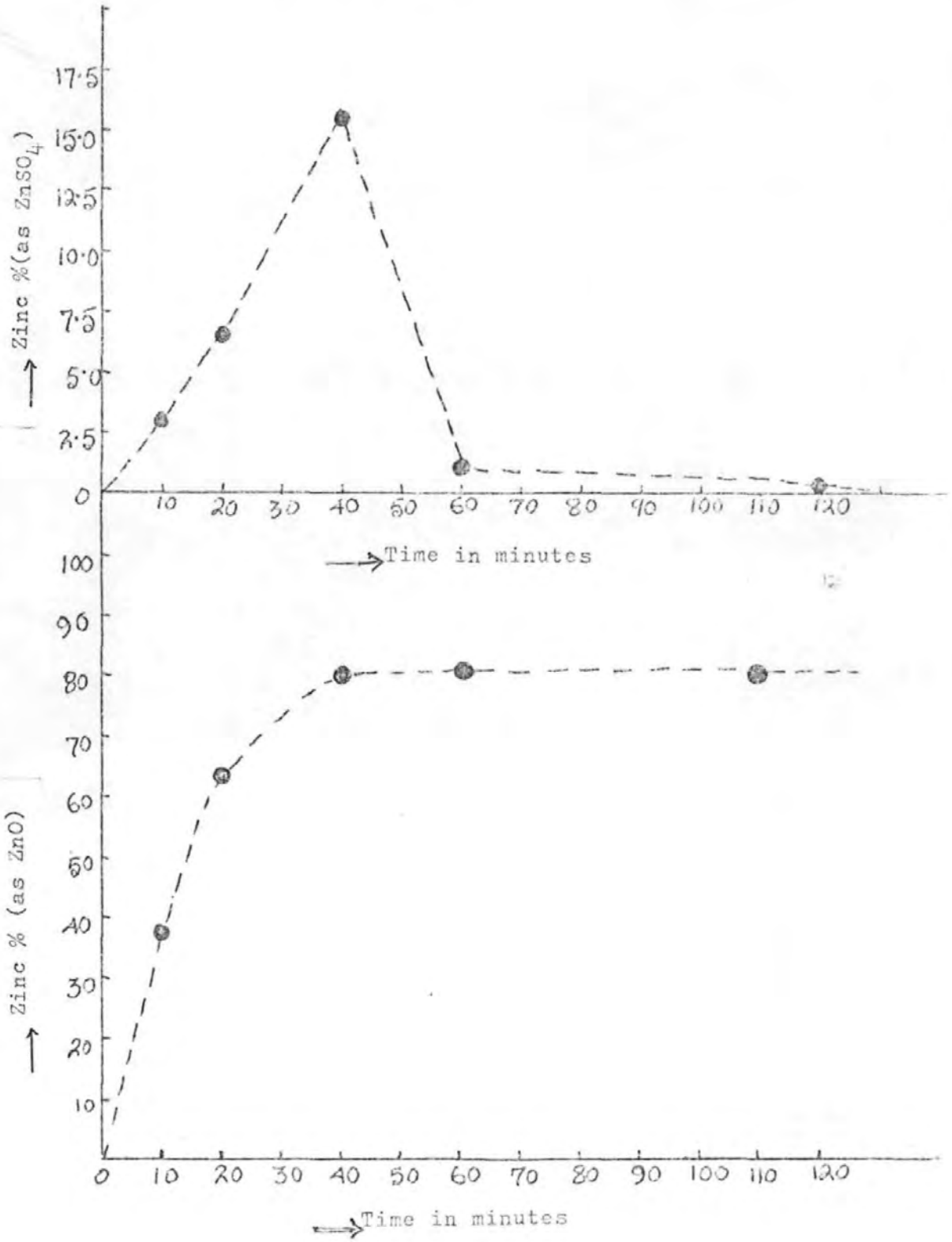

Figure 84

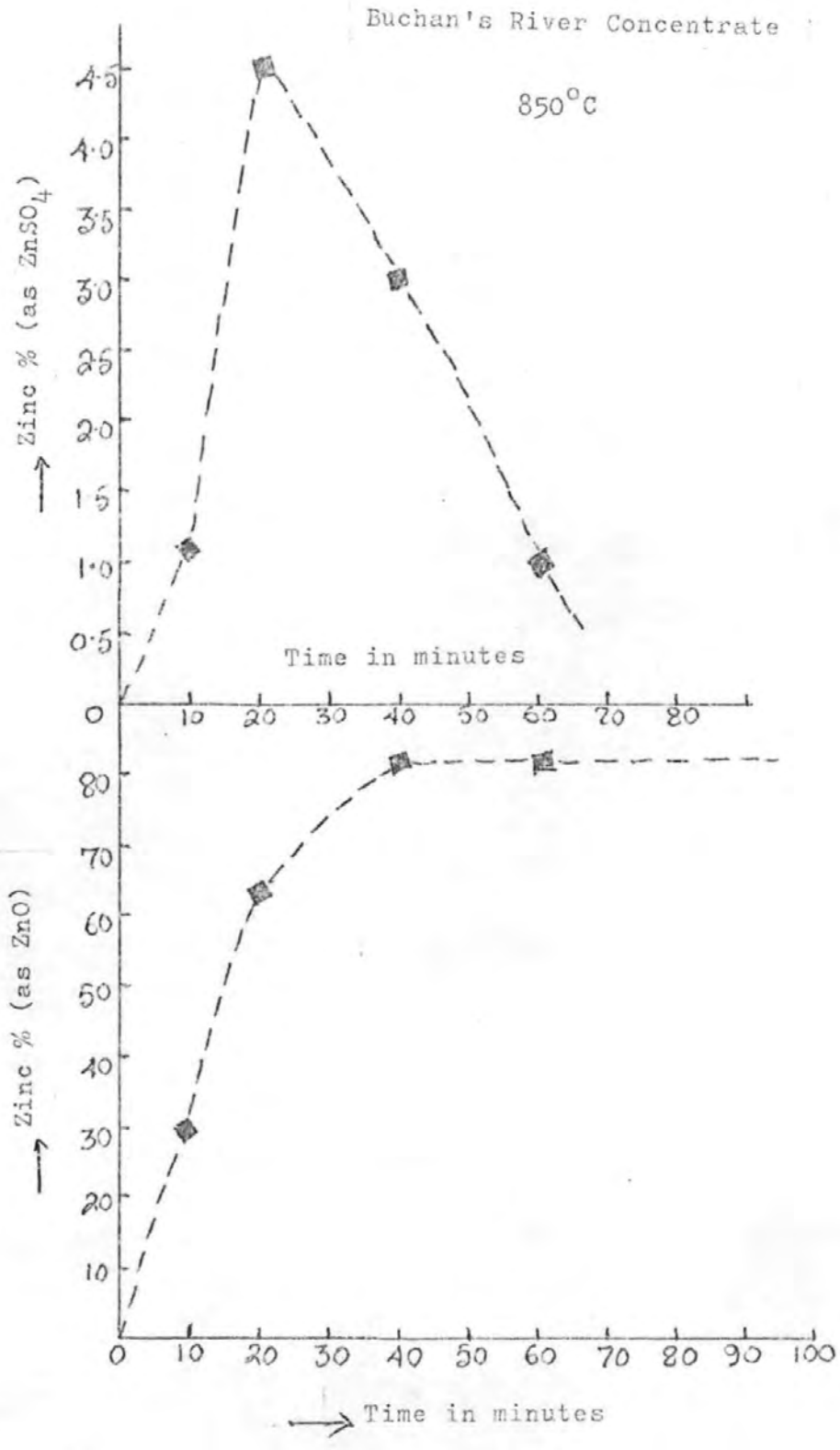
Buchan's River Concentrate
850°C
Zinc % (as $ZnSO_4$)
4·5
4·0
3·5
3·0
2·5
2·0
1·5
1·0
0·5
0
Time in minutes
10 20 30 40 50 60 70 80
Zinc % (as ZnO)
80
70
60
50
40
30
20
10
0 10 20 30 40 50 60 70 80 90 100
Time in minutes

Figure 85

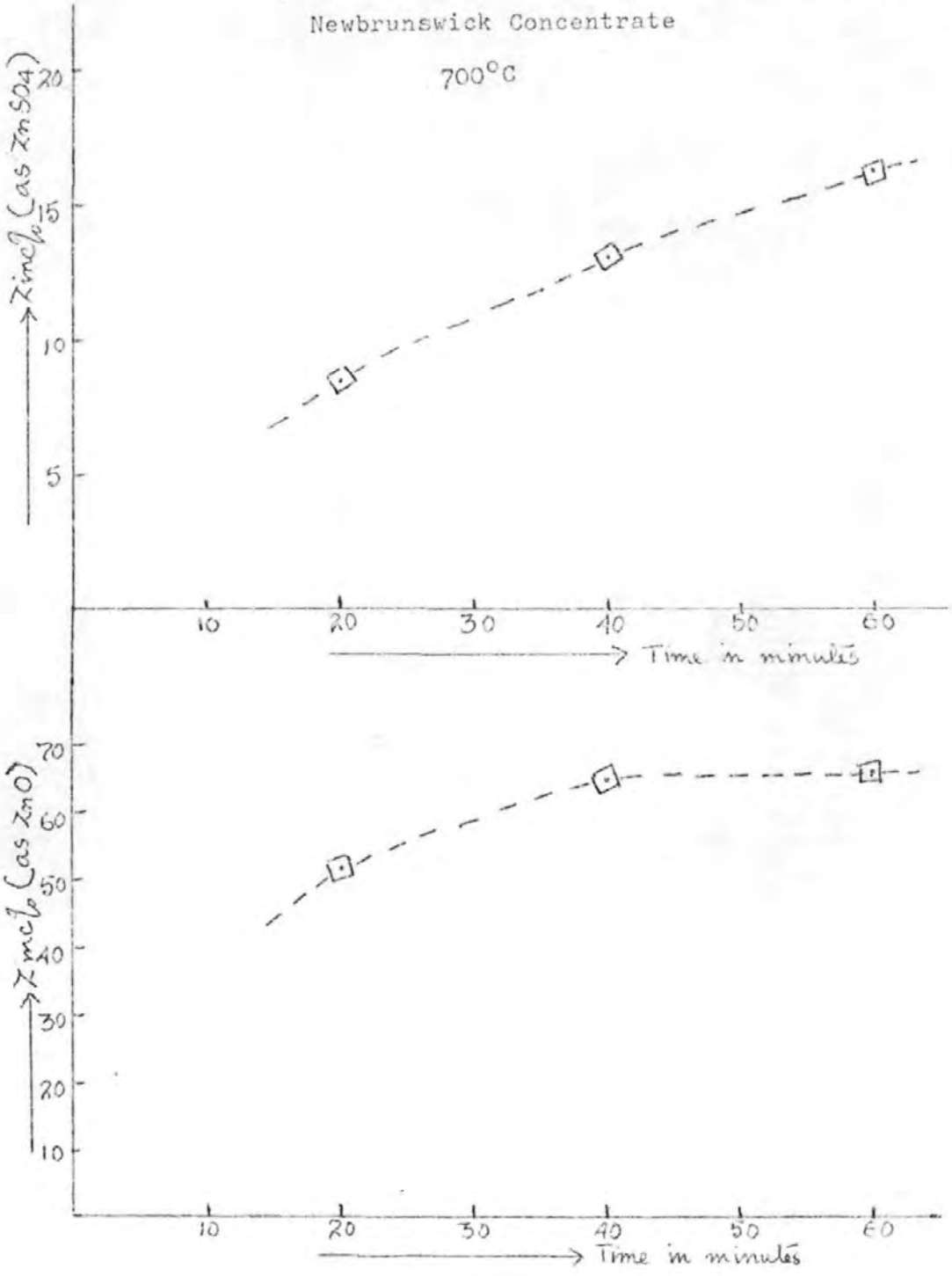


ROASTING BEHAVIOUR OF ZINC CONCENTRATES AT ISOTHERMAL TEMPERATURES

(1 g sample taken each time; zinc present in each constituent expressed as percentage of the total zinc in the roast).

Figure 86

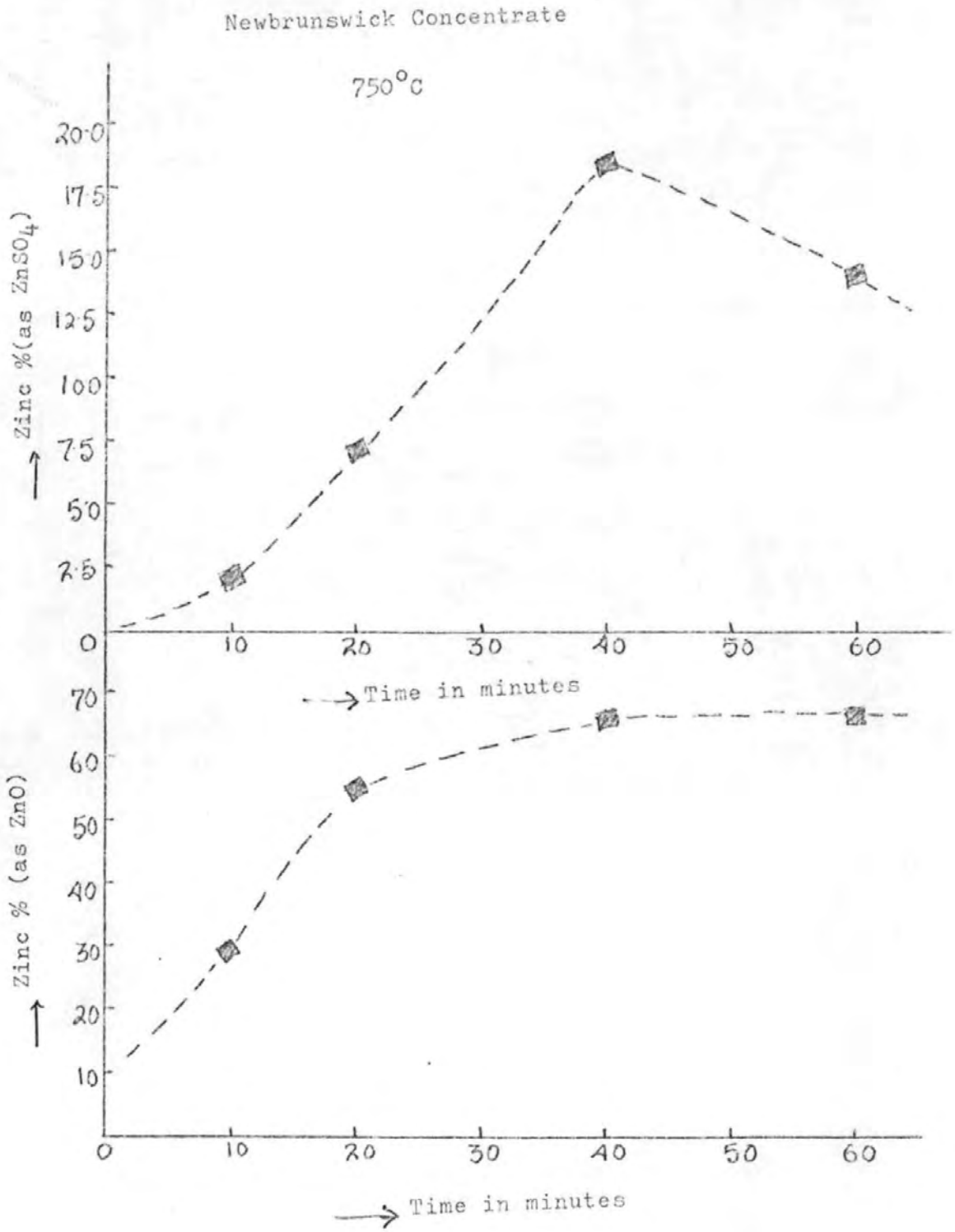
Newbrunswick Concentrate
750°C
Zinc %(as $ZnSO_4$)
20·0
17·5
15·0
12·5
10·0
7·5
5·0
2·5
0
10
20
30
40
50
60
Time in minutes
Zinc % (as ZnO)
70
60
50
40
30
20
10
0
10
20
30
40
50
60
Time in minutes

Figure 87

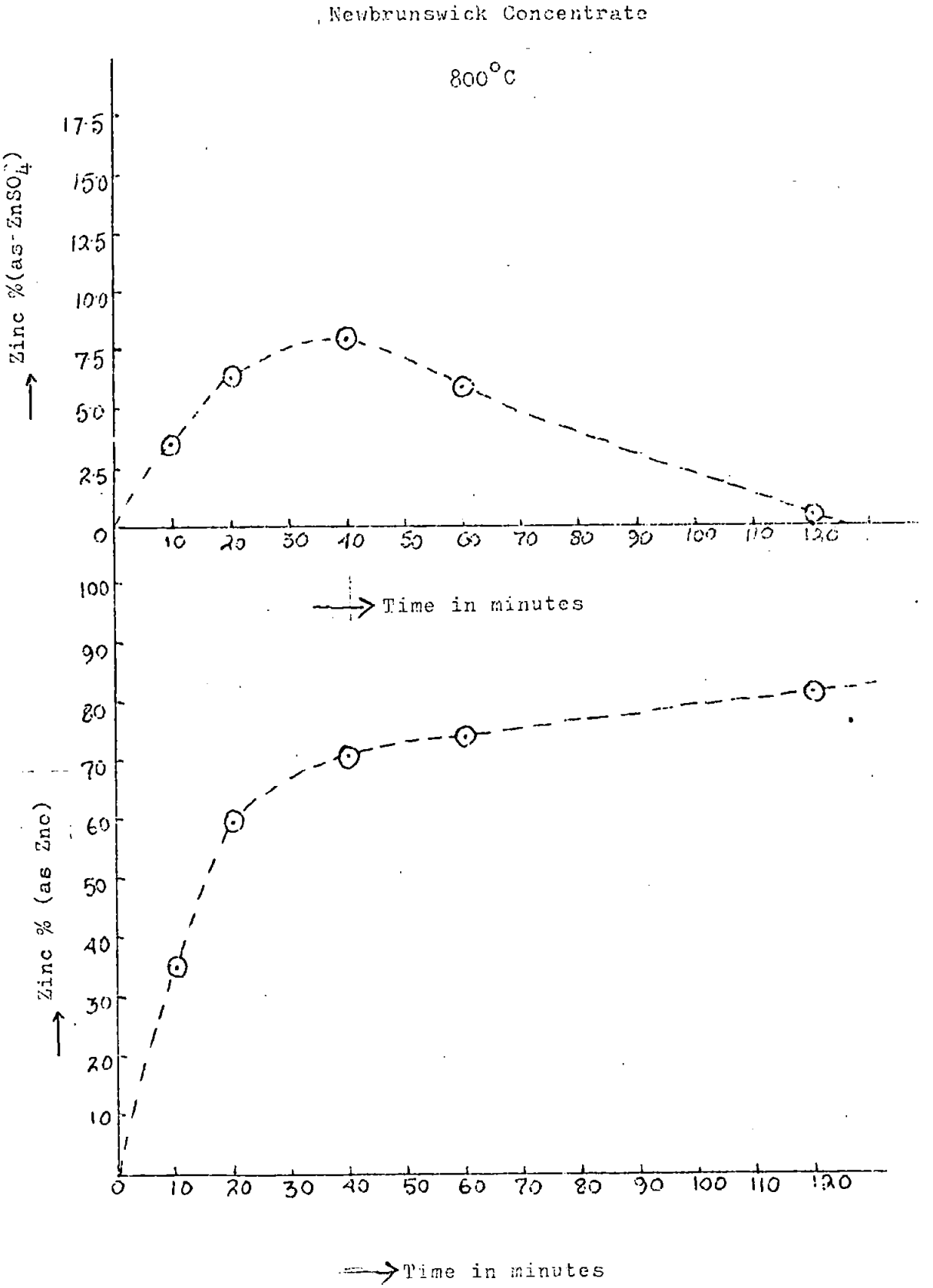
Newbrunswick Concentrate
800°C
Zinc %(as $ZnSO_4$)
17·5
15·0
12·5
10·0
7·5
5·0
2·5
0
10 20 30 40 50 60 70 80 90 100 110 120
Time in minutes
Zinc % (as Znc)
100
90
80
70
60
50
40
30
20
10
0 10 20 30 40 50 60 70 80 90 100 110 120
Time in minutes

Figure 88

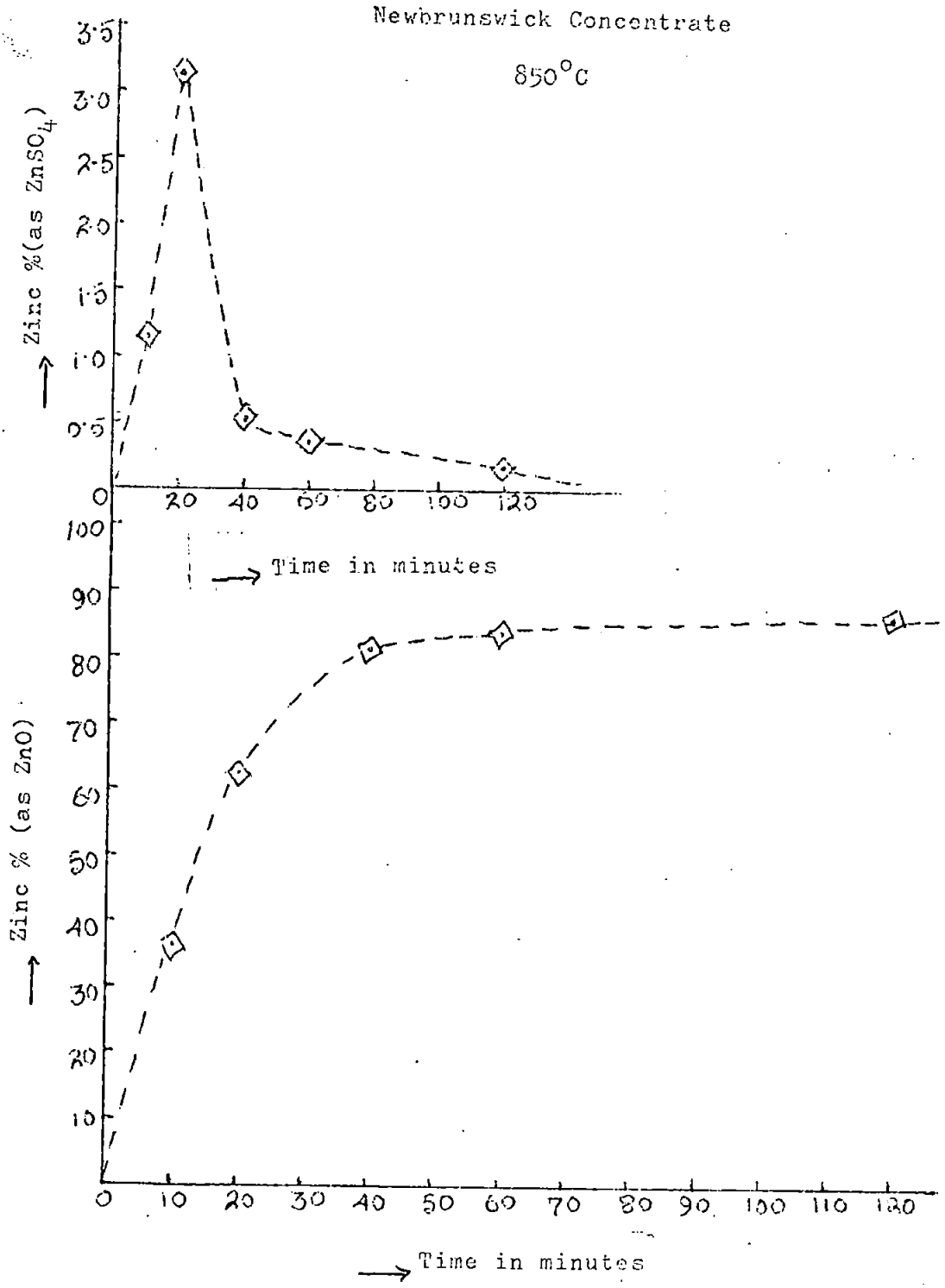
Newbrunswick Concentrate
850°C
Zinc %(as $ZnSO_4$)
3·5
3·0
2·5
2·0
1·5
1·0
0·5
0
20
40
60
80
100
120
Time in minutes
Zinc % (as ZnO)
100
90
80
70
60
50
40
30
20
10
0
10
20
30
40
50
60
70
80
90
100
110
120
Time in minutes

ROASTING BEHAVIOUR OF ZINC CONCENTRATES AT ISOTHERMAL TEMPERATURES

(1 g sample taken each time; zinc present in each constituent expressed as percentage of the total zinc in the roast).

Heathsteele Concentrate

700°C

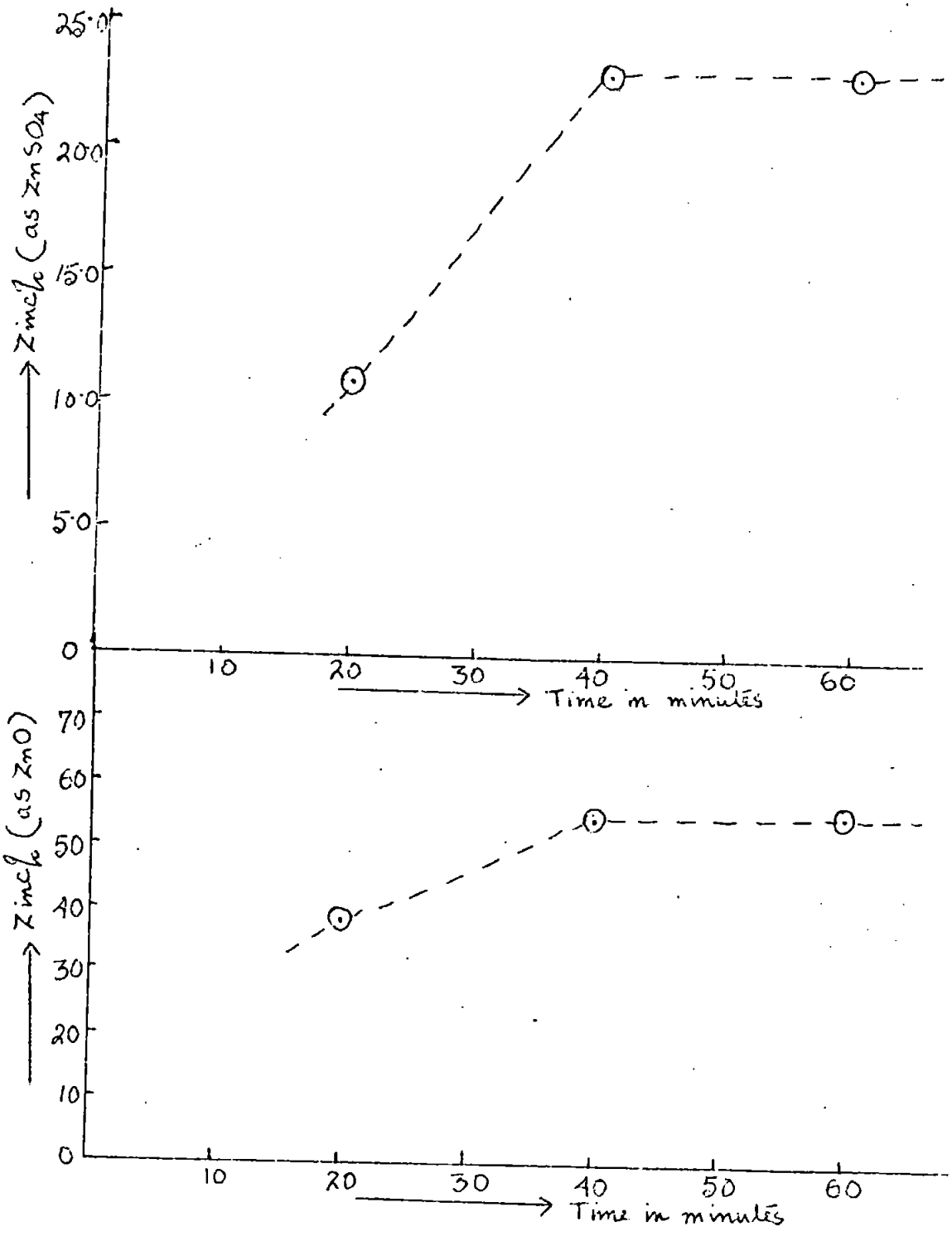


Figure 89

Figure 90

Heathsteele Concentrate

750°C

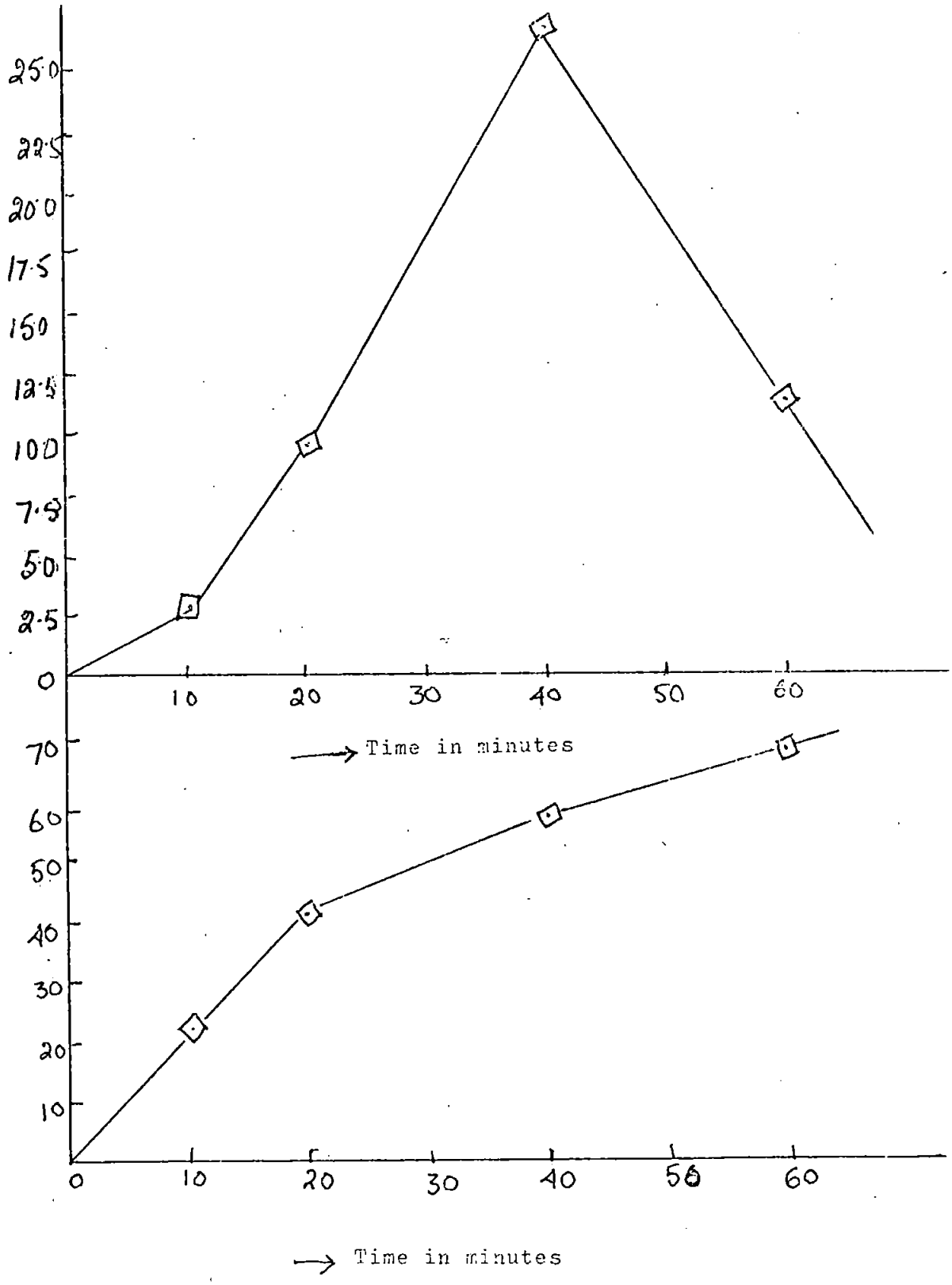

Figure 91

Heathsteele Concentrate

800°C

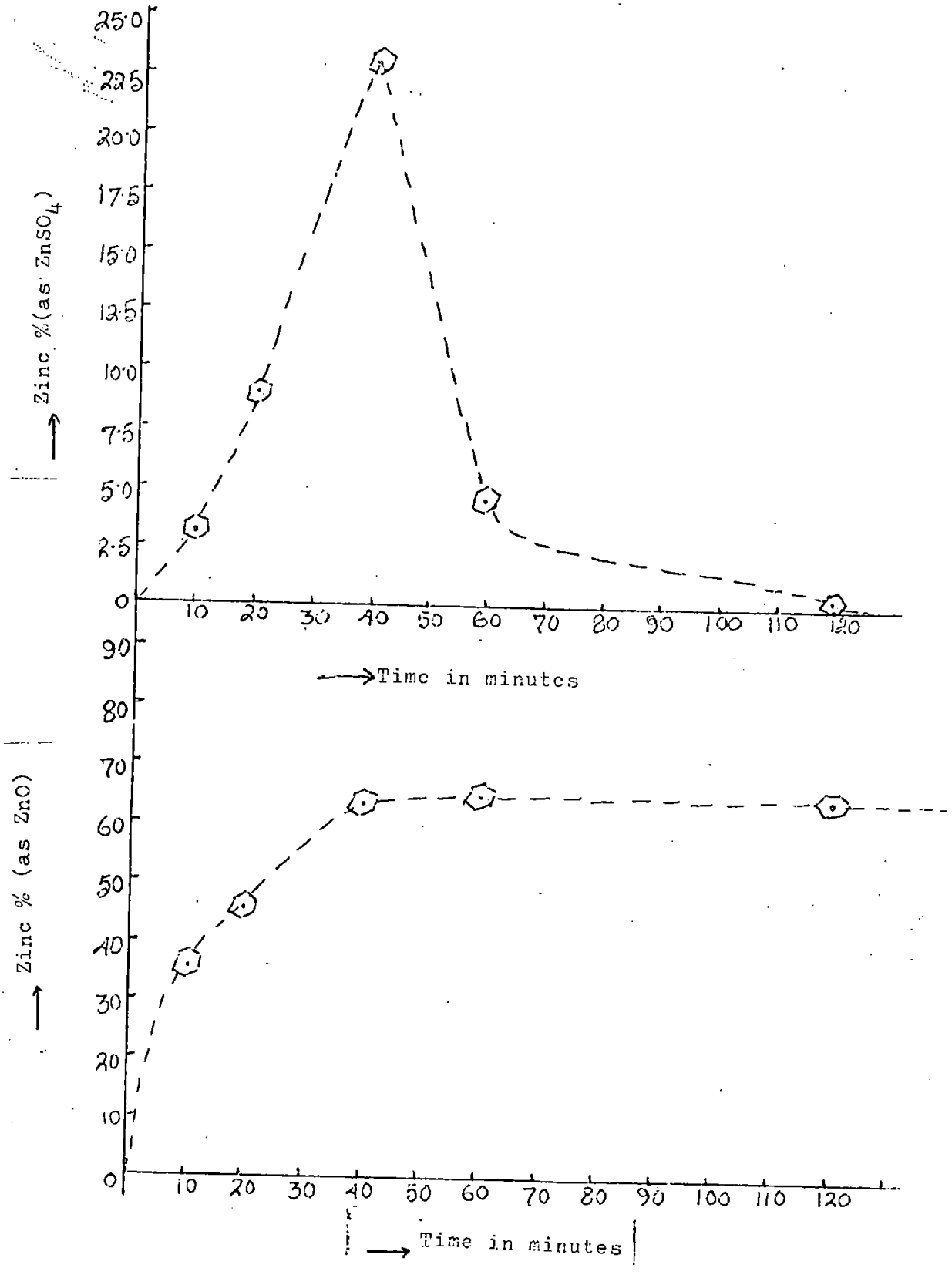

Figure 92

Heathsteele Concentrate

850°C

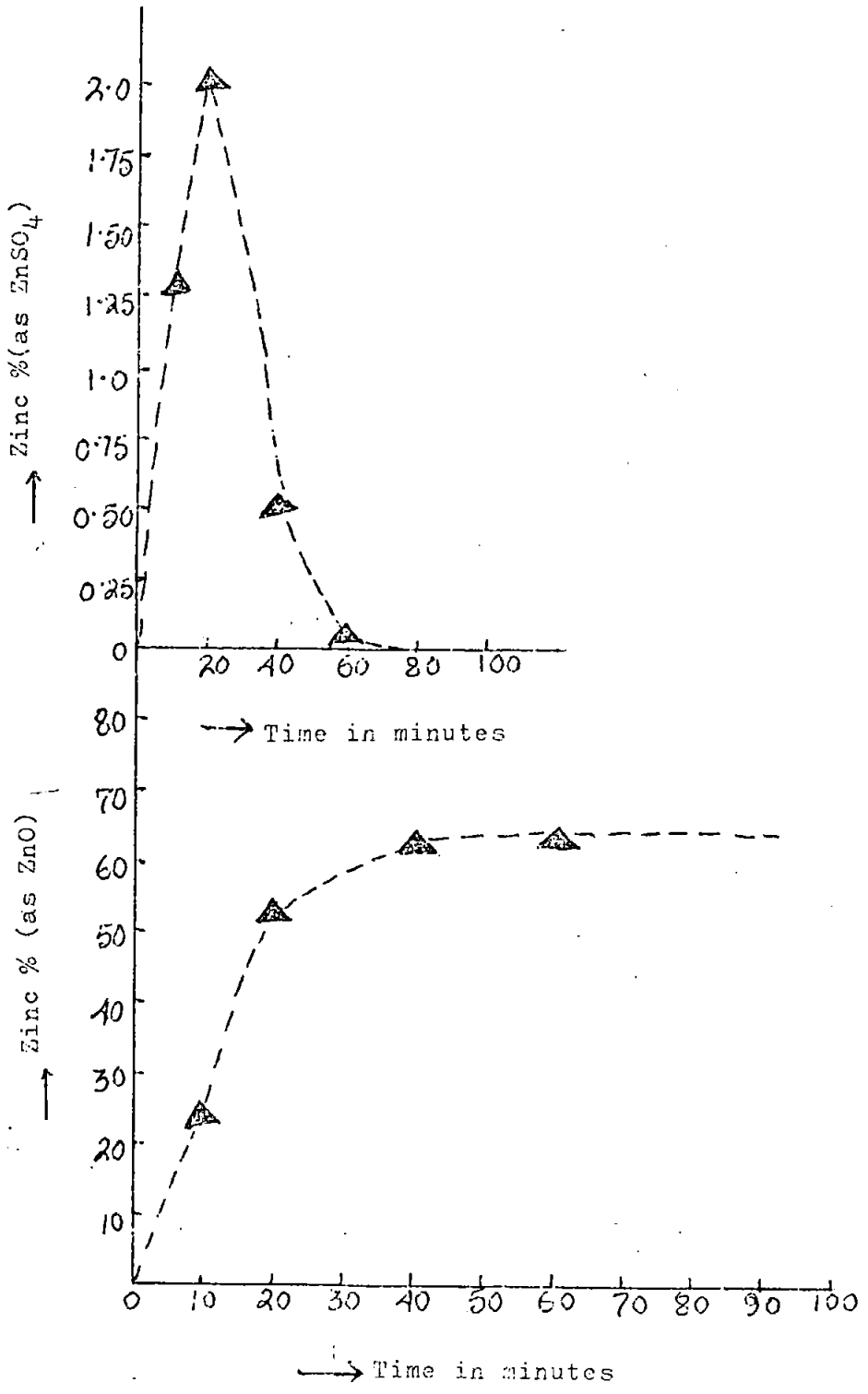

Figure 93

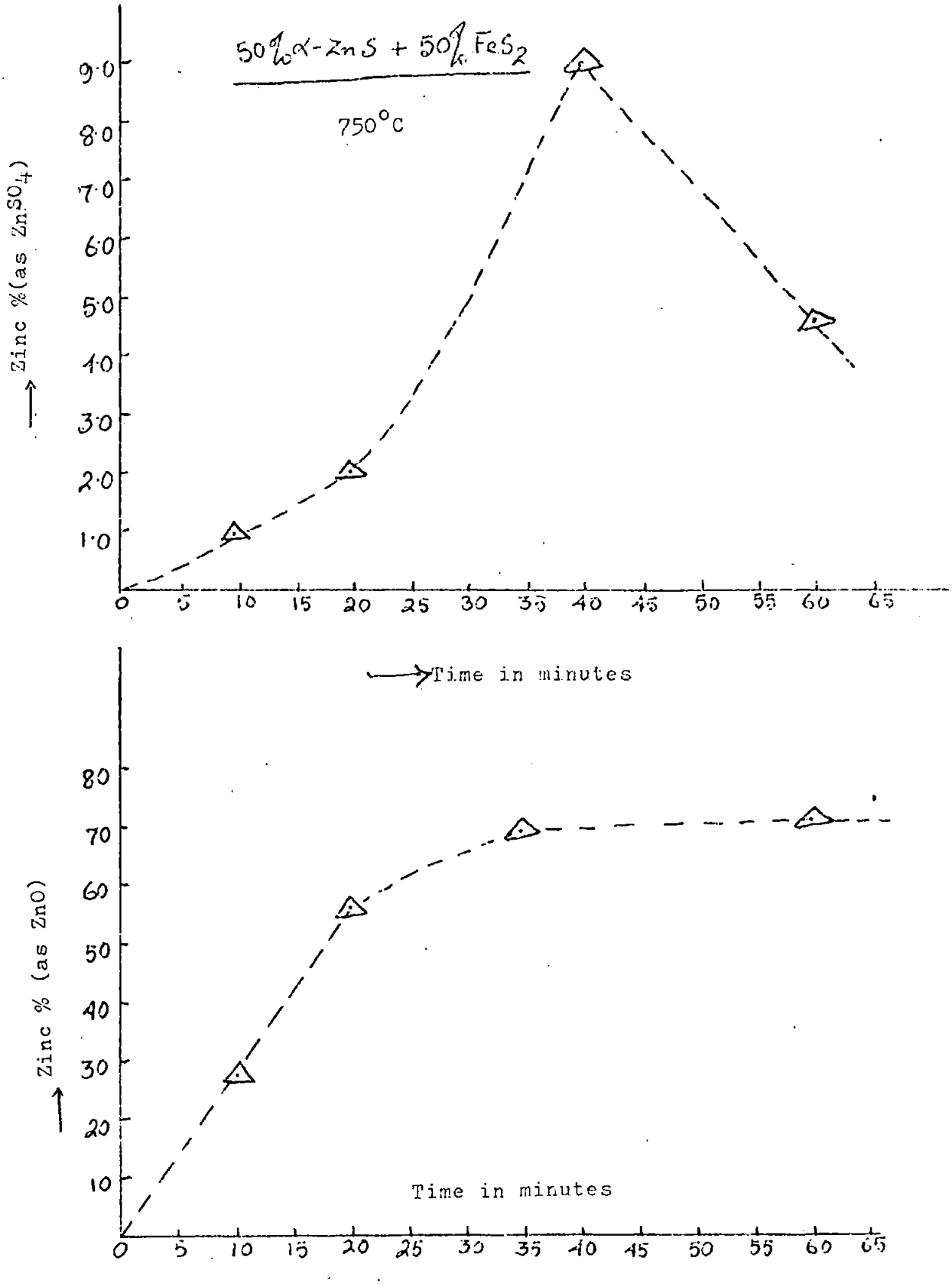


ROASTING BEHAVIOUR OF SYNTHETIC MIXTURE ($\alpha$-ZnS + $FeS_2$) AT ISOTHERMAL TEMPERATURES

(1 g sample taken each time; zinc present in each constituent expressed as percentage of the total zinc in the roast).

Figure 94

ROASTING BEHAVIOUR OF SYNTHETIC MIXTURE ($\alpha$-ZnS + $FeS_2$) AT ISOTHERMAL TEMPERATURES

(1 g sample taken each time; zinc present in each constituent expressed as percentage of the total zinc in the roast).

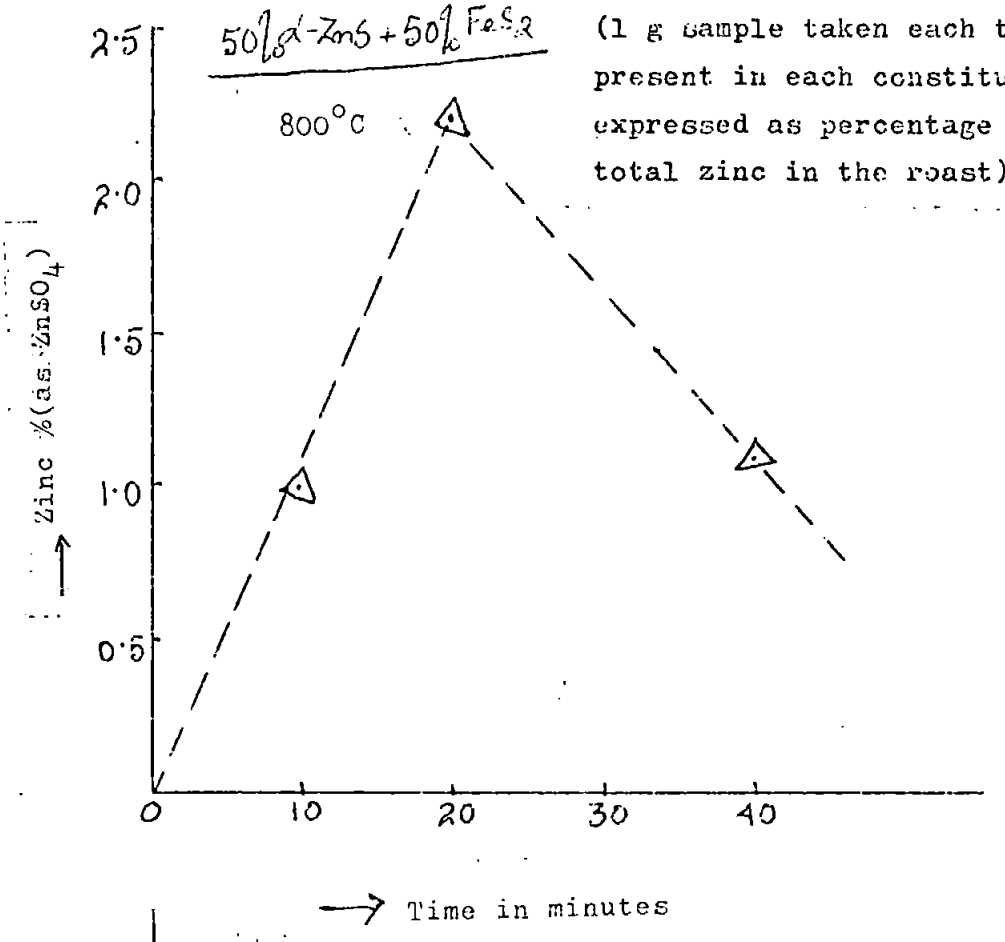


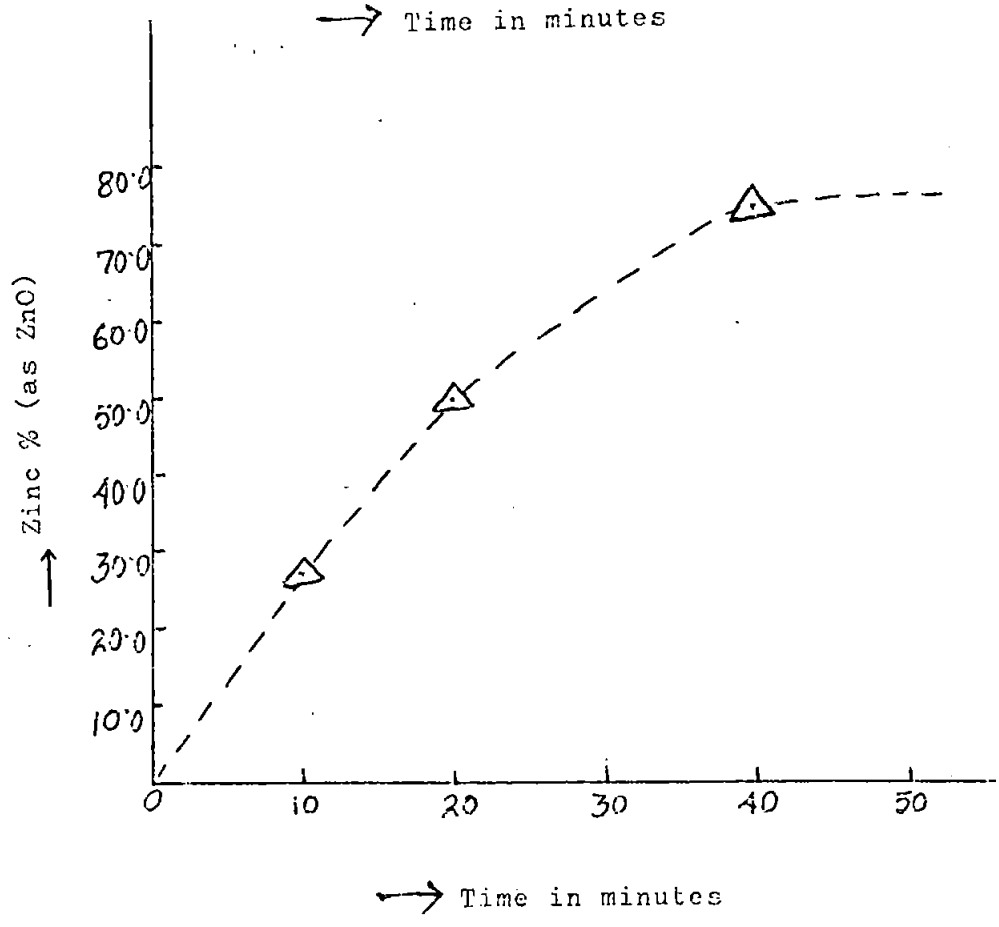

ZINC CONCENTRATES ROASTED FOR 40 MINUTES IN FLUIDISED BED

(1 g sample taken each time; zinc present in each constituent expressed as percentage of the total zinc in the roast).

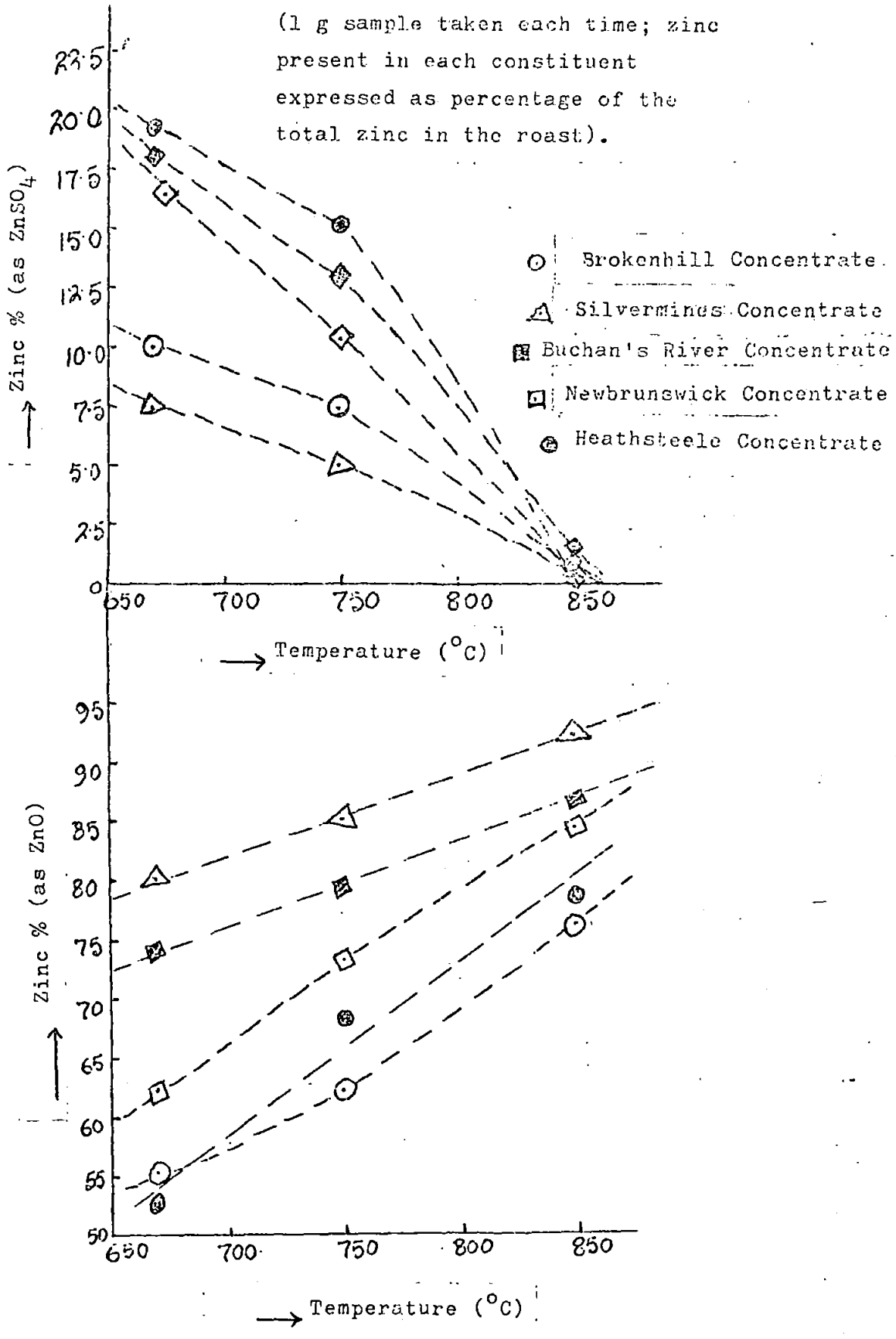


Figure 95

the order :

Heathsteele > New Brunswick > Broken Hill > Silvermines.

With an increasing $Fe_2O_3/ZnO$ ratio, the degree of sulphation of the zinc in the mixture increases, since the increased $Fe_2O_3$ "contact" surface promotes more complete oxidation of $SO_2$ to $SO_3$ (97). This has been confirmed by using synthetic mixtures of zinc sulphide - iron sulphide and zinc sulphide-iron oxide(Figs.71,72,93 & 94 and Table 24

In some of isothermal oxidations for different time intervals, the amount of zinc sulphate formed reached a maximum value (e.g. in 40 minutes at 750° and 800°C, but in 20 minutes for 850°C) during the early stages, and with further roasting the amount formed decreased (Figure 73-94 and Table 21-24). It is due to the fact that the $SO_2$ and $SO_3$ contents of the furnace gases decrease, whereas the oxygen pressure increases considerably towards the end of the roasting, which favours the decomposition of zinc sulphate.

It is interesting to note that in the sulphation of zinc concentrates at temperatures 800° and 850°C (Fig.73-94) in the initial stages high rates of sulphation are established in spite of the formation of ferrite. It may be assumed, therefore, that ferric oxide retains some of its catalytic power even when combined in a ferrite.

5.3.2 Formation of zinc ferrite and its effect on oxidation rate of zinc sulphide

According to the free energy data (91), zinc ferrite can be formed under ordinary roasting conditions. The extent to which zinc occurs as zinc ferrite in the calcine will depend on the relative amounts of zinc oxide and ferric oxide present, the time of contact between these two solids, and other factors like temperature which determine the kinetics between the two solids. X-ray diffraction studies indicate that practically all the ferric oxide in the calcine

at the end of roasting exists as ferrite and that oxygen-enrichment at any given temperature does not appreciably reduce the amount of ferrite formed at the end of the roasting period. This may be due to the fact that practically all the zinc sulphide in the concentrate is converted to zinc oxide within the first 25 minutes.

5.3.3 Roasting of zinc concentrates in fluidized turbulent layer

Roasting experiments were conducted in a silica-tube furnace. The reaction tube was made of silica. About 1g of sample was taken each time and introduced into the even-temperature zone of the reaction tube. Compressed air was then passed through the bed at the required rate through a calibrated flowmeter. Temperature was controlled to within $\pm$ 5°C.

Roasting experiments were conducted at temperatures ranging from 670° to 850°C. Preliminary experiments showed that when air was supplied at a rate greater than 450 $cm^3$/min, the oxidation was independent of the rate of flow of air (91). Therefore, in all experiments the zinc concentrates were roasted at an air flow rate $>$ 450 $cm^3$/min. At the end of experiment the roasted concentrate was analysed for zinc sulphate and zinc oxide.

Some experiments were also performed in oxygen-enriched air; oxygen taken from cylinders was introduced into the air system through flowmeters. The results are given in Table 25 Figure 95. In general, the oxidation rate increased in a fluidised bed and the maximum amount of sulphate was obtained at a temperature 670° compared with 750°C in a stationary layer.

It is seen from the data presented in Figures 96-97 that oxygen-enrichment increases the sulphate content at higher temperatures.

TABLE 25

Zinc Concentrates roasted for 40 minutes in fluidized bed

| Concentrate | Temp °C | Zinc % (in terms of total zinc in the product) | | |
|---|---|---|---|---|
| | | as $ZnSO_4$ | ZnO | ZnS + $ZnFe_2O_4$ |
| Heathsteele | 670° | 19.5 | 52.5 | 28.0 |
| " | 750° | 15.0 | 68.0 | 17.0 |
| " | 850° | 0.20 | 78.0 | 21.8 |
| Buchan's River | 670° | 18.0 | 74.0 | 8.0 |
| " | 750° | 13.0 | 79.0 | 8.0 |
| " | 850° | 1.3 | 86.5 | 12.2 |
| New Brunswick | 670° | 16.5 | 62.0 | 21.5 |
| " | 750° | 10.3 | 73.0 | 16.7 |
| " | 850° | 0.2 | 84.5 | 15.3 |
| Broken Hill | 670° | 10.0 | 55.0 | 35.0 |
| " | 750° | 7.5 | 62.0 | 30.5 |
| " | 850° | 0.75 | 76.0 | 23.25 |
| Silvermines | 670° | 7.5 | 80.0 | 12.5 |
| " | 750° | 5.0 | 85.0 | 10.0 |
| " | 850° | 0.50 | 92.0 | 7.5 |

Figure 96

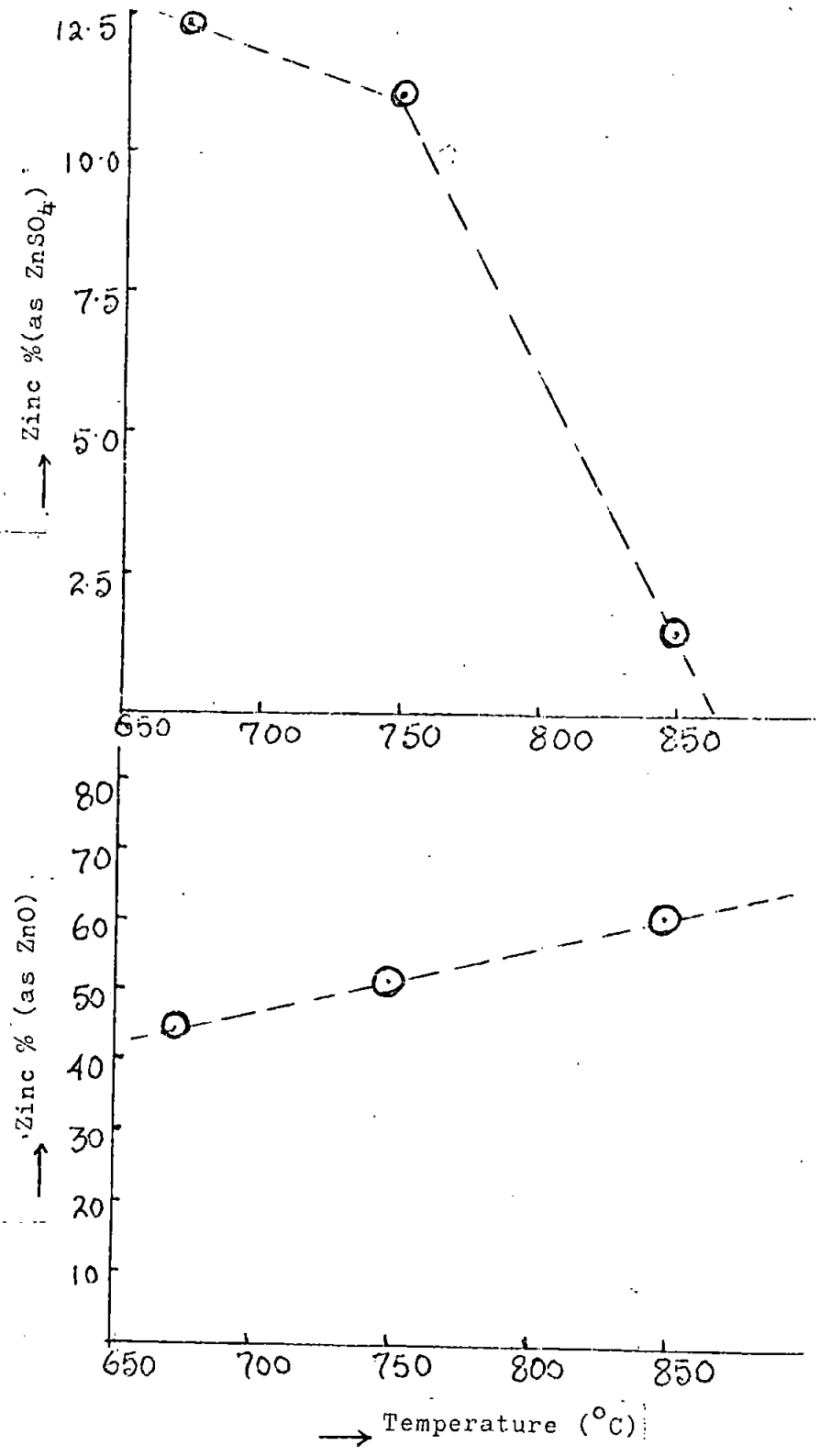


ROASTING BEHAVIOUR OF BROKENHILL CONCENTRATE IN FLUIDISED BED USING OXYGEN ENRICHED AIR

(1 g sample taken each time; zinc present in each constituent expressed as the percentage of the total zinc in the roast).

ROASTING BEHAVIOUR OF BROKENHILL CONCENTRATE IN FLUIDISED BED USING OXYGEN ENRICHED AIR AT 850°C

(1 g sample taken each time; zinc present in each constituent expressed as the percentage of the total zinc in the roast).

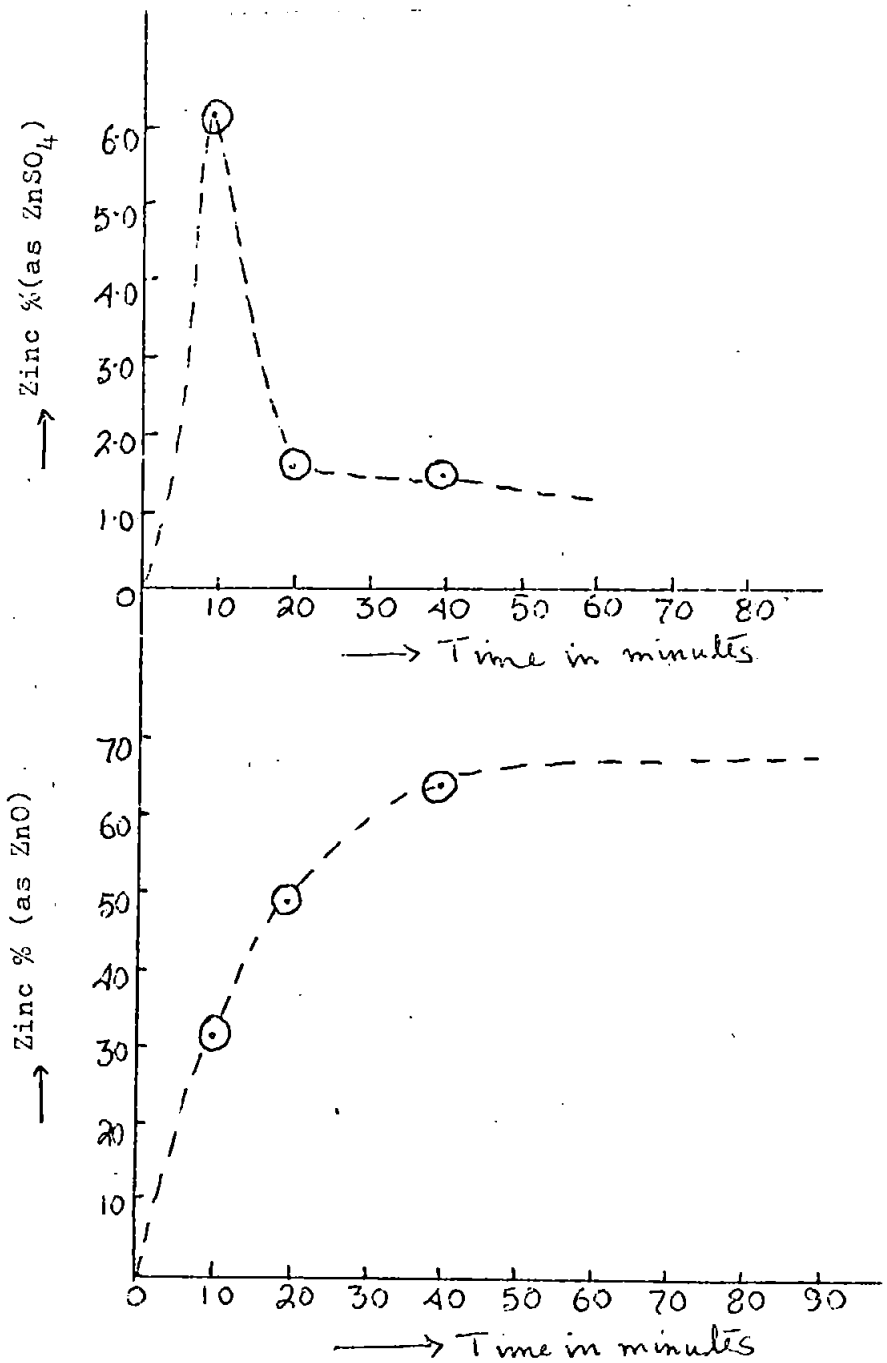


Figure 97

## 5.4 Differential thermal analysis (DTA) curve of zinc concentrates

Figs.98-108 show the DTA curves of the roasting of zinc concentrates of different compositions. The first exothermic peak at 449°C corresponds to the oxidation of iron sulphides. The height of this peak is lowest for Buchan's River concentrate as it contains the lowest percentage of iron and sulphides. For comparison DTA curves of iron-pyrites are shown in Figs.103-104 and Table 28.The second and third exothermic peaks in Figure 98 represent the oxidation of zinc sulphide. The endothermic peak at 750°C in Figure 98 and Table 26 corresponds to the decomposition of the sulphates formed in roasting.

In a static bed, i.e. with no flow of air through the bed, the exothermic peaks are very broad (Figure105), which indicates the slow oxidation rate of the sulphides in the concentrates.

The second and third exothermic peaks in the DTA curve can be explained as follows : The reaction probably nucleates and developes across the surface (first peak) and after a certain period required for the destruction of the crystal lattice to form a reaction interface it proceeds into the grain itself. This behaviour is similar to that found for pure zinc sulphide which also gives two peaks (Chapter 4). The presence of these two peaks can hardly be explained on the basis of differences in the chemical compositions of the sulphides, since all five zinc concentrates studied show the same two peaks although they all contain different amounts of iron sulphides.

### 5.4.1 D.T.A. Curve of zinc concentrates in oxygen-enriched air

Figs.109-113 and Table 26 show the DTA curve of zinc concentrates in oxygen-enriched air. The first exothermic peak corresponds to the oxidation of iron sulphide. The height of the peak is reduced quite considerably. The second exothermic peak

TABLE 26

D.T.A. Curves of Zinc Concentrates

| Concentrate | Flow rate | First Exothermic peak due to $FeS_2$ oxidation | | 2nd & 3rd Exothermic peaks due to ZnS oxidation | | Endo-thermic peak du to decc positic of 'Sulpha |
|---|---|---|---|---|---|---|
| | | Initial oxidation Temp °C | Intense oxidation Temp °C | Initial oxidation Temp °C | Intense oxidation Temp °C | |
| New Brunswick | $80cm^3$/min air | 389 | 449 | 542 | 625 & 660 | 750 |
| " | 0 | 460 | 525 | 662 | 725 | 806 |
| Heathsteele | $80cm^3$/min air | 389 | 437 | 542 | 625 & 660 | 825 |
| Broken Hill | " | - | - | 542 | 625 & 660 | - |
| " | 0 | - | - | 600 | 670 & 725 | - |
| Silvermines | 0 | 425 | 461 | 620 | 690 | 840 |
| " | $80cm^3$/min air | 389 | 419,425 & 445 | 542 | 643 & 660 | 736 |
| Buchan's River | 0 | 389 | 461 | 550 | 700 | 880 |
| " | $80cm^3$/min | 389 | 461 | 542 | 625 & 660 | 826 |
| New Brunswick | $80cm^3$/min $O_2$-enriched air | 389 | 485 | 600 | 650 | - |
| Buchan's River | " | 389 | 485 | 542 | 610 & 650 | 760 |
| Heathsteele | " | 437 | 460 | 475 | 490 | - |
| Broken Hill | " | - | - | 485 | 567 | 890 |
| Silvermines | " | - | - | 437 | 460 | - |

TABLE 27 :

D.T.A. Curves of synthetic mixture ($FeS_2$ + ZnS)

| Sample | Flow rate | First Exothermic peak due to $FeS_2$ oxidation | | 2nd & 3rd Exothermic peaks due to ZnS oxidation | | Endo-thermic peak du to decc positio of 'Sulpha |
|---|---|---|---|---|---|---|
| | | Initial oxidation Temp °C | Intense oxidation Temp °C | Initial oxidation Temp °C | Intense oxidation Temp °C | |
| β-ZnS + 20% $FeS_2$ | 80cm$^3$/min air | 389 | 430 & 442 | 542 | 595 | 715 |
| " | 80cm$^3$/min $O_2$-enriched air | 485 | 530 | 576 | 590 | - |
| α-ZnS + 20% $FeS_2$ | 80cm$^3$/min air | 365 | 420 | 542 | 600 & 610 | 715 |
| " | 80cm$^3$/min $O_2$-enriched air | - | - | 485 | 520 | - |

TABLE 28

D.T.A. Curves of Iron-pyrites

| Flow rate | First and 2nd Exothermic peaks due to oxidation of $FeS_2$ | | 3rd Exothermic peak due to oxidation of FeO or $Fe_3O_4$ to $Fe_2O_3$ | | Endothermic peak due to decomposition of 'Sulphate' |
|---|---|---|---|---|---|
| | Initial oxidation Temp °C | Intense oxidation Temp °C | Initial oxidation Temp °C | Intense oxidation Temp °C | |
| 80cm³/min air | 310 | 330 & 389 | 510 | 542 | 662 |
| 80cm³/min $O_2$-enriched air | 325 | 342 & 389 | 520 | 568 | - |

Figure 98

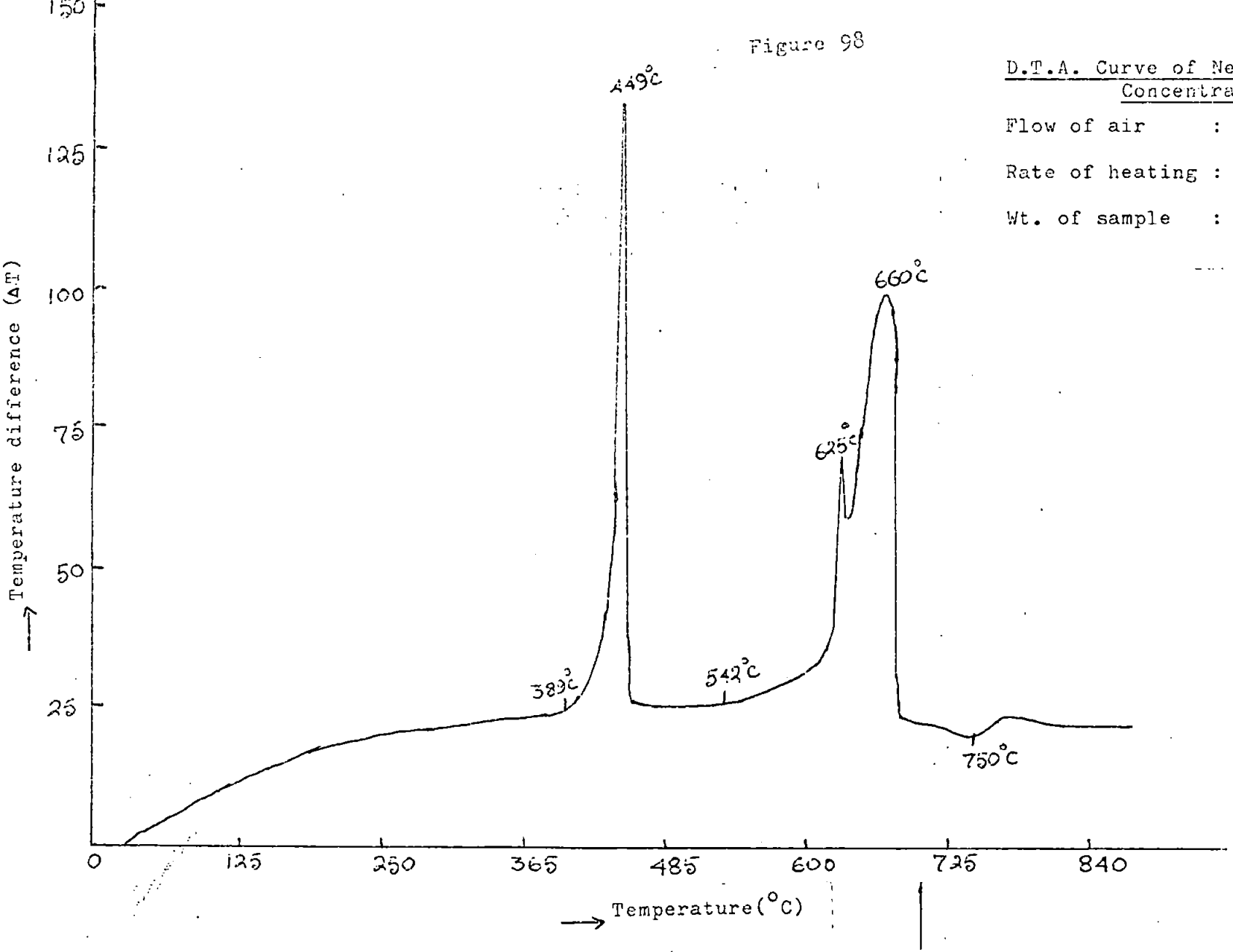
D.T.A. Curve of New Brunswick Concentrate
Flow of air : 80 cm³/min
Rate of heating : 10°C/min
Wt. of sample : 0.1 g
Temperature difference (ΔT)
150
125
100
75
50
25
449°C
660°C
625°C
389°C
542°C
750°C
0
125
250
365
485
600
725
840
Temperature (°C)

D.T.A. Curve of Buchan's River Concentrate

Figure 99

Flow of air : 80 cm $^3$/min

Rate of heating : 10°C/min

Wt. of sample : 0.1 g

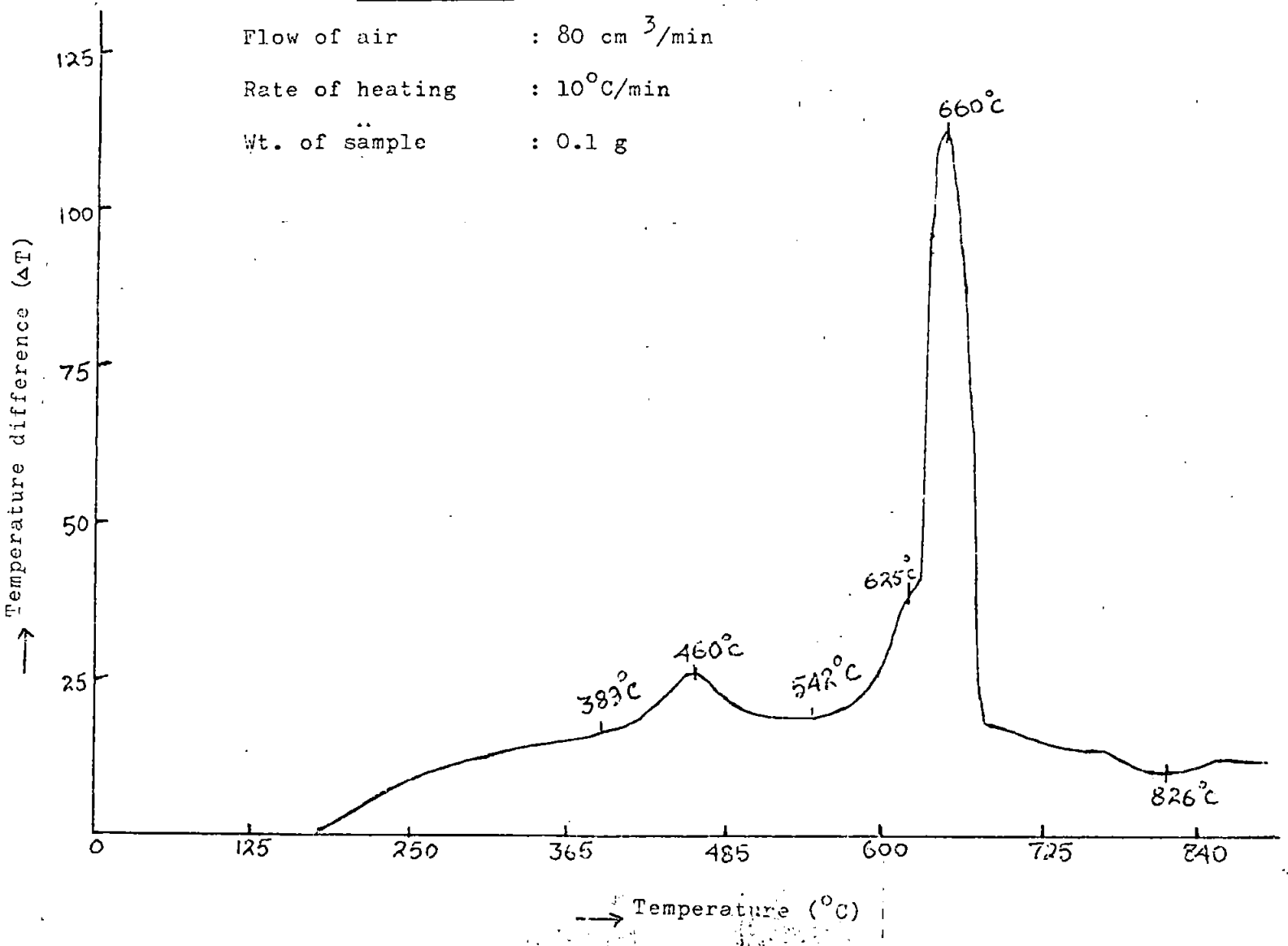

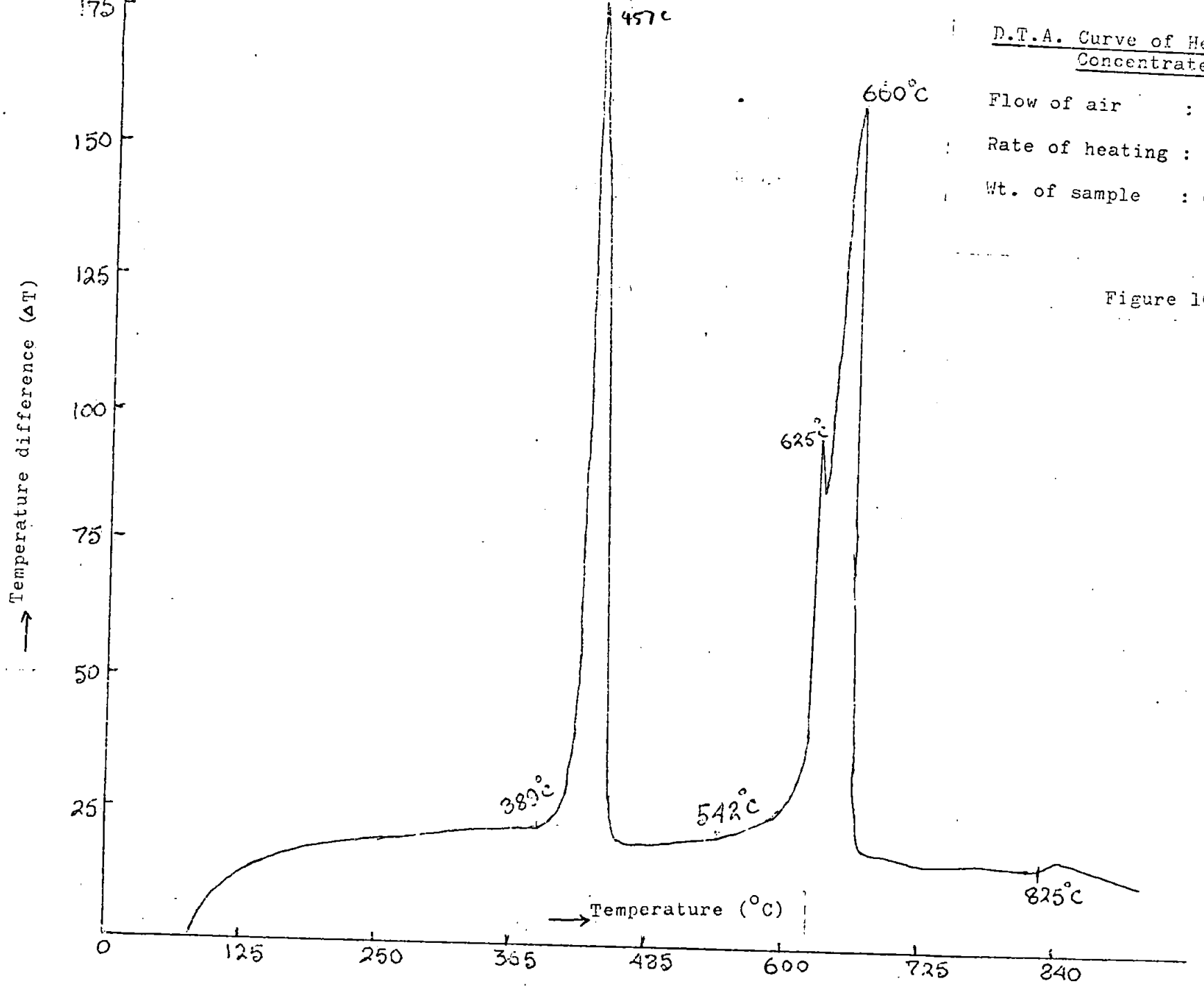


D.T.A. Curve of Heathsteele Concentrate

Flow of air : 80 cm $^3$/min

Rate of heating : 10°C/min

Wt. of sample : 0.1 g

Figure 100

D.T.A. Curve of Silvermines Concentrate

Flow of air : 80 cm $^3$/min

Rate of heating : 10°C/min

Wt. of sample : 0.1 g

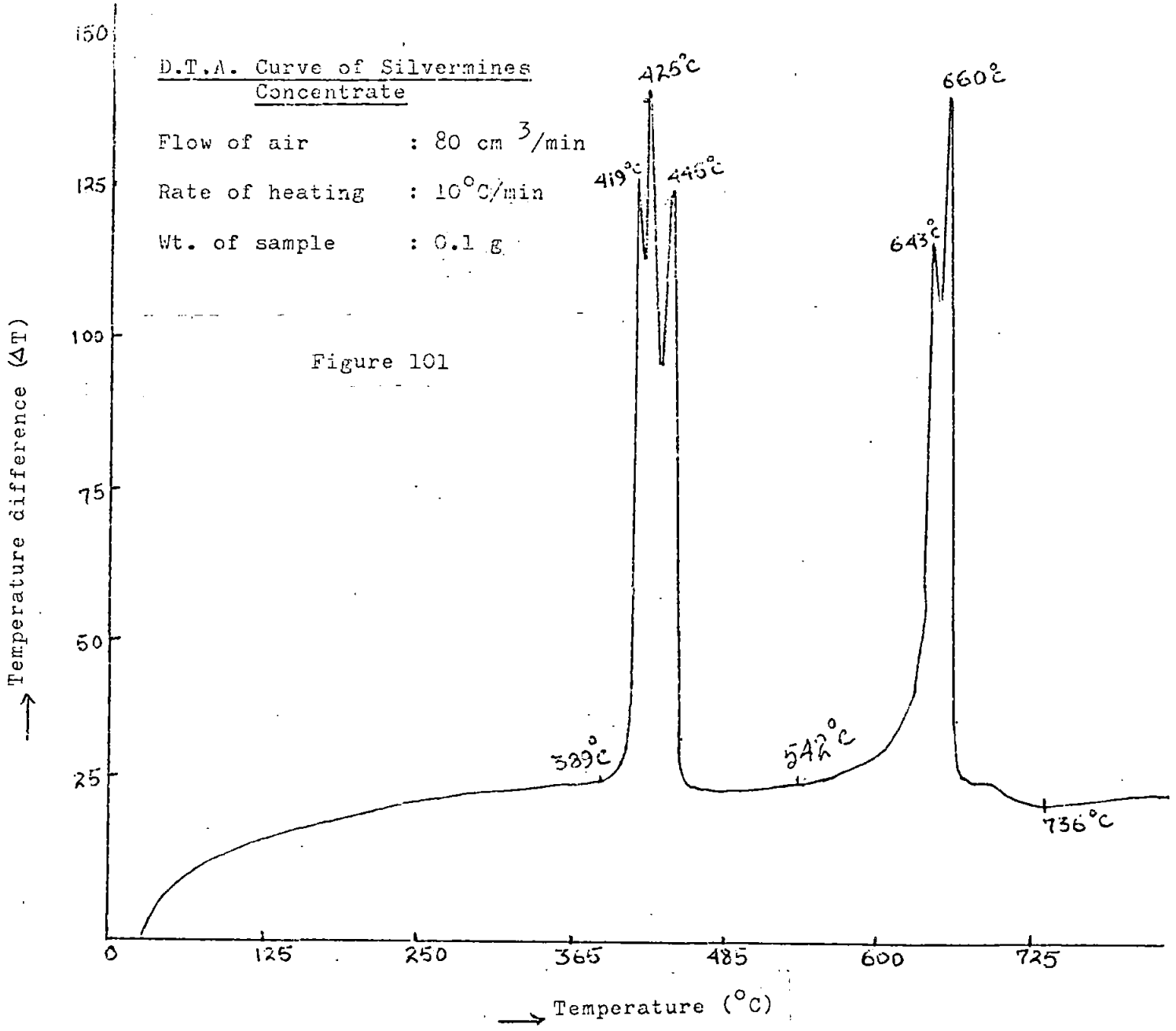


Figure 101

D.T.A. Curve of Broken Hill Concentrate

Flow of air : 80 $cm^3$/min

Rate of heating : 10°C/min

Wt. of sample : 0.1 g

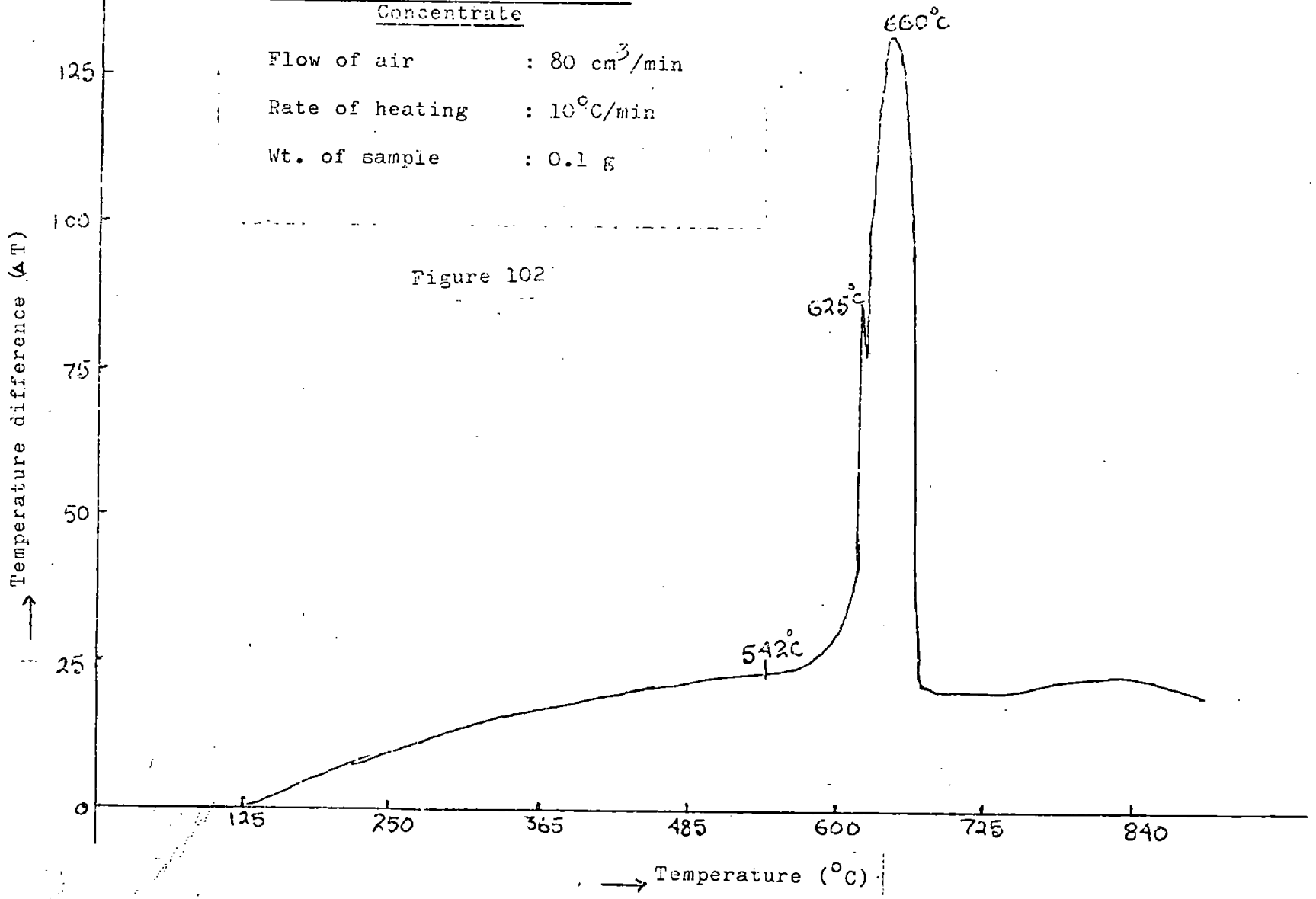


Figure 102

D.T.A. Curve of Iron pyrites

Flow of air : 80 cm $^3$/min

Rate of heating : 10°C/min

Wt. of sample : 0.1 g

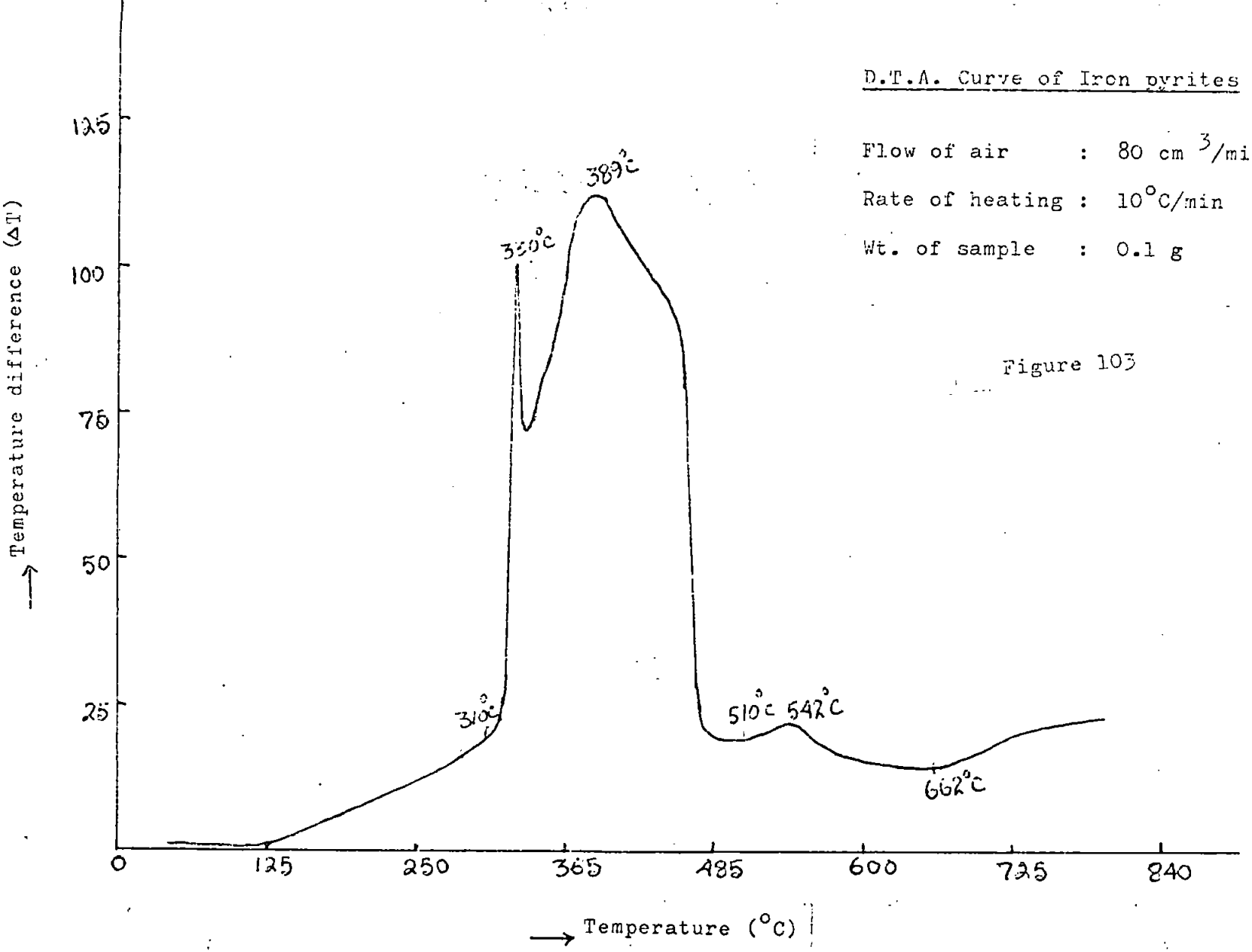


Figure 103

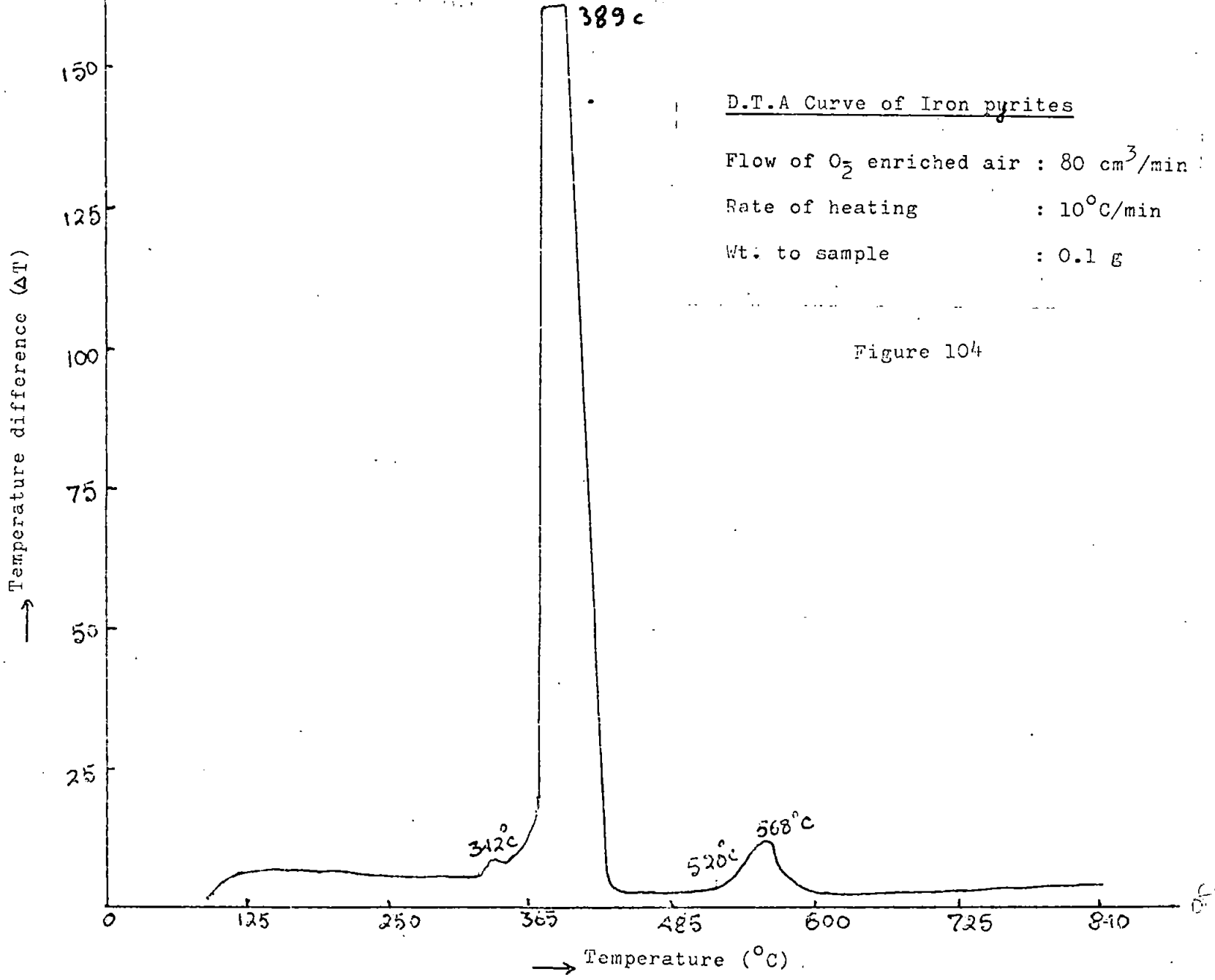


D.T.A Curve of Iron pyrites

Flow of $O_2$ enriched air : 80 $cm^3$/min

Rate of heating : 10°C/min

Wt. to sample : 0.1 g

Figure 104

Figure 105

D.T.A. Curve of Silvermines Concentrate in static bed

Rate of heating : 10°C/min

Wt. of sample : 0.1 g

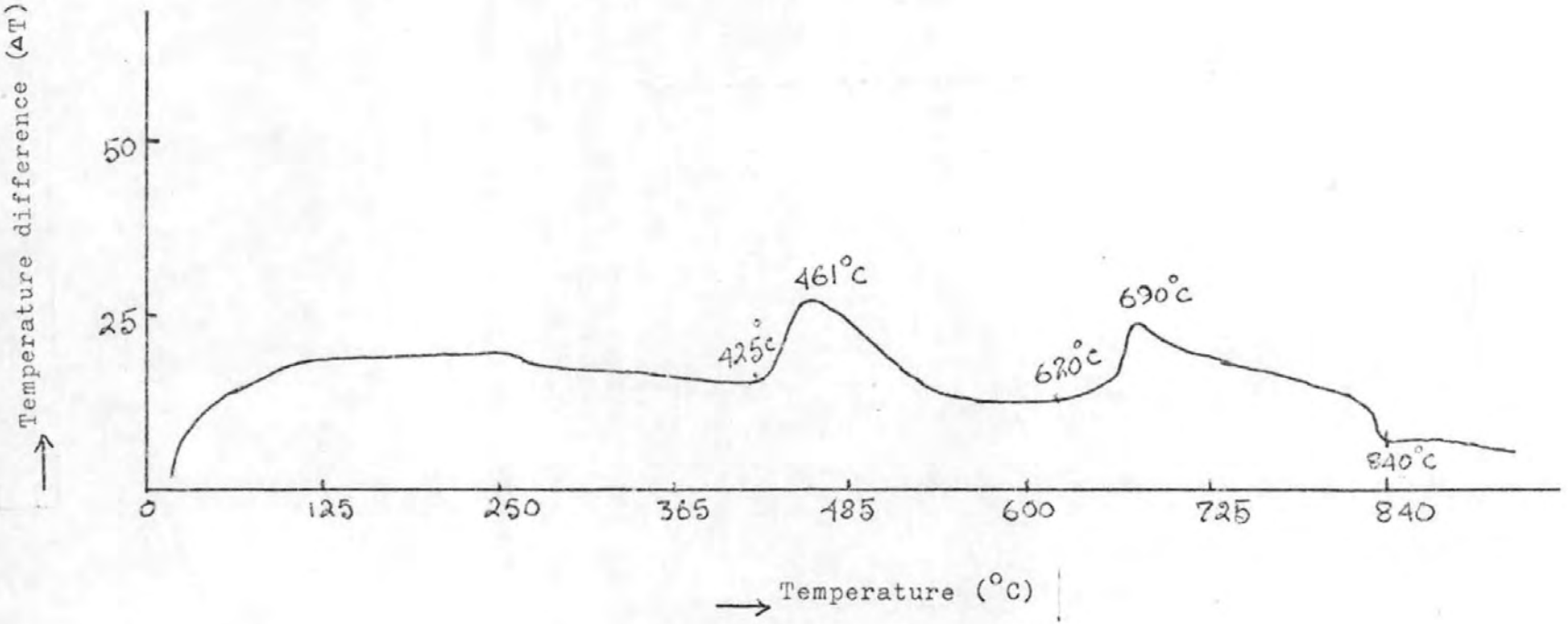

Figure 106

D.T.A. Curve of Buchan's River Concentrate in static bed

Rate of heating : 10°C/min

Wt. of sample : 0.1 g

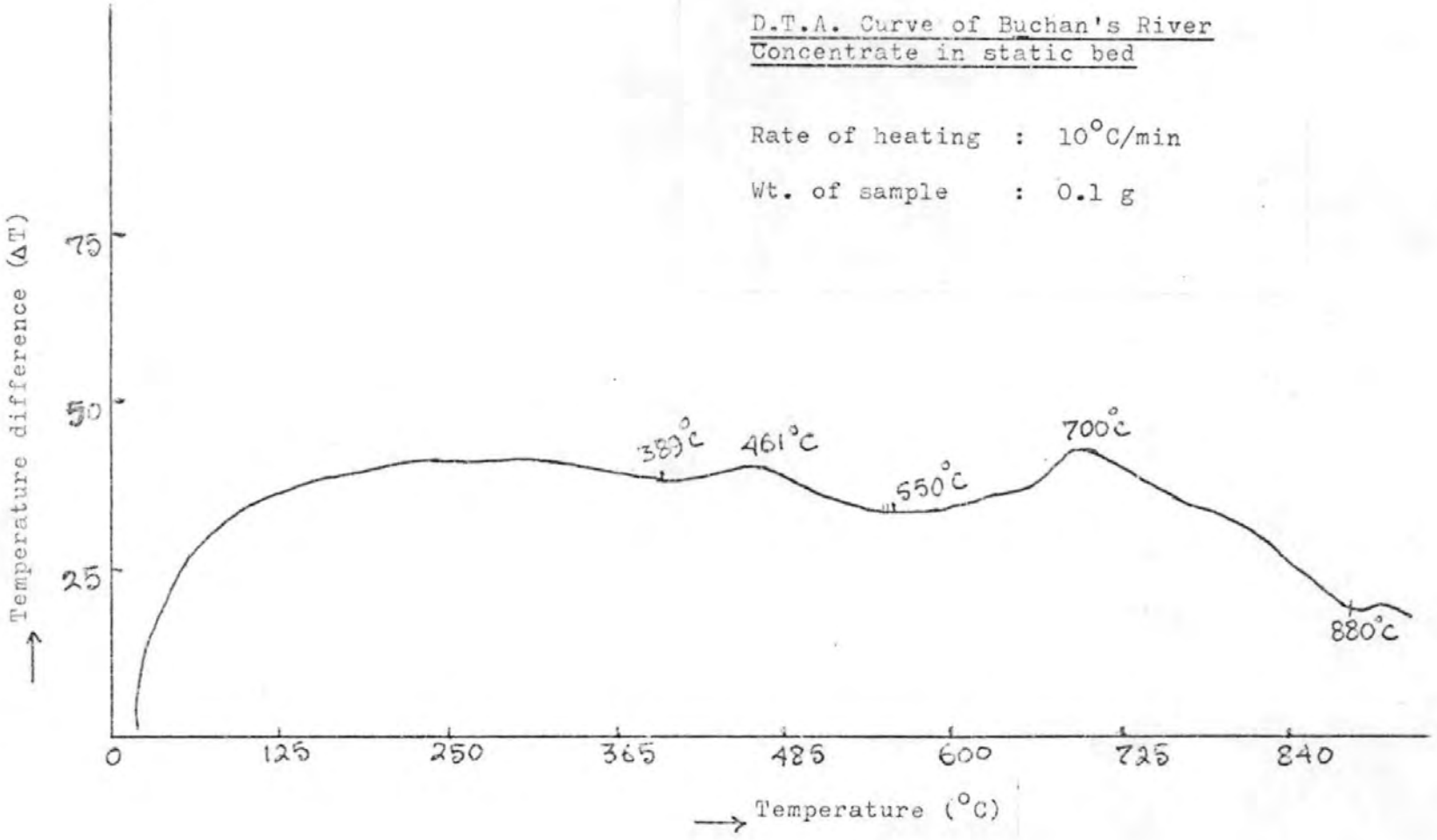

Figure 107

D.T.A Curve of New Brunswick Concentrate in static bed

Rate of heating : 10°C/min

Wt. of sample : 0.1 g

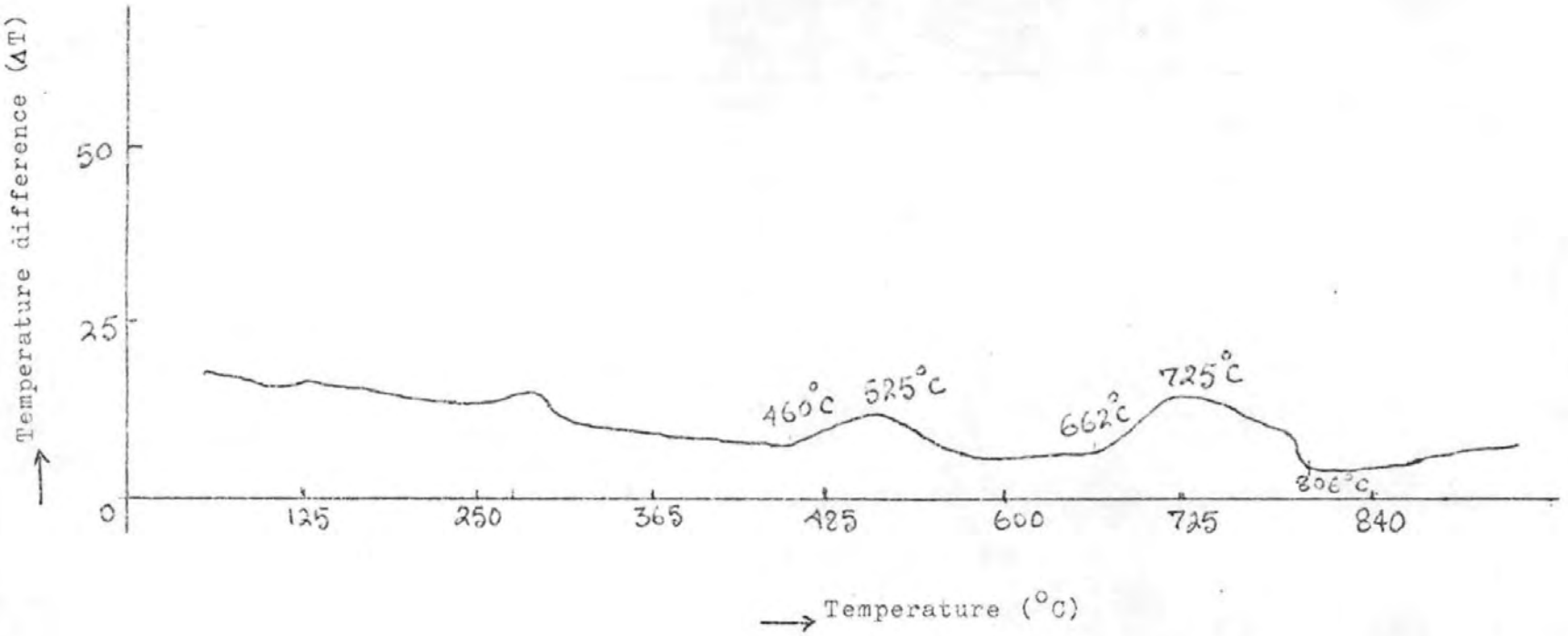

Figure 108

D.T.A Curve of Broken Hill Concentrate in static bed

Rate of heating : 10°C/min

Wt. of sample : 0. 1 g

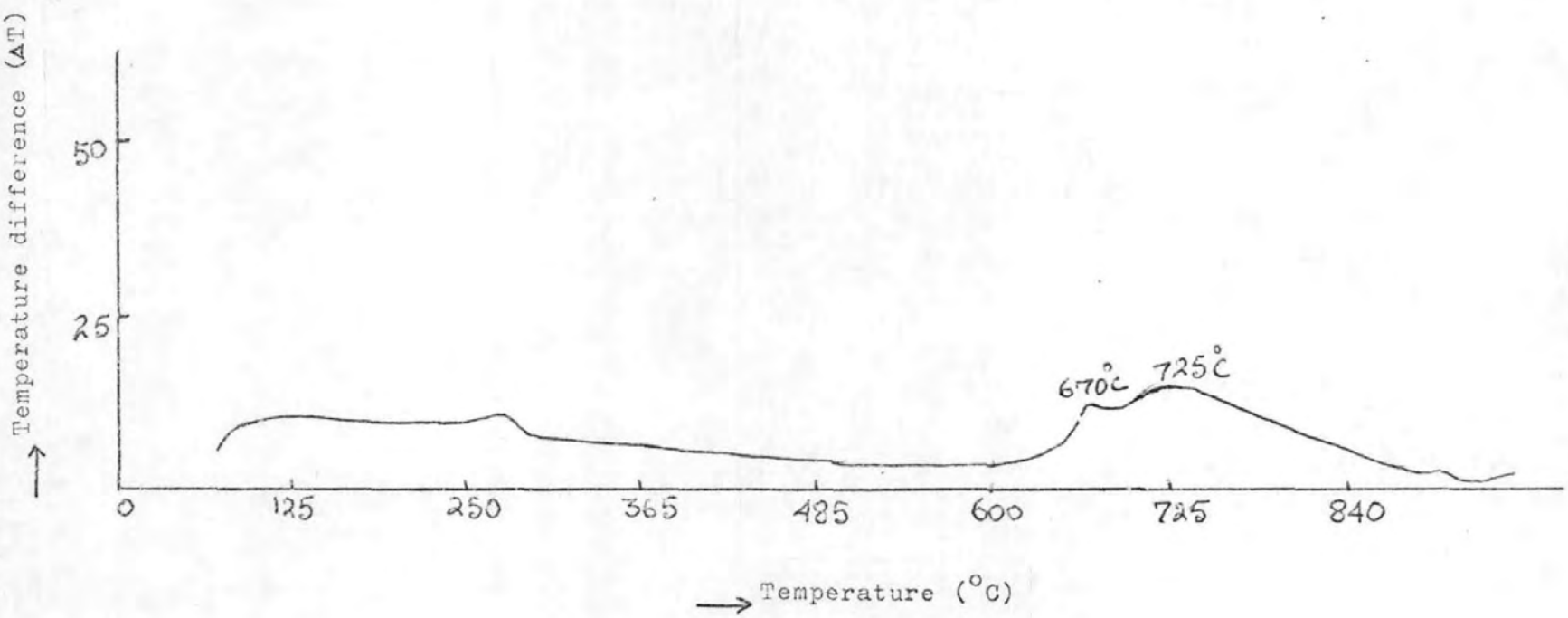

D.T.A. Curve of New Brunswick Concentrate

Flow of air ($O_2$-enriched) 80 $cm^3$/min

Rate of heating : 10°C/min

Weight of sample : 0.1 g

Figure 109

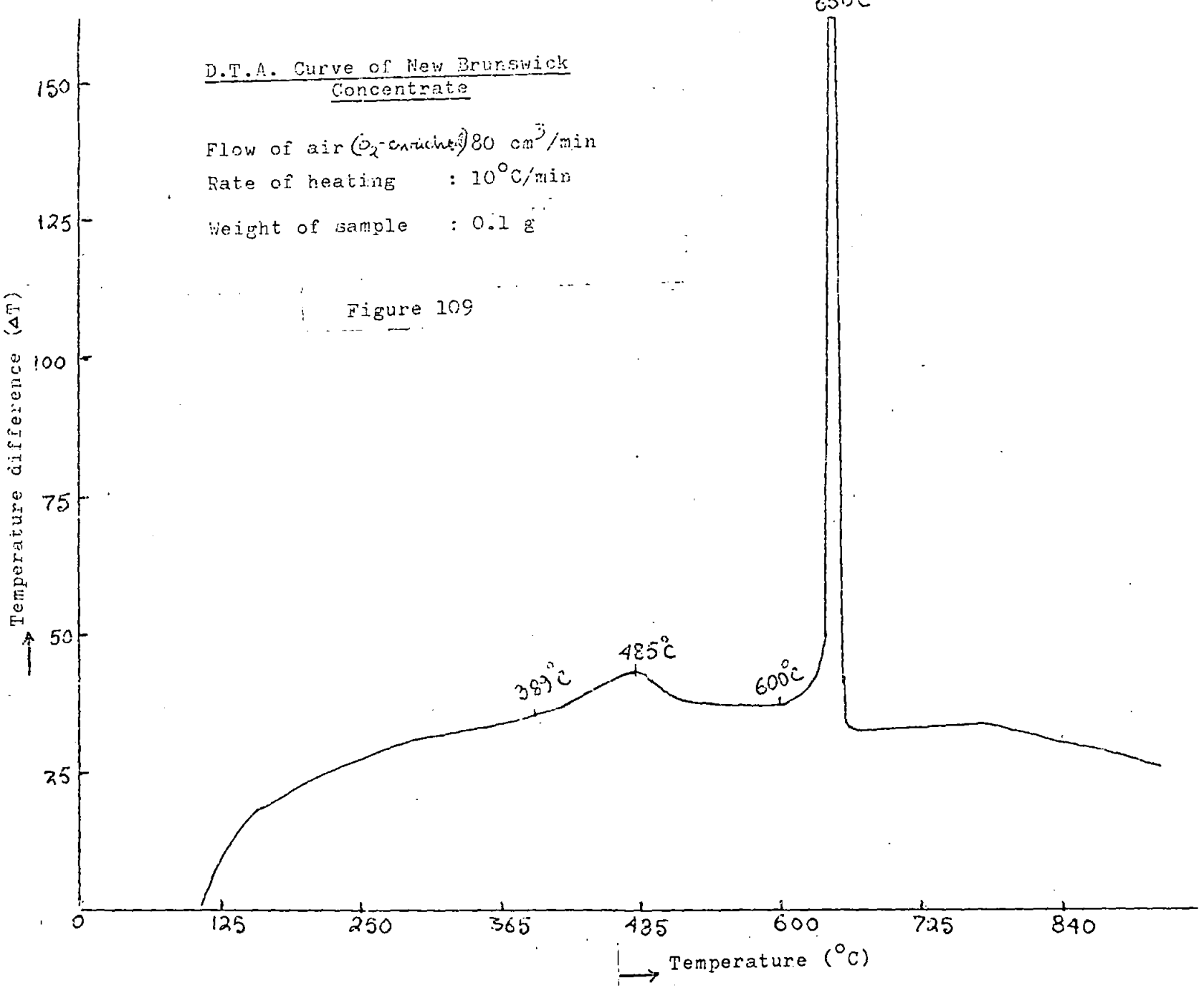

D.T.A. Curve of Buchan's River Concentrate

Flow of $O_2$ enriched air : 80 $cm^3$/min

Rate of heating : 10°C/min

Wt. of sample : 0.1 g

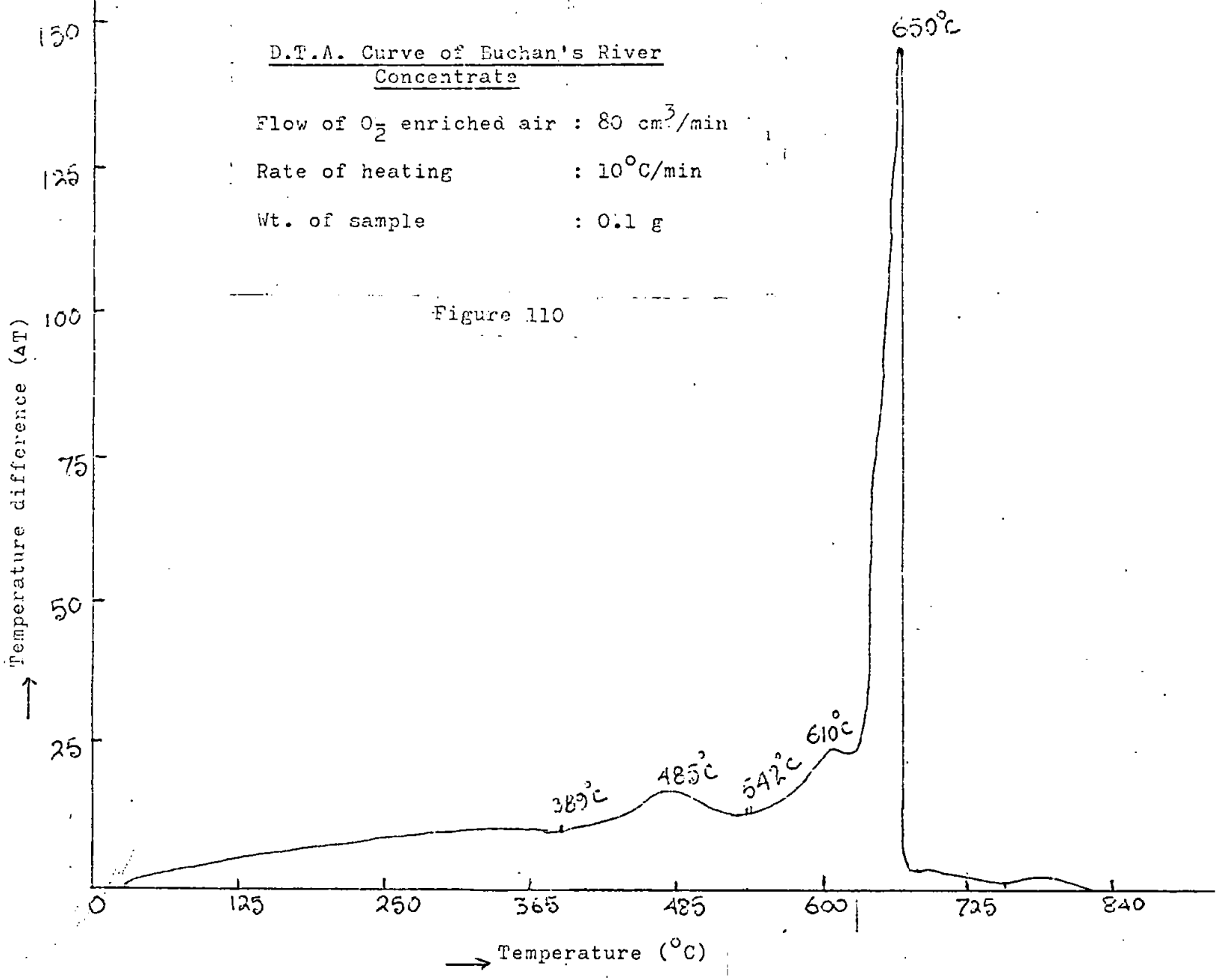


Figure 110

Figure 111

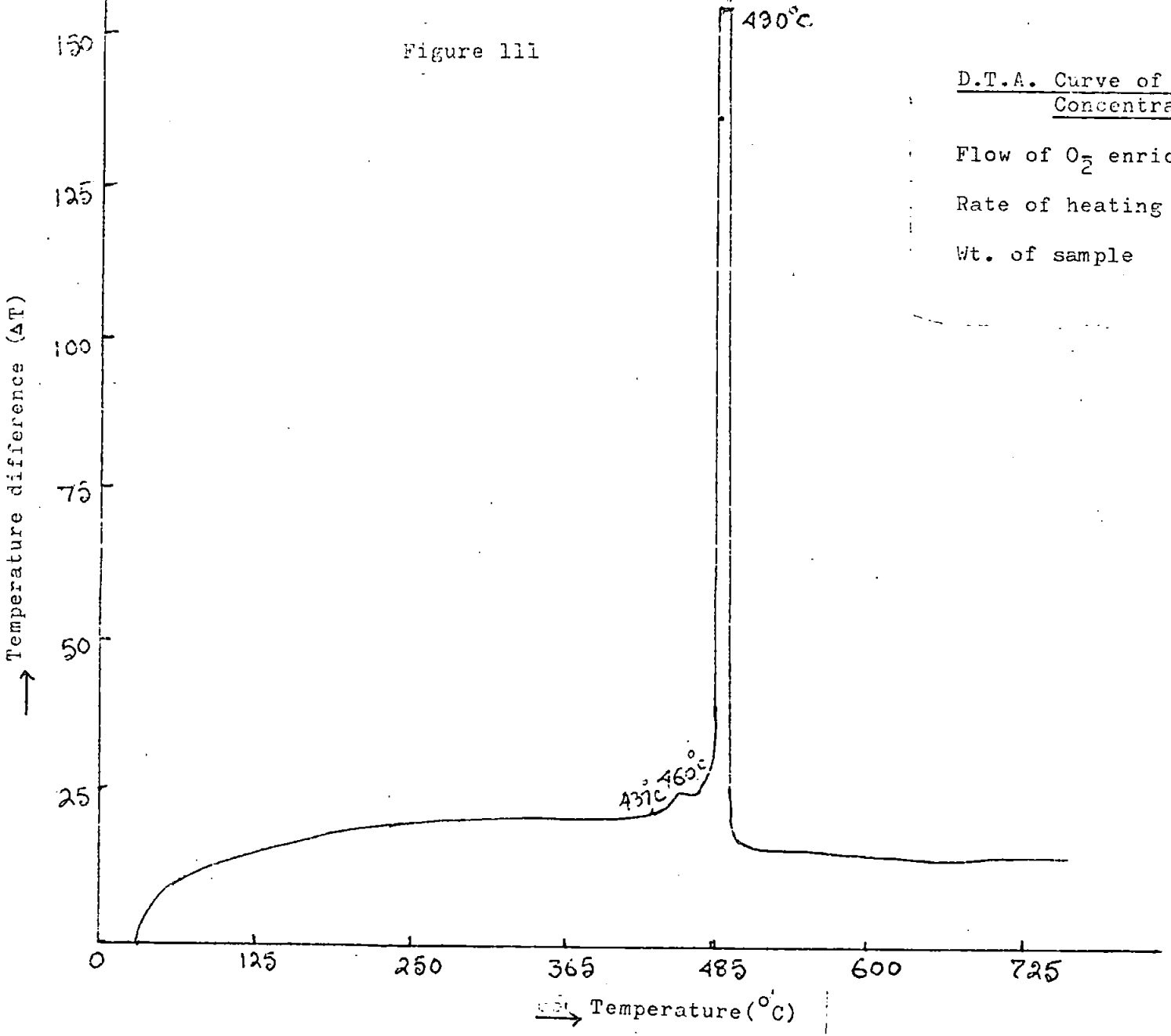


D.T.A. Curve of Heathsteele Concentrate

Flow of $O_2$ enriched air : 80 $cm^3$/min

Rate of heating : 10°C/min

Wt. of sample : 0.1 g

Figure 112

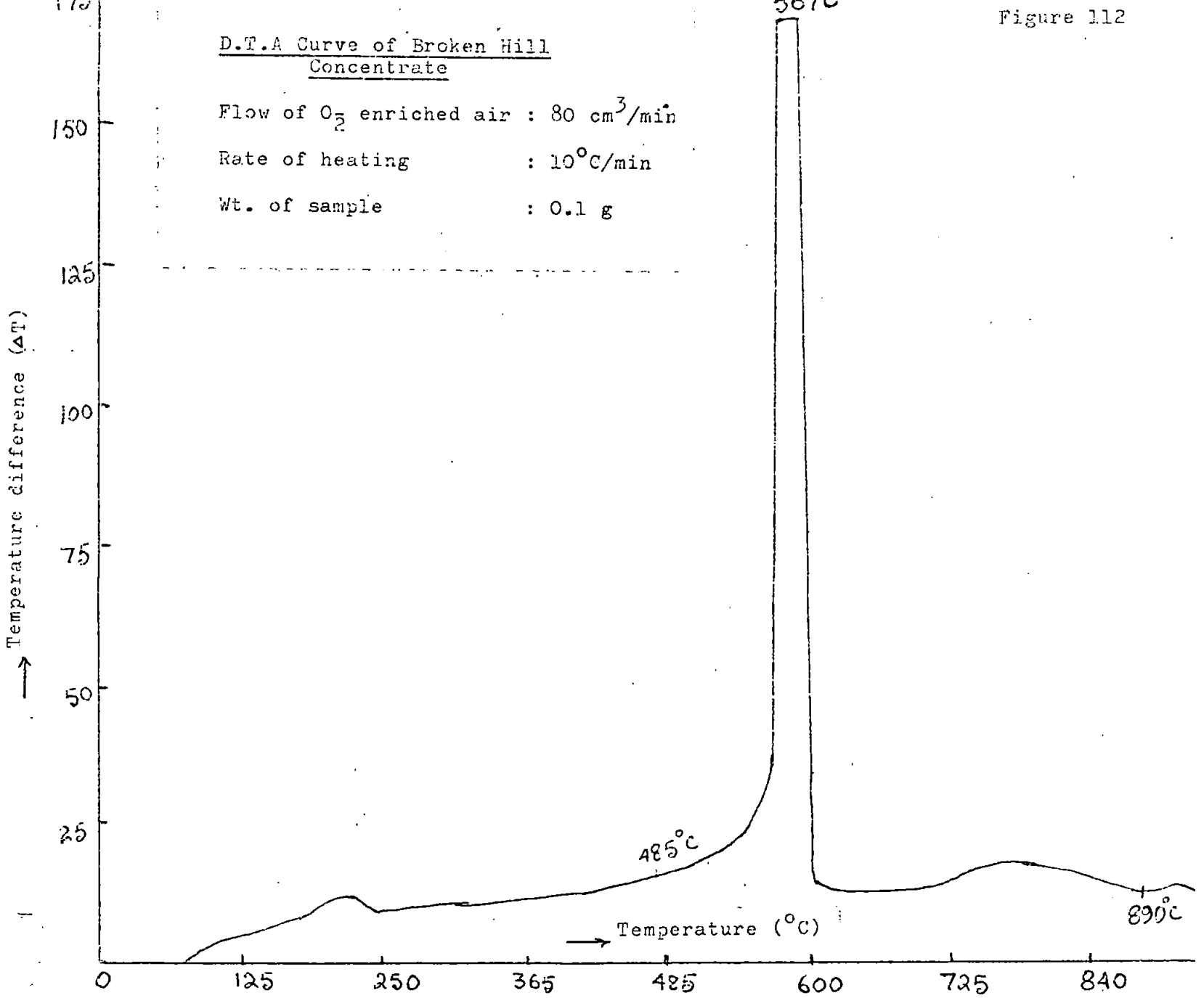
D.T.A Curve of Broken Hill Concentrate
Flow of $O_2$ enriched air : 80 $cm^3$/min
Rate of heating : 10°C/min
Wt. of sample : 0.1 g
Temperature difference (ΔT)
150
125
100
75
50
25
567°C
485°C
890°C
Temperature (°C)
0
125
250
365
485
600
725
840

Figure 113

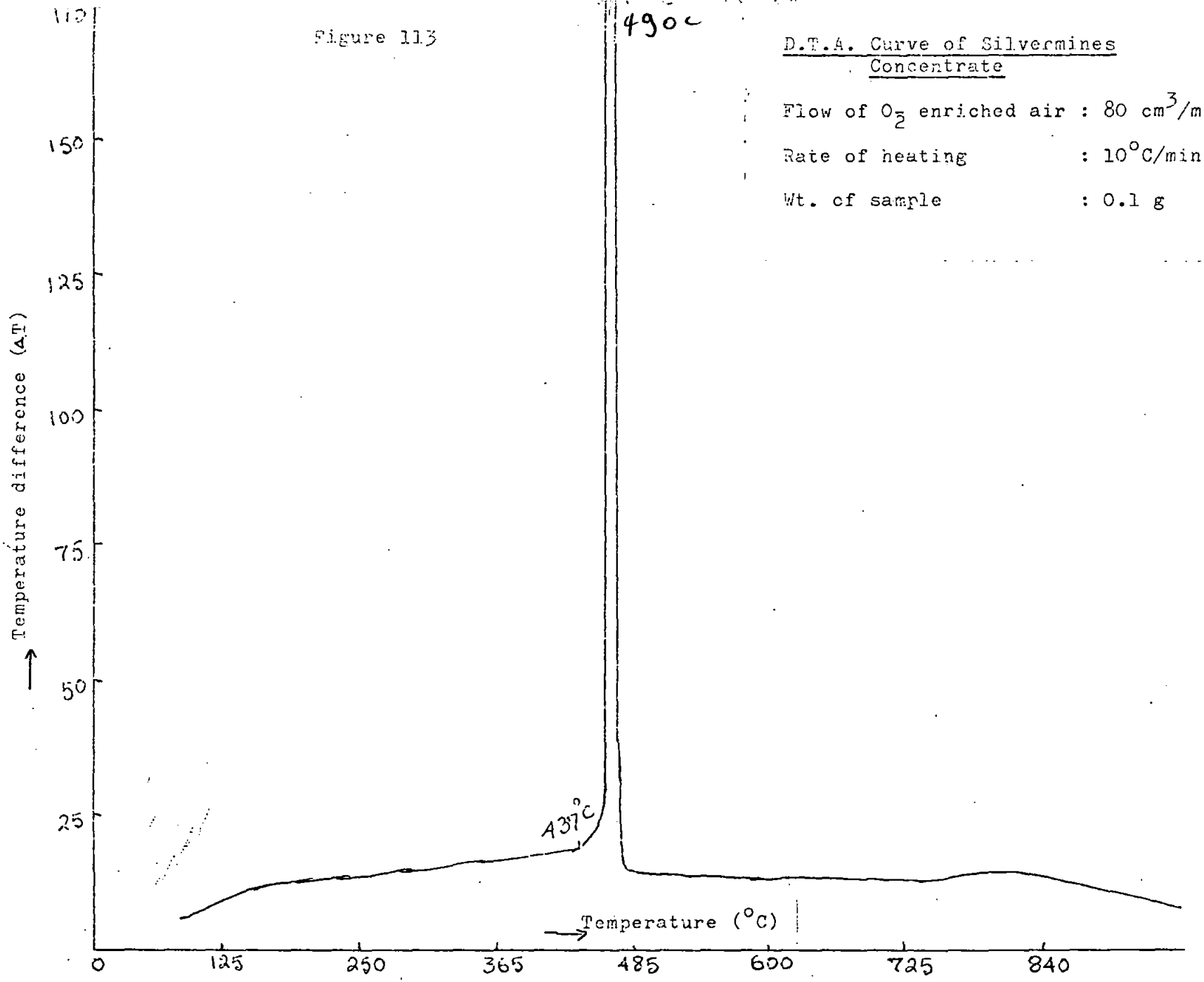


D.T.A. Curve of Silvermines Concentrate

Flow of $O_2$ enriched air : 80 $cm^3$/min

Rate of heating : 10°C/min

Wt. of sample : 0.1 g

represents the oxidation of zinc sulphide. The endothermic peak at 806°C in Fig.109 corresponds to the dissociation of the sulphate formed in roasting. As the oxidation proceeds more intensely, the exothermic peaks are shifted to lower temperatures and there is a narrowing of the temperature ranges of exothermic reactions. This indicates the intense rate of oxidation of zinc concentrates.

For comparison, we studied the DTA curves of synthetic mixture of zinc sulphide - iron sulphide (Figs.114-117 and Table 27).

The DTA curves of two zinc concentrates namely Buchan's River and New Brunswick follow the same pattern as a mixture of synthetic $\beta$-ZnS and 20% $FeS_2$. But the other three DTA curves of zinc concentrates namely Heathsteele, Silvermines and Broken Hill follow the DTA curve pattern of the synthetic mixture of $\alpha$-ZnS (hexagonal) and 20% $FeS_2$. The exothermic peaks in the DTA curves of Heathsteele, Silvermines and Broken Hill concentrates are shifted quite considerably to the lower temperature range in comparison with that of Buchan's River and New Brunswick concentrates. The same phenomenon have been observed in the DTA curves of the synthetic mixture zinc sulphide- iron sulphide. It could be explained in the following manner.

The Heathsteele, Silvermines and Broken Hill concentrates are sintered more in oxygen-enriched air than the Buchan's River and New Brunswick concentrates. The mixture of $\alpha$-ZnS (hexagonal) BDH and 20% $FeS_2$ is sintered more rapidly in oxygen-enriched air than the mixture of $\beta$-ZnS (cubic) and 20% $FeS_2$ at the same temperature. As the $\alpha$- sample sintered quite considerably, a protective layer of ferric oxide is formed outside the zinc sulphide layer, and so the diffusion of oxygen through the ferric oxide layer slows down; there is an increased tendancy of heat build-up at the surface of the sample due to uneven distribution of heat throughout the sample, leading to oxidation of

Figure 114

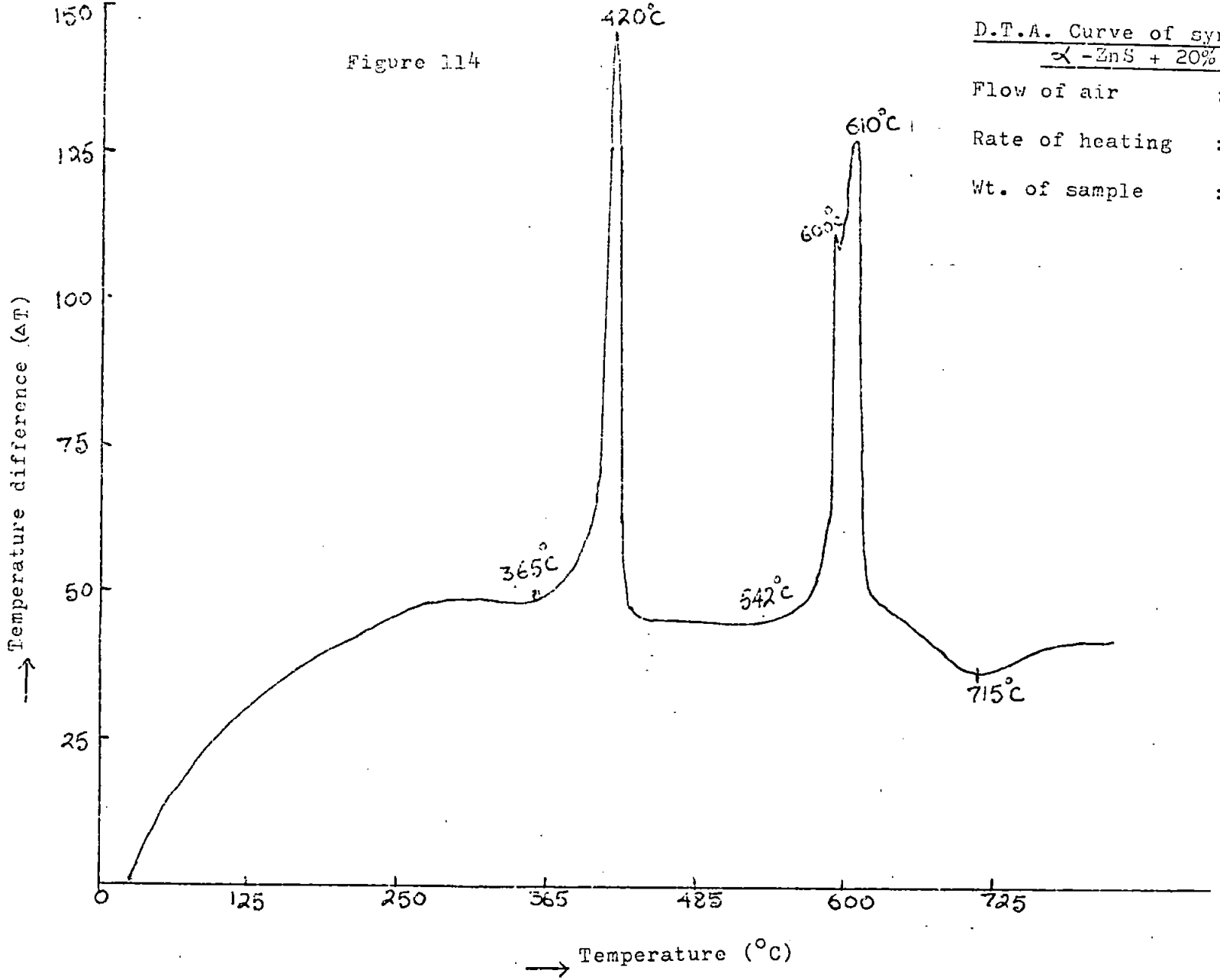


D.T.A. Curve of synthetic mixture, $\alpha$-ZnS + 20% $FeS_2$

Flow of air : 80 $cm^3$/min

Rate of heating : 10°C/min

Wt. of sample : 0.1 g

Figure 115

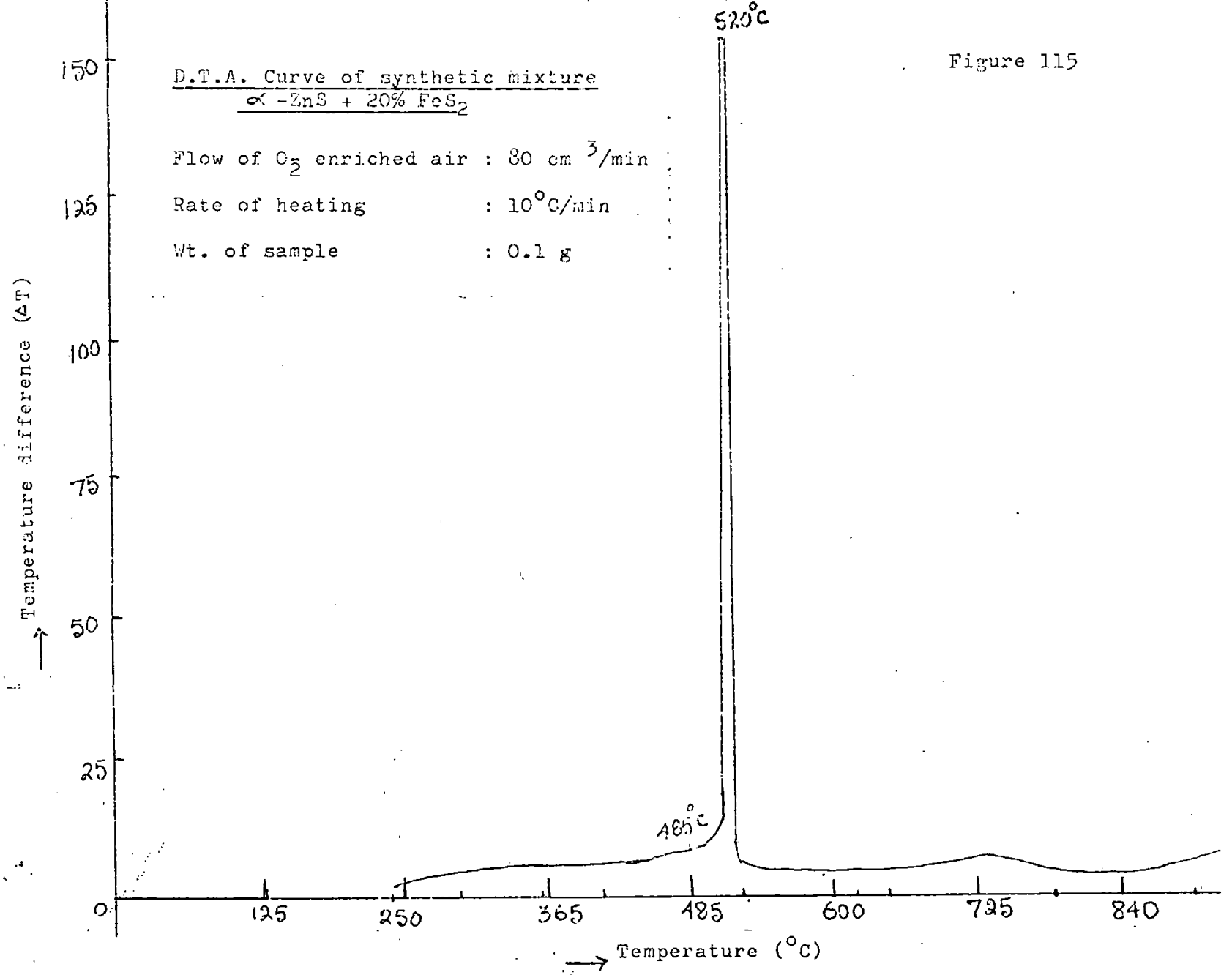
D.T.A. Curve of synthetic mixture
∝ -ZnS + 20% FeS2
Flow of O2 enriched air : 80 cm 3/min
Rate of heating : 10°C/min
Wt. of sample : 0.1 g
520°C
485°C
150
125
100
75
50
25
0
Temperature difference (ΔT)
125
250
365
485
600
735
840
Temperature (°C)

Figure 116

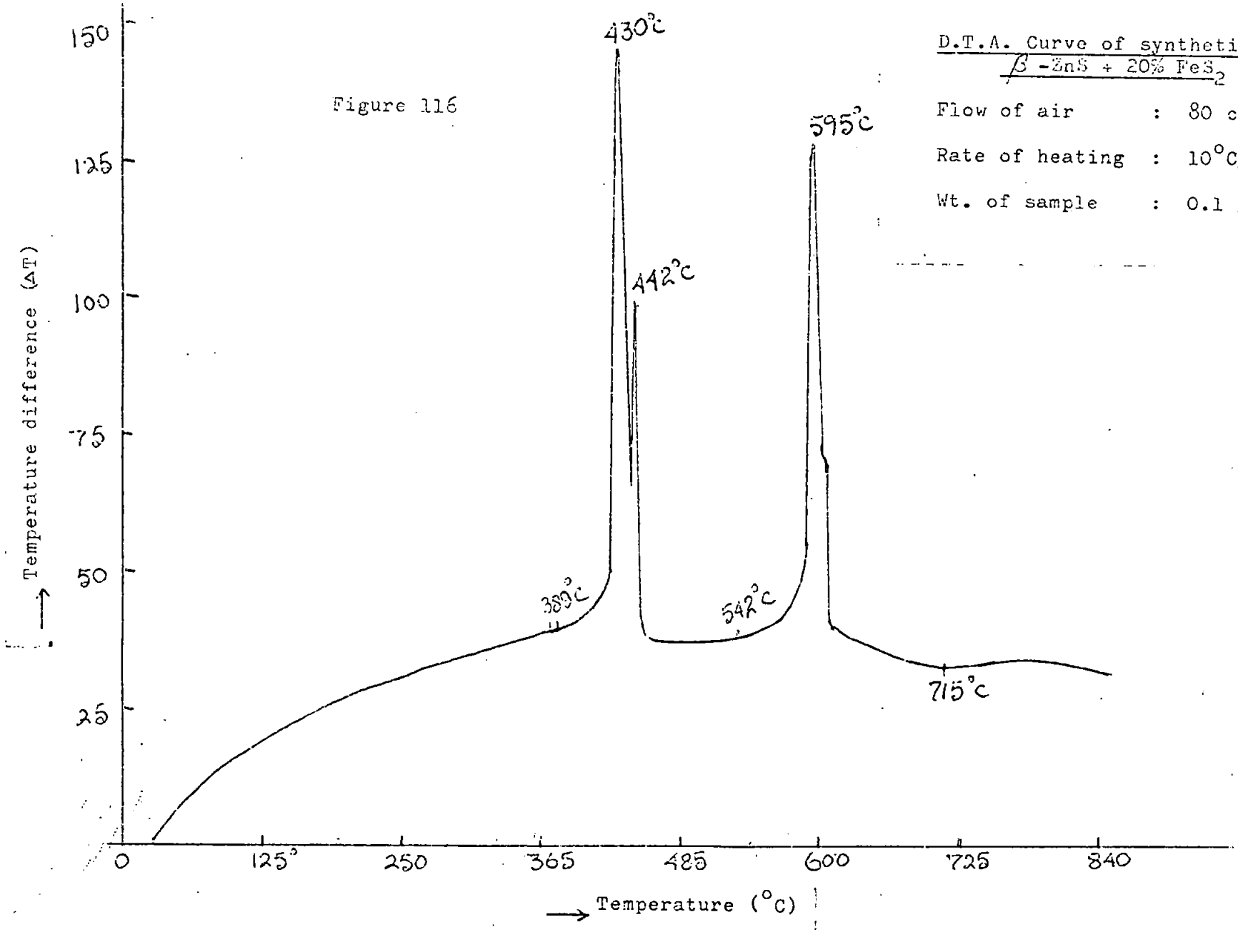


D.T.A. Curve of synthetic mixture, $\beta$-ZnS + 20% $FeS_2$

Flow of air : 80 cm $^3$/min

Rate of heating : 10°C/min

Wt. of sample : 0.1 g

Figure 117

D.T.A. Curve of synthetic mixture, $\beta$ -ZnS + 20% $FeS_2$

Flow of $O_2$ enriched air : 80 $cm^3$/min

Rate of heating : 10°C/min

Wt. of sample : 0.1 g

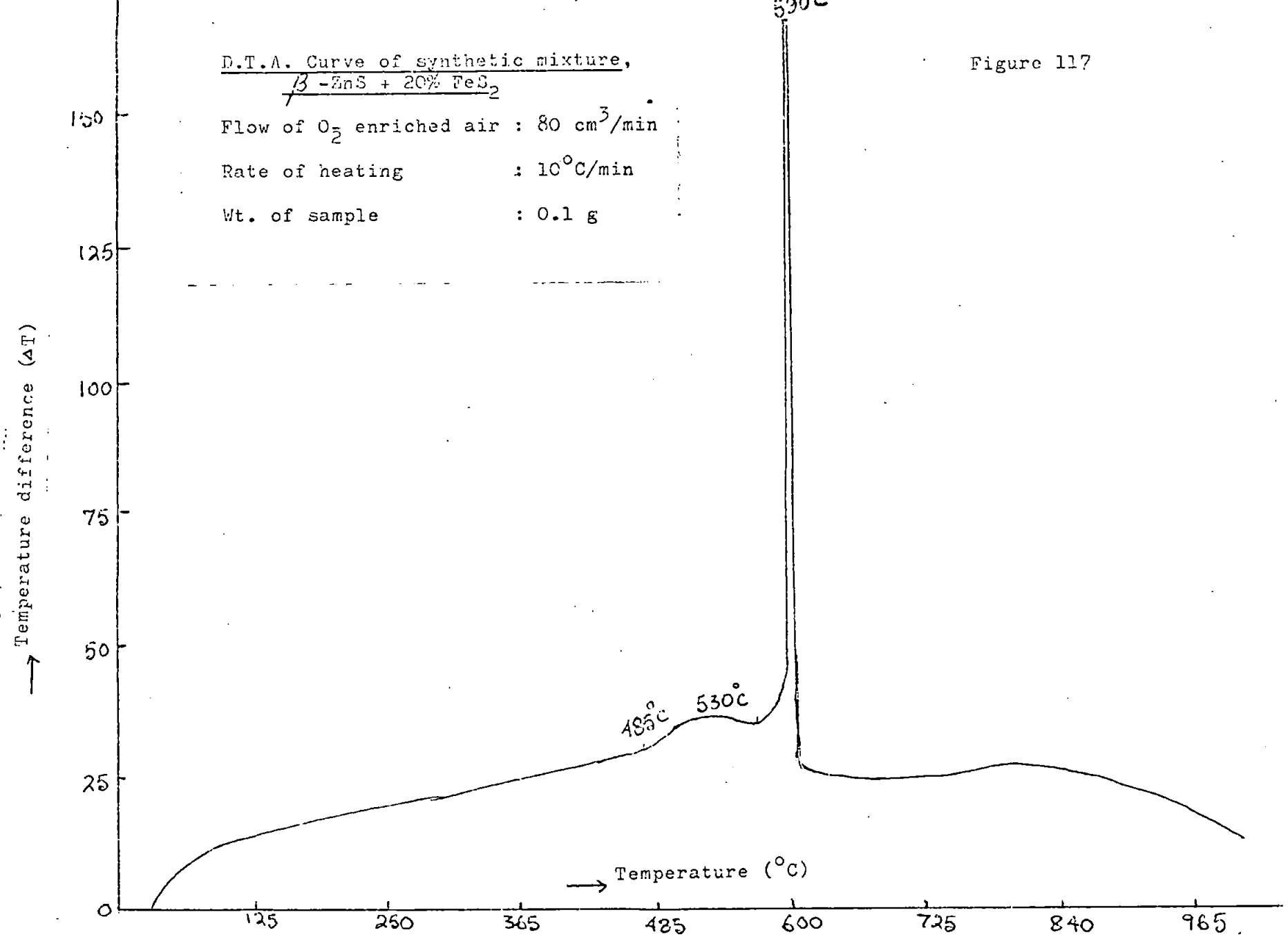

the zinc sulphide in the sample at a lower temperature. Thus, the zinc DTA peaks tend to merge with the iron and some ZnS remains unoxidised at the core of the sample. On examining the sample by X-ray diffraction, it has been found that the roasted samples of Heathsteele, Silvermines and Broken Hill concentrates in oxygen-enriched air contain more unroasted ZnS than the roasted samples of Buchan's River and New Brunswick concentrates at these peak temperatures.

5.4.2 Effect of additives (e.g. Iron sulphide) on sintering of zinc sulphide

At 850°C, when $ZnSO_4$ is absent, the addition of iron sulphide enhances sintering. Pure zinc sulphide after 5 h calcination has a specific surface of 2.0 $m^2g^{-1}$, compared with values of 1.5 and 1.1$m^2g^{-1}$ for samples containing 2.7% and 5% respectively of FeS.

At 600°C, specific surfaces of 5.4, 4.1 and 2.6 $m^2g^{-1}$ are recorded for the oxidation of the pure ZnS, ZnS + 2.7% FeS and ZnS + 5% FeS respectively.

In sphalerites, iron usually replaces zinc isomorphously, the Fe content ranging from a trace to as much as 15% or more (98). The sphalerite concentrate from New Brunswick, contains about 10% Fe.

The influence of small quantities of iron sulphide on the roasting of zinc sulphide was studied. The experiments were performed with zinc sulphide containing 25 to 75% iron sulphide as well as the five zinc concentrates which contain iron from 2.56 to 12%.

In the case of the synthetic mixture and the concentrates with the iron content below 5 % the rate of roasting was practically the same as that of pure zinc sulphide (Figure67).

However, with the zinc concentrates containing $\geq$ 10% iron, there was a decrease in the rate of roasting.

In the case of pure zinc sulphide, the only product of oxidation was zinc oxide, though almost negligible amounts of sulphate were formed at the lower temperature investigated.

For the mixture zinc sulphide - iron sulphide, the zinc oxide and iron oxide produced while roasting would further react to form the zinc ferrite, similar to its formation from the initial zinc sulphide - iron oxide mixtures. Lowering of oxidation rates for the concentrates and synthetic mixtures is ascribed to sintering caused by ferric oxide present. This oxide is formed preferentially to zinc oxide in the roastings, both thermodynamically and kinetically on the basis of a faster rate of diffusion of iron at the oxide boundary (98). This is in accordance with earlier research (99) which indicates that ferric oxide sinters extensively above 650°C (this being its Tammann Temperature - half melting point in °K) and thus it accelerates sintering of other oxides, e.g. lime and magnesia.

The presence of appreciable amounts of iron as sulphides in the zinc concentrates is undesirable not only because of the formation of the zinc ferrite from which zinc is not easily recovered in leaching process, but also because iron sulphide retards the roasting rates.

5.5. Zinc ore roasting at higher temperatures

Typical mixtures of zinc concentrates of varying composition were sintered. About 2g sample was taken in an alumina crucible and heated in a furnace for 2 hours at temperatures ranging from 900° to 1150°C. After roasting, the solid consists almost entirely of zinc oxide and zinc ferrite. At temperatures above 900°(to 1150°C), oxidation is rapidly completed and the content of zinc ferrite, $ZnO.Fe_2O_3$, decreases because of dissociation becoming appreciable above 1050°C. Volatilization of lead, cadmium and silver as well as zinc sulphide greatly increased above 1000°C. A considerable fraction of iron oxide was transferred also at high temperatures from the course

roaster to the flue dusts (100). Consequently, the crystals formed at the top of the sintered cake were ZnO and magneto plumbite, identified by X-ray diffraction and their optical micrographs are presented in Figure 118. Some of the ferric oxide is dissociated to magnetite; although the dissociation pressure is 1 atm at 1500°C, the low oxygen partial pressure at the oxide-sulphide interface permits the dissociation to occur at lower temperatures (1050° - 1150°C). Between 900° and 1050°C all of the iron is present as zinc ferrite, identified microscopically by its high reflectivity and red internal reflections (Figs.124-25). The light grayish grains in the pellets calcined at 1100°C to 1150°C do not exhibit internal reflections indicating that magnetite is present (Fig.126).

The overall dissociation of zinc ferrite above 1050°C produces zinc oxide vapour and finely-divided ferric oxide and magnetite, much of which is transferred readily from the sinter cake to the flue dusts. The residual calcined pellets exhibit a glazed surface with evidence of some coalescence with smaller grains of decomposed materials (101). Nevertheless, the average particle size is still smaller than that of the normal overflow in spite of some decrease in porosity caused by recrystallization and fusion (Figures 121-123).

## 5.6 Effects of lime and silica on the sintering of zinc concentrates

The experiments were performed with the addition of 18% $CaCO_3$ and 10% $SiO_2$ to the zinc concentrates at the temperature 1150°C. The phases present in sinters have been identified by X-ray diffraction. The outside of the sintered pellet contains mainly zinc silicate, calcium sulphate and unroasted zinc sulphide, whereas the inside contains some $\beta$-Zinc sulphide, zinc oxide and zinc ferrite. The loose powder at the top of the sintered pellet contains zinc oxide and magneto plumbite and their micrographs are presented in Figures 118-20.

FIGURE 118

PHOTOMICROGRAPHS

(a)

New Brunswick Concentrate roasted at 950°C with additives 18% $CaCO_3$ + 10% $SiO_2$ for 5 hours

(b)

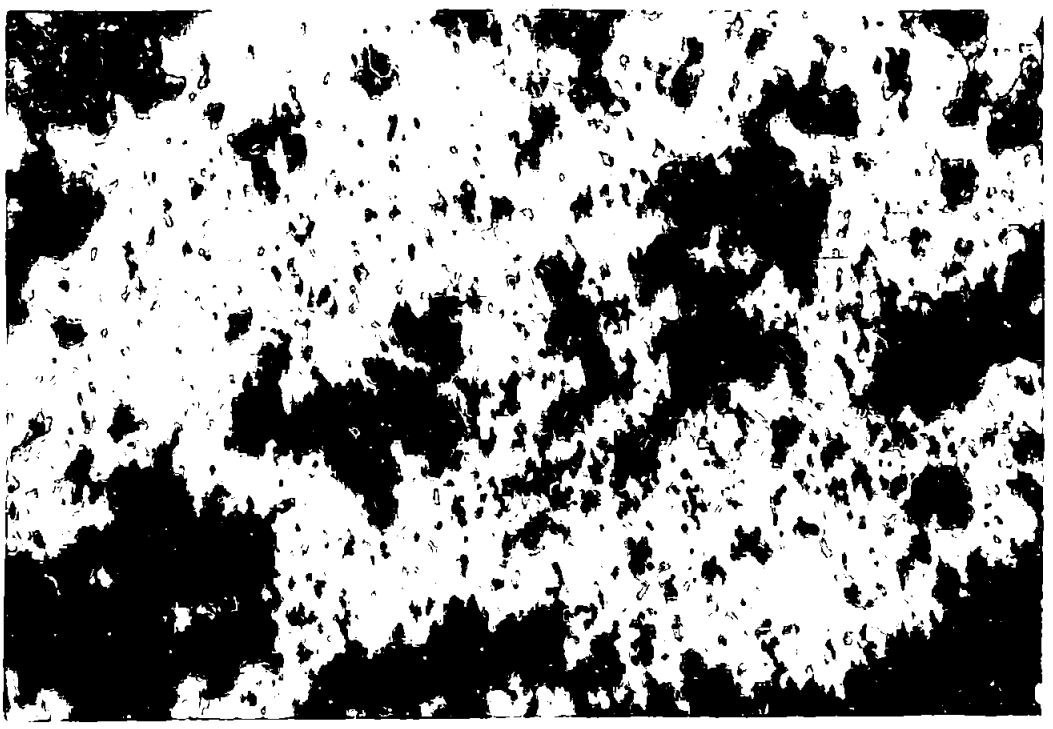

New Brunswick Concentrate ( 200 mesh)

FIGURE 119

(a)

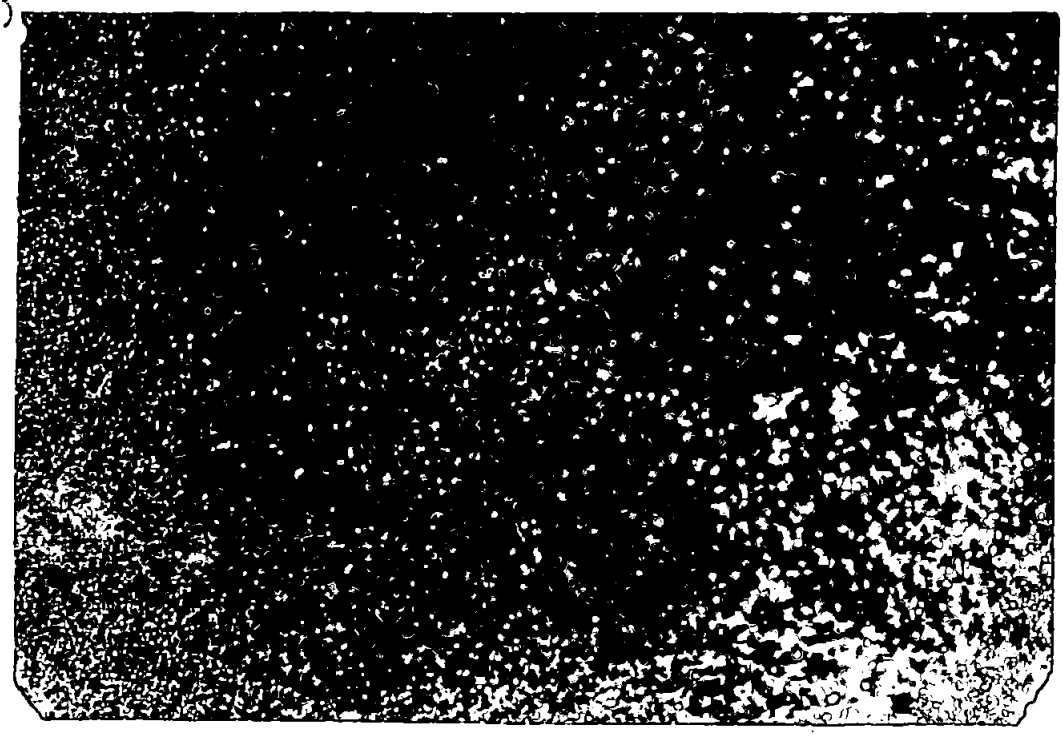

New Brunswick Concentrate ( 200 mesh) roasted for 2 hours at 1,150°C (outside surface of the sintered pellet)

(b)

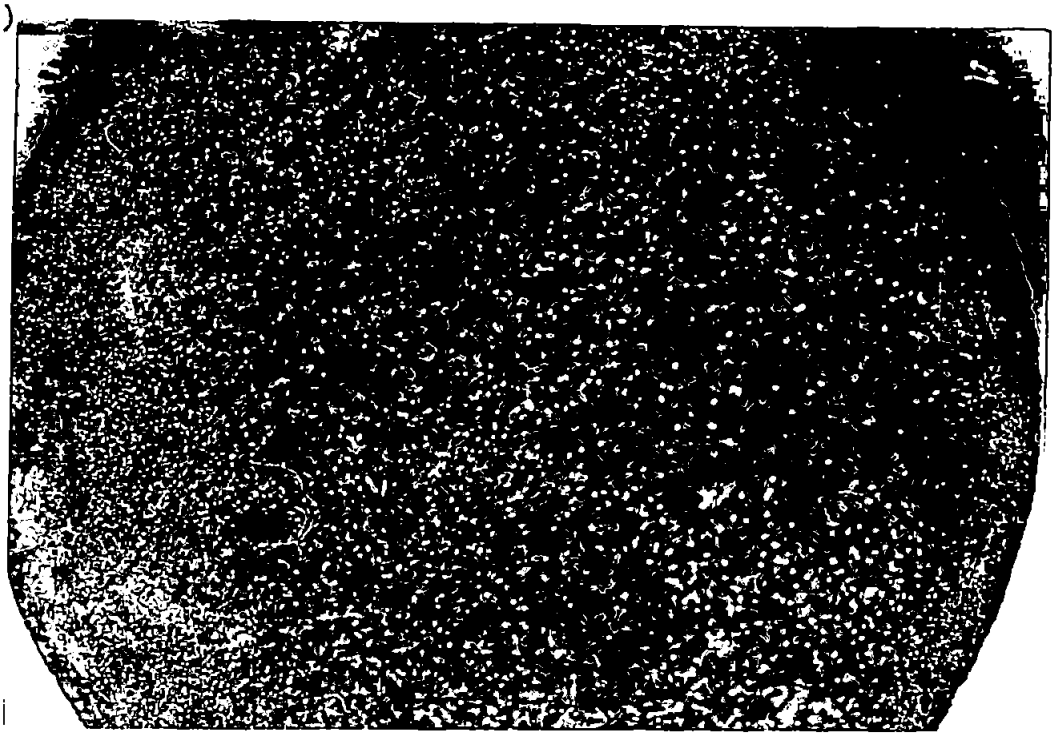

Broken Hill Concentrate ( 200 mesh) roasted for 2 hours at 1,150°C (outside surface of the sintered cake)

FIGURE 120

(a)

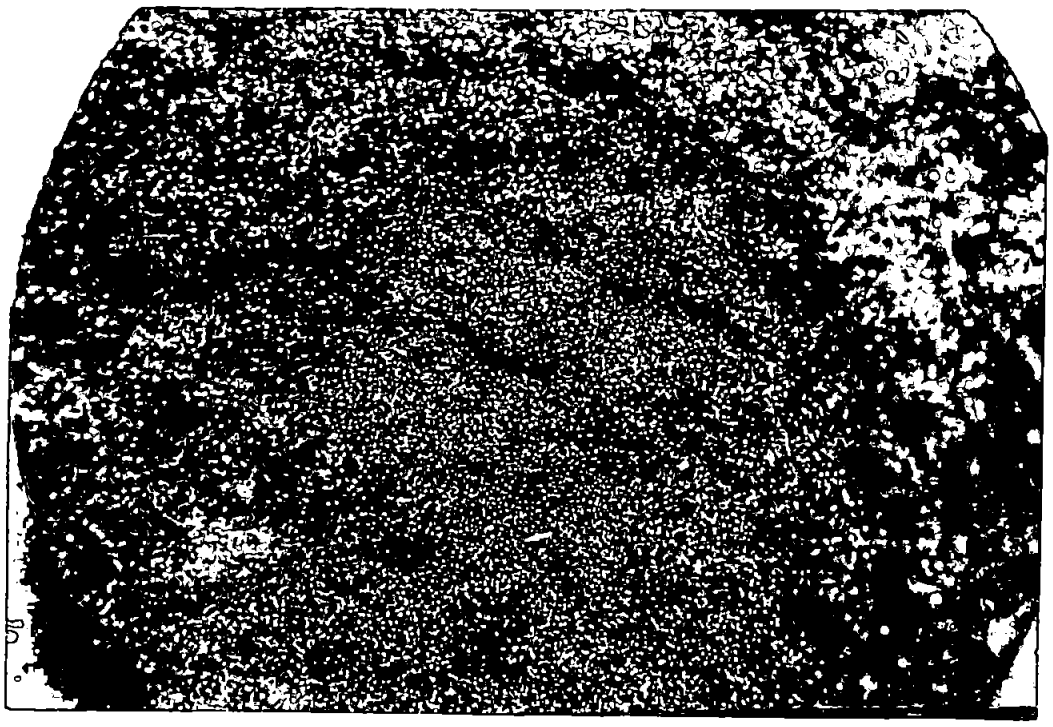

New Brunswick Concentrate ( 200 mesh) roasted for 2 hours at 1,150°C (inside surface of the sintered pellet)

(b)

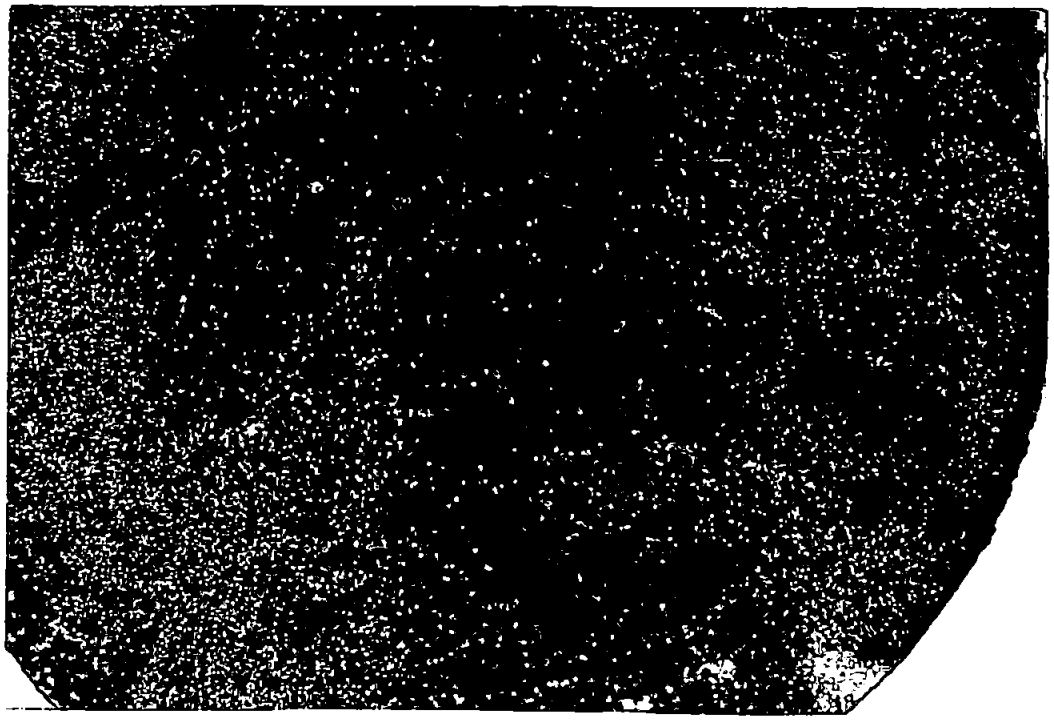

Broken Hill Concentrate ( 200 mesh) roasted for 2 hours at 1,150°C (inside surface of the sintered cake)

FIGURE 121

(a)

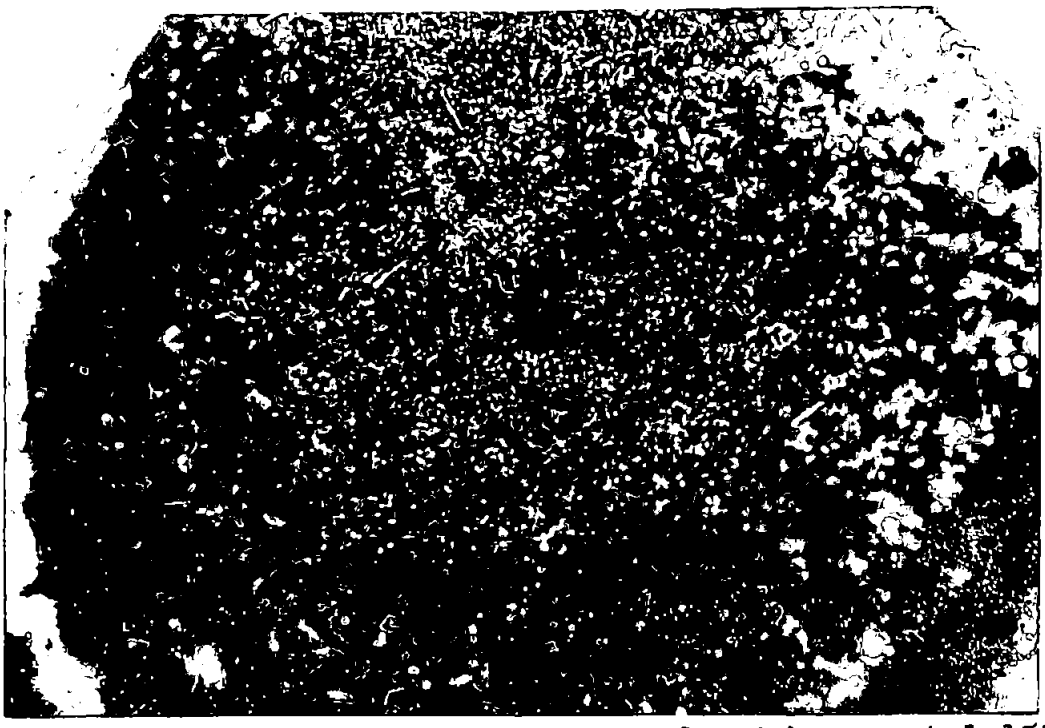

New Brunswick Concentrate roasted for 2 hours at 1,150°C
(white ring surrounding the sintered pellet)

(b)

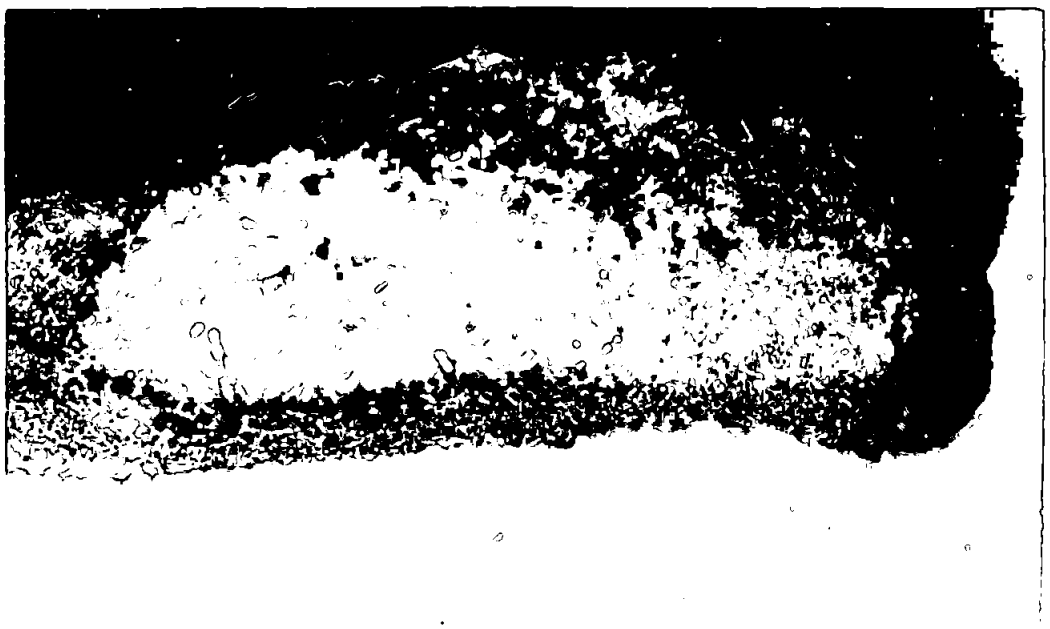

Buchan's River Concentrate roasted for 2 hours at 1,150°C
( white region in the sintered cake shows the formation of ZnO crystals)

FIGURE 122

OPTICAL MICROGRAPHS OF ZINC OXIDE CRYSTALS

(a)

Broken Hill Concentrate with additives (18% $CaCO_3$ + 10% $SiO_2$) roasted for 2 hours at 1,150°C (loose crystals formed at the top of the sintered cake)

Magnification: x 160

(b)

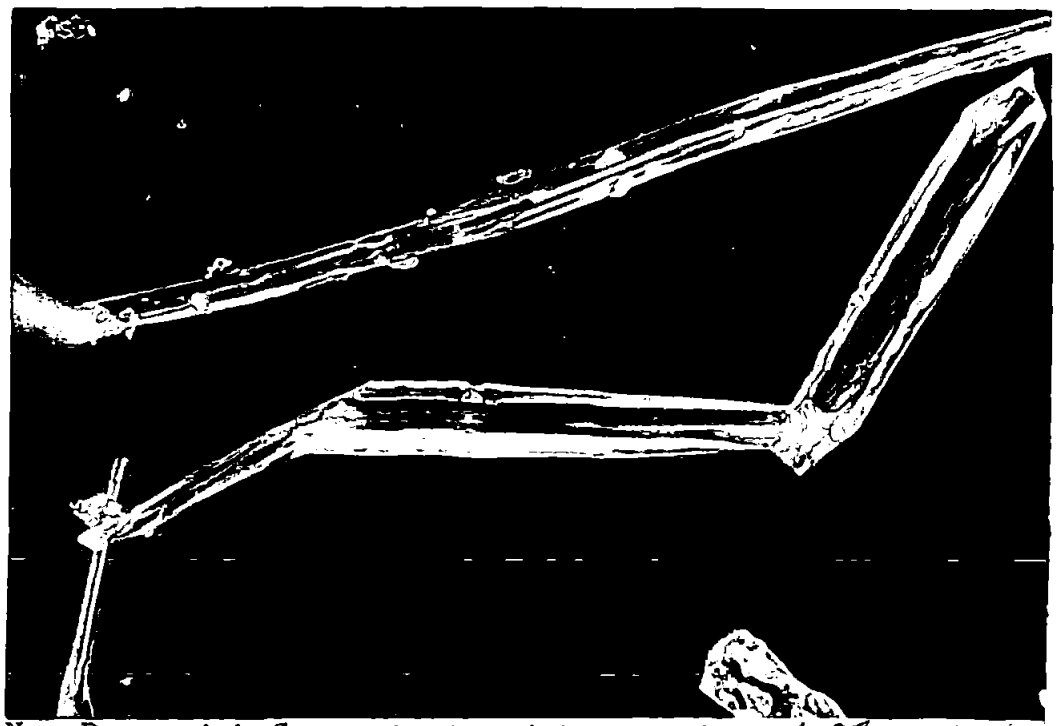

New Brunswick Concentrate with additives (18% $CaCO_3$ + 10% $SiO_2$) roasted for 2 hours at 1,150°C.

FIGURE 123

(a)

New Brunswick Concentrate ( 200 mesh) roasted for 2 hours at 1,150°C (loose powder formed at the top of the sintered cake)

Magnification: x 160

(b)

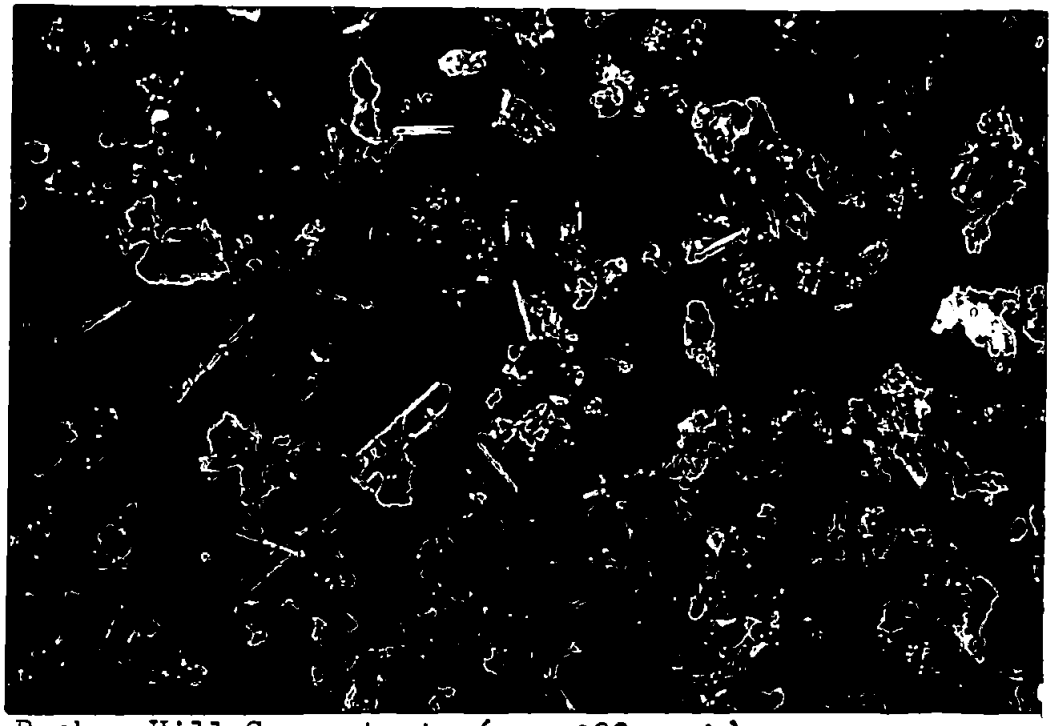

Broken Hill Concentrate ( 200 mesh) roasted for 2 hours at 1,150°C.

Magnification: x 160

Figure 123

(a)

New Brunswick Concentrate (~200 mesh) roasted for 2 hours at 1150°C (loose powder formed at the top of the sintered cake)
Magnification X160

(b)

Broken Hill Concentrate (~200 mesh) roasted for 2 hours at 1150°C Magnification X160

Figure 124

OPTICAL MICROGRAPHS (COLOUR)

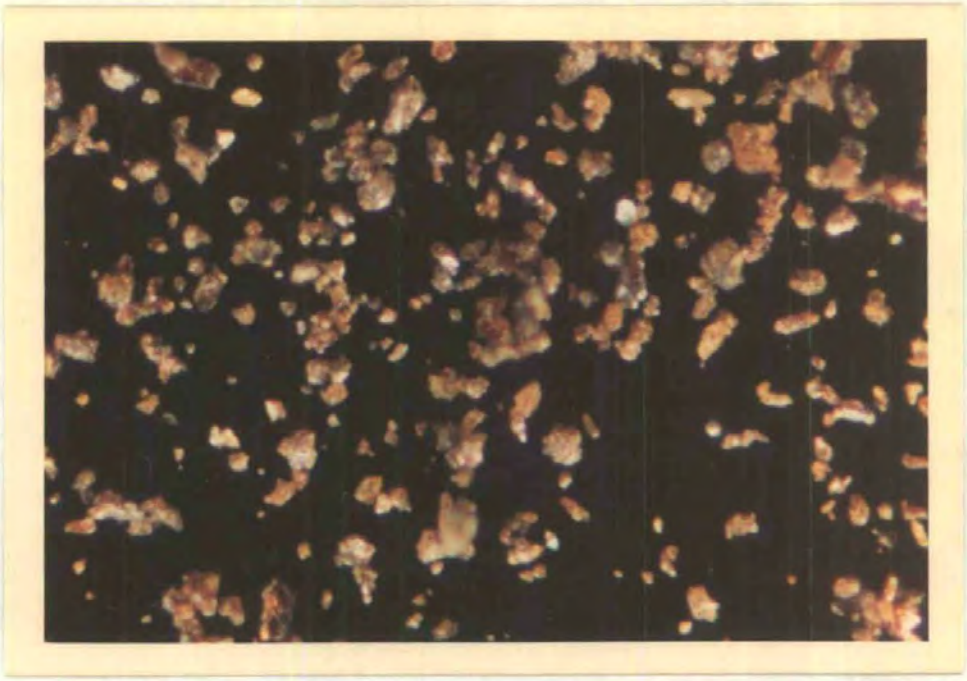

New Brunswick Concentrate ( 200 mesh)

Magnification: x 160

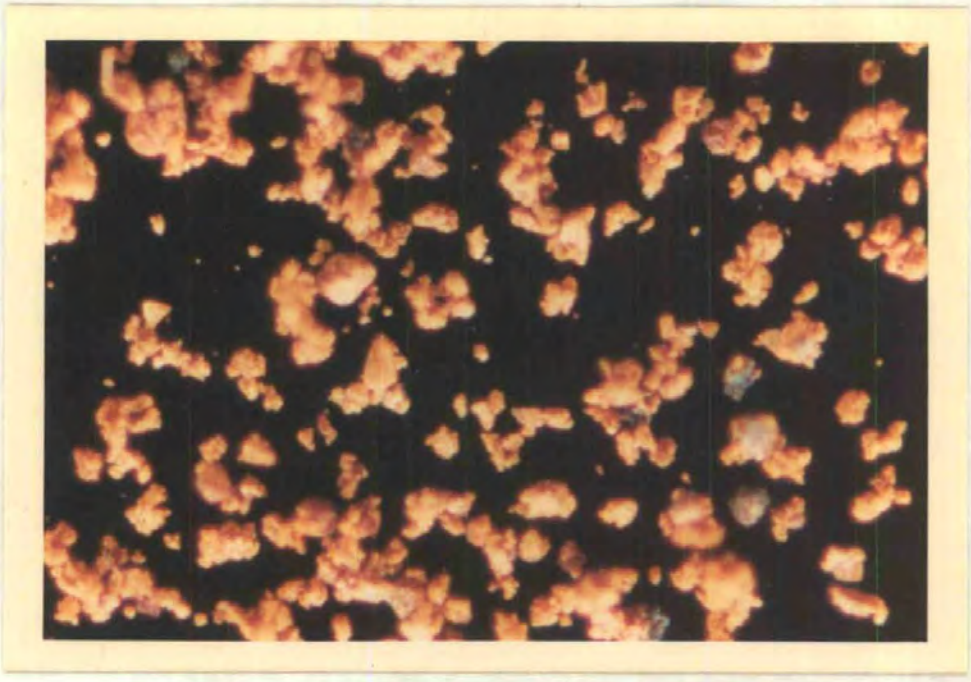

New Brunswick Concentrate ( 200 mesh)
roasted at 950°C for 5 hours.

Magnification: x 160

Figure 125

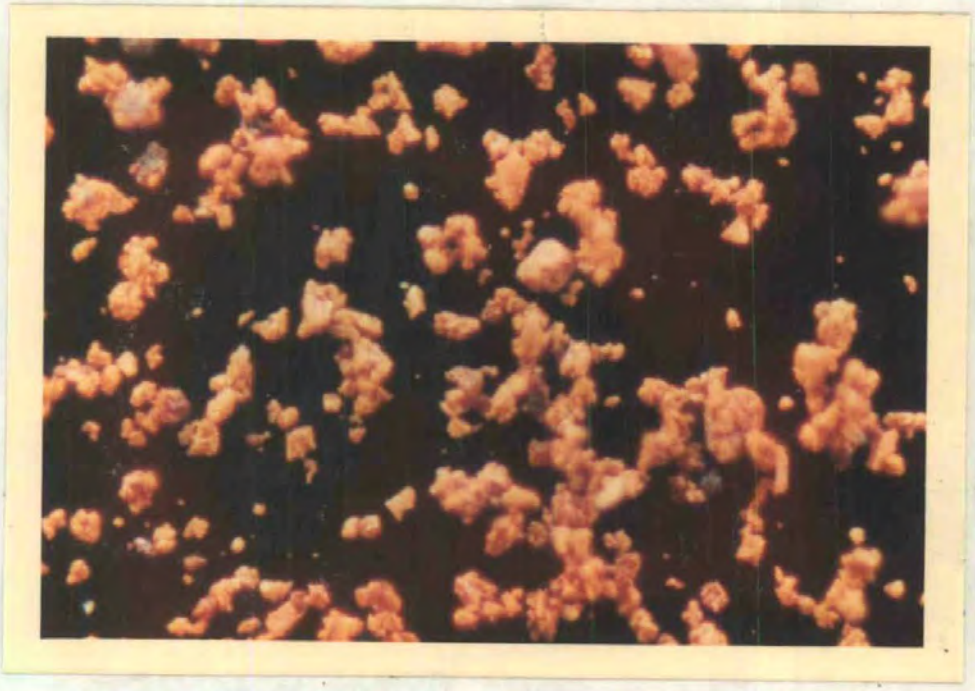

New Brunswick Concentrate ( 200 mesh)
with additives (18% $CaCO_3$ + 2% $SiO_2$)
roasted for 5 hours at 950°C.

Magnification: x 160

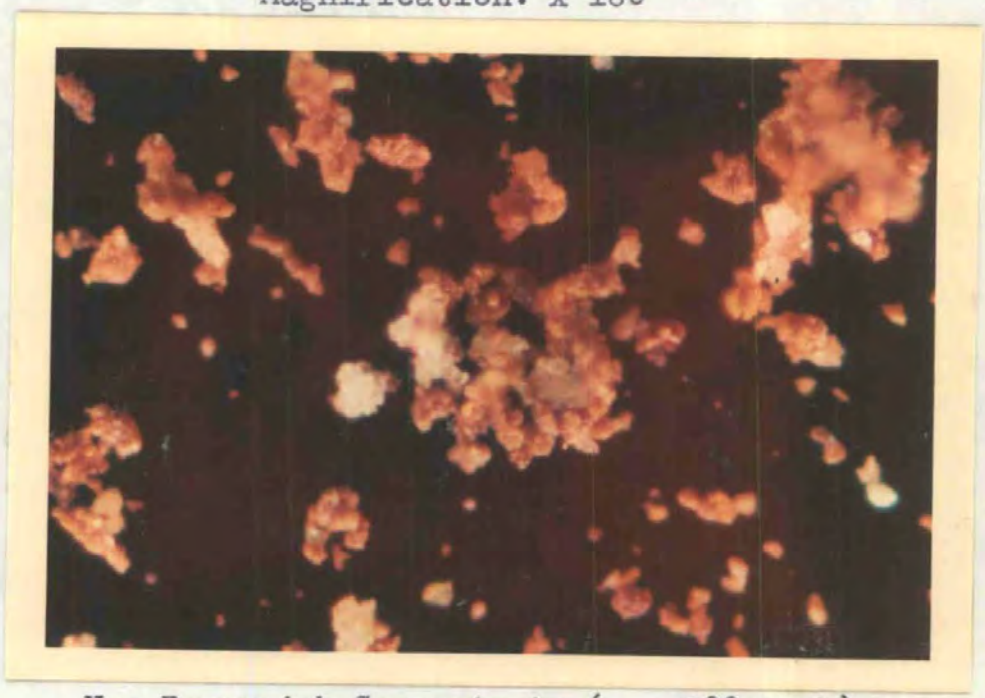

New Brunswick Concentrate ( 200 mesh)
with additives (18% $CaCO_3$ + 10% $SiO_2$)
roasted at 950°C for 5 hours.

Magnification: x 160

Figure 125

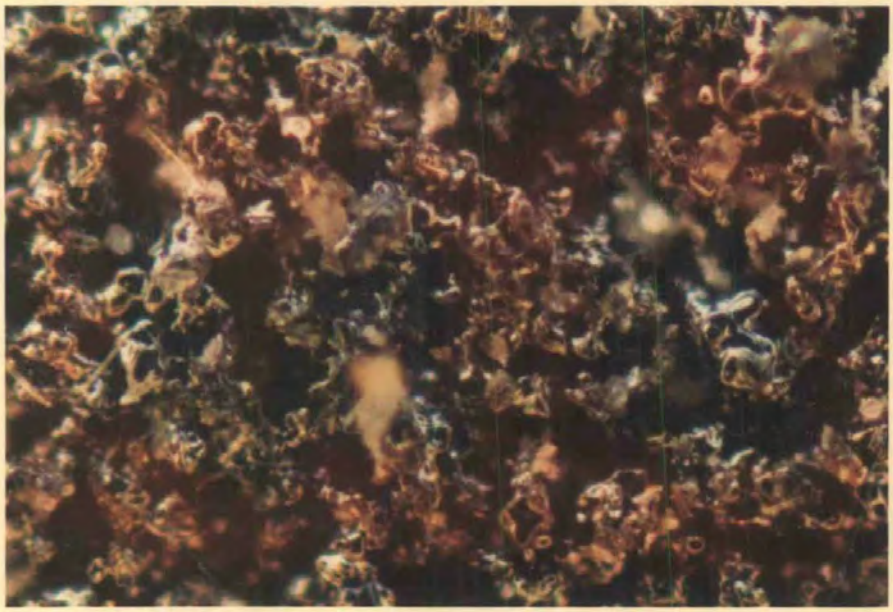

New Brunswick Concentrate ( 200 mesh)
roasted for 2 hours at 1,150°C.

Magnification: x 160

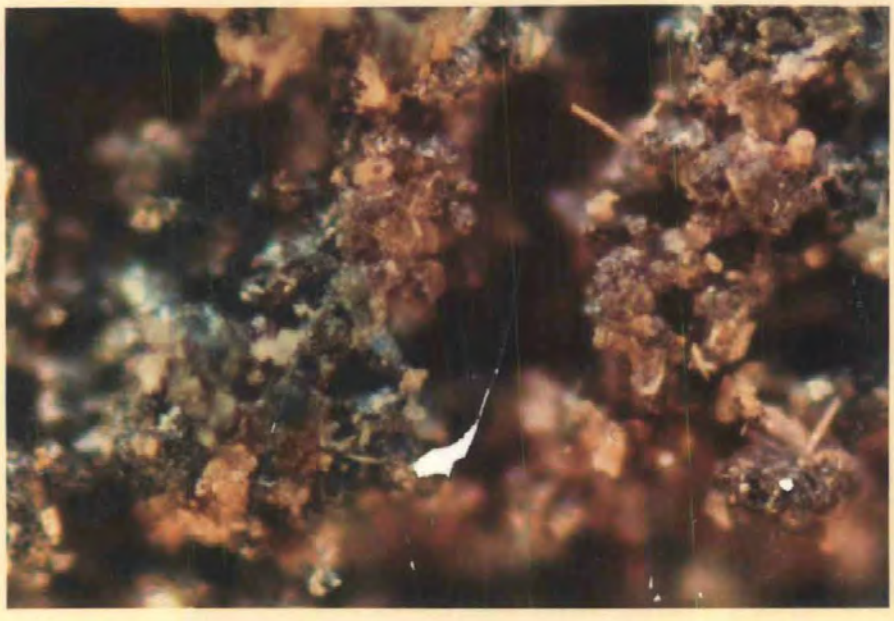

New Brunswick Concentrate ( 200 mesh)
with additives (18% $CaCO_3$ + 10% $SiO_2$)
roasted at 1,150°C for 2 hours.

Magnification: x 160

The main reaction is essentially diffusion of the sulphur outwards from the centre of each particle in exchange for oxygen diffusing inwards. Some zinc oxide formed evidently reacts with the silica (and possibly calcium silicate present) to form zinc silicate which migrates to the outside of the particles. Further reactions between the lime, sulphur dioxide and oxygen produce calcium sulphate either directly, viz. $2\ CaO + SO_2 + O_2 \rightleftharpoons 2\ CaSO_4$, or by intermediate formation of calcium sulphide by double decomposition with zinc sulphide, viz. $CaO + ZnS = CaS + ZnO$. The low melting point of the calcium sulphide would assist sulphur diffusion to the outside of the particles and also promote sintering. Since anhydrite appreciably decomposes to lime at temperatures above 900°C (102), the absence of sulphur dioxide after all of the zinc sulphide has been oxidised would lead to the migration of the calcium sulphate to the outside of the particles and its ultimate decomposition.

# Chapter 6

## Concluding Summary

### 6.1 Precipitation and Ageing of zinc sulphide

For basic oxidation studies, zinc sulphide samples of widely-different specific surfaces were prepared. They were precipitated from solution at various pH levels and in the presence of different concentrations of electrolyte.

In strongly acidic solution ($pH \lesssim 1$), irregular aggregates are formed of 0.001 to 0.01 $\mu$m size. Less acidic conditions produce a greater proportion of smaller particles, as found in precipitations from 0.1 M-$ZnSO_4$ or $ZnCl_2$ solutions and hydrogen sulphide. Here, the pH decreases from about 5 to 1 as precipitation proceeds and the average crystallite sizes (from specific surface measurements) are about 0.01 $\mu$m increasing to about 0.03 $\mu$m on ageing for 10 h at 20°C, and finally acquiring a comparatively slow growth rate. At electrolyte concentrations below 0.1 M, the greater coagulating effect of the divalent sulphate ion compared with the univalent chloride ion is not so prominent in promoting crystallite growth. Thus, the sulphides precipitated from these zinc sulphate and chloride solutions (and subsequently aged) have similar specific surfaces and average crystallite sizes. Values of the same order are obtained from X-ray line- (or peak -) broadening measurements; differences are explained in terms of the crystallite size distribution and porosity of the products.

Similar crystallite sizes are given initially when zinc sulphide is precipitated in alkaline conditions, viz. from salt solutions added to sodium sulphide or from zinc oxide dissolved in 3M $NH_3$ solution and treated with hydrogen sulphide. However,

subsequent ageing is slower than in acidic media. Precipitation at progressively increasing pH from about 5 to 7 (when sodium sulphide is added to zinc sulphate) is accompanied by hydrolysis of the zinc salt with considerable loss in surface area (and increase in crystallite size) of the product.

In the presence of additives such as sodium chloride, the zinc sulphide tends to crystallise as platelets. The changes have been correlated with the corresponding variation in the crystallite and aggregate sizes.

6.2 Oxidation of pure zinc sulphide

When pure zinc sulphide is roasted at temperatures above 400°C in air (or oxygen-enriched air), the main oxidation products are zinc oxide, zinc sulphate, sulphur dioxide or sulphur trioxide, and possibly a basic sulphate, $ZnO.\ 2ZnSO_4$. The last named has been identified by X-ray diffraction in the roasted sample, particularly at temperature $\geq$ 650°C for more finely-divided $\beta$-Zns and $\geq$ 700°C for coarser $\alpha$-Zns.

In the isothermal oxidations below 850°C, the amount of zinc sulphate formed in the earlier stages reached a maximum value, before decreasing on further roasting. The decomposition of the zinc sulphate results from the $SO_2$ and $SO_3$ contents of the furnace gases decreasing while the oxygen pressure increases considerably towards the end of roasting, giving high values of $Po_2/P_{(total)}$ at which the sulphate decomposes. Also, at these temperatures, the thermodynamics are favourable for the decomposition of zinc sulphate to oxide by interaction with zinc sulphide.

Three types of kinetics have been distinguished for the oxidation of zinc sulphide in a stationary layer. At low temperature, when the reaction rate is low in comparison with the rate of diffusion (kinetic region), the overall reaction rate is determined by the true kinetics at the surface and grows exponentially with temperature in agreement with the Arrheniu's law. However, this

growth continues only until the reaction rate becomes comparable with the diffusion rate. The process subsequently transfers to the diffusion region where its rate is determined entirely by the diffusion rate and grows only extremely slightly with temperature. With such a dependence of the rate of heat emission on temperature and under specific conditions of heat removal, three stationary heat modes are possible; the intermediate one is unstable, the upper corresponds to the diffusion region and the lower is in the kinetic region. The abrupt transfer from the lower to the upper stationary heat mode leads to ignition at the surface of the zinc sulphide.

The activation energies for the kinetic, intermediate and diffusion regions are (in K.cal/mole) 55.9, 20 and 2 for $\alpha$-ZnS and 42, 18 and 1.3 for $\beta$-ZnS respectively.

Sulphate formation is much more prominent in the presence of platinum (crucibles) which catalyses formation of $SO_3$ gas in the furnace atmospheres. Thus, up to 30 and 35% of $\alpha$ and $\beta$-zinc sulphides are converted to sulphate at 620°C, compared with less than 1% in the absence of platinum. The catalysis of the $2SO_2 + O_2 \longrightarrow 2\ SO_3$ reaction ensures a sufficient partial pressure of $SO_3$ to prevent the zinc sulphate decomposing until abnormally higher temperatures are reached. Hence, the amounts of zinc sulphate were correspondingly larger even up to 850°C, above which there was no sulphate formation in the oxidations in either air or oxygen-enriched air. The information obtained for the reaction of zinc oxide and sulphur trioxide at lower temperatures explains the formation of larger amounts of zinc sulphate in zinc roaster dusts compared with primary calcines.

A two-stage oxidation mechanism for $\alpha$- and $\beta$-zinc sulphides is indicated from 2 exothermic peaks being given in

DTA thermograms at lower air-flow rates, viz. (1) nucleation of zinc sulphide and development of the reaction across the surface of the particles (cf kinetic region) and (2) penetration of oxygen through the newly-formed zinc oxide layer, promoting further oxidation by an advancing interface mechanism inwards from the outside of each particle (cf diffusion region).

The oxidation rates, particularly in the diffusion region, are lowered by the sintering of the products at higher temperatures, which reduce the internal porosity and total surface area. Sintering of the zinc oxide by surface diffusion became appreciable about 500°C and extensive above 850°C when crystal lattice diffusion became operative. The sintering is accelerated between these temperatures by any zinc sulphate formed.

6.3 Roasting of zinc ore concentrates

In the roasting of the zinc ore concentrates, the rates of sulphate formation and oxidation to zinc oxide vary differently with time, because of increased amounts of sulphur trioxide gas in the furnace atmosphere in the presence of catalysts like ferric oxide, $Fe_2O_3$.

With an increasing $Fe_2O_3/ZnO$ ratio, the degree of sulphation of the zinc in the ore or synthetic mixture increases since the increased $Fe_2O_3$ 'contact' surface promotes more complete oxidation of the $SO_2$ to $SO_3$. In the initial stages of the sulphation of zinc concentrates at 800°C and 850°C, high sulphation rates are established, despite formation of zinc ferrite, i.e. the ferric oxide retains some of its catalytic power even when combined in a ferrite.

Tests on the influence of iron oxide on the roasting behaviour of zinc concentrates show that 5% iron present as

sulphide does not affect the roasting rates in air at 650°C to 850°C, whereas 10% or more iron as sulphide lowers the rates considerably. By comparison, pure ZnS oxidised only to ZnO, although almost negligible amounts of sulphate were formed at the lower temperatures investigated.

For zinc sulphide-iron sulphide mixtures, the zinc oxide and iron oxide produced while roasting would further react to form the zinc ferrite, similar to its formation from the initial zinc sulphide-iron oxide mixtures. Lowering of oxidation rates for the concentrates and synthetic mixtures is ascribed to sintering caused by ferric oxide present. This oxide is formed preferentially to zinc oxide in the roastings, both thermodynamically and kinetically on the basis of a faster rate of diffusion of iron at the oxide boundary (98). This is in accordance with earlier research (99) which indicates that ferric oxide sinters extensively above 650°C, (this being its Tammann temperature) and thus it accelerates sintering of other oxides, e.g. lime and magnesia.

A two-stage oxidation mechanism for ZnS in zinc concentrates is indicated by 2 exothermic peaks in the DTA thermograms. This could be explained in the same manner as for pure $\alpha$- and $\beta$-zinc sulphide oxidation, (Chapter 4).

In zinc ore roasting at higher temperatures, 900° - 1150°C, oxidation is completed rapidly. Between 900° to 1050°C all of the iron is present as zinc ferrite, the content of which decreases above 1050°C when dissociation becomes appreciable. Volatilisation of lead, cadmium and silver as well as zinc sulphide greatly increases above 1000°C. A considerable fraction of the iron oxide and some of the zinc oxide is dissociated to magnetite; although the dissociation pressure is 1 atm. at 1500°C, the low oxygen partial pressure at the oxide-sulphide interface permits the dissociation

to occur at lower temperatures (1050 - 1150°C).

The residual calcined pellets exhibit a glazed surface with evidence of some coalescence with smaller grains of decomposed materials. Nevertheless, the average particle size is still smaller than that of the normal overflow in spite of some decrease in porosity caused by recrystallisation and fusion.

In studies of the effects of lime and silica on the sintering of zinc concentrates, the phases present have been identified by X-ray diffraction. The outside of the sintered pellet contains mainly zinc silicate, calcium sulphate and unroasted zinc sulphide, whereas the inside contains some β-zinc sulphide, zinc oxide and zinc ferrite.

6.4 Other developments

This research forms part of a wider study of the low-temperature and spontaneous oxidation of zinc sulphide ore concentrates during storage and shipment; preventative measures require adequate addition of water, but in amounts just sufficient to form suspensions exhibiting thixotropic properties during transportation.

A further development envisaged is the application of the information obtained in the present study to roasting and sintering processes associated with lead ores.

Acquisition of new information regarding the oxidation of the sulphides at intermediate temperature (400° - 1000°C) is also of value in relation to the preliminary treatment of the ores in connection with the newer electrolytic refining processes.

Further useful background development work is required on industrial aspects of sulphide roasting and sintering including :

(i) Sintering of Pb/Zn sulphide concentrate mixes on a static

sinter pallet.

(ii) Laboratory and pilot plant studies of possible new roasting techniques.

(iii) Laboratory studies of thermodynamics of sulphates involved in the roasting process.

This work will supplement the basic researches by attempting to relate and scale up laboratory progress with pilot plant equipment.

## References


1. J.W. Mellor,"A comprehensive treatise on Inorganic and Theoretical chemistry", Longmans, 1946, P.398, P.587-92.
2. M.Hill, J.L. Peglar, D.P.Pepworth, R.N.F.Simpson and S.E.Woods, Imperial Smelting Corporation Ltd., Research Department, "Report of work on the spontaneous oxidation of Bafq. concentrates", June, 1970.
3. R.A. Laudise and A.A. Bateman, J.Phys.Chem. 61, 1960, PP.688.
4. E.T.Allen and J.L. Crenshaw, Am.J.Sci. 34, 1912, PP.341.
5. A.Kremheller and A.K.Levine, Sylvania Technologist, 67, 1957, PP.10.
6. R.Dimitrov, Competes rendus de l'Academe des Science, Tome 22, No.6, 1969.
7. Linus Pauling, "Nature of chemical bond", Cornell University, Press New York, 1960, P.244.
8. G.S.G.Beveridge, Agglomeration Interm.Symp. Philadelphia, 1961.
9. J.N.Ong, M.E.Wadsworth and W.M.Fassell, J.Metals, 8, 1959, PP.257.
10. K.J.Cannon and K.G.Denbigh, Chem.Eng.Sci.,6,1957,PP.145.
11. T.Wada and K.Niva, J.Fac.Sci.,Kokkaido Univ.Ser.III, 1957, 8, PP.857.
12. N.P.A.Diev, Doklady Akad Nauk, SSSR, 103, 1955, PP.857.
13. G.S. Balikhina and D.M. Chizhilov, Tseventnye Metal No.4, 1937, PP.72.
14. Y.Ongawa, Technol.Repts. Tohoku Univ., 9, 1929,PP.175.
15. Orlev and Nesterov, Chem.Abstr. 36, 1942, PP.21979.
16. K.Natesan and W.O.Philbrook, Trans.Soc. of A.M.I.E., 1969.

17. M.E.Wadsworth and W.M.Fascell,Jr.,Trans.A.I.M.E. 197, 1953, PP.1556-1558; Journal of Metals (1953).

18. K.J.Laidler, "Chemical Kinetics", 1950, P.152, N.Y. McGraw - Hill Book Co.Inc.

19. A.J.Shaler and J.Wulff, Ind. and Engl.Chem. 40, 1948, PP.838.

20. F.R.N.Nabarro, "Strength of solids", Physical Society, 1948.

21. C.Herring, J.Appl.Phys.,21, 1950, P.437.

22. Kuczynski, J.Appl.Phys.,21, 1950, P.437.

23. W.D.Kingery and M.Berg, J.Appl.Phys.,26, 1955, P.1205.

24. Coble, J.Amer.Ceram.Soc., 41, 1958, P.55.

25. Ellis, J.Amer.Ceram.Soc., 46, 1963, P.493.

26. Masakazu Sakaguchi, Denki Kagaku, 38(9), 1970, P.671-5.

27. A.E.Nielson, Croatica Chemica Acta, 42, 1970, P.319.

28. R.F.Stickland-Constable and R.E.A.Mason, Nature, 197, 1963, P.897.

29. R.Baker and W.Döring, Ann Physik, 24, 1935, P.719.

30. E.R.Buckle, Nature, 186, 1960, P.875.

31. H.J.De Nordwall and L.A.K.Staveley, J.Chem.Soc.,224, 1954.

32. A.E.Nielsen, "Kinetics of precipitation", Pergamon Press, Oxford,. 1964.

33. W.K.Burton, N.Calerera and F.C.Frank, Phil.Trans.Roy.Soc. A 243, 1951, P.299.

34. O.M.Todes, Zh.fiz.khim.,20, 1946, P.629.

35. F.C.Frank, Discussion Faraday Soc.,5, 1949, P.48.

36. W.K.Burton, Phil.Trans.Roy.Soc., A 243, 1951, P.299.

37. J.Th.G.Overbeek, Colloid Science, Ed.H.R.Kruyt, Chapter II, VI, VII and VIII, Elsewier, Amsterdam, 1952.

38. B.Tezak, Discussion Faraday Society, 18, 1954, P.63, P.194.

39. J.Kratshvil, M.Orhanovie and E.Malyevie, J.Phys. Chem., 64, 1960, P.1216.

40. O.M.Todes, Zh.fiz.khim, 21, 1946, P.629.

41. C.M.Lifshitz and V.V.Slyozov, Phys.Chem.Solids, 19, 1961, P.35.

42. E.Klein and Moiser, Ber.Bunsenges Physik Chemic, 67, 1963, P.349.

43. M.Kahlweit, Z. Physik.Chem.,N.F., 36, 1963, P.292.

44. G.R.Levi and C.G.Fontana,Alti.Accad.Naž Lincei, 7, 1928, P.502.

45. H.Ortmann and R.Piwonka, Mber.Dt.Akad.Wiss,2,1960,P.549.

46. H.Ortmann and R.Piwonka, ibid, 5, 1963, P.174.

47. E.Lendway, J.Schanda, K.Richter and M.Somagyi, Czech., J.Phys., 13, 1963, P.142.

48. R.A.Brown, Electrochem.Technol., 7-8, 1968, P.246.

49. E.M.Shishlyannikova, Izr.Nauch-Issled Inst.Nefte-Uglekhim Sin.Irkutsk Univ.,12, 1970, P.105.

50. R.L.Benner and H.Kenworthy, BuMines Rept., of Inv., 1966, PP.44.

51. T.R.Ingraham and H.H.Kellogg, Trans.Met.Soc.A.I.M.E. 227, 1963, PP.1419-1425.

52. G.E. Moore and K.K.Kelley, J.Am.Chem.Soc.,64, 1942, PP.2949-2951.

53. N.A.Warner and T.R.Ingraham, Canadian J.Chem.,38, 1960, PP.2196-2202.

54. W.E.Evans and D.D.Wagman, J.Research., N.B.S.,49, 1952, PP.141-148.

55. J.P.Coughlin, Bureau of Mines Bull, 542,1954, PP.80.

56. K.K.Kelley, Bureau of Mines Bull, 406,1937,PP.154.

56a. Y.Umethu and S.Suzuki, J.Min.Inst.,68, 1952, PP.529-532.

57. D.M.Chizhikov, G.S.Frents and B.I.Tratsevitskaya, Izvestiya Akademii Nank,SSSR, OTN (Moskva), 9,1949, PP.1352-1360; 12, 1950, PP.140-144; N.E.Pozin, A.M.Chirestling and Petsikovski, Zhurnal Prikladnai khimii, 3, 1954, PP.273; 4, PP.376, 1954; 5, 1955, PP.543; A.Podgornik, Rudarsko i Metalurgija,4, 1953, PP.1249-1255; K.Cazafura and B.Dobovisek, Rudarsko metalurski Zbornik, 3, 1956, PP.1249-1255; F.Opera, Rudarsko metalurski zbornik, 3, 1963, PP.197-212.

58. N.P.Diev and A.I.Okunev, DAN SSSR, XCVII(2), 1954; E.V.Margulis and V.D.Ponomarev, AN Kaz SSR, 3, 1960; V.V.Pechkovskii, Tsvetnye Metally, 1954, 2; V.I. Smirnov and A.R.Babenko, Sb.nauchn. tr.Uralsk Politekhn in-ta, 73, 1958.

59. A.A.Parfenov, Zapiski Leningradskogo Gornogo Instituta, 1970, 50(3), PP.70-75.

60. I.N.Piskunov, Tsvetnaya Metallurgiya, 1961, 6.

61. R.Dimitrov and A.Paulin, Rudarsko metalurski zbornik, No.3-4, 1965, PP.305-326.

61a. G.S.Frents, AN SSSR, Institut metallurgii im Baikova Izdatelstvo Nauk, 1964.

62. W.M.Latimer, J.Am.Chem.Soc., 73, 1951, PP.1480 - 1482.

63. G.S.Frents and E.I.Novikera, AN SSSR, Institut metallurgii im Baikova, 1964.

64. V.A.Kireev, Moskva; Metallurgizdat, 1960.

65. E.A.Pereti, Discussions of the Faraday Society (London), 4, 1948.

66. S.E.Woods and C.F.Harris, Sintering symposium Port. pirie, (Australian Institute of Mining and Metallurgy) 1958, PP.193-218.

67. C.F.Harris, J.L.Bryson and K.M.Sarkar, Institute of Mining and Metallurgy, C76, 1967, C 12-17.

68. A.V.Broad and D.A. Shutt, Sintering sumposium Port. pirie, 1958, PP.219-59.

69. S.E.Woods and C.F.Harris, Chemical engineering in the metallurgical industries, 1963, PP.77-86.

70. P.Scherer, Gottinger Nachrichten, 1918, 2, P.98.

71. F.W.Jones, Proc.R.Soc.(A), 16, 1938, P.166.

72. P.B.Hirsch, A.Howie, R.B.Nicholson, D.W.Pashley and M.J.Whelan, "Electron microscopy of thin crystals" Buttersworth, London, 1965.

73. D.H.Kay (Ed) "Techniques for Electron Microscopy", Blackwell, Oxford, 1965.

74. V.K.Zworykin, G.A.Morton, E.G.Ramberg, J.Hillier and A.W.Vance, "Electron optics and the electron microscope", J.Wiley, N.Y., 1945.

75. A.C.Van Dorsten, H.Niewdorf, A.Verhoeff, Phillips Tech.Rev., 12(2), 1950, P.33.

76. S.Brunauer, P.H.Emmett and E.Teller, J.Amer.Chem. Soc.,60, 1938, P.309.

77. Brunauer, Deming, Deming and Teller, J.Amer.Chem. Soc., 1940.,62, 1723.

78. S.J.Gregg and K.S.W.Sing "Adsorption, surface area and porosity", Academic Press, London, 1967.

79. S.J.Gregg, J.Chem.Soc.,1946, P.561, 1955, P.1438.

80. D.R.Glasson, J.Chem.Soc., 1956,P.1506.

81. British Standard 4359, part I, 1969.

82. D.R.Glasson, J.Appl.Chem., 14, 1964, P.121.

83. S.J.Gregg and G.W.Winsor, Analyst, London, 70, 1945, P.336.

84. H.S.Houldsworth and J.W. Cobb, Trams.Ceram.Soc., 22, 1922-23, P.111.

85. R.W. Grimshaw, E.Heaton and A.L.Roberts, Trams, Ceram.Soc., 44, 1945, P.76.

86. D.R.Glasson, J.Appl.Chem, 10, 1960, P.38.

87. S.J.Gregg, J.Chem.Soc., 1964, P.561; Sartorius-Werke, A-G, Gottingen, "Electrono-vacuum microbalances", 1963.

88. D.R.Glasson and S.A.A.Jayaweers, Soc.Chem.Ind., London, Monogr. No.28., 1968, P.353.

89. D.R.Glasson, J.Appl. Chem., 14, P.125.

90. B.Basak, D.R.Glasson and S.A.A.Jayaweera, Soc.Chem.Ind., symposium on particle growth in suspension, Brunel University, April 26-28, 1972.

91. M.M.Rao and K.P.Abraham, Indian J.Technology, 4(4), 1966, PP.59-62.

92. S.Arrhenius, Z.Physik.Chem (leipzig), 4:226, 1889.

93. L.G.Twidell and A.H.Larson, Trans.Soc.Mett.A.I.M.E., 236, 1966, P.1379.

94. A.I.Okuner, Doklady Akad Nank, SSSR, 103(5), 1955, PP.857-60.

95. M.R.Udupa, Curr.Sci., 9, 1970, PP.206-7.

96. M.M.Rao and K.P.Abraham, Indian J.Technology, 3(9), 1965, PP.291-3.

96a. Argent, B.B., & Phelps, B.; J.Less-Common Metals, 1960, 2, 181; Aylmore, D.W., Gregg, S.J., & Jepson, W.B., J.Electrochem.Soc., 1960

97. E.V.Margulis, V.F.Larin and S.M.Krasavina, Izv.Akad. Nauk., SSSR, 2, 1968, P.61-67.

98. M.M.Rao and K.P.Abraham, Indian J.Technology, No.3(9), 1965, P.291-3.

99. S.J.Gregg and R.J.Hill, J.Chem.Soc., 1953, P.394-5.; D.R.Glasson, J.Appl.Chem.Lond., 13, 1963, P.111-119.; ibid, 17, 1967, P.91-96.

100. E.C.Roggero, Trans. A.I.M.E., 227, 1963, P.105-111.

101. P.G.Thornhill and L.M.Pidgeon, 209, 1957, P.989-995.

102. D.R.Glasson and P.O'Neill, J.Appl.Chem.,Lond., 17, 1967, P.102-106.

APPENDICES

1. Curves for correcting line breadths for K$\alpha$-doublet and instrumental broadening in the method by Jones for determining intrinsic X-ray line- (or peak-) broadening.

2. Calculation of the angular separation of the $\alpha_1$ and $\alpha_2$-components of K-radiation.

3. I.B.M. 1130 Computer programme for B.E.T.gas sorption data.

4. Reprint of published paper Precipitation and Ageing of Zinc Sulphide, Soc. chem.Ind., symposium on "particle growth in suspensions", Colloid and surface chemistry Group, Brunel University, April 24 - 26, 1972.

# APPENDIX 1

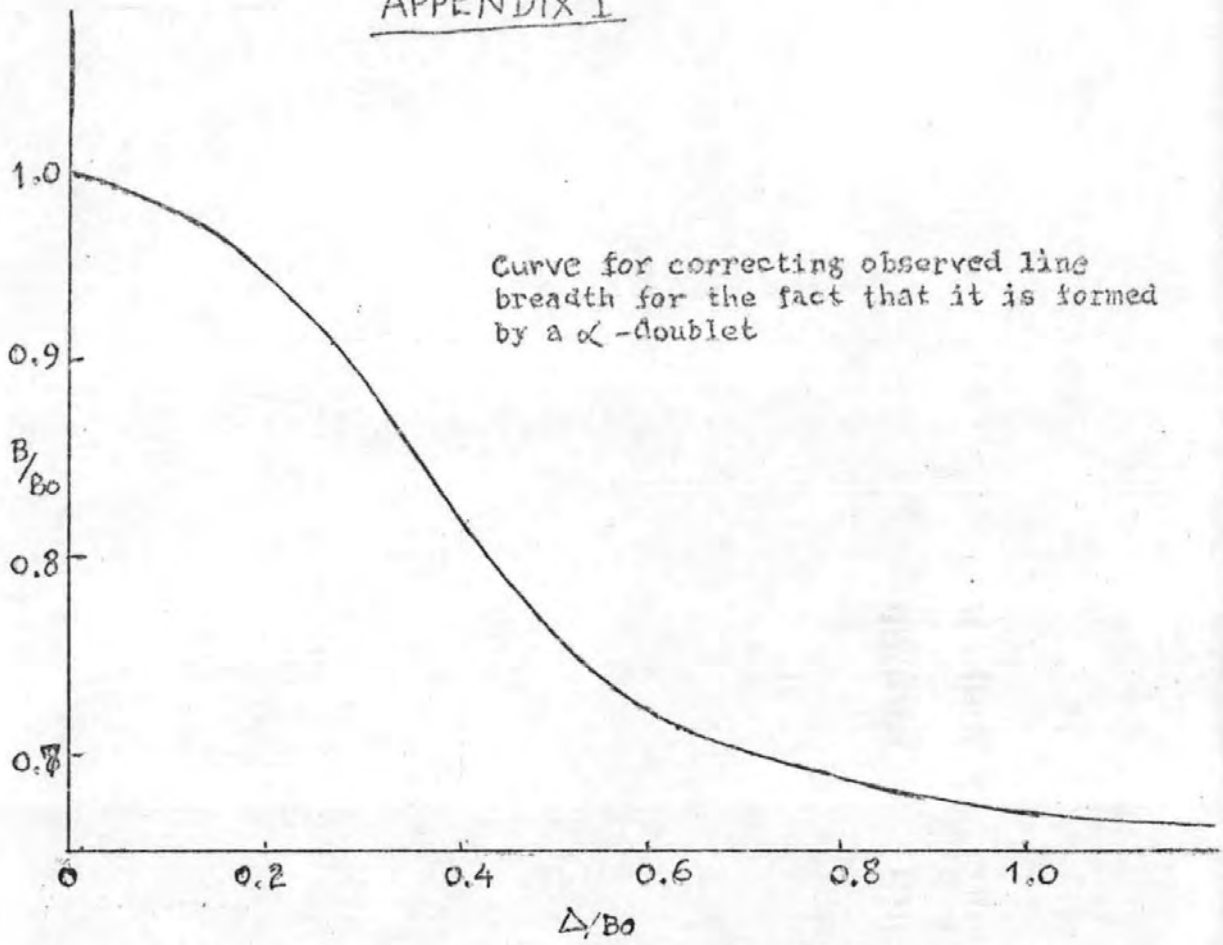


Curve for correcting observed line breadth for the fact that it is formed by a $\alpha$-doublet

Curve for correcting line breadth for the effect of instrumental broadening

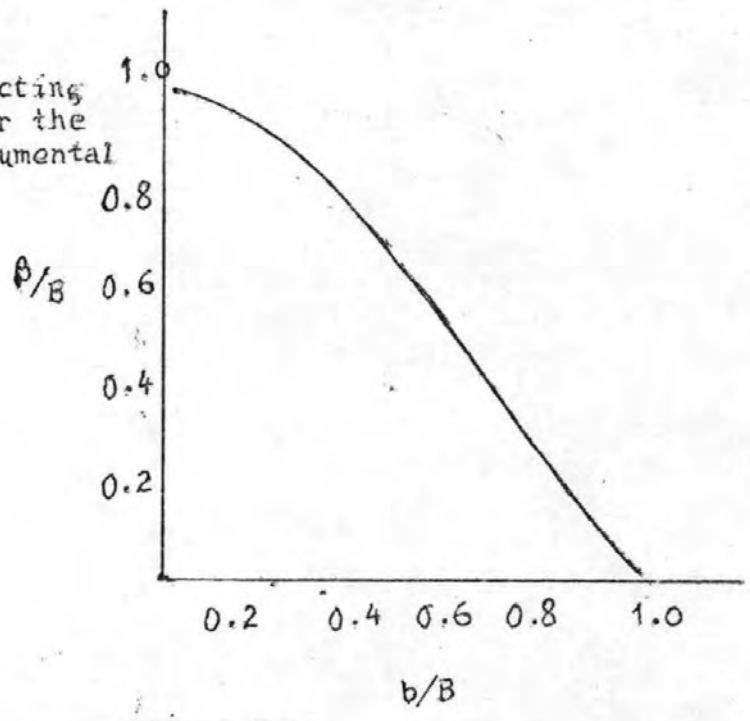

## Appendix 2

### Calculation of the angular separation of the $\alpha_1$ and $\alpha_2$ components of K radiation

Data for angular separation of the two components of various K radiations are given in the Internationale Tabellen* accurate to two significant figures. A direct calculation using the Bragg relationship

$$\sin\theta_1 = \frac{\lambda_{\alpha 1}}{2d} \qquad \sin\theta_2 = \frac{\lambda_{\alpha 2}}{2d}$$

wherein d is the crystal spacing and $\lambda$ is the wavelength in Angstrom units, is tedious and gives only two or three significant figures, because the two $\theta$ angles must be subtracted to obtain angular separation.

An equation for small values of $\theta$ was developed as follows: subtracting the above equations,

$$\frac{\lambda_{\alpha 2} - \lambda_{\alpha 1}}{2d} = \sin\theta_2 - \sin\theta_1 = 2\sin\tfrac{1}{2}(\theta_2 - \theta_1)\cos\tfrac{1}{2}(\theta_2 + \theta_1)$$

$$2\sin\tfrac{1}{2}(\theta_2 - \theta_1) = \frac{\lambda_{\alpha 2} - \lambda_{\alpha 1}}{2d\cos\theta_{av}}$$

Substituting

$$d = \frac{\lambda_{av.}}{2\sin\theta_{av.}}$$

$$2\sin\tfrac{1}{2}(\theta_2 - \theta_1) = \frac{\lambda_{\alpha 2} - \lambda_{\alpha 1}}{\lambda_{av.}}\tan\theta_{av.}$$

For very small angles, the sin is very nearly equal to the angle in radians, i.e.,

$$2 \sin \tfrac{1}{2} (\theta_2 - \theta_1) = \theta_2 - \theta_1$$

Thus,

$$\Delta = \frac{360}{\pi} \frac{\lambda_{\alpha 2} - \lambda_{\alpha 1}}{\lambda_{av.}} \tan \theta_{av.}$$

$$= C \tan \theta_{av.}$$

Various values of C for different X-ray tube targets are given below:

| K- Radiation | C |
|---|---|
| Cr | 0.195 |
| Fe | 0.233 |
| Co | 0.249 |
| Ni | 0.266 |
| Cu | 0.285 |
| Mo | 0.690 |
| Ag | 0.899 |

Example: Cu K-$\alpha$ radiation,

Bragg angle $\theta = 14^{\circ}43'$;

$$\Delta = 0.285 \tan 14^{\circ}43'$$

$$= 0.0746$$

* Internationale Tabellen zur Bestimmung von Kristallstrukturen, vol. 2., 1935, Gebrüder, Borntraeger, Berlin.

## APPENDIX 3

I.B.M. 1130 Computer Programme for the determination of Specific Surfaces by the B.E.T. Method using least squares method to determine the intercept and slope of the isotherm.

## APPENDIX 4

Reprint of paper presented at Symposium on "particle growth in suspensions", Colloid and surface chemistry Group, Brunel University, April 24 - 26, 1972.

*Society of Chemical Industry, Colloid and Surface Chemistry Group, Symposium on Particle Growth in Suspensions, Brunel University, April 24–26, 1972.*

# Precipitation and ageing of zinc sulphide

B. BASAK, D. R. GLASSON and S. A. A. JAYAWEERA

*John Graymore Chemistry Laboratories, Plymouth Polytechnic, England*

**Abstract**

Zinc sulphide samples have been precipitated from solution at various pH levels and in the presence of different concentrations of electrolytes. These experimental conditions have been correlated with changes in phase composition, surface area, and crystallite and aggregate sizes during the formation of the precipitates and their subsequent ageing in solution at various temperatures.

In strongly acidic solution (pH < 1), irregular aggregates are formed of 1 to 10 μm size. Less acidic conditions produce a greater proportion of smaller particles, as found in precipitations from 0·1 mol $dm^{-3}$ $ZnSO_4$ or $ZnCl_2$ solutions and hydrogen sulphide. Here, the pH decreases from about 5 to 1 as precipitation proceeds and the average crystallite sizes (from specific surface measurements) are about 10 nm increasing to about 30 nm on ageing for 10 h at 20°C, and finally acquiring a comparatively slow growth rate. At electrolyte concentrations below 0·1 mol $dm^{-3}$, the greater coagulating effect of the divalent sulphate ion compared with the univalent chloride ion is not so prominent in promoting crystallite growth. Thus, the sulphides precipitated from these zinc sulphate and chloride solutions (and subsequently aged) have similar specific surfaces and average crystallite sizes. Values of the same order are obtained from X-ray line- (or peak-) broadening measurements; differences are discussed in terms of the crystallite size distribution and porosity of the products.

Similar crystallite sizes are given initially when zinc sulphide is precipitated in alkaline conditions, viz, from salt solutions added to sodium sulphide or from zinc oxide dissolved in 3 mol $dm^{-3}$ $NH_4OH$ and treated with hydrogen sulphide. However, subsequent ageing is slower than in acidic media. Precipitation at progressively increasing pH from about 5 to 7 (when sodium sulphide is added to zinc sulphate) is accompanied by hydrolysis of the zinc salt with considerable loss in surface area (and increase in crystallite size) of the product.

Effects of additives on the crystal habit of the zinc sulphide precipitates are described, e.g. the tendency of the zinc sulphide to crystallize as platelets in the

presence of sodium chloride, and corresponding variations in crystallite and aggregate sizes are discussed.

## 1 Introduction

Previous researches on the precipitation of zinc sulphide from solution differ considerably with respect to the particle sizes of the products. Levi and Fontana[1] reported that the particle size was essentially the same, ~2 nm, for zinc sulphide precipitated by hydrogen sulphide from zinc sulphate solutions alone or with additions of ammonium hydroxide, sodium hydroxide and acetic acid. They suggested that the dissimilar behaviour of the precipitates was caused by differences in agglomeration rather than in particle size. However, Allen and Crenshaw[2] described newly-precipitated zinc sulphide as spherical particles 0·2 to 0·5 μm in diameter.

Ortmann and Piwonka[3,4] and Lendvay *et al.*[5] obtained samples with particle sizes of up to 30 μm and 100 to 200 μm by slowly precipitating zinc sulphide with hydrogen sulphide from acid solutions of a soluble zinc salt. Brown[6] showed that the pH of the surrounding solution had a marked effect on the particle size. Precipitation in strongly acidic solution resulted in the formation of aggregates of the order of 1 to 5 μm which were irregular globular masses. Production of finely-divided zinc sulphide with hydrogen sulphide from more dilute acidic zinc salt solutions (0·1 to 0·2 mol $dm^{-3}$ $ZnSO_4$ or $ZnCl_2$) has been described recently by Shishlyannikova.[7] Some of the products had specific surface areas of over 100 $m^2 g^{-1}$, corresponding to average crystallite sizes below 14·7 nm.

The products find application in zinc sulphide phosphors and in admixtures such as lithopone (with barium sulphate). This research forms part of a wider study of the low-temperature and spontaneous oxidation of zinc sulphide ore concentrates during storage and shipment; preventive measures require adequate addition of water, but in amounts just insufficient to form suspensions exhibiting thixotropic properties during transportation.

## 2 Experimental

Samples of zinc sulphide were precipitated in acidic media by passing hydrogen at a flow rate of 5 litre $h^{-1}$ through a gas-dispersion tube into solutions (50 to 500 $cm^3$) of 1·0, 0·25 and 0·1 mol $dm^{-3}$ $ZnSO_4$ or $ZnCl_2$ at 20°C or 85°C. After one hour the precipitates were filtered off and washed twice with 50 $cm^3$ portions of acetone to remove most of the water left in contact with them. This procedure arrests any further ageing, as in the treatment of calcareous materials.[8] The last traces of acetone and water were removed by outgassing the samples at 200°C *in vacuo* on an electrical sorption balance[9,10] before measurement of their surface areas by the BET method[11] from adsorption isotherms of nitrogen determined at −183°C.

$dm^{-3}$ $NH_4OH$ (providing a zinc concentration[13] of 0·1 mol $dm^{-3}$) and then treated with hydrogen sulphide, giving precipitation at pH values decreasing from about 11 to 9.

The zinc sulphide samples were X-rayed using a Solus–Schall diffractometer ($CuK_\alpha$ radiation) with a Geiger counter and ratemeter. Certain samples were examined further for morphology and aggregate sizes by optical and electron microscopes (Philips EM-100).

## 3 Results

In Fig. 1 the variations in specific surface $S$ and average crystallite size are shown for zinc sulphide samples aged for different lengths of time in acidic or alkaline media at low electrolyte concentrations ($\sim$0·1 mol $dm^{-3}$). The average crystallite sizes have been calculated (for a cubic habit) from the specific surface area measurements and the density of the zinc sulphide (4·09 g $cm^{-3}$) obtained from the X-ray diffraction pattern.

The X-ray patterns showed that the samples all consisted of the zinc blende (sphalerite) form of ZnS, except for those precipitated in less acidic media by the addition of 1 mol $dm^{-3}$ $Na_2S$ to 0·1 mol $dm^{-3}$ $ZnSO_4$ which contained some basic zinc salt. The half-peak widths of the 111, 200 and 220

Table 1
Zinc sulphide samples precipitated at different electrolyte concentrations

| Precipitation conditions (aged 1 h) | Surface area $S$ $m^2g^{-1}$ | Average crystallite size (nm) calculated from $S$ | Average crystallite size (nm) calculated from X-ray peaks |
|---|---|---|---|
| *Alkaline media* | | | |
| 1 mol $dm^{-3}$ $ZnSO_4$ added to 500 $cm^3$ 0·1 mol $dm^{-3}$ $Na_2S$ | 116·4 | 12·6 | 3·0 |
| 1 mol $dm^{-3}$ $ZnSO_4$ added to 50 $cm^3$ 1 mol $dm^{-3}$ $Na_2S$ | 94·0 | 15·7 | 3·0 |
| *Acidic media* | | | |
| 500 $cm^3$ 0·1 mol $dm^{-3}$ $ZnSO_4$ + $H_2S$ | 122·8 | 12·0 | 5·0 |
| 50 $cm^3$ 1 mol $dm^{-3}$ $ZnSO_4$ + $H_2S$ | 54·0 | 27·2 | 6·8 |
| 500 $cm^3$ 0·1 mol $dm^{-3}$ $ZnSO_4$ + 50 g NaCl + $H_2S$ | 80·0 | 18·4 | 3·9 |
| 500 $cm^3$ 0·1 mol $dm^{-3}$ $ZnCl_2$ + $H_2S$ | 129·4 | 11·4 | 4·4 |
| 500 $cm^3$ 0·25 mol $dm^{-3}$ $ZnCl_2$ + $H_2S$ | 59·8 | 24·5 | 3·9 |
| 500 $cm^3$ 0·25 mol $dm^{-3}$ $ZnCl_2$ + 50 g NaCl + $H_2S$ | 60·6 | 24·2 | 4·4 |

Zinc sulphide samples were precipitated in alkaline media by adding stoichiometric amounts of 1 mol $dm^{-3}$ $ZnSO_4$ or $ZnCl_2$ to 1·0 or 0·1 mol $dm^{-3}$ $Na_2S$. The specific surface areas of the zinc sulphide precipitates were practically independent of the rate of addition (standardized at 3 $cm^3$ per minute) of one reactant to the rapidly stirred solutions (50 to 500 $cm^3$) of the other. Only when the rate of addition was considerably increased (and/or the rate of stirring considerably decreased) did the specific surface area decrease appreciably, as a result of the concentration of the additive at the time of precipitation being increased. A similar situation exists for the precipitation of calcium carbonate from solution.[12] The samples were filtered off after one hour, and washed with acetone to remove most of the remaining water and thus prevent possible ageing, before drying and examination on the sorption balance in the same way as the samples precipitated in acidic media.

A few zinc sulphide samples were precipitated in the acidic or alkaline media in the presence of 50 g dissolved sodium chloride. Additional zinc sulphide samples were prepared in less acidic and less alkaline conditions. 1 mol $dm^{-3}$ $Na_2S$ was added to 0·1 mol $dm^{-3}$ $ZnSO_4$, giving precipitation at pH values increasing from about 5 to 7. Zinc oxide was dissolved in 3 mol

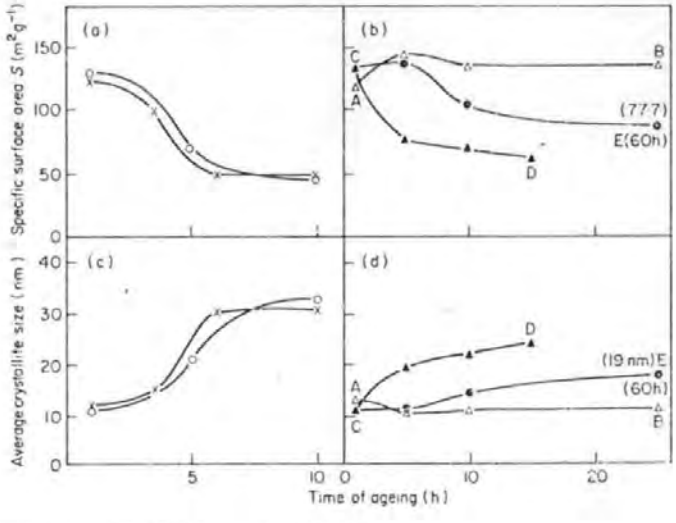


× 0·1 mol $dm^{-3}$ $ZnSO_4$ + $H_2S$ (20°C).
○ 0·1 mol $dm^{-3}$ $ZnCl_2$ + $H_2S$ (20°C).
△ 1 mol $dm^{-3}$ $ZnSO_4$ added to 0·1 mol $dm^{-3}$ $Na_2S$ (20°C).
▲ 1 mol $dm^{-3}$ $ZnSO_4$ added to 0·1 mol $dm^{-3}$ $Na_2S$ (85°C).
◉ Sample ▲ aged at 20°C after precipitation.

FIG. 1 Precipitation and ageing of zinc sulphide in acidic or alkaline conditions.

"reflections" of the cubic-*F* (zinc blende) crystal lattice were measured from some of the X-ray diffractometer traces. This also afforded approximate estimates of the average crystallite sizes,[14] using the Jones[15] method for calculating intrinsic line-broadening.

The specific surface areas and average crystallite sizes of the zinc sulphide samples newly precipitated in acidic or alkaline media at higher electrolyte concentrations (0·25 to 1·0 mol $dm^{-3}$) are summarized in Table 1, where they are compared with those for samples precipitated at lower electrolyte concentrations ($\sim$0·1 mol $dm^{-3}$).

Electron micrographs are presented in Fig. 2, showing differences in morphology and aggregate sizes when the zinc sulphide samples are precipitated and aged in acidic and in alkaline media.

## 4 Discussion

The pH conditions have a considerable effect on crystallite and aggregate size largely because they affect the solubility and hence the supersaturation ratio of the zinc sulphide. A greater supersaturation ratio causes nucleation to predominate over crystal growth, giving smaller crystallites. The ageing of the precipitates proceeds by Ostwald ripening supplemented by coagulation, especially in the presence of higher concentrations of surrounding electrolyte.

### 4.1 PRECIPITATION AND AGEING AT LOWER ELECTROLYTE CONCENTRATIONS

When zinc sulphide is precipitated by hydrogen sulphide from 0·1 mol $dm^{-3}$ $ZnSO_4$ or $ZnCl_2$, the pH progressively decreases from about 5 to 1. The average crystallite size of the products (calculated from specific surface area measurements) is about 10 nm, as shown in Fig. 1(a) and (c). Subsequently, these sizes increase to about 30 nm as the zinc sulphide ages for a total of 10 h at 20°C, finally acquiring a comparatively slow crystallite growth rate. The close similarity of the specific surface area (and average crystallite size) curves indicates that at electrolyte concentrations below 0·1 mol $dm^{-3}$ the greater coagulating effect of the divalent sulphate ion compared with the univalent chloride ion is not prominent in promoting crystallite growth.

Similar specific surface areas and average crystallite sizes are given initially when zinc sulphide is precipitated in alkaline conditions, viz. from zinc sulphate solutions added to 0·1 mol $dm^{-3}$ $Na_2S$ at 20°C, as in Fig. 1(b) and (d), curve *AB*. Subsequently, the specific surface area somewhat increases (and the average crystallite size decreases) before the material ages much more slowly than in acidic media. The initial increase may arise from removal of strains of defects in the newly-formed zinc sulphide as it recrystallizes to its normal lattice structure. This effect has been found previously with some newly-hydrated limes and magnesias.[8, 16]

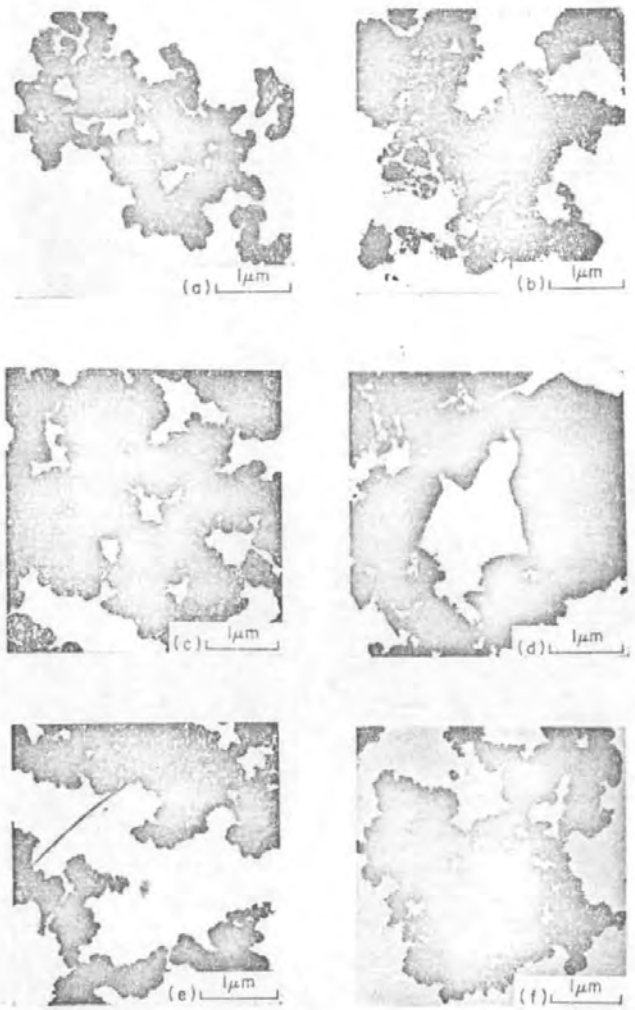


(a) 0·1 mol $dm^{-3}$ $ZnSO_4$ + $H_2S$ (3½ h ageing).
(b) 1 mol $dm^{-3}$ $ZnSO_4$ added to 0·1 mol $dm^{-3}$ $Na_2S$ (10 h ageing).
(c) 0·1 mol $dm^{-3}$ $ZnCl_2$ + $H_2S$ (1 h ageing).
(d) 1 mol $dm^{-3}$ $ZnCl_2$ added to 0·1 mol $dm^{-3}$ $Na_2S$ (1 h ageing).
(e) 0·25 mol $dm^{-3}$ $ZnCl_2$ + $H_2S$ (1 h ageing).
(f) 500 $cm^3$ 0·25 mol $dm^{-3}$ $ZnCl_2$ + 50 g NaCl + $H_2S$ (1 h ageing).

FIG. 2. Electron micrographs of zinc sulphide precipitated at 20°C in acidic or alkaline conditions.

The zinc sulphide precipitated at 85°C initially has a greater specific surface area (and smaller average crystallite size) than that prepared at 20°C (points *A* and *C* in Fig. 1(b) and (d)). Evidently, the nucleation is much faster at the higher temperature, which produces a larger number of smaller crystallites and more than compensates for the loss of surface caused by the increased rate of crystal growth. Thus, the zinc sulphide precipitated and aged at 85°C (curve *CD*) subsequently has a much smaller specific surface area (and larger average crystallite size) than that prepared and aged at 20°C (curve *AB*). As expected, the sample precipitated at 85°C ages afterwards at 20°C more slowly than it does at 85°C (curves *CE* and *CD*). However, this ageing at 20°C is faster than that of the sample initially prepared at 20°C (curves *CE* and *AB*). This is in accord with the sample precipitated at 85°C having initially a larger number of smaller crystallites (below a critical size) which redissolve and deposit on the larger crystallites in the Ostwald ripening process.[17]

Average crystallite size values of the same order as those calculated from specific surface areas have been obtained from X-ray line- (or peak-) broadening measurements. They are smaller but show the same general trends in variation as the materials are aged. Thus, in acidic media these average crystallite sizes vary from 5·0 to 8·8 nm with 0·1 mol $dm^{-3}$ $ZnSO_4$ and 4·4 to 8·8 nm with $ZnCl_2$. In alkaline media, the initial sizes and subsequent increases on ageing are somewhat smaller, viz. 3·0 to 3·4 nm and 2·8 to 4·4 nm for zinc sulphate added to 0·1 mol $dm^{-3}$ $Na_2S$ at 20°C and 85°C respectively; also 2·8 to 3·1 nm for the sample precipitated at 85°C and aged at 20°C.

In comparing the values of the average crystallite sizes determined from specific surface areas and X-ray line- (or peak-) broadening, there are 2 to 4-fold and 3 to 6-fold differences in acidic and alkaline media respectively. These are ascribed to differences in porosity, crystal strain and defects and especially crystallite size distribution. Variations due to porosity and crystal strain are comparatively small, since the nitrogen adsorption isotherms showed little hysteresis and the precipitation processes did not involve interconversion of solid material, only the more stable (cubic) form of zinc sulphide being obtained. The calculation of average crystallite sizes from specific surface areas assumes no particular crystallite size distribution, whereas that from X-ray measurements assumes a Gaussian distribution. Nevertheless, the X-ray measurements again indicate that the samples precipitated and aged in alkaline media (compared with acidic media) generally have the smaller crystallite sizes.

### 4.2 MORPHOLOGY AND AGGREGATE SIZES

In addition to differences in crystallite sizes, the samples vary also in morpho-

logy and aggregate sizes. Samples precipitated from acidic media appear to have smaller ranges of aggregate sizes than those from alkaline media. This is illustrated in Fig. 2 by comparing (a) and (b) for $ZnSO_4$ (0·1 to 0·2 μm and 0·1 to 1 μm) and (c) and (d) for $ZnCl_2$ (0·1 to 0·5 μm and 0·1 to 2 μm). In the latter case, the formation (and presence) of sodium chloride during the alkaline precipitation affects the crystal habit, causing the aggregates to have a plate-like morphology (Fig. 2(d)). Many of these aggregates are larger than those obtained in the corresponding precipitation from 0·1 mol $dm^{-3}$ $ZnSO_4$ in (b); the crystallites are about twice as large with $S = 56·3$ $m^2$ $g^{-1}$ and average crystallite size 26·1 nm, compared with 116·4 $m^2$ $g^{-1}$ and 12·6 nm.

### 4.3 PRECIPITATION IN LESS ACIDIC AND ALKALINE MEDIA

Smaller-sized zinc sulphide crystallites are obtained also in less alkaline conditions from zinc oxide dissolved in 3 mol $dm^{-3}$ $NH_4OH$ and treated with hydrogen sulphide, giving precipitation at pH values decreasing from about 11 to 9. Even after 15 h ageing at 20°C, the specific surface is 124 $m^2$ $g^{-1}$ and average crystallite size 11·9 nm (or 6·4 nm from X-ray peak-broadening). Much larger crystallite sizes are given in less acidic media when 1 mol $dm^{-3}$ $Na_2S$ is added to 0·1 mol $dm^{-3}$ $ZnSO_4$, with precipitation at pH values increasing from about 5 to 7. The precipitation is accompained by hydrolysis of the zinc salt, the newly-formed product having a specific surface area of only 14·9 $m^2$ $g^{-1}$ and an average crystallite size as large as 98·7 nm.

### 4.4 PRECIPITATION AND AGEING AT HIGHER ELECTROLYTE CONCENTRATIONS

The specific surface areas and corresponding average crystallite sizes of the zinc sulphide samples precipitated in alkaline media are not changed considerably when the concentration of the sodium sulphide is increased from 0·1 to 1 mol $dm^{-3}$ (see Table 1). The changes are more considerable in acidic media when the concentrations of zinc sulphate or zinc chloride are increased from 0·1 to 1 mol $dm^{-3}$ or 0·25 mol $dm^{-3}$ respectively (Table 1). Addition of sodium chloride to 0·1 mol $dm^{-3}$ $ZnSO_4$ also causes decreases in specific surface area and increases in corresponding average crystallite size, but it does not cause further changes of this type when added to 0·25 mol $dm^{-3}$ $ZnCl_2$. However, the presence of higher concentrations of chloride ions seems to change the crystallite size distributions, since the average crystallite sizes calculated from X-ray line- (or peak-) broadening give abnormally lower values. Nevertheless, the aggregate sizes (Fig. 2) increase somewhat from submicron sizes at the lower electrolyte concentrations, viz. (a) 0·1 to 0·2 μm for 0·1 mol $dm^{-3}$ $ZnSO_4 + H_2S$, and (c) 0·1 to 0·5 μm for 0·1 mol $dm^{-3}$ $ZnCl_2 + H_2S$, compared with (e) and (f) 0·2 to 3 μm for 0·25 mol $dm^{-3}$ $ZnCl_2 + H_2S$ alone or in the presence of sodium chloride.

ACKNOWLEDGEMENT

The authors thank Dr A. W. Richards, Imperial Smelting Corporation, for his interest and encouragement in this work; the University of London, Imperial Chemical Industries Ltd. and the Science Research Council for grants for apparatus; and the Governors of the Polytechnic for a Research Assistantship (for B. Basak).

## References

1. Levi, G. R. and Fontana, C. G. (1928). *Atti Accad. Naz. Lincei*, **7**, 502.
2. Allen, E. T. and Crenshaw, J. L. (1912). *Amer. J. Sci.* **36**, 341.
3. Ortmann, H. and Piwonka, R. (1960). *Mber. Dt. Akad. Wiss.* **2**, 549; Ortmann, H. and Piwonka, R. (1963). *Mber. Dt. Akad. Wiss.* **5**, 174.
4. Ortmann, N. and Piwonka, R. (1961). *Z. Phys. Chem.* **218**, 64.
5. Lendvay, E., Schanda, J., Richter, K. and Somagyi, M. (1963). *Czech J. Phys.* **13**, 142.
6. Brown, R. A. (1968). *Electrochem. Technol.* **6**, 246.
7. Shishlannikova, E. M. (1970). *Izv. Nauch-Issled. Inst. Nefte-Uglekhim. Sin. Irkutsk Univ.* **12**, 105.
8. Glasson, D. R. (1960). *J. Appl. Chem.* **10**, 38.
9. Gregg, S. J. (1946). *J. Chem. Soc.* 561.
10. "Electrono-vacuum Microbalances" (1963). Sartorius-Werke, A.-G., Gottingen.
11. Brunauer, S., Emmett, P. H. and Teller, E. (1938). *J. Amer. Chem. Soc.* **60**, 309.
12. Glasson, D. R. (1960). *J. Appl. Chem.* **10**, 42.
13. Glasson, D. R. and Jayaweera, S. A. A. (1968). *Soc. Chem. Ind. London, Monogr.* No. 28, p. 353.
14. Glasson, D. R. (1964). *J. Appl. Chem.* **14**, 121.
15. Jones, F. W. (1938). *Proc. Roy. Soc.* **166**, 16; Klugg, H. P. and Alexander, L. E. "X-ray Diffraction Procedures". John Wiley, New York.
16. Glasson, D. R. (1963). *J. Appl. Chem.* **13**, 119; Glasson, D. R. (1964). *J. Appl. Chem.* **14**, 125.
17. Nielsen, A. E. (1964). "Kinetics of Precipitation," p. 5. Pergamon Press, Oxford.

# APPENDIX 5

## The Heats of Formation and Dissociation of Zinc Sulphate

From the inter-relationship of $SO_3$, $SO_2$ and $O_2$ in reaction of the type

(1) $MSO_4 \rightleftharpoons MO + SO_2 + {}^1/_2O_2$

(2) $SO_2 + {}^1/_2O_2 \rightleftharpoons SO_3$

then at equilibrium at a given temperature $MSO_4$ and MO will have $SO_2$, $O_2$ and $SO_3$ present at values dictated by the K'S of the above reaction. The presence of platinum could not affect the position of equilibrium, or the stability of metal sulphate.

However, if we consider the sulphation of an oxide, then if the mechanism of sulphation depends on the $SO_3$ molecule, then in the presence of $SO_2$ and $O_2$ the attainment of equilibrium between solid and gas could be more rapid in the presence of a catalyst which allows reaction (2) to come to equilibrium more rapidly.

Based on the results given by Kellogg and Ingraham (1), we have been recalculating the high temperature free energies of the two decomposition reactions, giving

1. $ZnSO_4 = ZnO\ 2ZnSO_4 + SO_2 + {}^1/_2O_2$

   $\Delta H_T = 70{,}000 \quad \Delta S_T = 60.0$

2. ${}^1/_2\ (ZnO\ 2ZnSO_4) = {}^3/_2ZnO + SO_2 + {}^1/_2O_2$

   $\Delta H_T = 75{,}470 \quad \Delta S_T = 60.0$

Where T is in the range 1000 - 1200K.

The method was used

(a) from Kellogg and Ingraham's $P_{tot}$ and $P_{SO_3}$ derive $P_{SO_2}$ and $P_{O_2}$ (knowing $P_{tot} = P_{SO_2} + P_{SO_3} + P_{O_2}$ and $P_{SO_2} = 2P_{O_2}$)

(b) From logK calculate $\Delta H_T$ for each experiment[2] assuming $\Delta S_T = 60.0$

This latter value is an estimate which has been used for all sulphate decompositions to $SO_2 + {}^1/_2\ O_2$ and in most cases, we consider it to be more accurate than $\Delta S$ values calculated from a particular series of experiments.

(c) In this way one obtains a $\Delta H_T$ value from each experiment and the mean $\Delta H_T$ is quoted in the two equations above.

If the experimental points are plotted they are seen to be a good fit with lines drawn to the equations of (1) and (2).

We are now able to construct a plot similar to that in Fig. 4, P. 1425 of Kellogg and Ingraham (1). We enclose one for 800°C, similar plots can be made for other temperatures and one can use these plots in a number of ways, e.g. if one considers roasting gas with no false air then most compositions lie in the $ZnO.2ZnSO_4$ region; ZnO is stable only below 1% $SO_2$.

In one case with (presumably) an excess of air one might expect the stable phases to be as given in the table.

| % $SO_2$ | Temperature | | |
|---|---|---|---|
| | 700°C | 800°C | 900°C |
| 0.03 | ZnO | ZnO | ZnO |
| 0.1 | $ZnO.2ZnSO_4$ | ZnO | ZnO |
| 0.5 | $ZnO.2ZnSO_4$ and $ZnSO_4$ | ZnO | ZnO |
| 1.0 | $ZnSO_4$ | ZnO | ZnO |
| 2.0 | $ZnSO_4$ | ZnO and $ZnO.2ZnSO_4$ | ZnO |
| 5.0 | $ZnSO_4$ | $ZnO.2ZnSO_4$ | ZnO |
| 10.0 | $ZnSO_4$ | $ZnO.2ZnSO_4$ | ZnO |

We partly explain our results one the basis that the first oxidation is effected at very low $P_{SO2}$ due to the rapid removal from the surface of the particles. Hindrance of diffusion of $SO_2$ from the reaction surface may later allow higher $P_{SO2}$ to occur with sulphation of some of the oxide. In industrial practice the amount of excess air would be kept to a minimum - certainly not more than 100%; under these conditions the limits of stability of the sulphates are shown in Fig. 2.

Reference:


1. T.R. Ingraham and H.H. Kellogg, Trans. Met. Soc. AIME., 1963, 227, P.1419-1425

2. A.W. Richards, Journal of Applied Chemistry, 1959, 9, P.142-145.

Fig 1

Zn-S-O at 800°C

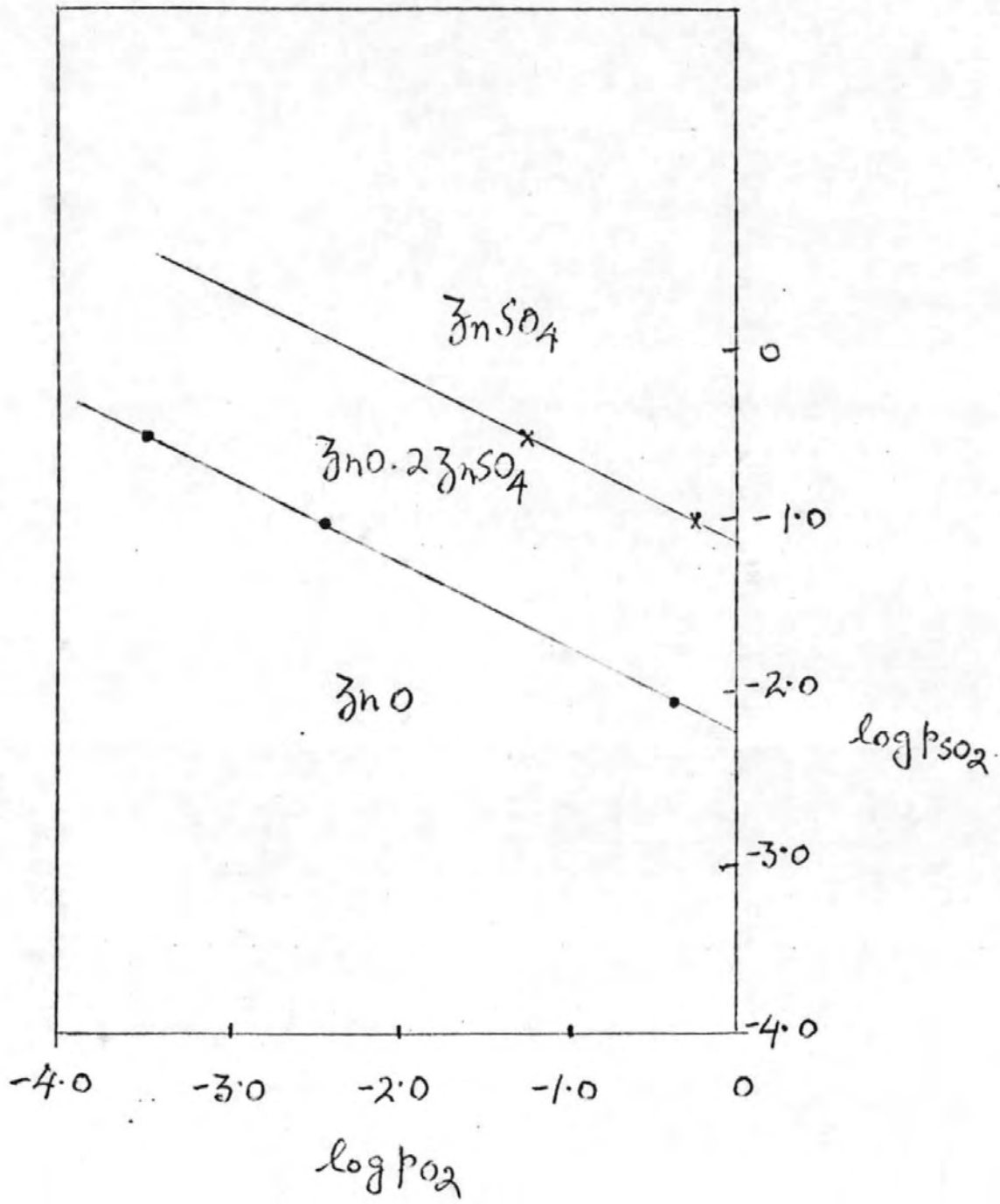

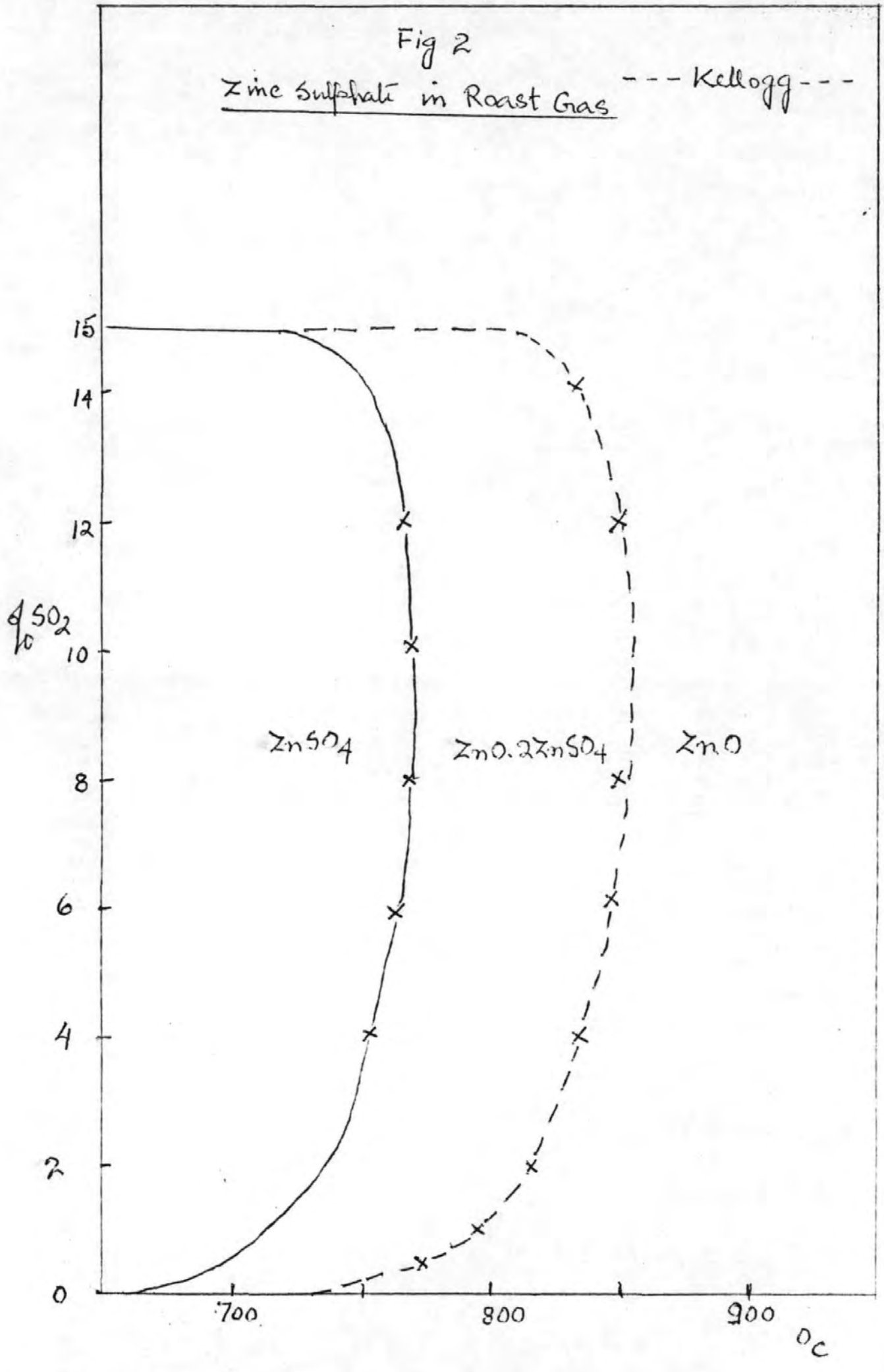
Fig 2
Zinc Sulphate in Roast Gas
--- Kellogg ---
15
14
12
10
8
6
4
2
0
% SO2
ZnSO4
ZnO.2ZnSO4
ZnO
700
800
900
°C

Academic Press—Particle Growth B. Basak etc, 10/12 maths. Ω 9

*Society of Chemical Industry, Colloid and Surface Chemistry Group, Symposium on Particle Growth in Suspensions, Brunel University, April 24–26, 1972.*

# Precipitation and ageing of zinc sulphide

B. BASAK, D. R. GLASSON and S. A. A. JAYAWEERA

*John Graymore Chemistry Laboratories, Plymouth Polytechnic, England*

**Abstract**

Zinc sulphide samples have been precipitated from solution at various pH levels and in the presence of different concentrations of electrolytes. These experimental conditions have been correlated with changes in phase composition, surface area, and crystallite and aggregate sizes during the formation of the precipitates and their subsequent ageing in solution at various temperatures.

In strongly acidic solution (pH < 1), irregular aggregates are formed of 1 to 10 μm size. Less acidic conditions produce a greater proportion of smaller particles, as found in precipitations from 0·1 mol $dm^{-3}$ $ZnSO_4$ or $ZnCl_2$ solutions and hydrogen sulphide. Here, the pH decreases from about 5 to 1 as precipitation proceeds and the average crystallite sizes (from specific surface measurements) are about 10 nm increasing to about 30 nm on ageing for 10 h at 20°C, and finally acquiring a comparatively slow growth rate. At electrolyte concentrations below 0·1 mol $dm^{-3}$, the greater coagulating effect of the divalent sulphate ion compared with the univalent chloride ion is not so prominent in promoting crystallite growth. Thus, the sulphides precipitated from these zinc sulphate and chloride solutions (and subsequently aged) have similar specific surfaces and average crystallite sizes. Values of the same order are obtained from X-ray line- (or peak-) broadening measurements; differences are discussed in terms of the crystallite size distribution and porosity of the products.

Similar crystallite sizes are given initially when zinc sulphide is precipitated in alkaline conditions, viz, from salt solutions added to sodium sulphide or from zinc oxide dissolved in 3 mol $dm^{-3}$ $NH_4OH$ and treated with hydrogen sulphide. However, subsequent ageing is slower than in acidic media. Precipitation at progressively increasing pH from about 5 to 7 (when sodium sulphide is added to zinc sulphate) is accompanied by hydrolysis of the zinc salt with considerable loss in surface area (and increase in crystallite size) of the product.

Effects of additives on the crystal habit of the zinc sulphide precipitates are described, e.g. the tendency of the zinc sulphide to crystallize as platelets in the

presence of sodium chloride, and corresponding variations in crystallite and aggregate sizes are discussed.

## 1 Introduction

Previous researches on the precipitation of zinc sulphide from solution differ considerably with respect to the particle sizes of the products. Levi and Fontana[1] reported that the particle size was essentially the same, ~2 nm, for zinc sulphide precipitated by hydrogen sulphide from zinc sulphate solutions alone or with additions of ammonium hydroxide, sodium hydroxide and acetic acid. They suggested that the dissimilar behaviour of the precipitates was caused by differences in agglomeration rather than in particle size. However, Allen and Crenshaw[2] described newly-precipitated zinc sulphide as spherical particles 0·2 to 0·5 μm in diameter.

Ortmann and Piwonka[3,4] and Lendvay *et al.*[5] obtained samples with particle sizes of up to 30 μm and 100 to 200 μm by slowly precipitating zinc sulphide with hydrogen sulphide from acid solutions of a soluble zinc salt. Brown[6] showed that the pH of the surrounding solution had a marked effect on the particle size. Precipitation in strongly acidic solution resulted in the formation of aggregates of the order of 1 to 5 μm which were irregular globular masses. Production of finely-divided zinc sulphide with hydrogen sulphide from more dilute acidic zinc salt solutions (0·1 to 0·2 mol $dm^{-3}$ $ZnSO_4$ or $ZnCl_2$) has been described recently by Shishlyannikova.[7] Some of the products had specific surface areas of over 100 $m^2$ $g^{-1}$, corresponding to average crystallite sizes below 14·7 nm.

The products find application in zinc sulphide phosphors and in admixtures such as lithopone (with barium sulphate). This research forms part of a wider study of the low-temperature and spontaneous oxidation of zinc sulphide ore concentrates during storage and shipment; preventive measures require adequate addition of water, but in amounts just insufficient to form suspensions exhibiting thixotropic properties during transportation.

## 2 Experimental

Samples of zinc sulphide were precipitated in acidic media by passing hydrogen at a flow rate of 5 litre $h^{-1}$ through a gas-dispersion tube into solutions (50 to 500 $cm^3$) of 1·0, 0·25 and 0·1 mol $dm^{-3}$ $ZnSO_4$ or $ZnCl_2$ at 20°C or 85°C. After one hour the precipitates were filtered off and washed twice with 50 $cm^3$ portions of acetone to remove most of the water left in contact with them. This procedure arrests any further ageing, as in the treatment of calcareous materials.[8] The last traces of acetone and water were removed by outgassing the samples at 200°C *in vacuo* on an electrical sorption balance.[9,10] before measurement of their surface areas by the BET method[11] from adsorption isotherms of nitrogen determined at −183°C.

Zinc sulphide samples were precipitated in alkaline media by adding stoicheiometric amounts of 1 mol $dm^{-3}$ $ZnSO_4$ or $ZnCl_2$ to 1·0 or 0·1 mol $dm^{-3}$ $Na_2S$. The specific surface areas of the zinc sulphide precipitates were practically independent of the rate of addition (standardized at 3 $cm^3$ per minute) of one reactant to the rapidly stirred solutions (50 to 500 $cm^3$) of the other. Only if the rate of addition were considerably increased (and/or the rate of stirring considerably decreased) did the specific surface area decrease appreciably, as a result of the concentration of the additive at the time of precipitation being increased, a similar situation exists for the precipitation of calcium carbonate from solution.[12] The samples were filtered off after one hour, and washed with acetone to remove most of the remaining water and thus prevent possible ageing, before drying and examination on the sorption balance in the same way as the samples precipitated in acidic media.

A few zinc sulphide samples were precipitated in the acidic or alkaline media in the presence of 50 g dissolved sodium chloride. Additional zinc sulphide samples were prepared in less acidic and less alkaline conditions. 1 mol $dm^{-3}$ $Na_2S$ was added to 0·1 mol $dm^{-3}$ $ZnSO_4$, giving precipitation at pH values increasing from about 5 to 7. Zinc oxide was dissolved in 3 mol

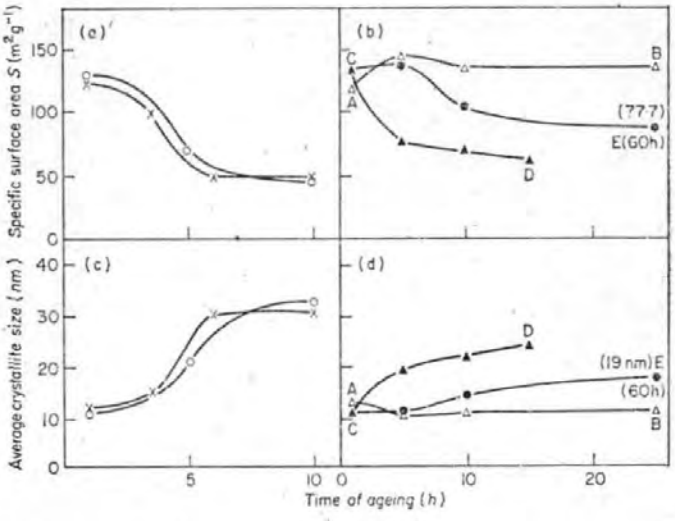


× 0·1 mol $dm^{-3}$ $ZnSO_4$ + $H_2S$ (20°C)
○ 0·1 mol $dm^{-3}$ $ZnCl_2$ + $H_2S$ (20°C).
△ 1 mol $dm^{-3}$ $ZnSO_4$ added to 0·1 mol $dm^{-3}$ $Na_2S$ (20°C).
▲ 1 mol $dm^{-3}$ $ZnSO_4$ added to 0·1 mol $dm^{-3}$ $Na_2S$ (85°C).
◐ Sample ▲ aged at 20°C after precipitation.

FIG. 1 Precipitation and ageing of zinc sulphide in acidic or alkaline conditions.

$dm^{-3}$ $NH_4OH$ (providing a zinc concentration[13] of 0·1 mol $dm^{-3}$) and then treated with hydrogen sulphide, giving precipitation at pH values decreasing from about 11 to 9.

The zinc sulphide samples were X-rayed using a Solus–Schall diffractometer (CuK$\alpha$-radiation) with a Geiger counter and rate-meter. Certain samples were examined further for morphology and aggregate sizes by optical and electron-microscopes (Philips EM-100).

## 3 Results

In Fig. 1 the variations in specific surface $S$ and average crystallite size are shown for zinc sulphide samples aged for different lengths of time in acidic or alkaline media at low electrolyte concentrations ($\sim$0·1 mol $dm^{-3}$). The average crystallite sizes have been calculated (for a cubic habit) from the specific surface area measurements and the density of the zinc sulphide (4·09 g $cm^{-3}$) obtained from the X-ray diffraction pattern.

The X-ray patterns showed that the samples all consisted of the zinc blende (sphalerite) form of ZnS, except for those precipitated in less acidic media by the addition of 1 mol $dm^{-3}$ $Na_2S$ to 0·1 mol $dm^{-3}$ $ZnSO_4$ which contained some basic zinc salt. The half-peak widths of the 111, 200 and 220

Table 1
Zinc sulphide samples precipitated at different electrolyte concentrations

| Precipitation conditions (aged 1 h) | Surface area $S$ $m^2g^{-1}$ | Average crystallite size (nm) calculated from $S$ | Average crystallite size (nm) calculated from X-ray peaks |
|---|---|---|---|
| *Alkaline media* | | | |
| 1 mol $dm^{-3}$ $ZnSO_4$ added to 500 $cm^3$ 0·1 mol $dm^{-3}$ $Na_2S$ | 116·4 | 12·6 | 3·0 |
| 1 mol $dm^{-3}$ $ZnSO_4$ added to 50 $cm^3$ 1 mol $dm^{-3}$ $Na_2S$ | 94·0 | 15·7 | 3·0 |
| *Acidic media* | | | |
| 500 $cm^3$ 0·1 mol $dm^{-3}$ $ZnSO_4$ + $H_2S$ | 122·8 | 12·0 | 5·0 |
| 50 $cm^3$ 1 mol $dm^{-3}$ $ZnSO_4$ + $H_2S$ | 54·0 | 27·2 | 6·8 |
| 500 $cm^3$ 0·1 mol $dm^{-3}$ $ZnSO_4$ + 50 g NaCl + $H_2S$ | 80·0 | 18·4 | 3·6 |
| 500 $cm^3$ 0·1 mol $dm^{-3}$ $ZnCl_2$ + $H_2S$ | 129·4 | 11·4 | 4·4 |
| 500 $cm^3$ 0·25 mol $dm^{-3}$ $ZnCl_2$ + $H_2S$ | 59·8 | 24·5 | 3·9 |
| 500 $cm^3$ 0·25 mol $dm^{-3}$ $ZnCl_2$ + 50 g NaCl + $H_2S$ | 60·6 | 24·2 | 4·4 |

"reflections" of the cubic-*F* (zinc blende) crystal lattice were measured from some of the X-ray diffractometer traces. This also afforded approximate estimates of the average crystallite sizes,[14] using the Jones[15] method for calculating intrinsic line-broadening.

The specific surface areas and average crystallite sizes of the zinc sulphide samples newly precipitated in acidic or alkaline media at higher electrolyte concentrations (0·25 to 1·0 mol $dm^{-3}$) are summarized in Table 1, where they are compared with those for samples precipitated at lower electrolyte concentrations ($\sim$0·1 mol $dm^{-3}$).

Electron micrographs are presented in Fig. 2, showing differences in morphology and aggregate sizes when the zinc sulphide samples are precipitated and aged in acidic and in alkaline media.

## 4 Discussion

The pH conditions have a considerable effect on crystallite and aggregate size largely because they affect the solubility and hence the supersaturation ratio of the zinc sulphide. A greater supersaturation ratio causes nucleation to predominate over crystal growth, giving smaller crystallites. The ageing of the precipitates proceeds by Ostwald ripening supplemented by coagulation, especially in the presence of higher concentrations of surrounding electrolyte.

### 4.1 PRECIPITATION AND AGEING AT LOWER ELECTROLYTE CONCENTRATIONS

When zinc sulphide is precipitated by hydrogen sulphide from 0·1 mol $dm^{-3}$ $ZnSO_4$ or $ZnCl_2$, the pH progressively decreases from about 5 to 1. The average crystallite size of the products (calculated from specific surface area measurements) is about 10 nm, as shown in Fig. 1(a) and (c). Subsequently, these sizes increase to about 30 nm as the zinc sulphide ages for a total of 10 h at 20°C, finally acquiring a comparatively slow crystallite growth rate. The close similarity of the specific surface area (and average crystallite size) curves indicates that at electrolyte concentrations below 0·1 mol $dm^{-3}$ the greater coagulating effect of the divalent sulphate ion compared with the univalent chloride ion is not prominent in promoting crystallite growth.

Similar specific surface areas and average crystallite sizes are given initially when zinc sulphide is precipitated in alkaline conditions, viz. from zinc sulphate solutions added to 0·1 mol $dm^{-3}$ $Na_2S$ at 20°C, as in Fig. 1(b) and (d), curve *AB*. Subsequently, the specific surface area somewhat increases (and the average crystallite size decreases), before the material ages much more slowly than in acidic media. The initial increase may arise from removal of strains of defects in the newly-formed zinc sulphide as it recrystallizes to its normal lattice structure. This effect has been found previously with some newly-hydrated limes and magnesias.[8, 16]

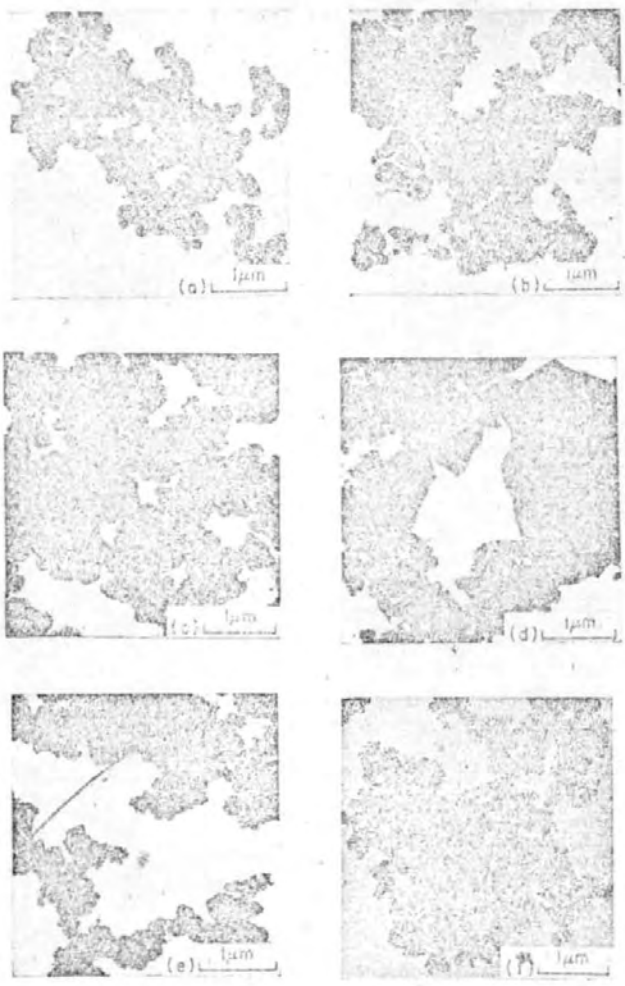


(a) 0·1 mol $dm^{-3}$ $ZnSO_4$ + $H_2S$ ($3\frac{1}{2}$ h ageing).
(b) 1 mol $dm^{-3}$ $ZnSO_4$ added to 0·1 mol $dm^{-3}$ $Na_2S$ (10 h ageing).
(c) 0·1 mol $dm^{-3}$ $ZnCl_2$ + $H_2S$ (1 h ageing).
(d) 1 mol $dm^{-3}$ $ZnCl_2$ added to 0·1 mol $dm^{-3}$ $Na_2S$ (1 h ageing).
(e) 0·25 mol $dm^{-3}$ $ZnCl_2$ + $H_2S$ (1 h ageing).
(f) 500 $cm^3$ 0·25 mol $dm^{-3}$ $ZnCl_2$ + 50 g NaCl + $H_2S$ (1 h ageing).

FIG. 2. Electronmicrographs of zinc [redacted] precipitated at 20°C in acidic or alkaline conditions.

The zinc sulphide precipitated at 85°C initially has a greater specific surface area (and smaller average crystallite size) than that prepared at 20°C (points *A* and *C* in Fig. 1(b) and (d)). Evidently, the nucleation is much faster at the higher temperature, which produces a larger number of smaller crystallites and more than compensates for the loss of surface caused by the increased rate of crystal growth. Thus, the zinc sulphide precipitated and aged at 85°C (curve *CD*) subsequently has a much smaller specific surface area (and larger average crystallite size) than that prepared and aged at 20°C (curve *AB*). As expected, the sample precipitated at 85°C ages afterwards at 20°C more slowly than it does at 85°C (curves *CE* and *CD*). However, this ageing at 20°C is faster than that of the sample initially prepared at 20°C (curves *CE* and *AB*). This is in accord with the sample precipitated at 85°C having initially a larger number of smaller crystallites (below a critical size) which redissolve and deposit on the larger crystallites in the Ostwald ripening process.[17]

Average crystallite size values of the same order as those calculated from specific surface areas have been obtained from X-ray line- (or peak-) broadening measurements. They are smaller but show the same general trends in variation as the materials are aged. Thus, in acidic media these average crystallite sizes vary from 5·0 to 8·8 nm with 0·1 mol $dm^{-3}$ $ZnSO_4$ and 4·4 to 8·8 nm with $ZnCl_2$. In alkaline media, the initial sizes and subsequent increases on ageing are somewhat smaller, viz. 3·0 to 3·4 nm and 2·8 to 4·4 nm for zinc sulphate added to 0·1 mol $dm^{-3}$ $Na_2S$ at 20°C and 85°C respectively; also 2·8 to 3·1 nm for the sample precipitated at 85°C and aged at 20°C.

In comparing the values of the average crystallite sizes determined from specific surface areas and X-ray line- (or peak-) broadening, there are 2 to 4-fold and 3 to 6-fold differences in acidic and alkaline media respectively. These are ascribed to differences in porosity, crystal strain and defects and especially crystallite size distribution. Variations due to porosity and crystal strain are comparatively small, since the nitrogen adsorption isotherms showed little hysteresis and the precipitation processes did not involve interconversion of solid material, only the more stable (cubic) form of zinc sulphide being obtained. The calculation of average crystallite sizes from specific surface areas assumes no particular crystallite size distribution, whereas that from X-ray measurements assumes a Gaussian distribution. Nevertheless, the X-ray measurements again indicate that the samples precipitated and aged in alkaline media (compared with acidic media) generally have the smaller crystallite sizes.

### 4.2 MORPHOLOGY AND AGGREGATE SIZES

In addition to differences in crystallite sizes, the samples vary also in morpho-

logy and aggregate sizes. Samples precipitated from acidic media appear to have smaller ranges of aggregate sizes than those from alkaline media. This is illustrated in Fig. 2 by comparing (a) and (b) for $ZnSO_4$ (0·1 to 0·2 μm and 0·1 to 1 μm) and (c) and (d) for $ZnCl_2$ (0·1 to 0·5 μm and 0·1 to 2 μm). In the latter case, the formation (and presence) of sodium chloride during the alkaline precipitation affects the crystal habit, causing the aggregates to have a plate-like morphology (Fig. 2d). Many of these aggregates are larger than those obtained in the corresponding precipitation from 0·1 mol $dm^{-3}$ $ZnSO_4$ in (b); the crystallites are about twice as large with $S = 56·3\ m^2\ g^{-1}$ and average crystallite size 26·1 nm, compared with 116·4 $m^2\ g^{-1}$ and 12·6 nm.

### 4.3 PRECIPITATION IN LESS ACIDIC AND ALKALINE MEDIA

Smaller-sized zinc sulphide crystallites are obtained also in less alkaline conditions from zinc oxide dissolved in 3 mol $dm^{-3}$ $NH_4OH$ and treated with hydrogen sulphide, giving precipitation at pH values decreasing from about 11 to 9. Even after 15 h ageing at 20°C, the specific surface is 124 $m^2\ g^{-1}$ and average crystallite size 11·9 nm (or 6·4 nm from X-ray peak-broadening). Much larger crystallite sizes are given in less acidic media when 1 mol $dm^{-3}$ $Na_2S$ is added to 0·1 mol $dm^{-3}$ $ZnSO_4$, with precipitation at pH values increasing from about 5 to 7. The precipitation is accompained by hydrolysis of the zinc salt, the newly-formed product having a specific surface area of only 14·9 $m^2\ g^{-1}$ and an average crystallite size as large as 98·7 nm.

### 4.4 PRECIPITATION AND AGEING AT HIGHER ELECTROLYTE CONCENTRATIONS

The specific surface areas and corresponding average crystallite sizes of the zinc sulphide samples precipitated in alkaline media are not changed considerably when the concentration of the sodium sulphide is increased from 0·1 to 1 mol $dm^{-3}$ (see Table 1). The changes are more considerable in acidic media when the concentrations of zinc sulphate or zinc chloride are increased from 0·1 to 1 mol $dm^{-3}$ or 0·25 mol $dm^{-3}$ respectively (Table 1). Addition of sodium chloride to 0·1 mol $dm^{-3}$ $ZnSO_4$ also causes decreases in specific surface area and increases in corresponding average crystallite size, but it does not cause further changes of this type when added to 0·25 mol $dm^{-3}$ $ZnCl_2$. However, the presence of higher concentrations of chloride ions seems to change the crystallite size distributions, since the average crystallite sizes calculated from X-ray line- (or peak-) broadening give abnormally lower values. Nevertheless, the aggregate sizes (Fig. 2) increase somewhat from submicron sizes at the lower electrolyte concentrations, viz. (a) 0·1 to 0·2 μm for 0·1 mol $dm^{-3}$ $ZnSO_4$ + $H_2S$, and (c) 0·1 to 0·5 μm for 0·1 mol $dm^{-3}$ $ZnCl_2$ + $H_2S$, compared with (e) and (f) 0·2 to 3 μm for 0·25 mol $dm^{-3}$ $ZnCl_2$ + $H_2S$ alone or in the presence of sodium chloride.

ACKNOWLEDGEMENT

The authors thank Dr A. W. Richards, Imperial Smelting Corporation, for his interest and encouragement in this work; the University of London, Imperial Chemical Industries Ltd, and the Science Research Council for grants for apparatus; and the Governors of the Polytechnic for a Research Assistantship (for B. Basak).

## References

1. Levi, G. R. and Fontana, C. G. (1928). *Atti Accad. Naz. Lincei* **7**, 502.
2. Allen, E. T. and Crenshaw, J. L. (1912). *Amer. J. Sci.* **36**, 341.
3. Ortmann, H. and Piwonka, R. (1960). *Mber. Dt. Akad. Wiss.* **2**, 549; Ortmann, H. and Piwonka, R. (1963). *Mber. Dt. Akad. Wiss.* **5**, 174.
4. Ortmann, N. and Piwonka, R. (1961). *Z. phys. Chem.* **218**, 64.
5. Lendvay, E., Schanda, J., Richter, K. and Somagyi, M. (1965). *Czech J. Phys.* **13**, 142.
6. Brown, R. A. (1968). *Electrochem. Technol.* **6**, 246.
7. Shishlannikova, E. M. (1970). *Izv Nauch-Issled Inst. Nefte-Uglekhim Sin. Irkutsk Univ.* **12**, 105.
8. Glasson, D. R. (1960). *J. Appl. Chem. London* **10**, 38.
9. Gregg, S. J. (1946). *J. Chem. Soc.* 561.
10. Sartorius-Werke (1963). "Electrono-vacuum Microbalances". Sartorius-Werke, A.-G., Gottingen.
11. Brunauer, S., Emmett, P. H. and Teller, E. (1938). *J. Amer. Chem. Soc.* **60**, 309.
12. Glasson, D. R. (1960). *J. Appl. Chem. London* **10**, 42.
13. Glasson, D. R. and Jayaweera, S. A. A. (1968). *Soc. Chem. Ind. Monogr.* No. 28, p. 353.
14. Glasson, D. R. (1964). *J. Appl. Chem. London* **14**, 121.
15. Jones, F. W. (1938). *Proc. R. Soc.* **166**, 16; Klugg, H. P. and Alexander, L. E. "X-ray Diffraction Procedures". John Wiley, New York.
16. Glasson, D. R. (1963). *J. Appl. Chem. London.* **13**, 119; Glasson, D. R. (1964). *J. Appl. Chem. London* **14**, 125.
17. Nielsen, A. E. (1964). "Kinetics of Precipitation," p. 5. Pergamon, Oxford.